

**Mathematical and Computational Analyses of Immunological Signaling Networks
Affecting *Mycobacterium tuberculosis* Infection**

by

Joe Christian Johnstone Ray

A dissertation submitted in partial fulfillment
of the requirements for the degree of
Doctor of Philosophy
(Microbiology and Immunology)
in The University of Michigan
2008

Doctoral Committee:

Associate Professor Denise E. Kirschner, Chair
Professor Gary B. Huffnagle
Professor Jennifer J. Linderman
Professor Alexander J. Ninfa
Professor Joel A. Swanson

© Joe Christian Johnstone Ray 2008

To Jodi

Acknowledgements

Denise allowed me the freedom to be independent while always expecting excellence, setting a standard that I should hope to take with me. Members of my committee provided deep insight and invaluable direction. John Chan and Jian Wang performed the experiments presented in Chapter 3, with advice. JoAnne Flynn provided expert guidance and direction on Chapter 4.

Family, friends and colleagues at many times, in many places, and in uncountable ways were indispensable. My father imparted a love of science, understanding, and progress; I have known no greater intellectual influence. My mother counseled, listened, cheered when appropriate, and lent me her time, effort and humanity. Charlie gave me hope for the future and occasional respite from the present.

Jodi's love, patience and perseverance saw me through.

Table of Contents

Dedication	ii
Acknowledgements	iii
List of Figures	v
List of Tables	viii
Abstract	x
Chapter 1. Introduction	1
Chapter 2. Requirement for Multiple Activation Signals by Anti-Inflammatory Feedback in Macrophages	26
Chapter 3. The Timing of TNF and IFN- γ Signaling Affects Macrophage Activation Strategies During <i>Mycobacterium tuberculosis</i> Infection	84
Chapter 4. Roles of Tumor Necrosis Factor Signaling in Granuloma Formation During <i>Mycobacterium tuberculosis</i> Infection	123
Chapter 5. Conclusions and Future Directions	204

List of Figures

Figure 1.1. Pathways of macrophage activation relevant to infection with <i>Mycobacterium tuberculosis</i> .	9
Figure 2.1. Schematic of the macrophage biochemical network involved in activation of nitric oxide production.	61
Figure 2.2. Response of nitric oxide to doses of LPS and IFN- γ .	62
Figure 2.3. Crosstalk of activation pathways induced by common feedback.	63
Figure 2.4. Significant partial rank correlations (statistical sensitivities) of parameters in Activation and Killing Module interactions to nitric oxide and labile iron pool levels.	64
Figure 2.5. Significant partial rank correlations (statistical sensitivities) of parameters in the Iron Regulation Module to nitric oxide and labile iron pool levels.	65
Figure 2.6. Example parameter spaces for mathematically controlled comparisons.	66
Figure 2.7. Parameter scores maximizing robustness of macrophage components to perturbations.	67
Figure 2.8. Response time of nitric oxide (x_6) from quiescent levels to within 5 % of the steady state or above.	68
Figure 3.1. Simulated experimental scenarios for macrophage activation that depend on the timing of IFN- γ and TNF signaling relative to infection.	105
Figure 3.2. Macrophage network schematic including interactions with an intracellular population of <i>Mycobacterium tuberculosis</i> (b) with parameter names and variable numbers depicted.	106
Figure 3.3. Calibration of the model to dose-response of ManLAM and IFN- γ .	107
Figure 3.4. Greater survival of <i>M. tuberculosis</i> in macrophages with negative feedback to NF- κ B by NO compared to positive feedback.	108

Figure 3.5. Stronger negative feedback improves macrophage activation time during infection with <i>M. tuberculosis</i> .	109
Figure 3.6. High cytokine concentrations that do not precede infection enhance killing under strong negative feedback.	110
Figure 3.7. Recruitment scenarios that tip the balance between bacterial killing and persistence based on timing of activation signals.	111
Figure 3.A1. Simulations and experimental data shown as time series over 96 hours.	117
Figure 4.1. Models of molecular signaling networks that affect granuloma formation during infection with <i>Mycobacterium tuberculosis</i> .	145
Figure 4.2. Structure of agent-based model environment.	146
Figure 4.3. Simulated kinetics of extracellular <i>M. tuberculosis</i> and typical granuloma structures at 200 days post-infection in baseline control and TNF deletion scenarios.	147
Figure 4.4. Distribution of average extracellular <i>M. tuberculosis</i> numbers at 200 days post-infection using parameter ranges in Table 4.1.	148
Figure 4.5. Time of bacterial clearance for simulations that predict complete elimination of bacteria depends on timing of innate and adaptive immune response.	149
Figure 4.6. Global Sensitivity analysis of granuloma simulations.	150
Figure 4.7. Depletion of TNF-induced apoptosis activity.	151
Figure 4.8. T cell kinetics for depletion of TNF-induced apoptosis activity in subsets of the macrophage population.	152
Figure 4.9. Effects of changing the probability of TNF-induced apoptosis activity on extracellular <i>M. tuberculosis</i> numbers and granuloma structures in the agent-based model.	153
Figure 4.10. Double and triple deletions of TNF-activities.	154
Figure 4.A1. Attainable granuloma structures 200 days post-infection from one run of global uncertainty analysis.	177
Figure 4.A2. Granuloma structures predicted for deletion and depletion of each specific TNF activity.	180

Figure 4.A3. Granuloma structures predicted for ten replicates of deletion and depletion of specific TNF activity combinations.	185
Figure 5.1. Conceptualization of a multi-scale model of intra- and inter-cellular signaling in <i>M. tuberculosis</i> infection.	213
Figure 5.2. Macrophage activation pathways involved with iNOS induction have layers of regulation from other genes regulated by Stat1.	214

List of Tables

Table 2.1. Definition and estimates of important parameters in the macrophage model.	69
Table 2.2. Parameters examined in the local detailed analysis.	70
Table 2.3. Lines of equivalent gain and the stability criterion used for local detailed analysis.	71
Table 2.4. Predicted parameter regions that best meet each criterion denoted by a score of $-$, 0 or $+$.	72
Table 3.1. Macrophage regulatory interactions optimizing killing of <i>M. tuberculosis</i> and temporal responsiveness	113
Table 3.2. Sensitivity of <i>M. tuberculosis</i> numbers (100 hours post-infection) to quantitative variations in regulatory interactions	114
Table 3.A1. Definitions and estimates of model parameters.	117
Table 3.A2. Parameter estimates from dose response experiments	118
Table 4.1. Parameters varied for Latin hypercube sampling	155
Table 4.2. Parameter relationships constrained for analyses	157
Table 4.3. Parameters not varied in uncertainty analysis	158
Table 4.4. Significant partial rank correlations between parameters and different granuloma outcome measures 20 and 200 days post-infection for several different outcome variables	159
Table 4.4. Significant partial rank correlations between parameters and different granuloma outcome measures 20 and 200 days post-infection for several different outcome variables	159
Table 4.5. Significant changes in granuloma variables at 200 days post-infection for deletion and depletion of all TNF activity (“Positive Control”), TNF-induced activation activity (“Activation”), and TNF-induced apoptosis activity (“Apoptosis”) versus the baseline control scenario.	160

Table 4.6. Significant changes in granuloma variables at 200 days post-infection for deletion and depletion of all TNF activity activity (“Positive Control”), TNF effects on cellular transendothelial migration activity (“Recruitment”), and TNF-induced secretion of chemokines/TNF activity (“Secretion”) versus the baseline control scenario.	161
Table 4.A1. Significant partial rank correlations between parameters and granuloma variables 200 days post-infection.	194
Table 4.A2. Significant partial rank correlations between parameters and granuloma variables 20 days post-infection (immediately preceding adaptive immunity).	195
Table 4.A3. Significant changes in granuloma variables at 200 days post-infection for deletion and depletion of combinations of two individual TNF activities versus the baseline control scenario.	196
Table 4.A4. Significant changes in granuloma variables at 200 days post-infection for deletion and depletion of combinations of three individual TNF activities versus the baseline control scenario.	197

Abstract

Immunological signaling pathways between and within cells are central determinants of the success of immune responses. One major characteristic of immune signaling is a balance that is struck between pro-inflammatory responses to pathogens and anti-inflammatory regulation that stabilizes and modulates immunity. *Mycobacterium tuberculosis* is a successful human pathogen that preferentially survives within host macrophages, the very immune cells that act to eliminate it. Exploitation of the balance between pro- and anti-inflammatory mechanisms may be a strategy for *M. tuberculosis* survival within macrophages. This work first explores the evolved design principles of intracellular macrophage activation pathways relevant to countering *M. tuberculosis* infection. I used a mathematical model of the macrophage intracellular signaling network to predict that multiple synergistic activation signals are balanced by negative (anti-inflammatory) feedback from a single output, the killing effector nitric oxide. Without the presence of two activation signals, the feedback is antagonistic toward high levels of activation. I next implemented a representation of a growing intracellular population of *M. tuberculosis* in the macrophage signaling model. This shows that negative feedback of nitric oxide to activation signaling may not optimally kill bacteria compared to a possible positive feedback design. However, the model predicts that negative feedback imparts a kinetic advantage to elevating nitric oxide levels. The kinetics of nitric oxide induction offset the disadvantage of negative feedback if the timing of activating cytokine delivery occurs near the time of macrophage infection. On a different biological scale, I explored

the roles of activation signals in *M. tuberculosis* infection with a computational agent-based model of granuloma formation. Model results suggest that multiple effects of the pleiotropic cytokine tumor necrosis factor- α (TNF) are an essential feature of TNF function: loss of single TNF activities did not result in granuloma structures comparable to deletion of all TNF activity. Perturbation of multiple TNF activities simultaneously showed synergistic and competitive effects of individual TNF activities in granuloma formation. Finally, I explored possible ways to integrate a single-cell stochastic model of macrophage gene regulation into an agent-based model to simulate the roles of intracellular signaling in the context of the granuloma environment.

Chapter 1

Introduction

Mycobacterium tuberculosis (Mtb) is among the most successful pathogens in the world, with approximately one third of the human population (two billion people) currently infected. Mtb is a slow-growing bacillus spread by small aerosol doses that survive in host lung macrophages. Infection induces an adaptive immune response that is usually successful at containing infection, but frequently fails to clear it, instead forming stable aggregates of immune cells called granulomas leading to a long-term latent state (reviewed in 20).

During any infection, immunological signaling events between and within cells are central determinants of the success of immune responses. Immune responses must effectively enable clearance of a constant onslaught of insults, including pathogens, non-pathogenic organisms and other foreign bodies. However, bactericidal effectors and pro-inflammatory signals are costly to host health. Thus, signaling must strike a balance between pro-inflammatory effects and anti-inflammatory regulation. The success of Mtb as a human pathogen may have arisen from exploiting this balance: if immune signals do not permit sufficient inflammation for bacterial clearance, the infection can indefinitely persist in a latent state. This represents a potential survival strategy for Mtb.

Clearly, the role of signaling— activation, de-activation, and coordination of immune responses— is an important element of host-pathogen interactions with Mtb.

Ongoing experimental work continually reveals increasing complexity, apparent redundancy, and counterintuitive effects for pro- and anti-inflammatory signals in immune responses to Mtb. This invites the application of mathematical and computational analysis that can explain subtle roles of immune signaling in Mtb infection that are currently inaccessible with other approaches.

1.1 Immunological events and infection with *M. tuberculosis*

1.1.1 Innate and adaptive immunity

Typical Mtb infection begins with inhalation of a small number of bacilli (on the order of 10) into the lung. Alveolar macrophages engulf the bacteria and possibly seed infection in lung parenchymal tissue, the highly vascularized environment of oxygen exchange comprised of at least 10% blood vessels and alveolar septa (29). During the initial stages of Mtb infection, infected neutrophils and macrophages produce the pro-inflammatory cytokine tumor necrosis factor- α (TNF) (12, 16, 36) and chemokines that recruit immune cells to the site of infection (30, 31, 49, 58). Macrophages infected with Mtb produce the cytokine IL-12 (34), which induces a cell-mediated Type-1 adaptive immune response.

Type-1 adaptive immunity is required to control infection in humans and in mouse models (11). In this type of response, activated CD4⁺ T cells from the draining lymph nodes migrate to the site of infection in the lung to provide the macrophage-activating cytokine interferon (IFN)- γ and contribute to production of TNF (67) in response to phagosome-derived antigen presented by macrophages. CD8⁺ T cells are recruited to the lungs from the draining lymph nodes of Mtb infected mice with similar

kinetics to CD4⁺ T cells (17, 60). These cells respond to cytoplasmic antigen presented by macrophages, producing pro-inflammatory cytokines (including IFN- γ) and lysing infected macrophages (reviewed in 20).

A third subset of T cells known as regulatory T cells (T_{reg}) have a modulatory role in adaptive immune responses (53). T_{reg}s are CD4⁺/Foxp3⁺ and comprise approximately 5-10% of all CD4⁺ T cells (3, 53). They suppress the action of pro-inflammatory T cells (63), possibly through cell-contact-mediated or immunosuppressive cytokine mechanisms (4). T_{reg} cells are present in mouse (40) and human (23) Mtb infections, and lower the effectiveness of the immune response at eliminating bacteria (46, 50).

1.1.2 Granuloma formation

The classic feature of pulmonary Mtb infection is the formation of granulomas in the lung. In humans and non-human primates with latent pulmonary infection, granulomas form as well-circumscribed masses in the lung parenchyma comprised of resting, infected and activated macrophages with a characteristic cuff of activated CD4⁺ and CD8⁺ T cells on the periphery (15, 48). At the level of a single granuloma, macrophages may fail to control infection, leading to caseous or necrotic granulomas harboring large numbers of bacteria within macrophages (15). TNF gene-disrupted mice have disorganized, dissolved granulomas in Mtb infections (5), underscoring the link between granuloma structure and effective containment of infection. However, the relationship between bacterial control in a single granuloma and the outcome of infection at the level of the entire host is not well established.

1.1.3 Molecular signals that activate macrophage responses to *M. tuberculosis*

Communication between immune cells depends on molecular-scale signals that coordinate immune cell responses. Pro-inflammatory cytokines TNF and IFN- γ are one facet of this communication network. TNF and IFN- γ activate macrophages in a complementary manner, promoting anti-microbial genetic programs (18, 19, 51) through separate intracellular signaling pathways that form a central component of host defense against Mtb infection (these are discussed in detail below). Differences in the functional roles of IFN- γ and TNF extend beyond macrophage activation. Unlike IFN- γ , TNF has several distinct functional activities: it also induces apoptotic cell death in macrophages (35) and has a direct role in cell recruitment via up-regulation of endothelial adhesion molecules (71), facilitating trans-endothelial migration of immune cells to the site of infection.

The spatial distribution of TNF and IFN- γ may also differ. IFN- γ is secreted by activated T cells directly to the immunological synapse (27), which forms at the interface with antigen presenting cells such as macrophages. In contrast, TNF was shown to be secreted multi-directionally from T cells (27) in addition to being produced by activated macrophages (12).

1.1.4 Molecular signals that coordinate immune cell recruitment

Chemokines, which direct immune cells to sites of infection, are a second facet of molecular scale immune signaling that induce trans-endothelial migration (reviewed in 65) and coordinate recruitment of immune cells to the site of infection by establishing a chemotactic gradient (reviewed in 61).

We constructed a simplified model of chemokines with three classes that affect recruitment of macrophages and T cells to the granuloma via binding of appropriate chemokine receptors on the cell surface. The α -chemoattractant class (CXCL9,10, and 11; formerly Mig, IP-10 and I-TAC, respectively) binds chemokine receptor CXCR3 on pro-inflammatory CD4⁺ and CD8⁺ T cells (42), but not regulatory T cells (33). CCL2 (formerly MCP-1) binds CCR2 on macrophages (64) and proportions of pro-inflammatory T cell populations (47). CCL5 (formerly RANTES) binds CCR5 on macrophages and T cells, and is necessary for migration of regulatory T cells to the site of Mtb infection (70).

1.2 Mechanisms, strategies and effects of macrophage activation

Typically, resident tissue macrophages readily clear foreign bodies by phagocytosis. Mtb is resistant to innate clearance mechanisms, requiring macrophages to receive T cell-derived signals to become activated sufficiently to kill intracellular bacteria (22). The adaptive immune response controls infection by inducing a genetic program in macrophages that produces toxic anti-microbial effectors in quantities that are potentially detrimental to long-term health of the host. Given the costs to the host associated with this, we reason that macrophage activation lies behind a threshold that makes it a relatively rare occurrence. This threshold is of interest when considering Mtb infections, since it provides an evolutionary goal for Mtb survival in the host (namely, to exploit mechanisms that maintain the quiescent or near-quiescent macrophage state). We now examine mechanisms by which macrophages may balance the requirement of its typical

goal to maintain a stable quiescent state with the potential for reaching highly activated states.

1.2.1 NF- κ B and JAK/STAT intracellular signaling pathways

Activation signals, including TNF, IFN- γ and bacterial products, induce intracellular second messengers that lead to transcriptional reprogramming of macrophages receiving these signals. In Mtb infection, two signaling pathways stand out as central to bacterial control: NF- κ B and JAK/STAT.

The NF- κ B signaling pathway (59) is pro-inflammatory and general, operating in most cell types (21). Signals that are transduced from toll-like receptor (TLR)-antigen binding (reviewed in 8) or TNF-TNFR1 binding (reviewed in 67) on the macrophage cell surface result in ubiquitin-mediated degradation of inhibitor of NF- κ B (I κ B). This leads to the release of formerly captive NF- κ B into a transcriptionally active form capable of translocating into the nucleus (21, 59). NF- κ B may be activated by products from Mtb, including lipoarabinomannan (LAM) (9).

The Janus kinase (JAK)/signal transducer and activator of transcription (STAT) pathway depends on auto-phosphorylation of JAK due (in the relevant pathway here) to dimerization of IFNR1 (1). This results in phosphorylation and homodimerization of Stat1- α into a transcriptionally active form that binds the γ -Activating Sequence motif of gene promoters.

1.2.2 Transcriptionally regulated nitric oxide production

NF- κ B and Stat1 regulate a number of genes, but one stands out as especially important for responses to Mtb: inducible nitric oxide synthase (iNOS), the enzymatic producer of nitric oxide (NO) (reviewed in 44). (69). Binding sequences for NF- κ B and Stat1 homodimer appear in the mouse and human promoter regions of the iNOS gene, and the NF- κ B pathway is complementary to and synergistic with Stat1 in iNOS transcriptional activation in mouse macrophage cultures (38).

Of the known mechanisms of pathogen killing by macrophages, NO and other reactive nitrogen intermediates (RNIs) appear to be the sole effective mechanisms *in vitro*. NO is a free radical that interacts promiscuously with other molecules, lending generality to its anti-microbial effects, and making it a regulator of multiple intracellular mechanisms. In particular, it feeds back to NF- κ B in either an inhibitory, stimulatory, or bi-modal manner (i.e. inhibitory in some circumstances, stimulatory in others; (10)). Like NF- κ B, Stat1 appears to be regulated by RNIs as well, apparently in an anti-inflammatory manner (37). The resulting picture of macrophage activation affecting iNOS transcription is of multiple, synergistic signals regulated in a feedback manner by RNIs.

1.2.3 Nitric oxide interaction with iron regulation

Another complexity arising from the reactivity of RNIs is that free intracellular iron in the labile iron pool (LIP) readily interacts with it, and the two are co-regulated (32). In addition to this, iron is the growth-limiting nutrient for nearly all intracellular pathogens, including Mtb (56). In both ways iron regulation is an important consequence of infection and macrophage activation.

As extracellular iron from blood or surrounding tissue circulates, it is chelated into transferrin or lactoferrin, and resident tissue macrophages clear it by internalization via the transferrin receptor (TfR) or phagocytotic ingestion (43). A homeostatic intracellular apparatus regulates the levels of intracellular iron by directly sensing iron concentrations in the cytoplasm: Free iron binds to iron regulatory proteins (IRPs) with high affinity, freeing IRPs from causing translational arrest of the production of ferritin, a large shell-like chelator of intracellular iron (62). Therefore, the resulting increase in cytoplasmic iron levels permits ferritin-mediated iron chelation. Several studies point to nitric oxide/RNI-mediated regulation of IRP1 and IRP2, sometimes with conflicting results: RNIs may differentially regulate the IRPs (7, 68). The link between iNOS regulation and iron homeostasis involves feedback as well: elevated cytoplasmic iron is associated with inhibition of iNOS transcription through C/EBP- β (formerly NF-IL6)(14). This factor is necessary but not sufficient for iNOS transcription (24), allowing suppression, but not activation, of iNOS transcription by changes in intracellular iron levels.

1.3 Design principles of integrated macrophage function

The macrophage subsystems presented in the previous sections form a biochemical network responsible for regulating activation in response to extracellular signals (Figure 1.1). The entire network is comprised of three primary functions, referred

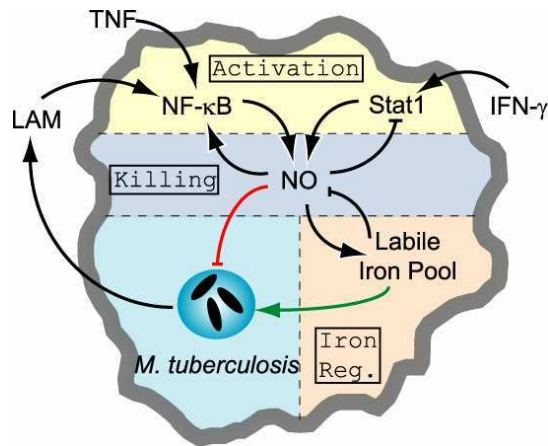


Figure 1.1 Pathways of macrophage activation relevant to infection with *Mycobacterium tuberculosis*. These include NF- κ B- and Stat1-induced transcriptional upregulation of inducible nitric oxide synthase, producer of the free radical nitric oxide (NO) that regulates many components of the macrophage and acts as an anti-microbial effector against intracellular mycobacteria. Relevant macrophage components can be split into three individual functions that are co-regulated, referred to as functional modules: Activation, Killing, and Iron Regulation.

to herein as functional modules: Activation, Killing, and Iron Regulation. The components in each module interact reciprocally with one or more neighboring modules, forming an integrated system whose response to macrophage activation is affected by intermodule interactions.

In some cases (e.g. RNI feedback to NF- κ B), these interactions are poorly understood from experimental work. That is, the magnitude of the interaction (strong versus weak) may be unknown and the sign of the interaction (i.e. whether it is stimulatory or inhibitory) is ambiguous or unknown. Even where it is known what type of interaction occurs, the consequences of this to the integrated system calls for further elucidation.

We reason that the intermodule interactions of the macrophage network have undergone evolutionary selection, which has gradually optimized the process of macrophage activation to meet the functional needs of macrophages, including a balance between a quiescent state and the rare need for high activation levels. Therefore, based on possible selective advantages of certain types of intermodule interactions, we hypothesize that the system has evolved according to underlying design principles. One major goal of this work is to determine the design principles of macrophage activation based on the types of intermodule interactions that optimize macrophage function.

1.4 Dynamic interactions of macrophage components with intracellular *M. tuberculosis*

A successful intracellular parasite exploits host cell machinery for survival, forming a micro-environment favorable to growth. In the case of Mtb infection, this appears to start with the inhibition of phagosome-lysosome fusion in macrophages (2, 13). Once inside a mycobacterial phagosome, Mtb bacilli depend on intracellular iron for continued growth (45).

Mtb within host macrophages survive if bactericidal levels of macrophage activation have not been reached (c.f. Section 1.2), and during an ongoing adaptive immune response, the location and timing of TNF and IFN- γ signals may differ (c.f. Section 1.1.3), affecting activation kinetics. For instance, if one or both of TNF and IFN- γ signals precede infection, so that macrophages are to some degree already activated before infection, is this favorable to the host?

Alternative macrophage network designs may also affect the kinetics of response; for instance, in other systems negative feedback has been shown to speed response times

in some inducible circuits (52). We therefore extend the concept of design principles to interactions with intracellular Mtb by asking what effects different possible macrophage network designs have on effective killing of Mtb. If an optimal activation strategy exists, this in turn may be subject to exploitation by a specialized pathogen. Therefore, understanding the kinetic roles of activation timing during infection may also suggest mycobacterial strategies to prevent bactericidal immune responses.

1.5 A mathematical formalism for studying macrophage design principles

1.5.1 Biochemical Systems Theory

Biochemical Systems Theory (BST) is a mathematical formalism developed for studying the integrative behavior of complex biochemical networks encompassing a number of tools developed to address the question of network design principles. This makes it a natural choice for studying the behavior of macrophage activation signals at the scale of interest here.

The basic concept underlying BST models is linearization of biochemical fluxes using logarithms (55). In logarithmic space, many functions are accurately approximated with a piecewise linear model, including non-linear sigmoidal and saturating functions appropriate for representing biochemical processes. This allows the estimation of a biochemical flux (dependent on n regulators X_i) in logarithmic coordinates using a first-order (i.e. linear) Taylor approximation that is local to a nominal set-point. For a flux V dependent on n regulators (X_i), the Taylor polynomial is of the form

$$\log V = a + \sum_{i=1}^n g_i \log X_i + O\left(\sum_{i=1}^n [\log X_i]^2\right).$$

Near the set point, the higher order terms are small; discarding them for this approximation and transforming back to linear coordinates gives an approximate quantitation of the flux as a product of power laws:

$$V = e^a X_1^{g_1} X_2^{g_2} \dots X_n^{g_n} = \alpha X_1^{g_1} X_2^{g_2} \dots X_n^{g_n} .$$

The BST formalism provides a *canonical* mathematical form (66). That is, the underlying mathematical structure is uniform with differences between models completely specified by the topology of the network under study. Therefore, analytical results from these models are very general, and applicable to any network with the same characteristics. The model can be further generalized with the use of piecewise power law approximations that allow the modeler to set a threshold where the parameter values are changed to improve the accuracy of the model far from the set-point (54).

We represent the network describing macrophage activation pathways shown in Figure 1.1 with an S-system type of BST model. In an S-system model, each variable, X_i , is dynamic, with single aggregate terms representing production or consumption flux, so that the model is specified by a system of ODEs of the form:

$$\frac{dX_i}{dt} = \alpha_i \prod_{j=1}^{n+m} X_j^{g_{ij}} - \beta_i \prod_{j=1}^{n+m} X_j^{h_{ij}} \text{ with } n \text{ dependent and } m \text{ independent variables.}$$

1.5.2 Mathematically controlled comparison

One of the primary advantages of mathematical models is the ability to easily manipulate components of the model. However, determining the effects of these changes in a model is not necessarily a trivial task. Studying design principles of the network calls for a rigorous method for determining the performance of alternative design possibilities.

We argue that high-performing designs have selective advantages over inferior designs (e.g. stimulatory versus inhibitory regulation of one component by another improves overall system performance by some criteria). The method of mathematically controlled comparisons (28) was developed for rigorous comparisons of alternative design possibilities for individual regulatory pathways of interest (local analysis). For global analysis of parameter space, we use statistical sensitivity and uncertainty methods (Section 1.7 below).

One requirement for local analysis is that we determine functional criteria by which to judge the effectiveness of alternative designs. The specific choice of criteria depends on the functional goal of the system. For the macrophage model, we use three criteria previously shown to predict design principles in other inducible gene circuits (25): stability, robustness, and dynamic responsiveness. Stability refers to the ability of the system to return to steady state after a small change in component levels, determined in this system with the Routh-Hurwitz method. Robustness means the relative insensitivity of model variables and production/consumption rates to perturbations in parameters and other external components, measured by logarithmic gains of each dependent variable (X_i) and flux (V_i) in response to independent variable and parameter perturbations. (Logarithmic gains are mathematically defined as $\partial \log \hat{X} / \partial \log p$, intuitively meaning a quantitation of the level of perturbation of molecule X by changes in parameter p when the system is in steady state.) Finally, responsiveness represents a fast temporal change in NO levels after activation signals, reaching the activated steady state as quickly as possible after induction. Stability and robustness are, in principle, determined analytically from the model; this lends the analysis a level of independence

from choices of parameter values. Responsiveness requires choosing realistic parameter values for numerical simulations.

With these criteria defined, we alter regulatory interactions of interest in a manner constrained to ensure that the systems under comparison are as nearly identical as possible, the only remaining changes therefore confidently attributable to the parameter under study. Two parameter constraints are introduced to achieve this: internal and external equivalence. Internal equivalence requires all parameters not part of the regulatory flux of interest (e.g. V_i^+ for parameter g_{ij} under study) to be equal. The second requirement, external equivalence, introduces corrections for parameters in the regulatory flux of interest based on holding constant an external, observable behavior of the model: in the case of the macrophage model, gain of iNOS protein from activation signals. This is necessary since non-linearities in the model may introduce irrelevant differences from varying the regulatory parameter under study.

1.6 Multi-scale computational model of signaling in a mycobacterial granuloma

The ordinary differential equation modeling framework has historically been the most fruitful route for building predictive models of any kind of physical system. However, its limitations, particularly in a biological context, become obvious when seeking an integrated understanding of very complex systems. In the dynamics of immune responses to Mtb, individual macrophages and T cells interact with each other and with molecular scale signals. A realistic model of this system should integrate all relevant spatio-temporal scales. Spatially, this ranges from the molecular to the tissue to organismal scales with temporal events occurring on the order of second to years. One

promising method for capturing all the relevant scales and interactions is an agent-based model (ABM). An ABM is a computer algorithm that encompasses any interactions capable of being programmed. Therefore, continuous and discrete spatiotemporal effects may be represented in any level of detail within the constraints of computational power.

ABMs are developed based on four considerations: *agents*, the *rules* that describe the agents and their interactions, the *environment* on which the agents reside and the *timescales* on which events are defined. Molecular scale events may be represented continuously with either discretized ordinary or partial differential equations while each immune cell is a discrete entity with a location and conserved properties over time. Algorithms in the model represent genetic and biochemical programs in cells that allow each cell to respond, deterministically or probabilistically (as appropriate) to stimuli. The details of the algorithms are determined from experimental data. The passage of time is discretized into the smallest appropriate step, set by the fastest process in the model. Cell movements and interactions are updated at appropriate intervals based on model algorithms. A remarkable outcome of this type of model is emergent behavior: that is, simulations show system-wide behaviors that are the result of agents interacting locally.

Previously, Segovia-Juarez *et al* (57) developed a simple ABM of granuloma formation during infection with Mtb using two cell types and a non-specific chemokine for cell recruitment. This model was able to reproduce different types of granulomas (that both contain infection and fail to do so), but it lacks sufficient mechanisms to study the specific roles of cytokines, chemokines and specific cell types in granuloma formation and function. We have extended this previous model to study the role of pro-inflammatory cytokines and multiple T cell subtypes in determining resulting granuloma

formation. We distinguishing between three possible outcomes at the level of a single granuloma: elimination of bacteria, controlled growth (i.e. a latent state), and uncontrolled bacterial growth.

1.7 Statistical methods for parameter space sampling and sensitivity analysis

Mathematical and computational models that represent detailed mechanisms involved in biological processes inherently contain many parameters, and in most cases realistic values are difficult or impossible to determine. Thus, sophisticated methods are necessary for determining how parameters, which represent specific mechanisms in the system, affect model outcomes. In a statistical approach to this problem, each parameter is given a plausible interval and values in this interval are selected in a Monte Carlo sampling scheme; randomly combined values from each parameter give N sets that represent a statistical sample of the entire plausible parameter space. Here we use Latin hypercube sampling (41), a stratification method that ensures high-efficiency sampling of the parameter space. Ideally, the choice of parameter distributions and intervals in this method should represent both an unbiased sampling of parameter space and physically or biologically plausible ranges for each parameter. In practice, the best choice of distributions and intervals is a trade-off between these two goals.

With a statistical sample of the parameter space, partial rank correlations (PRCs) quantify the effect of each parameter on a chosen model output. PRCs vary between -1 and 1 , respectively representing inverse and direct correlations. PRCs permit the output to be non-linear due to the ranking, but the relationship between the output and each parameter should be monotonic. In the case of models that have aleatory uncertainty (i.e.

uncertainty arising from random processes in the model), the monotonicity requirement may not be met. This situation occurs in ABMs. However, parameters with a particular effect on an output variable will continue to have this effect on average during simulations. Therefore, repeated simulations for each sampled parameter set will allow the average output of the model to be monotonic, allowing the use of uncertainty and sensitivity analysis with ABMs.

Significance tests have been developed to determine if the PRC is different from zero (6) and to determine if two PRCs differ from one another (26). This allows discrimination between strong and weak parameter effects, and allows the determination of relative effects of different parameters on the model output (39).

1.8 Understanding roles of immunological signaling in macrophage activation and infection with *Mycobacterium tuberculosis*

During infections with Mtb, immunological signaling is central in determining the success of host defenses. Massive experimental efforts and increasingly sophisticated experimental methods have resulted in a large list of components involved in immunological signaling and its role in mycobacterial infections. However, deeper understanding of the principles of immune signaling, and an integrated view of its role in larger-scale effects of infection, require systems-oriented approaches.

The aim of this work is to construct and analyze mathematical and computational models that capture several facets of immunological signaling involved with *Mycobacterium tuberculosis* infection. First, we analyze the role of the intracellular regulatory network involved with macrophage activation of nitric oxide production with a mathematical model. Second, we extend this model to understand the role of activation

signal timing during intracellular *M. tuberculosis* infection. Finally, we analyze the roles of signaling using an agent-based model in the larger-scale setting of pulmonary granuloma formation.

1.9 References

1. **Aaronson, D. S., and C. M. Horvath.** 2002. A road map for those who know JAK-STAT. *Science* **296**:1653--1655.
2. **Armstrong, J. A., and P. D. Hart.** 1971. Response of cultured macrophages to *Mycobacterium tuberculosis*, with observations on fusion of lysosomes with phagosomes. *J Exp Med* **134**:713--740.
3. **Asano, M., M. Toda, N. Sakaguchi, and S. Sakaguchi.** 1996. Autoimmune disease as a consequence of developmental abnormality of a T cell subpopulation. *J Exp Med* **184**:387-396.
4. **Baatar, D., P. Olkhanud, K. Sumitomo, D. Taub, R. Gress, and A. Biragyn.** 2007. Human Peripheral Blood T Regulatory Cells (Tregs), Functionally Primed CCR4+ Tregs and Unprimed CCR4- Tregs, Regulate Effector T Cells Using FasL. *J Immunol* **178**:4891-4900.
5. **Bean, A., D. Roach, H. Briscoe, M. France, H. Korner, J. Sedgwick, and W. Britton.** 1999. Structural Deficiencies in Granuloma Formation in TNF Gene-Targeted Mice Underlie the Heightened Susceptibility to Aerosol *Mycobacterium tuberculosis* Infection, Which Is Not Compensated for by Lymphotoxin. *J Immunol* **162**:3504-3511.
6. **Blower, S. M., and H. Dowlatabadi.** 1994. Sensitivity and Uncertainty Analysis of Complex Models of Disease Transmission: an HIV Model, as an Example. *Int Stat Rev* **62**:229--243.
7. **Bouton, C., L. Oliveira, and J. C. Drapier.** 1998. Converse modulation of IRP1 and IRP2 by immunological stimuli in murine RAW 264.7 macrophages. *J Biol Chem* **273**:9403--9408.
8. **Carmody, R. J., and Y. H. Chen.** 2007. Nuclear factor-kappaB: activation and regulation during toll-like receptor signaling. *Cell Mol Immunol* **4**:31-41.
9. **Chan, E. D., K. R. Morris, J. T. Belisle, P. Hill, L. K. Remigio, P. J. Brennan, and D. W. Riches.** 2001. Induction of Inducible Nitric Oxide Synthase-NO by Lipoarabinomannan of *Mycobacterium tuberculosis* Is Mediated by MEK1-ERK, MKK7-JNK, and NF- κ B Signaling Pathways. *Infect Immun* **69**:2001-2010.
10. **Connelly, L., M. Palacios-Callender, C. Ameixa, S. Moncada, and A. J. Hobbs.** 2001. Biphasic regulation of NF-kappa B activity underlies the pro- and anti-inflammatory actions of nitric oxide. *J Immunol* **166**:3873--3881.

11. **Cooper, A., D. Dalton, T. Stewart, J. Griffin, D. Russell, and I. Orme.** 1993. Disseminated tuberculosis in interferon gamma gene-disrupted mice. *J Exp Med* **178**:2243-2247.
12. **Decker, T., M. L. Lohmann-Matthes, and G. E. Gifford.** 1987. Cell-associated tumor necrosis factor (TNF) as a killing mechanism of activated cytotoxic macrophages. *J Immunol* **138**:957-962.
13. **Deretic, V., S. Singh, S. Master, J. Harris, E. Roberts, G. Kyei, A. Davis, S. de Haro, J. Naylor, H.-H. Lee, and I. Vergne.** 2006. Mycobacterium tuberculosis inhibition of phagolysosome biogenesis and autophagy as a host defence mechanism. *Cellular Microbiology* **8**:719-727.
14. **Dlaska, M., and G. Weiss.** 1999. Central role of transcription factor NF-IL6 for cytokine and iron-mediated regulation of murine inducible nitric oxide synthase expression. *J Immunol* **162**:6171--6177.
15. **Emile, J. F., N. Patey, F. Altare, S. Lamhamedi, E. Jouanguy, F. Boman, J. Quillard, M. Lecomte-Houcke, O. Verola, J. F. Mousnier, F. Dijoud, S. Blanche, A. Fischer, N. Brousse, and J. L. Casanova.** 1997. Correlation of granuloma structure with clinical outcome defines two types of idiopathic disseminated BCG infection. *Journal of Pathology* **181**: 25-30.
16. **Falddt, J., C. Dahlgren, and M. Ridell.** 2002. Difference in neutrophil cytokine production induced by pathogenic and non-pathogenic mycobacteria. *APMIS* **110**:593-600.
17. **Feng, C., A. Bean, H. Hooi, H. Briscoe, and W. Britton.** 1999. Increase in Gamma Interferon-Secreting CD8+, as Well as CD4+, T Cells in Lungs following Aerosol Infection with Mycobacterium tuberculosis. *Infect. Immun.* **67**:3242-3247.
18. **Flesch, I., and S. Kaufmann.** 1987. Mycobacterial growth inhibition by interferon-gamma-activated bone marrow macrophages and differential susceptibility among strains of *Mycobacterium tuberculosis*. *J Immunol* **138**:4408-4413.
19. **Flesch, I. E., and S. H. Kaufmann.** 1990. Activation of tuberculostatic macrophage functions by gamma interferon, interleukin-4, and tumor necrosis factor. *Infect Immun* **58**:2675-2677.
20. **Flynn, J. L., and J. Chan.** 2001. Immunology of tuberculosis. *Annu Rev Immunol* **19**:93--129.

21. **Ghosh, S., M. May, and Elizabeth.** 1998. NF- κ B AND REL PROTEINS: Evolutionarily Conserved Mediators of Immune Responses. *Annual Review of Immunology* **16**:225-260.
22. **Gordon, S.** 2003. Alternative activation of macrophages. *Nat Rev Immunol* **3**:23-35.
23. **Guyot-Revol, V., J. A. Innes, S. Hackforth, T. Hinks, and A. Lalvani.** 2006. Regulatory T cells are expanded in blood and disease sites in patients with tuberculosis. *Am J Respir Crit Care Med* **173**:803-810.
24. **Hentze, M. W., and L. C. Kuhn.** 1996. Molecular control of vertebrate iron metabolism: mRNA-based regulatory circuits operated by iron, nitric oxide, and oxidative stress. *Proc Natl Acad Sci U S A* **93**:8175--8182.
25. **Hlavacek, W. S., and M. A. Savageau.** 1995. Subunit structure of regulator proteins influences the design of gene circuitry: analysis of perfectly coupled and completely uncoupled circuits. *J Mol Biol* **248**:739--755.
26. **Howell, D.** 1987. *Statistical Methods for Psychology*. Duxbury Press, Boston.
27. **Huse, M., B. r. Lillemeier, M. Kuhns, D. Chen, and M. Davis.** 2006. T cells use two directionally distinct pathways for cytokine secretion. *Nature Immunology* **7**:247-255.
28. **Irvine, D.** 1991. The Method of Controlled Mathematical Comparison, p. 90-109. *In* E. Voit (ed.), *Canonical Nonlinear Modeling. S-System Approach to Understanding Complexity*. Van Nostrand Reinhold, New York.
29. **Itoh, H., M. Nishino, and H. Hatabu.** 2004. Architecture of the Lung: Morphology and Function. *J Thorac Imaging* **19**:221-227.
30. **Kasahara, K., I. Sato, K. Ogura, H. Takeuchi, K. Kobayashi, and M. Adachi.** 1998. Expression of chemokines and induction of rapid cell death in human blood neutrophils by Mycobacterium tuberculosis. *J Infect Dis* **178**:127-137.
31. **Kasahara, K., T. Tobe, M. Tomita, N. Mukaida, S. Shao-Bo, K. Matsushima, and K. Kobayashi.** 1994. Selective Expression of Monocyte Chemoattractant Protein 1 in Human Blood Monocytes by Mycobacterium Tuberculosis. *The Journal of Infectious Diseases* **170**: 1238-1247.
32. **Kim, S., and P. Ponka.** 2003. Role of nitric oxide in cellular iron metabolism. *Biometals* **16**:125--135.
33. **Kristensen, N. N., M. Gad, A. R. Thomsen, B. Lu, C. Gerard, and M. H. Claesson.** 2006. CXC chemokine receptor 3 expression increases the disease-

- inducing potential of CD4⁺ CD25⁻ T cells in adoptive transfer colitis. *Inflamm Bowel Dis* **12**:374-381.
34. **Ladel, C. H., G. Szalay, D. Riedel, and S. H. Kaufmann.** 1997. Interleukin-12 secretion by Mycobacterium tuberculosis-infected macrophages. *Infect Immun* **65**:1936-1938.
 35. **Laster, S. M., J. G. Wood, and L. R. Gooding.** 1988. Tumor necrosis factor can induce both apoptotic and necrotic forms of cell lysis. *J Immunol* **141**:2629-2634.
 36. **Law, K., M. Weiden, T. Harkin, K. Tchou-Wong, C. Chi, and W. N. Rom.** 1996. Increased release of interleukin-1 beta, interleukin-6, and tumor necrosis factor-alpha by bronchoalveolar cells lavaged from involved sites in pulmonary tuberculosis. *Am J Respir Crit Care Med* **153**:799-804.
 37. **Llovera, M., J. D. Pearson, C. Moreno, and V. Riveros-Moreno.** 2001. Impaired response to interferon-gamma in activated macrophages due to tyrosine nitration of STAT1 by endogenous nitric oxide. *Br J Pharmacol* **132**:419--426.
 38. **Lorsbach, R. B., W. J. Murphy, C. J. Lowenstein, S. H. Snyder, and S. W. Russell.** 1993. Expression of the nitric oxide synthase gene in mouse macrophages activated for tumor cell killing. Molecular basis for the synergy between interferon-gamma and lipopolysaccharide. *J Biol Chem* **268**:1908--1913.
 39. **Marino, S., I. Hogue, C. Ray, and D. Kirschner.** submitted 2007. A Methodology For Performing Global Uncertainty And Sensitivity Analysis In Systems Biology.
 40. **Mason, C. M., E. Porretta, P. Zhang, and S. Nelson.** 2007. CD4⁺CD25⁺transforming growth factor--producing T cells are present in the lung in murine tuberculosis and may regulate the host inflammatory response. *Clinical & Experimental Immunology* **148**:537-545.
 41. **McKay, M. D., W. J. Conover, and R. J. Beckman.** 1979. A comparison of three methods of selecting values of input variables in the analysis of output from a computer code. *Technometrics* **21**:239--245.
 42. **Mohan, K., Z. Ding, J. Hanly, and T. B. Issekutz.** 2002. IFN-gamma-inducible T cell alpha chemoattractant is a potent stimulator of normal human blood T lymphocyte transendothelial migration: differential regulation by IFN-gamma and TNF-alpha. *J Immunol* **168**:6420-6428.
 43. **Mulero, V., S. Searle, J. M. Blackwell, and J. H. Brock.** 2002. Solute carrier 11a1 (Slc11a1; formerly Nramp1) regulates metabolism and release of iron

acquired by phagocytic, but not transferrin-receptor-mediated, iron uptake. *Biochem J* **363**:89-94.

44. **Nathan, C., and M. U. Shiloh.** 2000. Reactive oxygen and nitrogen intermediates in the relationship between mammalian hosts and microbial pathogens. *Proc Natl Acad Sci U S A* **97**:8841--8848.
45. **Olakanmi, O., L. S. Schlesinger, A. Ahmed, and B. E. Britigan.** 2002. Intraphagosomal *Mycobacterium tuberculosis* acquires iron from both extracellular transferrin and intracellular iron pools. Impact of interferon-gamma and hemochromatosis. *J Biol Chem* **277**:49727--49734.
46. **Ordway, D., M. Henao-Tamayo, M. Harton, G. Palanisamy, J. Troudt, C. Shanley, R. Basaraba, and I. Orme.** 2007. The Hypervirulent Mycobacterium tuberculosis Strain HN878 Induces a Potent TH1 Response followed by Rapid Down-Regulation. *J Immunol* **179**:522-531.
47. **Peters, W., J. G. Cyster, M. Mack, D. SchlÄ¶ndorff, A. J. Wolf, J. D. Ernst, and I. F. Charo.** 2004. CCR2-dependent trafficking of F4/80dim macrophages and CD11cdim/intermediate dendritic cells is crucial for T cell recruitment to lungs infected with Mycobacterium tuberculosis. *J Immunol* **172**:7647-7653.
48. **Ridley, M., C. J. Heather, I. Brown, and D. A. Willoughby.** 1983. Experimental epithelioid cell granulomas tubercle formation and immunological competence: An ultrastructural analysis. *The Journal of Pathology* **141**:97-112.
49. **Riedel, D. D., and S. H. Kaufmann.** 1997. Chemokine secretion by human polymorphonuclear granulocytes after stimulation with Mycobacterium tuberculosis and lipoarabinomannan. *Infect Immun* **65**:4620-4623.
50. **Roberts, T., N. Beyers, A. Aguirre, and G. Walzl.** 2007. Immunosuppression during active tuberculosis is characterized by decreased interferon- gamma production and CD25 expression with elevated forkhead box P3, transforming growth factor- beta , and interleukin-4 mRNA levels. *J Infect Dis* **195**:870-878.
51. **Rook, G. A., J. Steele, M. Ainsworth, and B. R. Champion.** 1986. Activation of macrophages to inhibit proliferation of Mycobacterium tuberculosis: comparison of the effects of recombinant gamma-interferon on human monocytes and murine peritoneal macrophages. *Immunology* **59**:333-338.
52. **Rosenfeld, N., M. B. Elowitz, and U. Alon.** 2002. Negative autoregulation speeds the response times of transcription networks. *J Mol Biol* **323**:785-793.
53. **Sakaguchi, S., N. Sakaguchi, M. Asano, M. Itoh, and M. Toda.** 1995. Immunologic self-tolerance maintained by activated T cells expressing IL-2

- receptor alpha-chains (CD25). Breakdown of a single mechanism of self-tolerance causes various autoimmune diseases. *J Immunol* **155**:1151-1164.
54. **Savageau, M. A.** 2002. Alternative designs for a genetic switch: analysis of switching times using the piecewise power-law representation. *Math Biosci* **180**:237--253.
 55. **Savageau, M. A.** 1969. Biochemical systems analysis. I. Some mathematical properties of the rate law for the component enzymatic reactions. *J Theor Biol* **25**:365--369.
 56. **Schaible, U. E., and S. H. E. Kaufmann.** 2004. Iron and microbial infection. *Nature Reviews Microbiology* **2**:946--953.
 57. **Segovia-Juarez, J. L., S. Ganguli, and D. Kirschner.** 2004. Identifying control mechanisms of granuloma formation during *M. tuberculosis* infection using an agent-based model. *J Theor Biol* **231**:357-376.
 58. **Seiler, P., P. Aichele, S. Bandermann, A. E. Hauser, B. Lu, N. P. Gerard, C. Gerard, S. Ehlers, H. J. Mollenkopf, and S. H. Kaufmann.** 2003. Early granuloma formation after aerosol *Mycobacterium tuberculosis* infection is regulated by neutrophils via CXCR3-signaling chemokines. *Eur J Immunol* **33**:2676-2686.
 59. **Sen, R., and D. Baltimore.** 1986. Inducibility of [kappa] immunoglobulin enhancer-binding protein NF-[kappa]B by a posttranslational mechanism. *Cell* **47**:921-928.
 60. **Serbina, N., and J. Flynn.** 1999. Early Emergence of CD8+ T Cells Primed for Production of Type 1 Cytokines in the Lungs of *Mycobacterium tuberculosis*-Infected Mice. *Infect. Immun.* **67**:3980-3988.
 61. **Stein, J., and C. Nombela-Arrieta.** 2005. Chemokine control of lymphocyte trafficking: a general overview. *Immunology* **116**:1-12.
 62. **Theil, E. C.** 2003. Ferritin: at the crossroads of iron and oxygen metabolism. *J Nutr* **133**:1549S--1553S.
 63. **Thornton, A. M., and E. M. Shevach.** 1998. CD4+CD25+ immunoregulatory T cells suppress polyclonal T cell activation in vitro by inhibiting interleukin 2 production. *J Exp Med* **188**:287-296.
 64. **Valente, A. J., D. T. Graves, C. E. Vialle-Valentin, R. Delgado, and C. J. Schwartz.** 1988. Purification of a monocyte chemotactic factor secreted by nonhuman primate vascular cells in culture. *Biochemistry* **27**:4162-4168.

65. **van Buul, J., and P. Hordijk.** 2004. Signaling in Leukocyte Transendothelial Migration. *Arterioscler Thromb Vasc Biol* **24**:824-833.
66. **Voit, E.** 2000. *Computational Analysis of Biochemical Systems : A Practical Guide for Biochemists and Molecular Biologists.* Cambridge University Press.
67. **Wajant, H., K. Pfizenmaier, and P. Scheurich.** 2003. Tumor necrosis factor signaling. *Cell Death Differ* **10**:45-65.
68. **Wang, J., G. Chen, and K. Pantopoulos.** 2005. Nitric oxide inhibits the degradation of IRP2. *Mol Cell Biol* **25**:1347--1353.
69. **Yu, K., C. Mitchell, Y. Xing, R. S. Magliozzo, B. R. Bloom, and J. Chan.** 1999. Toxicity of nitrogen oxides and related oxidants on mycobacteria: *M. tuberculosis* is resistant to peroxynitrite anion. *Tuber Lung Dis* **79**:191--198.
70. **Yurchenko, E., M. Tritt, V. Hay, E. Shevach, Y. Belkaid, and C. Piccirillo.** 2006. CCR5-dependent homing of naturally occurring CD4+ regulatory T cells to sites of *Leishmania major* infection favors pathogen persistence. *J. Exp. Med.* **203**:2451-2460.
71. **Zhou, Z., M. C. Connell, and D. J. Macewan.** 2007. TNFR1-induced NF-kappaB, but not ERK, p38MAPK or JNK activation, mediates TNF-induced ICAM-1 and VCAM-1 expression on endothelial cells. *Cell Signal* **19**:1238-1248.

Chapter 2

Requirement for Multiple Activation Signals by Anti-Inflammatory Feedback in Macrophages

2.1 Introduction

One of the primary roles of macrophages in the immune response is killing of internalized pathogens. Macrophages attain strong activation states for killing based on external signals received but must balance capability of activation with the need to stay quiescent in the absence of decisive stimuli. A resulting question is how the macrophage biochemical network balances alternate demands of different activation states. Our focus is the macrophage killing mechanism where exogenous cytokine and pathogen-derived endotoxin signals induce a genetic program resulting in the production of nitric oxide (NO) and NO-derived reactive nitrogen intermediates (51, 69), (based primarily on the well-studied mouse macrophage model). These NO-related species have the ability to directly kill internalized pathogens (8) while also acting as intracellular signals (25) in feedback that regulates activation pathways (39, 42, 43) and iron homeostasis regulation (32). The link between NO and iron homeostasis can alter NO production (67) and the availability of iron as a nutrient for pathogens (e.g. 59). The resulting picture is of an interconnected network with systemic consequences of macrophage activation depending on the presence of activating signals and exogenous iron (Figure 2.1).

Due to the energetic demands of macrophage activation coupled with the toxic and perturbative nature of nitric oxide to surrounding tissues, macrophages must remain

quiescent in the absence of a decisive need for activation. When and only when the macrophage biochemical network receives a definite signal for activation, it must supply a sufficiently strong response: an integrated change in cellular state that induces conditions leading to growth inhibition and killing of internalized pathogens. This system has a modular organizational scheme; the integrated behavior of macrophages during activation is determined by factors within and between these modules. One possibility for controlling the trade-off between quiescence and activation is based on how the functional modules interact. To address the trade-off between quiescent and activated states we have developed a mathematical model of the biochemical network operating in macrophages that reflects this organizational scheme.

Analysis of this model allows us to assess the influence of every interaction under both quiescent and activated macrophage conditions. We apply two levels of analysis here. A global statistical analysis allows us to determine the relative importance of each model parameter on macrophage activation outcomes. Local analyses of specific interactions yield network motifs that best meet evolutionary criteria for effective macrophage function. Together these analyses have revealed what network motifs allow the conflicting demands of macrophage quiescence and activation to be met. We define three functional modules of the macrophage biochemical network assessed with this approach: *activation*, *killing* and *iron regulation* (Figure 2.1).

The *activation module* (AM) represents receipt of external stimuli that signal parallel second messengers: LPS-inducible NF- κ B and IFN- γ -inducible Stat1. These signals transcriptionally induce production of inducible nitric oxide synthase (iNOS) (1) in a synergistic manner (40). The *killing module* (KM) represents the iNOS

transcriptional program, a cascade resulting in production of NO, which serves as a signaling molecule whose products in turn regulate NF- κ B (10, 43) and Stat1 (39) in the AM. For simplicity we emphasize NO and its effects over other killing mechanisms such as superoxide (O_2^-).

NO levels regulate amounts of iron in the labile iron pool (LIP) (32), an intracellular quantity of elemental iron that is either free or loosely bound to miscellaneous weak chelators (53) and available for metabolic use by many processes (30). LIP regulation is the primary goal of the *iron regulation module* (IRM), comprising cellular mechanisms of iron internalization and sequestration. LIP levels are increased by intake from extracellular transferrin-bound sources, and decreased by sequestration into a complex with ferritin. The IRM is coregulated with the KM via NO regulation of iron response proteins (IRPs) 1 and 2 (23, 31, 65) with indirect transcriptional regulation of iNOS by the LIP (67). Thus levels of KM and IRM components are interdependent.

Our global and local analyses of the macrophage model suggest that anti-inflammatory (negative) feedback by NO from the KM to the AM allows maintenance of a system that is robust to perturbations and generally more functionally effective than the equivalent system with no or positive feedback. This negative feedback scheme allows macrophages to stay quiescent or relatively minimally activated in the absence of decisive immune activation or under a single activation signal. However, it also allows for strong activation, but only in the presence of both endotoxin and cytokine activation signals. Only under sufficiently strong, multiple-signal activation conditions is the interaction between iNOS transcriptional regulators synergistic, a requirement for strong activation in this model. This effect partially results from NO-induced crosstalk between

activation signals that suppresses one signal when the other is active. We also demonstrate that the co-regulation of NO and iron regulation in the presence of normal iron loads is asymmetric: elevated iron levels slightly suppress NO synthesis but cytokine and endotoxin signaling more dramatically upregulates the intake and sequestration of iron. Under partial activation conditions and high iron loads the influence of these two modules on each other reaches parity; the asymmetric relationship is mostly restored under complete activation.

2.2 Methods

We have developed a mathematical model describing macrophage biochemical processes based on three functional modules: *activation*, *killing* and *iron regulation*. The model is built on published experimental data primarily from mouse macrophage and human cell systems. We first describe the model and then discuss the methods for how the model is analyzed. The model equations and a discussion of parameter estimation are presented in the Appendix.

2.2.1 Mathematical model representation

We require a representation of the macrophage biochemical network that is dynamic, accurate over a wide range of molecular concentrations and allows analytical study. The local S-system representation of the power-law formalism (58) usually meets these requirements, sometimes requiring a piecewise representation for large deviations in concentrations (56). We choose this formalism over other model types due to the straightforward canonical representation of network motifs and previously developed

analytical methods allowing conclusions to be drawn about the evolution of intermodule interactions.

In an S-system setting, each molecular component in the macrophage is represented by one variable described by an ordinary differential equation (ODE). An n -variable S-system is of the form $dX_i/dt = V_i^+ - V_i^-$ where each $V_i^+ = \alpha_i \prod_{j=1}^n X_j^{g_{ij}}$ and $V_i^- = \beta_i \prod_{j=1}^n X_j^{h_{ij}}$ is an aggregate power law flux describing the production and consumption of molecule X_i . Parameters α_i and β_i are rate constants for production and consumption reactions, respectively. Parameters g_{ij} and h_{ij} are generalized kinetic orders that describe the influence of the variable X_j on the rate of X_i production or consumption (57). If a variable does not influence a given flux, the kinetic order is zero. If the influence is stimulatory, the kinetic order is positive; if it is inhibitory, the kinetic order is negative. The logarithmic gain $L(x, z) = (\partial \ln x / \partial \ln z)_0$ and sensitivity $S(x, p) = (\partial \ln x / \partial \ln p)_0 = (p/x_0)(\partial x / \partial p)_0$ are useful steady state measures of the model's response where x is any dependent variable or flux, z is an independent variable, p is a kinetic order or rate constant parameter and the subscript 0 indicates values determined at steady state. Despite the formally identical definitions of gains and sensitivities, we distinguish between them because logarithmic gains represent the system's response to external signals and precursors while sensitivity refers to the consequence of small perturbations in parameters.

Our macrophage model consists of a 9-variable S-system whose mathematical specification is derived from a schematic representation of the system topology (Figure 2.1). The complete set of equations is presented in the Appendix. We now highlight the

representation of some key interactions; for other interactions that are relatively straightforward, we leave the details to the Appendix.

2.2.2 Activation Module

We include only those variables necessary to reflect activation signaling in the context of the full model. We represent these pathways as concentrations of activated nuclear NF- κ B and Stat1. Due to the relative speed of their activation upon signaling (on the order of minutes (21, 52) in a model that operates on the order of hours), we assume an instantaneous effect of cytokines and LPS on NF- κ B and Stat1 nuclear translocation. This is an idealized model with mechanisms of feed-forward and feedback within the AM omitted. For NF- κ B, we define the terms representing activation and feedback as

$$V_1^+ = \alpha_1 X_{11}^{g_{111}} X_6^{g_{16}} \text{ and for Stat1, } V_2^+ = \alpha_2 X_{12}^{g_{212}} X_6^{g_{26}} \text{ where } \alpha_1 \text{ and } \alpha_2 \text{ are rate constants,}$$

X_{11} and X_{12} are independent variables representing respective level of pathway activation from exogenous LPS and IFN- γ , and X_6 is the dependent variable [NO]. The kinetic orders g_{111} and g_{212} (both positive) scale the level of activation from respective LPS or IFN- γ signal while g_{16} and g_{26} scale NO feedback respectively (see Table 2.1 for specific definitions of parameters in the model). Both feedback interactions are predominantly considered negative (39, 42, 43), but not in every case for the feedback to NF- κ B, where low [NO] may have a stimulatory effect (10). Loss of NF- κ B (52) and Stat1 (20) activity from the nucleus due to inactivation and export are constitutive processes dependent on [NF- κ B] and [Stat1], respectively. The NF- κ B and Stat1 pathways represent parallel signals with a symmetric relationship in the model structure

(Figure 2.1, Activation Module). This symmetry is quantitatively divided by parameter values specific to the signaling cascade.

A partial activation state is defined by receiving only one of the two activation signals. Under the partial activation state induced by treatment with LPS alone, the resultant slightly elevated [NO] may have a negative feedback effect that suppresses Stat1 activation (V_2^+) below the quiescent steady state as long as $g_{26} < 0$. Whether or not this is plausible, or if the quiescent level of Stat1 activity cannot be further suppressed is unknown. Similarly, under activation by IFN- γ alone elevated [NO] may have a feedback effect suppressing NF- κ B activation (V_1^+) below the quiescent steady state if $g_{16} < 0$ in the model. We use a piecewise power law representation (56) to prevent this suppression in a few instances to determine the effect of these assumptions (outlined in the Appendix).

2.2.3 Killing Module

We represent iNOS transcriptional regulation with an mRNA production rate law:

$$V_3^+ = \alpha_3 X_1^{g_{31}} X_2^{g_{32}} X_7^{g_{37}}. \text{ NF-}\kappa\text{B and Stat1 regulate transcriptional initiation (12, 13)}$$

according to the kinetic orders g_{31} and g_{32} , respectively. We assume the mechanism of synergism between the activation signals here to be at the transcriptional level (37) but it may exist earlier in the signaling cascade; see e.g. (28). The LIP (X_7) regulates transcription indirectly via C/EBP- β (NF-IL6), a transcription factor required for initiation (11, 17, 23). Substituting LIP concentration into the flux term eliminates the need for representing C/EBP- β in the model. Parameter g_{37} scales the quantitative

influence of the LIP on the rate of iNOS transcription initiation. We omit post-translational modification of iNOS and assume that concentrations of L-Arginine, NADPH + H⁺, and O₂ precursors to NO in iNOS catalysis are not rate-limiting (49). At the scale of interest here, iNOS catalyzes NO + Citrulline production via the intermediate N^ω-hydroxyarginine (NHA) (16). The resulting simplified pathway tracks production of NHA and NO catalyzed by iNOS (Figure 2.1, KM).

2.2.4 Iron Regulation Module

The IRM tracks iron response protein (IRP) regulation with a resultant influence on LIP and apoferritin levels (Figure 2.1, IRM). The link between the KM and the IRM occurs through IRP regulation by NO with a resulting feedback on iNOS transcription (above). We base the network topology on the interaction between IRP2 and the cationic nitrosonium ion NO⁺ (a product that forms as a result of nitric oxide production), which presents an interaction with sufficient data for estimation of some parameters (β_9 and g_{89} from (31)). This gives the NO control point of the IRM as the rate of IRP degradation $V_9^- = \beta_9 X_6^{h_{96}} X_7^{h_{97}} X_9^{h_{99}}$. The majority of IRP in the cell is IRP1, which has qualitatively identical iron regulatory properties as IRP2 but possibly an opposite response to NO (Wang (65) and references therein). To implement the assumption that either IRP1 or IRP2 is the predominant mechanism we set $h_{96} < 0$ (IRP1 or possibly IRP2) or $h_{96} > 0$ (IRP2). We assume IRP-regulated transcript stabilization of the transferrin receptor (reviewed in Thomson et al. (63)) is directly controlled by IRPs. This is included in the iron influx term V_7^+ . Lastly, IRPs translationally control apoferritin production (63). Apoferritin subunits form a shell structure that holds the sequestered iron atoms within.

The ratio of iron atoms to ferritin protein complexes is about 4000:1 in the iron-rich ferritin complex (see Theil (61) for a short review). Iron accumulates in the ferritin complex relatively slowly, continuing for up to 24 hours after initial iron loading (24). Based on the rate of this process, we assume that the variable X_8 represents the molarity of binding capacity held by ferritin rather than the raw number of molecules. The iron-rich ferritin complex is stored by macrophages for use by other cells, maturing into hemosiderin under conditions of iron overload (19). The primary source of LIP is presumably transferrin-bound extracellular iron. Low extracellular iron results in degradation of the ferritin complex to replenish the LIP in red blood cells (34). Since we do not simulate low iron conditions, and since the iron-rich ferritin complex is stored for long periods by macrophages, the fate of this complex is beyond the scope of the model.

2.2.5 Parameter estimates

Our goal is to derive order-of-magnitude estimates for model parameters resulting in behavior that reflects the known data for the physical macrophage system. Uncertainty and sensitivity analyses can then be used to explore the parameter space and determine variations in system outcome. The macrophage model contains 44 parameters whose values require estimation before numerical model simulations can be performed. Complete details of this process are given in the Appendix and summarized in Table 2.1. Here we outline some key steps.

First, we reduce the number of estimates needed using non-dimensionalization. The non-dimensionalized model is used for numerical simulations, but we use the dimensionalized model for calculation of stability and robustness, which do not require

numerical simulations (see Local Analysis, below). Non-dimensionalization of the model gives a normalized form with concentrations relative to the quiescent steady state; the effect of kinetic orders across the two model forms is the same.

Substituting levels of each variable X_i relative to quiescent steady state \hat{X}_i gives the nondimensional value $x_i = X_i/\hat{X}_i$ (we use the \hat{y} notation to distinguish the particular quiescent steady state of y from the generic steady state denoted by y_0). In this type of model, a unique steady state always exists as long as the determinant of the matrix \mathbf{A} of kinetic order differences is non-zero (i.e. $\det \mathbf{A} = \det [g_{ij} - h_{ij}] \neq 0$; see (64) p. 200-201).

At the steady state, $\alpha_i \prod_{j=1}^{n+m} X_{j0}^{g_{ij} - \delta_{ij}} = \beta_i \prod_{j=1}^{n+m} X_{j0}^{h_{ij} - \delta_{ij}} = a_i$ where $\delta_{ij} = \begin{cases} 1, & i = j \\ 0, & i \neq j \end{cases}$ and m is

the number of independent variables (six here). Then $\hat{x}_i = 1$ for $i = 1, \dots, 9$ represents the quiescent steady state in the nondimensionalized model. Table 2.1 gives estimated values for turnover rates and kinetic orders for most of the parameters. Several kinetic order parameters are omitted from Table 2.1 as they are set to the value 1 (see Appendix for details).

2.2.6 Software and simulations

We used two platforms to perform simulations to ensure that convergence to the same solutions occurs in different settings. Mathematica (Wolfram Research) was used for most calculations. The results were confirmed with a second program written by our group in C++ incorporating standard ODE solvers. An algorithm for uncertainty and sensitivity analysis was implemented in both and the results compared for accuracy. Steady state analysis, including dose-response and calculation of logarithmic gains and

sensitivities were done using Mathematica's algebraic Solve function.

2.2.7 Global statistical analysis

Estimating parameters for any mathematical model is complicated by lack of or variability in experimental data. This leads to uncertainty in the quantities used for parameters. We have implemented statistical uncertainty and sensitivity analyses (22) that allow simultaneous exploration of the entire biologically plausible parameter space.

We used a type of stratified Monte Carlo sampling known as Latin Hypercube Sampling (LHS) to partition wide parameter ranges into a number, N , of equiprobable subintervals for high efficiency sampling (3, 45). This method prescribes sampling once per subinterval. Therefore, the greater the partition number N , the more accurate the estimates of sensitivity will be. We chose a partition number of $N = 1000$ and randomly combined the sampled numerical values, one value per parameter. In the absence of further data on their actual distributions, each parameter interval was sampled assuming a uniform distribution for the ranges specified in Table 2.1. The intervals chosen for the kinetic order parameters represent a sampling of the parameter within a region corresponding to one type of regulation; i.e. always positive or negative. Distinguishing between the qualitative differences in regulatory motifs (positive, negative or no regulation) is left to the local analysis discussed below. Note that the intervals for two parameters (g_{89} and h_{97}) were slightly reduced to avoid numerical stiffness resulting from x_8 ($[\text{apoferritin}]/[\text{apoferritin}]_0$) becoming too small during simulation.

We perform simulations of the system for a 100-hour time frame after simulating a constant stimulus of LPS, IFN- γ , and/or exogenous iron starting from quiescent steady

state conditions. This analysis uses the non-dimensionalized model for numerical simulations. Due to the non-dimensionalization, the quiescent steady state concentration of each molecule in the model is 1. Statistical measures describe the output with a lognormal distribution when the system is near steady state. Here, the output is the distribution of values for the dependent variable x_6 representing $[\text{NO}]/[\text{NO}]_0$. Our goal in choosing the treatment levels (which are arbitrary) is to induce distinct *activation states* above this steady state given by particular levels of exogenous LPS, IFN- γ and iron (x_{11} , x_{12} and x_{17} , respectively).

Activation of the AM from LPS or IFN- γ is set to 100-fold induction of NF- κ B or Stat1, respectively. This quantity is chosen to represent a level of activation that is definite and distinguishable from an insignificant stimulus but well below high activation levels that cause signal saturation. Therefore, $x_{11} = 100$ and $x_{12} = 100$ under conditions of complete activation. Under partial activation conditions, either NF- κ B or Stat1 is subject to 100-fold activation, but not both. The quiescent level of activation is given by $x_{11} = 1$, $x_{12} = 1$.

Under iron-rich conditions, the intake of exogenous iron into the LIP is increased 10-fold (over low iron conditions of $x_{17} = 1$); that is, $x_{17} = 10$. This simulates conditions of high iron levels and their effects on overall macrophage activation. There is a constant background level of the LIP that is measurable under homeostatic conditions (see for example Petrat et al (53)). Therefore, in contrast to the second messengers in the model, a relatively small fold-change in iron intake will simulate iron-rich conditions.

When performing the LHS analysis described above, we are able to measure

uncertainty in the outcome variable ($x_6 : [\text{NO}]/[\text{NO}]_0$) due to changes in the parameter values. What remains to do is to correlate the observed variations to specific parameters. This can be accomplished using a partial rank correlation (PRC; see (3)) as a *statistical sensitivity*. The resulting correlation coefficients, γ_{iy} , have a magnitude between 0 and 1, and a sign (+/-) describing the relationship of the i th input parameter to the y th variable. The PRC may be calculated at any time point during the simulation; many of the correlations are dynamic. A significance test has been determined for γ_{iy} (versus $\gamma_{iy} = 0$) that approximates a Student's T (3). The PRC is valid when considering solutions with a monotonic relationship with respect to the input parameter (22) as is the case here. We have also implemented a Z test for comparisons of PRC coefficients against one another to determine the relative statistical sensitivity of variables to different parameters in a particular activation state (27 p. 240-241). We refer to the magnitude of the PRC without regard to sign as the *absolute* PRC.

2.2.8 Local detailed analysis

To evaluate the role of specific parameters within the macrophage biochemical model, we apply a local detailed analysis. We view the macrophage as a modular system where signals from a given module co-regulate other modules resulting in a new cellular state. Thus, parameters governing the interaction of the three functional modules are of particular interest toward understanding the trade-off between macrophage quiescence and activation.

In this setting we apply mathematically controlled comparisons (MCCs) that allow evaluation of the intermodule parameters and their influence on model outcomes

according to a set of *Criteria for Functional Effectiveness* (CFE) (29). This method is analogous to a gene knockout experiment where part or all of a specific pathway is deleted from a system. In our case, a component of the pathway (e.g. gene product) is not deleted but one effect of the component on another member of the pathway is neutralized, increased, decreased or reversed. We refer to the interaction under study this way as a “knockout” parameter. The knockout system is compared to the wild-type (control using the default parameter values in Table 2.1, column 3) based on their conformity to the CFE. The CFE used to assess changes in functional effectiveness as a parameter varies are three well-defined criteria that have been applied to study other inducible systems (26). The first, *stability*, is the ability of the system to return to steady state after a transient perturbation as evaluated by the last Routh-Hurwitz criterion (outlined in (64) pp. 208–213; for this model given in Table 2.3). Second, *robustness*, is insensitivity of dependent variables and fluxes to perturbation by independent variables and parameters; this is measured by steady state logarithmic gains and sensitivities. Lastly, *responsiveness* is the minimal time for $[\text{NO}]/[\text{NO}]_0$ (x_6) to reach a new steady state from the quiescent steady state after a stimulus. Induction of NO under a decisive signal is also a requirement for a functionally effective system, but this will be indirectly required for all parameter values tested to meet an equivalence requirement as part of the MCC (below) and thus need not be an explicit criterion. Each of the six knockout parameters that we explored in local analysis are listed in Table 2.2 columns 1–2.

Mathematically, stability and robustness can be determined from the system at steady state making no specific choices for parameter values (using the dimensionalized model). This lends generality to the results. For the stability and robustness criteria, we

were able to perform the analysis in the most general setting, making no assumptions on the numerical values for the parameters. The results are often shown with default parameter values (Table 2.1) substituted for simplicity of presentation. Unlike stability and robustness, the responsiveness criterion requires numerical simulations with specific values for each parameter using the non-dimensional model.

As part of the MCC, we force the value of a knockout parameter to change. To control for changes as this parameter is varied, we require the model to maintain equivalence with the wild-type (default parameter value) case over the parameter range in two ways: internally and externally (57). *Internal equivalence* requires that the parameters not associated with the flux containing the knockout parameter under study remain the same. *External equivalence* requires the external behavior of the model to remain the same as the parameter under study is varied; this then requires correction of other parameter values in the same flux as the knockout parameter. In each case we use iNOS induction to measure external behavior. iNOS levels are a direct readout of gene expression, reflecting equivalence in the macrophage gene expression program across values of the knockout parameter. (We could as easily use NO as the external measure of behavior, with the process almost identical and the conclusions unchanged.) At wild-type iNOS levels for a given activation stimulus, we must adjust the other parameters in the flux containing the knockout parameter under study. Two requirements for iNOS levels must be met: as the knockout parameter is varied, the model must have an identical quiescent steady state (\hat{X}_4) and identical total logarithmic gain ($L_s = L(X_4, X_{11}) + L(X_4, X_{12}) + L(X_4, X_{17})$) with respect to exogenous signals that influence the macrophage activation state (LPS, IFN- γ , and extracellular iron levels).

Table 2.2, column 3, shows which parameters require adjustment to meet the external equivalence requirement. The number of parameters requiring correction in the flux determine the degrees of freedom for the interaction of interest. The corrected parameters are both kinetic orders and rate constants. In the nondimensionalized system (used for numerical simulations) finding the equivalence for rate constants is unnecessary because the normalized quiescent steady state is the same for any chosen value of the parameter of interest. Thus we only correct the kinetic orders in this case, and find a *line of equivalent gain* (LEG) over the range of the parameter under study that gives the parameter corrections for external equivalence. Note that the computation of stability is also independent of rate constants (Table 2.3, Stability Criterion) leaving only the robustness criterion requiring correction of rate constants during the comparison.

In the examination of the robustness criterion for various g_{31} , g_{32} and g_{37} , we also require correction of g_{313} by holding $L(X_4, X_{13})$ constant, allowing the unbiased determination of systemic sensitivities. This correction is not required for the other criteria: stability is independent of g_{313} and the non-dimensional model is identical for changes in this parameter because levels of precursors are assumed not to be perturbed during the calculation of responsiveness.

As an example of the MCC method, we outline the procedure for g_{16} , which represents the feedback of nitric oxide (X_6) in the KM to the activating second messenger NF- κ B (X_1) in the AM (Figure 2.1). We require

$L_s = L(X_4, X_{11}) + L(X_4, X_{12}) + L(X_4, X_{17})$ for every g_{16} quantity investigated. From this relationship we find the correction factor for parameters in the same flux term as the

knockout parameter examined, in this case g_{111} . This corrects g_{111} so that:

$$g_{111} = \frac{-p_2(p_7h_{97} - p_8) + L_s(p_6p_7 - (p_3 + p_4 - p_5)(p_7h_{97} - p_8))}{g_{31}g_{43}h_{22}h_{66}(p_7h_{97} - p_8)}$$

(Table 2.3). This is the LEG for the NO feedback parameter g_{16} , ensuring external equivalence in the model for the MCC.

Clearly, alteration of L_s can change the slope of the LEG, and possibly change results for very large changes in L_s . Here we restrict L_s to approximate what is experimentally found in mouse macrophage cell culture (see Parameter Estimation above). In principle, representation of this network in other cell types or species with much lower or higher L_s may require adjustment of the slope of the LEG.

We visualize three possible regions in a parameter space with the knockout parameter of interest on the x -axis and the parameter corrected to ensure external equivalence on the y -axis (for example, Figure 2.6A for g_{16}). Each point on the LEG represents one set of parameters for model evaluation according to the CFE. Notice that g_{16} has one degree of freedom, giving a 2-dimensional parameter space. The distance d on the LEG represents the distance between a stable parameter value choice and the line generated from the stability criterion, allowing the determination of stability by d . Robustness and responsiveness of the system represented by a given point on the LEG are determined with the calculations or simulations specified by the definition of the CFE above.

We have found the LEG for parameter g_{16} as an example of applying MCC to one of the six interactions between the functional modules. Certain considerations are necessary to generalize the process to the other five knockout parameters (Table 2.2).

Applying MCC for the KM feedback to Stat1 (g_{26}) follows directly from the above process. However, an additional degree of freedom is found for the other MCCs due to the higher number of components regulating the processes. For instance, parameters g_{31} , g_{32} and g_{37} each require correction of either of the other two parameters for equivalence (Table 2.2), leading to a plane of equivalent iNOS logarithmic gain in 3-dimensional parameter space. For simplicity we choose to reduce the degrees of freedom in these cases by holding one parameter constant and meeting the equivalent gain requirement by correcting the other (Table 2.2). The parameter held constant is given the default wild-type value in Table 2.1. In this way all of the MCCs are performed in the constrained parameter space given in Table 2.2.

For each of the six parameters we evaluated using the CFE (Table 2.2), we assign a *score* for each criterion of + (stimulation of a process), - (inhibition of a process) or 0 (no regulation of a given process). Then the overall score is calculated based on the individual score for each criterion. The overall score represents the type of regulation that is assigned as *optimally functionally effective* for a given interaction. Recall each knockout parameter represents the regulation of a rate of production or consumption of a molecular component of the model. Thus the overall CFE score for a parameter predicts the type of regulation that optimizes the overall macrophage performance.

2.3 Results

Macrophages require maintenance of a quiescent state to conserve energy and minimize host damage while oppositely needing to be sufficiently activated under appropriate conditions to best control or kill pathogens. Our aim is to understand and predict necessary requirements for the trade-off between these macrophage states. To this end, we have developed a mathematical model representing the biochemical network operating within macrophages that is based on a framework of functional modules. Here we present results from our analyses of the model in three parts: validation simulations, global uncertainty and statistical sensitivity analysis, and a local analysis of functional effectiveness based on three specified criteria.

2.3.1 Conditional synergistic activation by two signals

To validate the model system, we compared the model's predicted steady state dose-response [NO] with simulated LPS and IFN- γ doses to data from macrophage cell culture (Figure 2.2). With only quiescent levels of LPS-induced NF- κ B stimulation even a significant increase in IFN- γ -induced Stat1 levels leads to very low NO induction above $[\text{NO}]_0$. Results with increasing amounts of LPS and IFN- γ stimulation show a capacity for synergistic induction of iNOS and resultant NO production (Figure 2.2A). This has been previously observed in experiments using sub-saturation levels of LPS and IFN- γ measuring nitrite output of J774.1 macrophage cell cultures (Figure 2.2B). In the model, the mechanism behind this phenomenon arises from the flux term V_3^+ (iNOS transcriptional regulation) from the interactions of NF- κ B and Stat1.

The model predicts a dual role for transcriptional activation parameters,

exhibiting either a synergistic or non-synergistic influence on transcriptional activation (Figure 2.3, $g_{16}, g_{26} < 0$). Under dosing of only one activator (for example, LPS) low-dose levels of IFN- γ (less than \ddagger in Figure 2.3B) do not allow a synergistic influence of NF- κ B and Stat1 interactions on transcription, while higher levels of IFN- γ alter the sensitivity of NO to transcriptional activation such that the interaction of NF- κ B and Stat1 is synergistic. The model mechanism causing this phenomenon is negative feedback on Stat1 by NO, induced from the LPS/NF- κ B-activation pathway. This feedback induces the IFN- γ /Stat1 pathway to be at or below its quiescent steady state level.

This crosstalk is confirmed by comparing the sensitivity $S(x_6, g_{32})$ when varying the feedback parameter g_{26} (Figure 2.3A). The non-synergistic activation state is abolished in the absence of this feedback ($g_{26} = 0$) or when it is positive ($g_{26} > 0$). We thus find that negative feedback crosstalk (that is, feedback on Stat1 under primarily LPS signaling or feedback on NF- κ B under primarily IFN- γ signaling) contributes to maintenance of a quiescent macrophage state in the absence of multiple decisive activation signals. The possibility of low [NO] having a positive feedback effect for NF- κ B (10) brings this effect into question under conditions of partial activation with high IFN- γ signaling but low LPS signal (Figure 2.3A). If the level of NO induced by IFN- γ alone is high enough to surpass this proposed low-level positive feedback threshold then the effect can occur (and indeed is predicted by the model). Note that for optimal maintenance of quiescence we predict negative feedback ($g_{16} < 0$) for this low-level activation (discussed below).

2.3.2 Global analysis: statistical sensitivities of parameters under different activation stimuli and exogenous iron treatments

To determine global statistical sensitivity of chosen model outputs with respect to changes in parameter values from Table 2.1, we applied uncertainty and statistical sensitivity analyses using LHS and PRC, respectively, with a sampling partition of $N = 1000$ as described in Methods. With the non-dimensionalized model form used for this part of the analysis, references to concentrations of components (e.g. [NO]) refer to the normalized concentration. This analysis was performed under six different activation signaling states: LPS alone, IFN- γ alone, LPS + IFN- γ and each of the above together with exogenous iron. We find PRCs for [NO] (x_6) at a time point of $t = 100$ hrs after initial stimulation, which is at (or near) the steady state for the 1000 simulations. The results are summarized in Figures 2.4–2.5. In Figure 2.4, Panel A indicates sensitivities of [NO] to parameters on the interface of the AM and KM, while Panel B indicates sensitivities of LIP level to these parameters. In Figure 2.5, Panel A indicates PRC coefficients in the absence of exogenous iron and Panel B indicates PRC coefficients in the presence of exogenous iron for parameters in the IRM, including those on the interface of the KM and IRM.

Because we performed the analysis with [NO] near steady state, we find that turnover rates (a_i) do not have a significant influence on outcome variable (NO / x_6 or LIP / x_7) levels. Carrying out a statistical sensitivity analysis under pre-steady state conditions revealed that some turnover rates have significant but minor PRCs:

$\gamma_{a_i, x_i} < \pm 0.25$. This is almost always the case for iNOS mRNA and protein turnover rates

a_3 and a_4 and in some cases NO and LIP turnover rates a_6 and a_7 as well. As

component levels change over time after stimulation, the kinetic order PRCs (γ_{g_{ij}, x_i} and γ_{h_{ij}, x_i}) change in a predictable manner: those related to the AM and KM generally follow [NO] while those related to the IRM generally follow [LIP]. These transient PRCs are in line with intuition, but in this work we emphasize steady state correlations due to our focus on distinct activation states.

Under the various stimuli, one obvious result is that kinetic order parameters have a much stronger PRC with [NO] when their corresponding pathway is activated than when it is not activated. For example, g_{111} , the kinetic order characterizing the change of NF- κ B activation levels with LPS treatment (Figure 2.4) has a high PRC under stimuli that include LPS but not during treatment with IFN- γ alone, with or without exogenous iron. As we would expect, most parameters involved in either the AM or KM (Figure 2.4) have stronger absolute PRCs with [NO] than those of the IRM (Figure 2.5).

2.3.3 Interactions between the Activation and Killing Modules

The interaction between the AM and KM is determined by parameters representing transcriptional activation (g_{31}, g_{32}) and feedback by NO (g_{16}, g_{26}). We find the PRCs to be primarily dependent on the activation state with regard to LPS and IFN- γ but only slightly on the level of exogenous iron (Figure 2.4). For each activation state we assume that NF- κ B and Stat1 can be regulated both up and slightly down. If we assume that the AM cannot be downregulated below the quiescent state (see the piecewise model variant in Methods and Appendix) we find some PRCs that are non-significant (Figure 2.4 †).

Under both model variants NO crosstalk contributes to maintenance of quiescence. Under signaling conditions biased strongly to one signal or the other (i.e. LPS or IFN- γ alone) we find the PRCs for the two transcriptional activation parameters (g_{31} and g_{32}) to have opposite signs (+ in one, – in the other) while the statistical sensitivity of [NO] to KM feedback to the AM is negative. Recall that $g_{16}, g_{26} < 0$ here; thus, a positive PRC means a negative correlation between strength of feedback and [NO] (Figure 2.4). This effect is abolished under full activation: both transcriptional activation parameters have positive correlations with [NO], resulting in the synergistic interaction of the two signals in iNOS/NO production (as in Figure 2.3). As the loss of statistical sensitivity of [NO] to some parameters in the piecewise model variant shows (Figure 2.4, Panel A †), the crosstalk effect raises the threshold for decisive positive iNOS/NO regulation without the small antagonistic effect seen in the model variant that allows AM suppression. In either case, the PRCs of the transcriptional activation parameters shows cooperativity in the two signaling pathways only under full activation signaling.

The statistical sensitivity profile of [LIP] is almost the same as for [NO] for the AM/KM interface parameters due to increased iron uptake under cytokine and endotoxin-induced activation conditions, with significant differences only in g_{111} and g_{31} (Figure 2.4; compare PRCs marked * for [NO] (Panel A) with the PRC for the same parameter and activation state for [LIP] in Panel B). Under exogenous iron treatment there are more parameters with significant differences between the sensitivities of [NO] and [LIP] to them (Figure 2.4, compare both * and ** in Panel A to the PRC with the same parameter and activation state in Panel B). Furthermore, under exogenous iron treatment the PRC of [LIP] with some interactions is significantly lowered compared to no iron treatment

(Figure 2.4 Panel B, ‡).

2.3.4 Interactions between the Killing and Iron Regulation Modules

We find the statistical sensitivity of [NO] (x_6) to variations in the parameters in the IRM including those between the KM and IRM to be lower than those parameters between the AM and KM (compare Figure 2.5 top panels to Figure 2.4 Panel A). However, exogenous iron treatment induces a significant change in the PRCs of [NO] for most IRM parameters (Figure 2.5 Panel B, top; significance test not shown). The exception is h_{96} , NO-induced regulation of the IRM, in the fully activated state.

Statistical sensitivity of [LIP] (x_7) to IRM parameters is predictably much higher, and generally opposite to [NO] sensitivities (Figure 2.5, top * versus bottom). Recall that [LIP] sensitivities to AM/KM parameters mirrored those of [NO]. The best explanation for the reversal in PRCs to IRM parameters between [NO] and [LIP] is that, while an increase in NO production tends to increase iron intake into the LIP, an increase in exogenous iron and resultant [LIP] increase tends to inhibit iNOS transcription and result in a lowering of [NO].

We are therefore interested in which module dominates the immune response under high iron conditions, as [NO] is sensitive to the IRM parameters, and [LIP] is less sensitive to AM/KM parameters under treatment with exogenous iron. By comparing the statistical sensitivity of [NO] to g_{37} (the parameter representing the regulation of iNOS transcription by the LIP), γ_{g_{37},x_6} , to the statistical sensitivity of [LIP] to h_{96} (the parameter representing the regulation of the IRM by NO), γ_{h_{96},x_7} , we can determine

which module is dominant under different conditions. For cases without exogenous iron (Figure 2.5 Panel A, †) the statistical sensitivity of [LIP] to h_{96} (bottom) is significantly higher than the statistical sensitivity of [NO] to g_{37} (top) in every activation state. This changes during elevated exogenous iron conditions (Figure 2.5 Panel B, † and ‡), when the absolute PRC of [LIP] with h_{96} is either not significantly different, or slightly significantly smaller than the absolute PRC of [NO] to g_{37} in partial activation states. However, under complete activation, we find the absolute PRC of [LIP] with h_{96} to be elevated, restoring the relationship seen under no iron treatment above.

We conclude that with complete activation, the synergistic interaction of LPS and IFN- γ activation pathways overcome the KM inhibition by the IRM even in conditions of elevated iron, leaving only incremental differences in parameter statistical sensitivity. However, under partial activation conditions, the statistical sensitivity of the KM to the IRM is approximately in parity with that of the IRM to the KM.

2.3.5 Local analysis: evolutionary requirements for inter-module interactions

Each interaction coupling the functional modules may be stimulatory or inhibitory. The types of interactions present determine the functional effectiveness of the macrophage and ensure that the parameter values giving the trade-off between quiescence and strong activation in this model are biologically plausible. For each interaction between the functional modules (Table 2.2) we have evaluated the model according to three CFE (see Methods), scoring each parameter as stimulatory (+), inhibitory (-) or zero (0) according to the type of interaction that meets the requirements of each criterion

(Table 2.4). We illustrate the evaluation of two parameters, NF- κ B transcription (g_{31}) and NO feedback to NF- κ B (g_{16}) (Figures 2.6–2.8), according to the CFE.

As discussed in Methods, several interactions in the model are idealized and may be stimulatory or inhibitory depending on the predominant mechanism assumed in the model. We consider this plausible for the interactions of nitric oxide with other system components (g_{16} , g_{26} and h_{96}). The transcriptional regulation parameters (g_{31} , g_{32} and g_{37}) have known or postulated mechanisms of either stimulation or inhibition, though they may differ based on cell type (12). Regardless, we examine these three parameters assuming any type of interaction is possible. This allows us to see (i) confirmation that this model predicts the correct interaction type, (ii) how the evolution of positive transcriptional regulation may be favored even in a system with many possible negative side effects (i.e. nitric oxide production), and (iii) how the coupling of iron regulation to NO production affects macrophage activation and iron regulation.

For each criterion, we consider the parameter under investigation to be wild-type if it is at its baseline estimated value (Table 2.1). We vary the parameter along the line of equivalent gain (LEG; Table 2.3) and determine which parameter value score, +, –, or 0, best fits the criterion.

2.3.6 Stability: return to steady state after a small transient perturbation

The first criterion we explore is stability, or the ability of a system to return to steady state after a transient perturbation. The local stability analysis of this system is a function of several parameters defined by the appropriate Routh-Hurwitz criterion (see Methods). The stability criterion is represented graphically as dashed lines in Figure 2.6.

Notice that as different parameter values from equivalent systems are chosen along the lines of equivalent gain, the margin of stability, defined as d , correspondingly changes. This distance is independent of the macrophage activation state. The score for this criterion for each parameter is given by the type of interaction giving the largest d . Thus, for the parameter g_{31} (Figure 2.6A) we have $d(-) < d(0) < d(+)$, giving a score of + for g_{31} in terms of stability. Similarly, for the parameter g_{16} (Figure 2.6B) d is maximized for $g_{16} < 0$, giving a score of - (see Table 2.4, Stability column for the scores of all the tested parameters).

2.3.7 Robustness: minimal sensitivity of component levels to perturbation

The most functionally effective macrophage is insensitive to small perturbations, or robust. That is, in the absence of decisive activation signals, the macrophage must stay as close to quiescence as possible. We tested system robustness for each parameter of interest by computing the steady state logarithmic gains $L(x_i, x_j)$ and $L(v_i, x_j)$ of the dependent variables x and fluxes v for each independent variable, and the sensitivities $S(x_i, p)$ and $S(v_i, p)$ for each kinetic order p (Figure 2.7; see Figure 2.1 for the role of each precursor/independent variable in the model). In some situations a gain may preferentially be large, such as the gain of [NO] in the presence of cytokine. However, each gain calculated here is from a single signal at a time, not the multiple-signal situation required for complete activation as in Figure 2.2. We therefore assume that gains to individual signals are preferentially low.

For transcriptional regulation parameters g_{31} , g_{32} and g_{37} , a clear plurality or

majority of the gains and sensitivities do not support a single score (Figure 2.7A shows the profile for g_{31}). For transcriptional activation by second messengers (g_{31} and g_{32}) we find 32.12% support +, 32.82% support 0 and 35.05% support –. Here perturbation of AM and KM parameters predominantly supports + and perturbation of IRM parameters supports –. For iron regulation of transcription (g_{37}) we find 21.27% support +, 37.37% support 0 and 41.36% support –. In this case perturbation of AM and KM parameters predominantly supports – while perturbation of IRM parameters predominantly supports 0. We do not consider one score to be definitively supported by the robustness criterion in these cases, and rely on the other criteria for the overall score (Table 2.4).

The interactions of NO with other model components (represented by parameters g_{16} , g_{26} and h_{96}) show clear pluralities or majorities of one score over the others. In each of the cases a negative value is most robust (48.79% of the gains and sensitivities for g_{16} and g_{26} and 52.47% for h_{96}). The remaining gains and sensitivities are split between a score of 0 (31.88% for g_{16} and g_{26} ; 32.58% for h_{96}) and + (19.33% for g_{16} and g_{26} ; 14.94% for h_{96}), leaving – as the favored score. This is shown for g_{16} in Figure 2.7B.

2.3.8 Responsiveness: fast NO elevation after stimulus

A functionally effective system minimizes the time to steady state after stimulus. We explore the response time under which levels of NO (x_6) come within 5 percent of the activated steady state or above (i.e. we do not penalize the system for overshoot because the goal for killing pathogen should be to get nitric oxide levels up to at least a certain level or above). We examine responsiveness for each of the three activation states

with LPS/IFN- γ (Figure 2.8). Results with exogenous iron treatment are similar (not shown). As expected, each activation state shows a distinct pattern of response times, but in every case examined, they yield the same score (summarized in Table 2.4).

The dynamic and specific nature of the numerical simulations leave open several possible situations deserving consideration. If the system starts from a partially activated steady state (i.e. constant stimulus from one signal, say LPS), response times after stimulation from the other signal (here, IFN- γ) are the same as if the system had started in the quiescent steady state. We have also investigated cases with initiation of the two stimulation signals staggered over various short intervals, before the system has reached steady state from the first signal (not shown). The exact profiles differ slightly but in each case the results support the same hypothesis as for other cases. We conclude that examination of the three activation states shown suffice to draw conclusions regarding the responsiveness criterion.

It is possible to achieve a minimal response time representing baseline [NO] that is undisturbed by the activation signal. This is observed for g_{31} (\dagger and \ddagger in Figure 2.8A), as well as g_{32} , g_{26} and g_{37} for reasonable parameter ranges. We consider these “non-response” cases to be trivial. Slightly different activation states can change the exact parameter value where this phenomenon occurs. Thus, achieving an artificial minimal response time is likely not relevant since multiple activation signals and the possibility of strong activation are necessary for proper macrophage function. Parameter values less than this no-response point in Figure 2.8A represent repressible systems, causing NO levels to decrease in response to stimulus. Determining the response time for g_{16} (Figure 2.8B) and h_{96} is more straightforward than the previous cases as levels of NO

are induced to a steady state level above that of the quiescent state for biologically reasonable parameter choices.

With the above considerations in mind we conclude that a single score emerges for each parameter examined (Table 2.4). Therefore g_{31} (Figure 2.8A) scores + for responsiveness and g_{16} scores –.

2.4 Discussion

The process of macrophage activation for killing of internalized pathogens has evolved a trade-off between a robustly quiescent state and decisive activation under a definitive signal. Experimental study of this system in mouse and human cells has characterized components of what are apparently the most important aspects of macrophage activation and killing. This has allowed us to construct a mathematical model for system-level investigation, with a view toward the interaction of functional modules that determine the outcome of activation signaling. Using this model, we have shown that the configuration of intermodule regulatory interactions can permit a near-quiescent state in the presence of partial activation, while allowing complete activation upon receipt of multiple activation stimuli. Our model suggests that there must exist a synergistic response to multiple signals in order to overcome stabilizing interactions for complete macrophage activation. The role of iron regulation in the activation of iNOS and NO production appears to be an asymmetric relationship: iron levels respond to activation as part of the overall response in a pattern consistent with sequestration of iron from extracellular space under normal iron conditions. Mechanisms of killing become sensitive to iron regulation parameters under exogenous iron treatment, but this is most

apparent only under partial activation conditions; under complete activation killing mechanisms again predominate.

Each member of an intermodule pair of regulatory interactions (i.e. g_{31}/g_{16} , g_{32}/g_{26} and h_{96}/g_{37}) has a dependence on the other in the pair for the predicted interaction score based on the CFE. Thus, as we know that g_{31} is positive (shown experimentally) then g_{16} is predicted to be negative by the CFE. We also find that anti-inflammatory feedback allows and enforces a system with positive transcriptional regulation as compared to lack of feedback or positive feedback (Figures 2.6, 2.7 and 2.8 B). We therefore see with these interactions how a system that must remain quiescent most of the time can maintain quiescence robustly. This reasoning applies to each of the other pairs of interactions as well. With the KM/IRM interactions (h_{96}/g_{37}) the resultant pair of scores is -- (Table 2.4).

AM signaling induces anti-inflammatory feedback to both NF- κ B and Stat1 in this model. The overall effect is to increase the functional effectiveness of the macrophage system (Table 2.4) by preventing activation in the absence of multiple activating signals. Crosstalk feedback by NO on Stat1 increases the threshold for activation under LPS signaling alone (Figures 2.3 and 2.4). Crosstalk to NF- κ B by IFN- γ signaling also shows this effect to a lesser extent. We explain these results as follows: For transcriptional activation of iNOS, activated NF- κ B, Stat1 and other transcription factors must occupy their promoter regions for transcription initiation and resultant iNOS/NO production. In the absence of an activating signal, the probability of these being together on the promoter is low. When a single activation signal is present (e.g. LPS), the level of NF- κ B increases, raising the probability of transcription initiation.

However, the slight increase of NO and resultant negative feedback to Stat1 lowers the probability of Stat1 presence for initiation, or possibly keeps it at a quiescent level, due to a crosstalk anti-inflammatory feedback effect (Figure 2.3). We have shown that this crosstalk-inhibition effect is caused by the negative feedback of NO to the unstimulated activator (Figure 2.3). The transcriptional signals are only working in concert under conditions in which both of the signals are sufficiently active. When this is the case the two signals act synergistically to induce NO production (Figure 2.2). The activation of multiple signals thus allows the macrophage system to overcome anti-inflammatory feedback for complete activation.

The interactions between the KM and IRM help determine the outcome of LIP levels during activation and the outcome of macrophage activation under iron-rich conditions. The exact effect of macrophage activation on LIP levels may depend on different interactions (32, 65). We find that the most functionally effective motif results in NO production inducing the influx of iron into the LIP via IRPs (i.e. $h_{96} < 0$), increasing LIP levels on the path to sequestration of iron from plasma, consistent with hypoferremia (66). Note that one need not argue for a direct benefit of hypoferremia against extracellular pathogens for this interaction to be functionally effective.

This result shows an indirect negative feedback to iNOS/NO production via the IRM during activation. Under iron-rich conditions this result implies a direct signaling effect of iron influx on iNOS transcription, leading us to question which functional module is dominant. Under a definitive activation signal, the macrophage must show high induction of iNOS and NO in the KM, but this could be inhibited, with potentially impairing results on the immune response, under conditions of high iron in the IRM. We

have addressed this with global statistical analysis, which shows a generally higher statistical sensitivity of [LIP] to AM and KM parameters than [NO] shows to IRM parameters under lower level iron conditions. Under iron-rich conditions these statistical sensitivities are brought into near-parity under partial activation conditions (comparing the sensitivity of [NO] to g_{37} to the sensitivity of [LIP] to h_{96} ; Figure 2.5), but become asymmetric again under complete activation. Thus exogenous iron appears to play an incremental role in suppressing macrophage activation, particularly important under partial activation conditions. However, this can be overcome so that activation of the KM predominates under complete activation conditions. While the effect of [LIP] on NO production is clear (11, 18, 67), the possible role of this interaction in exacerbating disease processes deserves more study; this model suggests a role for iron in suppressing NO expression by macrophages that depends on the macrophage activation state. This implies that mechanisms required for robust macrophage response may also worsen response to infection under pathological iron conditions.

Since macrophage activation involves many mechanisms beyond cytokine and endotoxin-induced nitric oxide production, the scope and applicability of our current work is an important part of thinking about the system. Depending on the mix of cytokines present, macrophages may become activated in a classical or alternative manner (e.g. 15). We have included a subset of mechanisms for classical activation here. Our focus is on quantitative regulation of the model's components; spatial considerations, especially mechanisms of phagocytosis, comprise an important facet of macrophage function that may alter the capability of nitric oxide to access internalized pathogen (e.g. 48, 50). Finally, de-activation is a naturally important step in the cycle of macrophage

immunological function (reviewed in (15)) that has its own set of regulatory apparatus beyond the scope of this model, which is concerned with the process of moving from a quiescent state to activation.

We propose several possible avenues of extension based on our results for the mechanisms of macrophage function presented here. We note first the importance of nitric oxide signaling to transcription factors that regulate iNOS transcription. This may be examined in macrophage culture by detection of nitrosylation crosstalk between signaling pathways. For instance, detecting nitrosylation of Stat1 and other IFN- γ -inducible signals under LPS stimulation (and of NF- κ B and other LPS-inducible signals under IFN- γ stimulation) may further elucidate the roll of NO in activation. Further, the effect of the NO feedback effect may be assessed with consideration for more complex AM interactions not captured here, such as transcriptionally controlled feedback mechanisms. The usefulness of this model may be extended by studying macrophage interactions with a growing population of intracellular bacteria, particularly the superoxide-resistant *Mycobacterium tuberculosis*. Implementation of this extension into the model allows another criterion for macrophage functional effectiveness, namely clearance of bacteria (c.f. Chapter 3).

Our results show the usefulness of approaching questions regarding the immune response with a view toward the integrated function of the system. We propose that known mechanisms for macrophage activation allow contradictory demands of different contexts to be met with a strong activation signal only in the presence of synergistic activation of multiple signals stabilized by anti-inflammatory feedback from a common output of the signaling cascade. With this in mind other immune signaling cascades may

show similar topology and behavior, explaining in part the evolutionary need for multiple signals and complex cytokine networks to overcome robustness to perturbations.

Figures

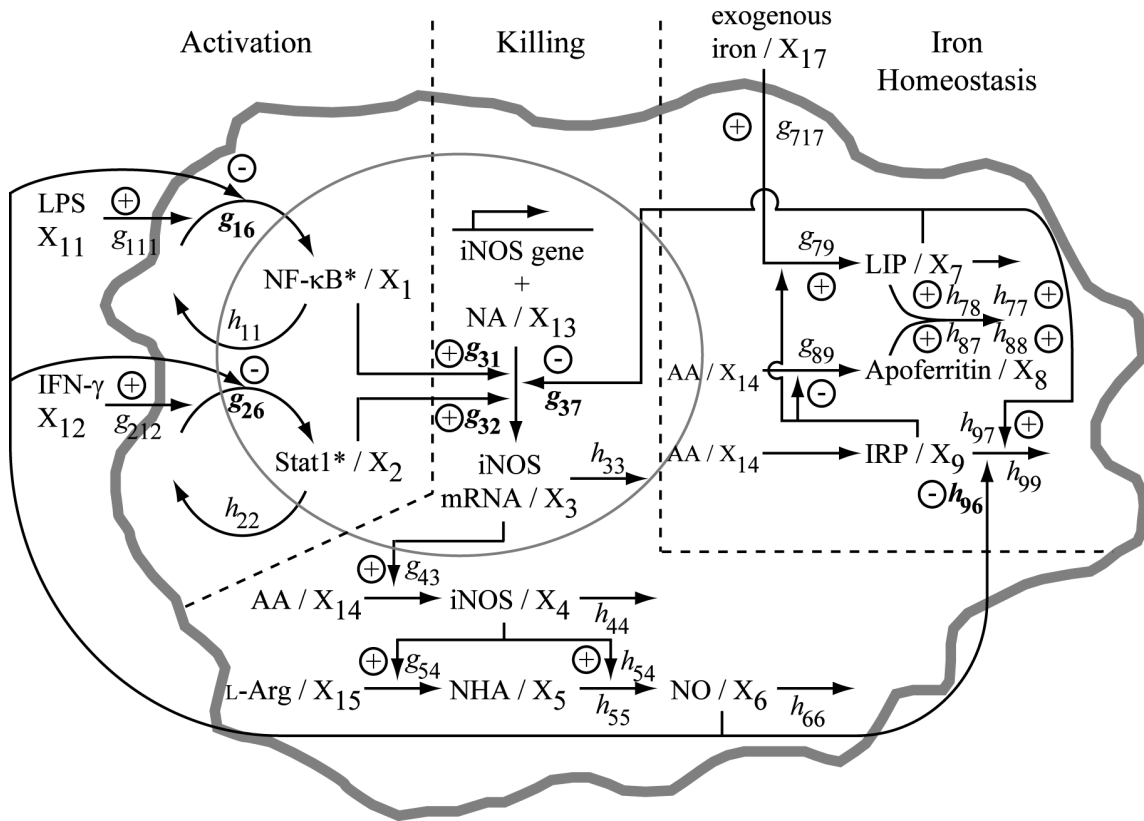


Figure 2.1: Schematic of the macrophage biochemical network involved in activation of nitric oxide production. Each X_i represents one model variable. Arrows pointing to or from variables represent synthetic, degradatory or cycling processes while those pointing to other arrows represent regulatory interactions. Parameters are labeled with their putative regulatory phenotype, stimulatory (+) or inhibitory (-). Three functional modules (Activation, Killing, Iron Regulation) are marked. Bold parameters are subject to local detailed analysis (Methods). NA (X_{13}), pool of nucleic acid precursors to mRNA; AA (X_{14}), pool of amino acid precursors to protein. Note that the parameter h_{77} represents the weighted average of the kinetic orders from both depicted labile iron pool consumption processes.

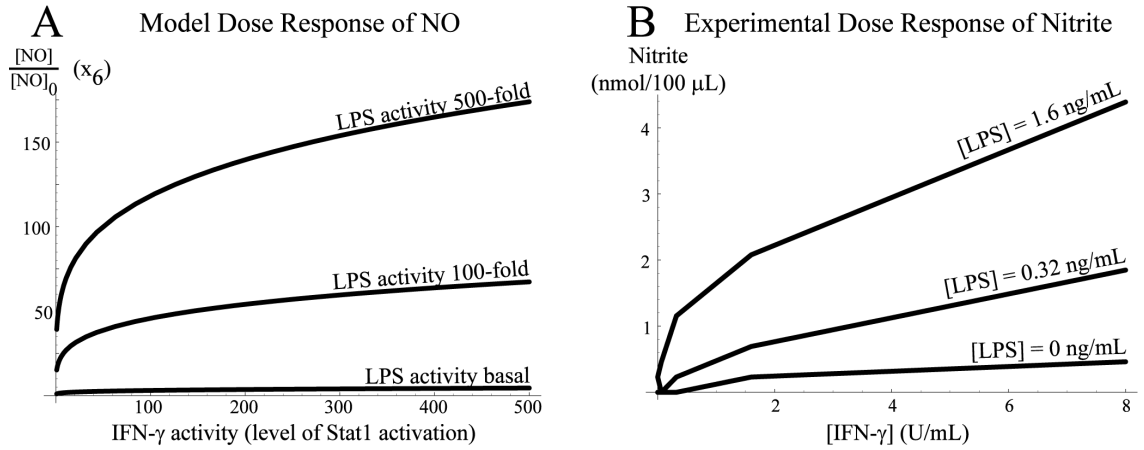


Figure 2.2. Response of nitric oxide to doses of LPS and IFN- γ . (A) Steady state dose response of NO (x_6) in the macrophage model for various levels of NF- κ B and Stat1 induction by LPS (x_{11}) and IFN- γ (x_{12}), respectively, shows synergistic activation by multiple activation signals. (B) Dose response of nitrite to various concentrations of LPS and IFN- γ in J774A.1 mouse macrophages shows a similar synergistic activation. Data are from(9); we selected a subset of the data that are below saturation.

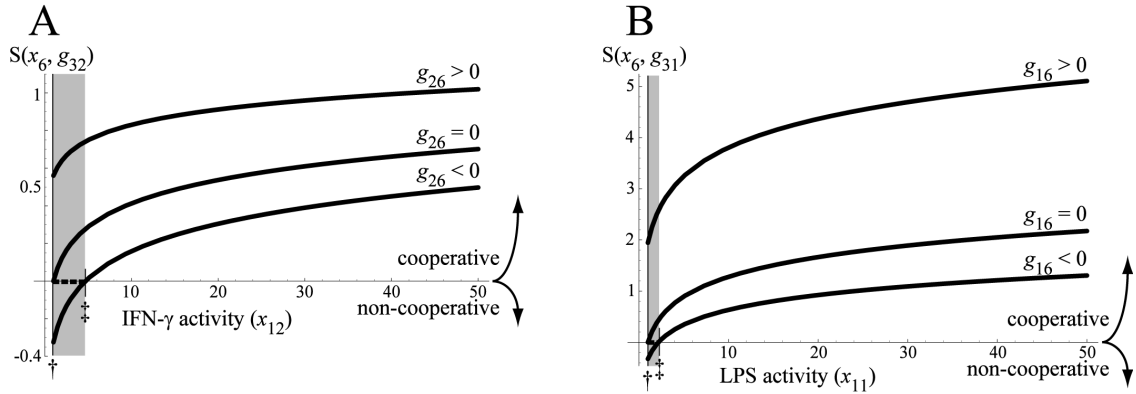


Figure 2.3. Crosstalk of activation pathways induced by common feedback. (A) The sensitivity of [NO] to alterations in Stat1 transcription effect (g_{32}) under constant LPS activity ($x_{11} = 100$) shows a dependence on IFN- γ activity (x_{12}). During activation from LPS but low IFN- γ signaling, the negative feedback by NO to Stat1 can cause it to have a non-cooperative influence on iNOS transcriptional activation (gray shaded region). Above a certain threshold of IFN- γ -induced Stat1 activation (marked \ddagger) the interaction is cooperative, or synergistic ($S(x_6, g_{32}) > 0$). (B) Sensitivity of [NO] to alterations in NF- κ B transcription effect (g_{31}) under constant IFN- γ activity ($x_{12} = 100$) shows a parallel effect. This effect in both cases is altered under cases lacking feedback ($g_{26}, g_{16} = 0$, respectively) or with positive feedback ($g_{26}, g_{16} > 0$, respectively) where the sensitivity measure does not reach zero above the quiescent steady state (marked \dagger). The dashed lines (between \dagger and \ddagger on the x -axis) represent S for negative feedback when a piecewise model is used to prevent suppression of the activation module below the quiescent steady state (see text for explanation). Values of g_{16} and g_{26} are chosen with the constraints of lines of equivalent gain described in Methods.

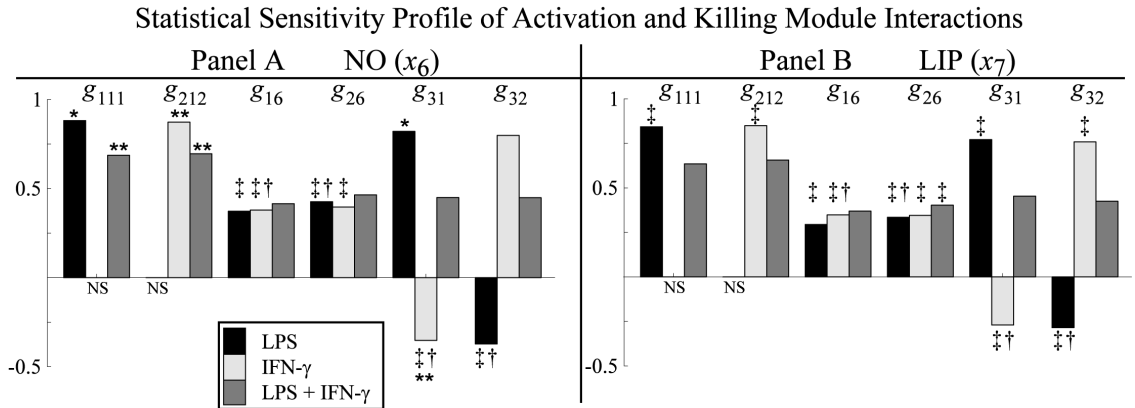


Figure 2.4. Significant partial rank correlations (statistical sensitivities) of parameters in Activation and Killing Module interactions to nitric oxide and labile iron pool levels. Each parameter is shown for three activation states (LPS, IFN- γ and LPS + IFN- γ) at $t = 100$ hrs. NS: the PRC is not significantly different from zero ($p > 0.01$). Correlations marked ‡ are significantly reduced in absolute value under treatment with exogenous iron ($x_{17} = 10$, $p < 0.01$). Correlations marked † are not significantly different from zero when a piecewise model is used to prevent suppression of the activation module below the quiescent steady state during partial activation (see text for explanation). *, **: Correlations for the same parameter in the same activation state significantly differ between x_6 and x_7 under both treatment and lack of treatment with exogenous iron (*) or under treatment with exogenous iron only (**). The interaction represented by each parameter is shown in Figure 2.1.

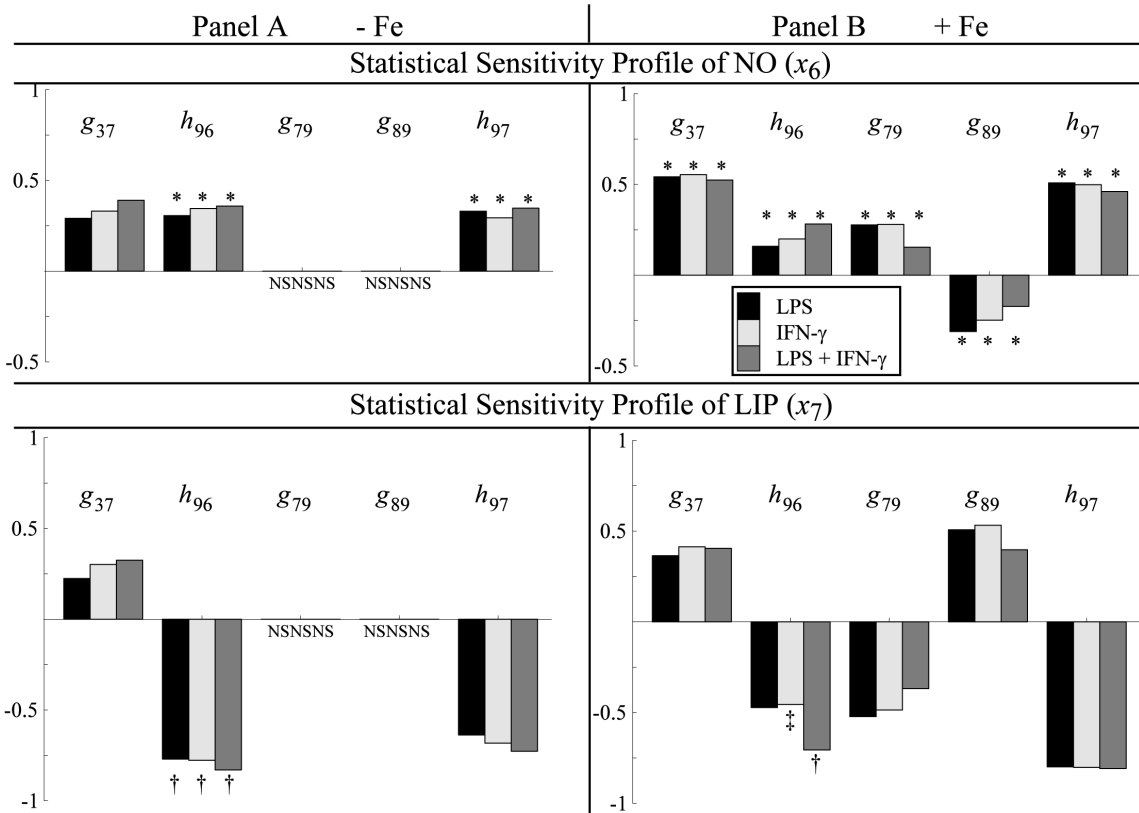


Figure 2.5. Significant partial rank correlations (statistical sensitivities) of parameters in the Iron Regulation Module to nitric oxide and labile iron pool levels. Each parameter is shown for three activation states (LPS, IFN- γ and LPS + IFN- γ) with or without supplemental iron ($x_{17} = 10$) at $t = 100$ hrs. NS: the PRC is not significantly different from zero ($p > 0.01$). *: Correlations for the same parameter in the same activation state significantly differ between x_6 and x_7 . †: the absolute PRC is significantly greater than $|\gamma_{g_{37},x_6}|$ in the same activation state; ‡: the absolute PRC is significantly less than $|\gamma_{g_{37},x_6}|$ in the same activation state. The interaction represented by each parameter is shown in Figure 2.1.

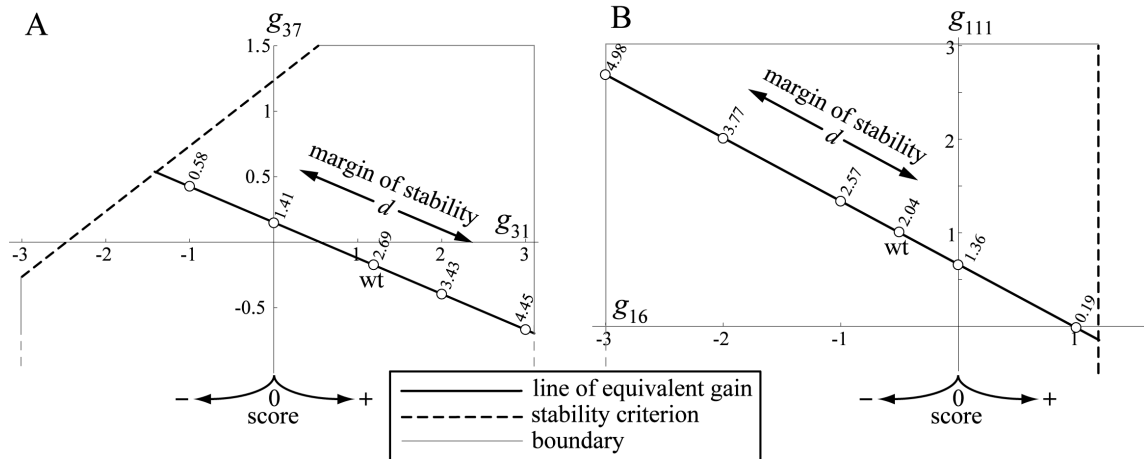


Figure 2.6. Example parameter spaces for mathematically controlled comparisons. A single point represents a set of parameter values for the mathematical model. On the x -axis is the knockout parameter (see text). Models meeting the equivalence requirements (Methods; Table 2.2) are compared along the solid line of equivalence (given in Table 2.3). This line specifies a value of the parameter on the y -axis that must be chosen to ensure equivalence between versions of the model compared while varying the x -axis parameter. The dashed line represents the Routh-Hurwitz criterion that determines model stability (see Methods). The boundary line represents plausible limits of biological relevance for parameter values. The exact value of each boundary is unknown, but need not be specified for this analysis. The margin of stability d is a measure of distance from a point on the line of equivalent gain to the critical stability line, so that the region with the highest d gives the score for the stability criterion. (A) Parameter space for the transcriptional activation parameter g_{31} . (B) Parameter space for the feedback parameter g_{16} . Points on the line of equivalent gain to the right of the y -axis give a model with a stimulatory interaction represented by the parameter of interest; to the left, the interaction is inhibitory and on the y -axis it is nullified.

Macrophage Robustness to Perturbation

NF-κB Activation of Transcription (g_{31})

A

Dependent Fluxes / Variables x

	X_1	X_2	X_3	X_4	X_5	X_6	X_7	X_8	X_9	V_1	V_2	V_3	V_4	V_5	V_6	V_7	V_8	V_9
Y_{11}	+	0	0	0	0	0	0	0	0	+	0	0	0	0	0	0	0	0
Y_{12}	+	-	+	+	+	+	+	+	+	+	-	+	+	+	+	+	+	+
Y_{13}	+	+	-	+	+	+	+	+	+	+	+	-	+	+	+	+	+	+
Y_{14}	+	+	-	-	-	-	-	-	0	-	-	-	-	-	-	-	+	+
Y_{15}	-	-	-	-	-	-	-	-	0	-	-	-	-	-	-	-	-	-
α_1	+	0	0	0	0	0	0	0	0	+	0	0	0	0	0	0	0	0
β_1	+	0	0	0	0	0	0	0	0	0	0	0	0	0	0	0	0	0
α_2	+	-	+	+	+	+	+	+	+	+	-	+	+	+	+	+	+	+
β_2	+	-	+	+	+	+	+	+	+	+	+	+	+	+	+	+	+	+
α_3	+	+	+	+	+	+	+	+	+	+	+	+	+	+	+	+	+	+
β_3	+	+	+	+	+	+	+	+	+	+	-	+	+	+	+	+	+	+
α_4	+	+	-	+	+	+	+	+	+	+	+	-	+	+	+	+	+	+
β_4	+	+	-	+	+	+	+	+	+	+	+	-	+	+	+	+	+	+
α_5	+	+	-	-	+	+	+	+	+	+	-	+	+	+	+	+	+	+
β_5	+	+	-	-	+	+	+	+	+	+	-	+	+	+	+	+	+	+
α_6	+	+	-	-	-	+	+	+	+	+	+	-	+	+	+	+	+	+
β_6	+	+	-	-	-	+	+	+	+	+	+	-	+	+	+	+	+	+
α_7	-	-	-	-	-	-	-	-	-	-	-	-	-	-	-	-	-	-
β_7	-	-	-	-	-	-	-	-	-	-	-	-	-	-	-	-	-	-
α_8	-	-	-	-	-	-	-	-	-	-	-	-	-	-	-	-	-	-
β_8	-	-	-	-	-	-	-	-	-	-	-	-	-	-	-	-	-	-
α_9	-	-	-	-	-	-	-	-	-	-	-	-	-	-	-	-	-	-
β_9	-	-	-	-	-	-	-	-	-	-	-	-	-	-	-	-	-	-
g_{16}	+	0	0	0	0	0	0	0	0	+	0	0	0	0	0	0	0	0
g_{26}	+	-	+	+	0	+	+	0	+	-	+	+	0	+	+	+	+	0
g_{31}	0	0	0	0	0	0	0	0	0	0	0	0	0	0	0	0	0	0
g_{32}	+	+	+	+	0	+	+	+	0	+	+	+	+	+	+	+	+	0
g_{37}	-	-	-	0	-	-	-	0	-	-	-	-	0	-	-	-	-	0
g_{43}	+	+	-	+	0	+	+	0	+	+	-	+	0	+	+	+	+	0
g_{79}	-	-	-	0	-	-	-	-	-	-	-	-	0	-	-	-	-	-
g_{89}	-	-	-	0	-	-	-	-	-	-	-	-	0	-	-	-	-	-
h_{11}	0	0	0	0	0	0	0	0	0	0	0	0	0	0	0	0	0	0
h_{22}	+	-	+	+	+	+	+	0	+	-	+	+	0	+	+	+	+	0
h_{33}	+	+	+	+	+	+	+	+	+	+	-	+	+	+	+	+	+	0
h_{44}	+	+	-	+	0	+	+	+	+	+	-	0	+	+	+	+	+	0
g_{54}	+	+	-	-	+	+	+	0	+	+	-	-	+	+	+	+	+	0
h_{54}	0	0	0	-	0	0	0	0	0	0	0	-	0	0	0	0	0	0
h_{55}	0	0	0	0	-	0	0	0	0	0	0	-	0	0	0	0	0	0
h_{66}	+	+	-	-	0	+	+	+	+	+	-	-	+	+	+	+	+	0
h_{77}	-	-	+	0	-	-	-	-	-	-	+	-	-	-	-	-	-	-
h_{96}	-	-	-	0	-	-	-	-	-	-	+	-	-	-	-	-	-	-
h_{97}	-	-	-	0	-	-	-	-	-	-	+	-	-	-	-	-	-	-
h_{99}	-	-	-	0	-	-	-	-	-	-	+	-	-	-	-	-	-	-
g_{111}	+	0	0	0	0	0	0	0	0	+	0	0	0	0	0	0	0	0
g_{212}	-	-	+	+	0	+	+	0	+	-	+	+	0	+	+	+	+	0
g_{313}	+	+	-	-	0	+	+	-	0	+	-	0	+	+	+	+	+	0
g_{414}	+	+	-	+	0	+	+	+	0	+	-	+	+	+	+	+	+	0
g_{515}	-	-	-	-	0	-	-	-	-	-	-	-	-	-	-	-	-	-
g_{717}	-	-	-	0	-	-	-	-	-	-	-	-	-	-	-	-	-	-
g_{814}	-	-	-	0	-	-	-	-	-	-	-	-	-	-	-	-	-	-
g_{914}	-	-	-	0	-	-	-	-	-	-	-	-	-	-	-	-	-	-

└ Independent Variables y / Parameters p

Predicted robust value of independent variable shown: Predicted robust value of parameter shown:

$$\min |L(x, y)|$$

$$\min |S(x, p)|$$



No

Preference

B

NO Feedback on NF-κB (g_{16})

Dependent Fluxes / Variables x

	X_1	X_2	X_3	X_4	X_5	X_6	X_7	X_8	X_9	V_1	V_2	V_3	V_4	V_5	V_6	V_7	V_8	V_9
Y_{11}	+	+	+	+	+	+	+	+	+	+	+	+	+	+	+	+	+	+
Y_{12}	0	-	-	-	-	-	-	-	-	0	+	-	-	-	-	-	-	-
Y_{13}	0	-	-	-	-	-	-	-	-	0	-	-	-	-	-	-	-	-
Y_{14}	0	-	+	-	-	-	-	-	-	0	-	+	-	-	-	-	-	-
Y_{15}	0	-	-	-	-	-	-	-	-	0	-	-	-	-	-	-	-	-
Y_{17}	0	-	-	-	-	-	-	-	-	0	-	-	-	-	-	-	-	-
α_1	-	-	-	-	-	-	-	-	-	-	-	-	-	-	-	-	-	-
β_1	-	-	-	-	-	-	-	-	-	-	-	-	-	-	-	-	-	-
α_2	0	+	-	-	-	-	-	-	-	-	+	-	-	-	-	-	-	-
β_2	0	+	-	-	-	-	-	-	-	-	+	-	-	-	-	-	-	-
α_3	0	-	-	-	-	-	-	-	-	-	0	-	-	-	-	-	-	-
β_3	0	-	-	-	-	-	-	-	-	-	0	-	-	-	-	-	-	-
α_4	0	-	-	-	-	-	-	-	-	-	0	-	-	-	-	-	-	-
β_4	0	-	-	-	-	-	-	-	-	-	0	-	-	-	-	-	-	-
α_5	0	-	+	+	-	-	-	-	-	-	0	-	+	+	-	-	-	-
β_5	0	-	+	+	-	-	-	-	-	-	0	-	+	+	-	-	-	-
α_6	0	-	+	+	+	-	-	-	-	-	0	-	+	+	+	-	-	-
β_6	0	-	+	+	+	-	-	-	-	-	0	-	+	+	+	-	-	-
α_7	0	-	-	-	-	-	-	-	-	-	0	-	-	-	-	-	-	-
β_7	0	-	-	-	-	-	-	-	-	-	0	-	-	-	-	-	-	-
α_8	0	-	-	-	-	-	-	-	-	-	0	-	-	-	-	-	-	-
β_8	0	-	-	-	-	-	-	-	-	-	0	-	-	-	-	-	-	-
α_9	0	-	-	-	-	-	-	-	-	-	+	+	+	0	-	-	-	+
β_9	0	-	-	-	-	-	-	-	-	-	+	+	+	0	-	-	-	+
g_{16}	0	0	0	0	0	0	0	0	0	0	0	0	0	0	0	0	0	0
g_{26}	0	+	-	-	0	-	-	0	-	-	0	+	-	-	0	-	-	0
g_{31}	0	-	-	-	-	-	-	-	-	-	0	-	-	-	-	-	-	-
g_{32}	0	-	-	-	-	-	-	-	-	-	0	-	-	-	-	-	-	-
g_{37}	0	-	-	-	-	-	-	-	-	-	0	-	-	-	-	-	-	-
g_{43}	0	-	-	-	-	-	-	-	-	-	0	-	-	-	-	-	-	-
g_{79}	0	-	-	-	-	-	-	-	-	-	+	+	+	0	-	-	-	+
g_{89}	0	-	-	-	-	-	-	-	-	-	+	+	+	0	-	-	-	+
h_{11}	0	+	-	-	-	-	-	-	-	-	0	+	-	-	-	-	-	0
h_{22}	0	+	-	-	-	-	-	-	-	-	0	+	-	-	-	-	-	0
h_{33}	0	-	-	-	-	-	-	-	-	-	0	-	-	-	-	-	-	0
h_{44}	0	-	-	-	-	-	-	-	-	-	0	-	-	-	-	-	-	0
g_{54}	0	-	+	+	0	-	-	-	-	-	0	-	-	-	-	-	-	0
h_{54}	0	-	+	+	0	-	-	-	-	-	0	-	-	-	-	-	-	0
h_{55}	0	-	+	+	0	-	-	-	-	-	0	-	-	-	-	-	-	0
h_{66}	0	-	+	+	0	-	-	-	-	-	0	-	-	-	-	-	-	0
h_{77}	0	-	-	-	-	-	-	-	-	-	0	-	-	-	-	-	-	0
h_{96}	0	-	-	-	-	-	-	-	-	-	0	-	-	-	-	-	-	0
h_{97}	0	-	-	-	-	-	-	-	-	-	0	-	-	-	-	-	-	0
h_{99}	0	-	-	-	-	-	-	-	-	-	0	-	-	-	-	-	-	0
g_{111}	+	+	+	+	-	-	-	-	-	-	+	+	+	+	-	-	-	+
g_{212}	+	+	-	-	-	-	-	-	-	-	-	+	-	-	-	-	-	+
g_{313}	0	-	-	-	-	-	-	-	-	-	-	0	-	-	-	-	-	-
g_{414}	0	-	-	-	-	-	-	-	-	-	-	0	-	-	-	-	-	-
g_{515}	0	-	+	+	+	-	-	-	-	-	-	0	-	-	-	-	-	-
g_{7																		

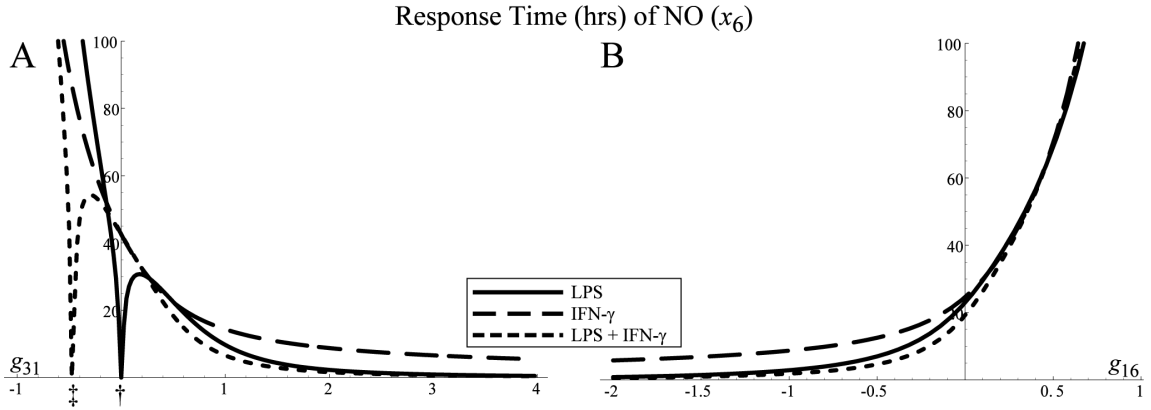


Figure 2.8. Response time of nitric oxide (x_6) from quiescent levels to within 5 % of the steady state or above. We varied levels of (A) NF- κ B transcriptional regulation (g_{31}) and (B) NO feedback to NF- κ B (g_{16}). The knockout parameter of interest is varied along its line of equivalent gain (Table 2.3). The minimal response time indicates a score of (A) + and (B) -. Depending on the activation state, the profile differs slightly, but a common minimum response parameter value is shared by all activation states in every case. In (A), two of the cases show a trivial minimal response time for $g_{31} = 0$ (marked \dagger) or $g_{31} < 0$ (marked \ddagger). These cases are irrelevant as the system represented by those parameter values is completely non-responsive to the simulated activation stimuli. No such non-responsive state exists for treatment by IFN- γ alone because of the equivalence requirements imposed on the system (Table 2.2).

Tables

Table 2.1. Definition and estimates of important parameters in the macrophage model.

Parameter ^a	Definition	Estimated Value	Sampling Interval ^b
a_1	NF- κ B turnover rate (nondim)	1.73 hr ⁻¹	[0.885, 41.6]
a_2	Stat1 turnover rate (nondim)	8.32 hr ⁻¹	[4.62, 41.6]
a_3	iNOS mRNA turnover rate (nondim)	0.173 hr ⁻¹	[0.116, 0.347]
a_4	iNOS turnover rate (nondim)	0.0693 hr ⁻¹	[0.0365, 0.693]
a_5	NHA turnover rate (nondim)	5.55 μ mol/hr	[0.0277, 166]
a_6	NO turnover rate (nondim)	2.77 hr ⁻¹	[0.0277, 166]
a_7	LIP turnover rate (nondim)	32.20 μ mol/hr	[2.58, 61.8]
a_8	apoFt turnover rate (nondim)	40 μ mol/hr	[3.72, 89.2]
a_9	IRP turnover rate (nondim)	36.7 μ mol ⁻¹ hr ⁻¹	[29.2, 44.1]
g_{111}	LPS-induced activation of NF- κ B	1	[0.1, 2]
g_{212}	IFN- γ -induced activation of Stat1	1	[0.1, 2]
g_{31}	NF- κ B transcriptional regulation of iNOS	1.19	[0.1, 2]
g_{16}	NO feedback to NF- κ B	-0.5	[-2, -0.1]
g_{32}	Stat1 transcriptional regulation of iNOS	0.48	[0.1, 2]
g_{26}	NO feedback to Stat1	-0.5	[-2, -0.1]
g_{37}	iron transcriptional regulation of iNOS	-0.177	[-2, -0.1]
h_{96}	NO-induced alteration of IRP	-0.5	[-2, -0.1]
g_{79}	indirect IRP-induced gain of iron influx	0.5	[0.1, 2]
g_{89}	IRP-induced translational control of ferritin	-0.645	[-1.7, -0.1]
h_{97}	iron-induced loss of IRP	0.5	[0.3, 2]

^a Boldface parameters are examined further in the local detailed analysis.

^b Reduced interval sizes in g_{89} and h_{97} prevent parameter combinations that result in pathological results from the numerical solver due to stiffness in the system (see text).

Table 2.2. Parameters examined in the local detailed analysis.

Parameter ^a	Function	Corrected Pars	Constrained Par Space
g_{31}	NF- κ B transcription	$g_{32}; g_{37}; g_{313}; \alpha_3$	$g_{31} \times g_{37}$
g_{32}	Stat1 transcription	$g_{31}; g_{37}; g_{313}; \alpha_3$	$g_{32} \times g_{37}$
g_{16}	NO feedback to NF- κ B	$g_{111}; \alpha_1$	$g_{16} \times g_{111}$
g_{26}	NO feedback to Stat1	$g_{212}; \alpha_2$	$g_{26} \times g_{212}$
g_{37}	Iron control of transcription	$g_{31}; g_{32}; g_{313}; \alpha_3$	$g_{37} \times g_{31}$
h_{96}	NO control of iron regulation	$h_{97}; h_{99}; \beta_9$	$h_{96} \times h_{97}$

^a Shown for each parameter is its definition, a set of other parameters in the same flux term corrected to ensure external equivalence requirements in each case, and a constrained parameter space used for its line of equivalent gain that ensures a controlled comparison (see Methods).

Table 2.3. Lines of equivalent gain and the stability criterion used for local detailed analysis.

Parameter(s)	Line of Equivalent Gain			
g_{31}, g_{32}	$g_{37} = \frac{(p_1 + p_2 + L_s(p_3 + p_4 - p_5))(p_7 h_{97} - p_8)}{g_{43} g_{54} h_{11} h_{22} h_{96} L_s p_7}$			
g_{37}	$g_{31} = \frac{-p_2(p_7 h_{97} - p_8) + L_s(p_6 p_7 + (-p_4 + p_5)(p_7 h_{97} - p_8))}{g_{43} h_{22} (g_{111} h_{66} + g_{16} g_{54} L_s)(p_7 h_{97} - p_8)}$			
g_{16}	$g_{111} = \frac{-p_2(p_7 h_{97} - p_8) + L_s(p_6 p_7 - (p_3 + p_4 - p_5)(p_7 h_{97} - p_8))}{g_{31} g_{43} h_{22} h_{66} (p_7 h_{97} - p_8)}$			
g_{26}	$g_{212} = \frac{-p_1(p_7 h_{97} - p_8) + L_s(p_6 p_7 - (p_3 + p_4 - p_5)(p_7 h_{97} - p_8))}{g_{32} g_{43} h_{11} h_{66} (p_7 h_{97} - p_8)}$			
h_{96}	$h_{97} = \frac{p_1 p_8 + p_2 p_8 + L_s(p_6 p_7 + (p_3 + p_4 - p_5) p_8)}{(p_1 + p_2 + L_s(p_3 + p_4 - p_5)) p_7}$			
Stability Criterion				
$p_6 p_7 - (p_3 + p_4 - p_5)(h_{97} p_7 - p_8) > 0$				
Abbreviation	Value	Abbreviation	Value	
p_1	$g_{111} g_{31} g_{43} h_{22} h_{66}$	p_5	$h_{11} h_{22} h_{33} h_{44} h_{66}$	
p_2	$g_{212} g_{32} g_{43} h_{11} h_{66}$	p_6	$g_{37} g_{43} g_{54} h_{11} h_{22} h_{96}$	
p_3	$g_{16} g_{31} g_{43} g_{54} h_{22}$	p_7	$g_{89} h_{78} - g_{79} h_{88}$	
p_4	$g_{26} g_{32} g_{43} g_{54} h_{11}$	p_8	$(-h_{78} h_{87} + h_{77} h_{88}) h_{99}$	

Table 2.4. Predicted parameter regions that best meet each criterion denoted by a score of $-$, 0 or $+$.

Parameter	Stability	Responsiveness	Robustness ^a	Overall Score
g_{31}	+	+	\approx	Positive
g_{32}	+	+	\approx	Positive
g_{16}	-	-	-	Negative
g_{26}	-	-	-	Negative
g_{37}	-	-	\approx	Negative
h_{96}	-	-	-	Negative

^a In some cases for robustness criterion, there was not a clear score derived from gains and sensitivities (see Figure 2.7); however, taken together, the other two criteria suggest a clear overall score. See text for details.

2.5 Appendix

2.5.1 Model equations

We represent the macrophage network S-system shown in Figure 2.1 as a series of differential equations:

$$\begin{aligned}
 \frac{dX_1}{dt} &= \alpha_1 X_{11}^{g_{111}} X_6^{g_{16}} - \beta_1 X_1^{h_{11}} & \frac{dX_6}{dt} &= \beta_5 X_4^{h_{54}} X_5^{h_{55}} - \beta_6 X_6^{h_{66}} \\
 \frac{dX_2}{dt} &= \alpha_2 X_{12}^{g_{212}} X_6^{g_{26}} - \beta_2 X_2^{h_{22}} & \frac{dX_7}{dt} &= \alpha_7 X_{17}^{g_{717}} X_9^{g_{79}} - \beta_7 X_7^{h_{77}} X_8^{h_{78}} \\
 \frac{dX_3}{dt} &= \alpha_3 X_{13}^{g_{313}} X_1^{g_{31}} X_2^{g_{32}} X_7^{g_{37}} - \beta_3 X_3^{h_{33}} & \frac{dX_8}{dt} &= \alpha_8 X_{14}^{g_{818}} X_9^{g_{89}} - \beta_8 X_7^{h_{87}} X_8^{h_{88}} \\
 \frac{dX_4}{dt} &= \alpha_4 X_{14}^{g_{414}} X_3^{g_{43}} - \beta_4 X_4^{h_{44}} & \frac{dX_9}{dt} &= \alpha_9 X_{14}^{g_{919}} - \beta_9 X_6^{h_{96}} X_7^{h_{97}} X_9^{h_{99}} \\
 \frac{dX_5}{dt} &= \alpha_5 X_{15}^{g_{515}} X_4^{g_{54}} - \beta_5 X_4^{h_{54}} X_5^{h_{55}}
 \end{aligned}$$

In practice we reduce the number of parameters with basic assumptions about the kinetics as well as non-dimensionalization (see Parameter Estimation below). This makes numerical simulations possible and gives the following system:

$$\begin{aligned}
 \frac{dx_1}{dt} &= a_1 (x_{11}^{g_{111}} x_6^{g_{16}} - x_1) & \frac{dx_6}{dt} &= a_5 (x_4 x_5 - x_6) \\
 \frac{dx_2}{dt} &= a_2 (x_{12}^{g_{212}} x_6^{g_{26}} - x_2) & \frac{dx_7}{dt} &= a_7 (x_{17} x_9^{g_{79}} - x_7 x_8) \\
 \frac{dx_3}{dt} &= a_3 (x_1^{g_{31}} x_2^{g_{32}} x_7^{g_{37}} - x_3) & \frac{dx_8}{dt} &= a_8 (x_9^{g_{89}} - x_7 x_8) \\
 \frac{dx_4}{dt} &= a_4 (x_3 - x_4) & \frac{dx_9}{dt} &= a_9 (1 - x_6^{h_{96}} x_7^{h_{97}} x_9^{h_{99}}) \\
 \frac{dx_5}{dt} &= a_5 (x_4 - x_4 x_5)
 \end{aligned}$$

2.5.2 Alternate representation of Activation Module

Under partial activation conditions the model predicts a level of transcription factor activity below the quiescent steady state. To address differences between this model and a model where this is not possible we represent the fluxes v_1^+ and v_2^+ in a

piecewise manner (56) in some instances:

$$v_{1p}^+ = \begin{cases} a_1 x_{11}^{g_{111}} x_6^{g_{16}}, & x_{11}^{g_{111}} x_6^{g_{16}} \geq 1 \\ a_1, & x_{11}^{g_{111}} x_6^{g_{16}} < 1 \end{cases}$$

$$v_{2p}^+ = \begin{cases} a_2 x_{12}^{g_{212}} x_6^{g_{26}}, & x_{12}^{g_{212}} x_6^{g_{26}} \geq 1 \\ a_2, & x_{12}^{g_{212}} x_6^{g_{26}} < 1 \end{cases}.$$

We avoided the need for identifying an upper limit by simulating LPS and IFN- γ doses low enough to be below signal saturation.

2.5.3 Parameter estimation

2.5.3.1 Rate constants

We have estimated the turnover rates a_i for equations 1, 2, 3, 4 and 6 from half life data (2, 6, 35, 39, 52, 67, 70).

$a_5 = \beta_6 (X_{60}/X_{50}) = a_6 (X_{60}/X_{50})$ at some operating point. Estimation of the NO:NHA ratio is difficult because actual NO levels are rarely measured in experiments. However, at most levels there is more nitrite than NHA, suggesting that there is more NO than NHA (7, 47). We assume this ratio to be 2, giving $a_5 = 2a_6$.

$a_7 = \beta_7 X_{80}$. In erythrocytes the turnover half-life of the LIP is about 1 hour (5).

Estimates for ferritin mass in macrophages range from 3.55×10^{-4} to 8.5×10^{-3} ng/cell (44, 60, 68). Given an approximate macrophage cell volume of $4990 \mu\text{m}^3$ (36) and average apoferritin subunit size of 19.1 kDa (19) we estimate $X_{80} \in [3.7 \times 10^{-6}, 8.5 \times 10^{-5}]$ m, giving $a_7 \in [2.58, 61.8] \mu\text{mol/hr}$. We take the mean as the default value. This overestimates the levels of apoferritin, because the variable X_8 is for unbound only. It

also underestimates it, because it counts molarity of subunits, not molarity of binding capacity. Nevertheless the sensitivity analysis shows that this will suffice for our analysis.

$a_8 = \beta_8 X_{70}$. Assuming an approximately 2-hour half life of ferritin (31) and 1 μ m LIP level (30) gives an estimate of 40 μ mol/hr. The LIP level is probably an overestimate but we sufficiently vary the parameter during the uncertainty analysis to account for this.

$a_9 = \alpha_9/X_{90}$. Assuming a 1.8 hour half-saturation time for IRP2 during return to steady state after depletion (31), and total IRP2 levels in the cell of 0.00874 to 0.0132 μ m (derived from IRP1 numbers (23) and estimated IRP1/IRP2 ratios (54)) we estimate $a_9 \in [29.2, 44.1]$ $\text{hr}^{-1} \mu \text{m}^{-1}$. We take the mean 36.7 as the default value.

2.5.3.2 Kinetic orders

General methods for estimation of kinetic orders are found in(64). Several kinetic order parameters correspond to simple first order processes. When this occurs, the kinetic order is 1. This has been shown experimentally for the following parameters: h_{11} (52), h_{22} (20), h_{33} (6), h_{44} (55), h_{66} (62) (see below) and h_{99} (33). The process of translation is 1-to-1 from mRNA to protein subunit so $g_{43} = 1$. The kinetic orders of iNOS substrate catalysis (g_{54} and h_{54}) are 1 because of the proportionality of iNOS to NO production (41).

We set $h_{55} = 1$, accurate for low levels of NHA. Under high activation conditions, this parameter may be lower (e.g. 0.5 near the $K_m = 15\mu\text{M}$ (14)). However, this only affects the steady state of NHA, not any other model components. This would require

greater consideration if we were concerned with NHA regulation of arginase (4), but for the aims of this study it suffices to set $h_{55} = 1$.

The kinetic order of NO loss in the intact cellular system $h_{66} = 1$ in hepatocytes (62); the second-order loss often observed in reaction with O_2 is predominant in cell-free systems or extracellular space (e.g. 38), not relevant here.

Parameters g_{31} , g_{32} , and g_{37} represent transcriptional regulation of the iNOS gene. Based on (46) we estimate $g_{31} = 1.19$ and $g_{32} = 0.47$ using linear regression of sub-saturation dose response of NO_2^- to LPS and IFN- γ . g_{37} can be estimated to a certain extent by a study showing a 50 percent decrease in macrophage iNOS mRNA with approximately a 50-fold increase in iron (67) (assuming a 1 μ M LIP steady state (30); the estimate does not change significantly even for a substantially lower LIP steady state). Assuming that mRNA stability and other significant components are not altered by the change in iron levels, $g_{37} = \frac{\log 0.5}{\log 50} \approx -0.177$.

The parameters h_{77} , h_{78} , h_{87} , and h_{88} represent the relationship between iron and ferritin and metabolic consumption of the LIP. As discussed in Methods, we represent the ferritin binding capacity instead of the raw number of subunits or complexes. Then one mole of iron takes one mole of ferritin binding capacity and the parameters of this process (h_{78} , h_{87} , and h_{88}) equal 1. Since X_8 (apoferritin) is an intermediate, its loss due to degradation is negligible. h_{77} represents the weighted average of kinetic orders for loss due to metabolic consumption and chelation by apoferritin. In aggregate, the loss is first order so $h_{77} = 1$ (5).

The parameter g_{89} represents the influence of IRP (X_9) on ferritin (X_8) translation. When IRP2 levels are decreased by the addition of NO^+ , ferritin levels increase linearly over time (31). Assuming this assay detected all forms of ferritin, $g_{89} \approx -0.645$.

We set all kinetic orders of independent variables to 1. This has no effect on the model in most cases because the levels of independent variables are arbitrary and usually non-rate limiting. During the course of analysis we choose a value other than 1 for g_{111} and g_{212} for controlled comparisons in some cases (see Local Detailed Analysis in Methods).

The remaining unestimated parameters, h_{96} , h_{97} , g_{79} , g_{16} and g_{26} , represent regulatory interactions for which there exist no quantitative data to our knowledge that would allow us to estimate them. In the default case they are ± 0.5 , equivalent to a Michaelis-Menten process working at the operating point (64).

2.6 References

1. **Alderton, W. K., C. E. Cooper, and R. G. Knowles.** 2001. Nitric oxide synthases: structure, function and inhibition. *Biochem J* **357**:593-615.
2. **Andrews, R. P., M. B. Ericksen, C. M. Cunningham, M. O. Daines, and G. K. Hershey.** 2002. Analysis of the life cycle of stat6. Continuous cycling of STAT6 is required for IL-4 signaling. *J Biol Chem* **277**:36563-36569.
3. **Blower, S. M., and H. Dowlatabadi.** 1994. Sensitivity and Uncertainty Analysis of Complex Models of Disease Transmission: an HIV Model, as an Example. *Int Stat Rev* **62**:229-243.
4. **Boucher, J. L., J. Custot, S. Vadon, M. Delaforge, M. Lepoivre, J. P. Tenu, A. Yapo, and D. Mansuy.** 1994. N omega-hydroxyl-L-arginine, an intermediate in the L-arginine to nitric oxide pathway, is a strong inhibitor of liver and macrophage arginase. *Biochem Biophys Res Commun* **203**:1614-1621.
5. **Breuer, W., S. Epsztejn, and Z. I. Cabantchik.** 1995. Iron acquired from transferrin by K562 cells is delivered into a cytoplasmic pool of chelatable iron(II). *J Biol Chem* **270**:24209-24215.
6. **Brown, D. H., W. P. Lafuse, and B. S. Zwillig.** 1997. Stabilized expression of mRNA is associated with mycobacterial resistance controlled by Nramp1. *Infect Immun* **65**:597-603.
7. **Buga, G. M., R. Singh, S. Pervin, N. E. Rogers, D. A. Schmitz, C. P. Jenkinson, S. D. Cederbaum, and L. J. Ignarro.** 1996. Arginase activity in endothelial cells: inhibition by NG-hydroxy-L-arginine during high-output NO production. *Am J Physiol* **271**:H1988-1998.
8. **Chakravorty, D., and M. Hensel.** 2003. Inducible nitric oxide synthase and control of intracellular bacterial pathogens. *Microbes Infect* **5(7)**:621-627.
9. **Chauhan, V., D. Breznan, P. Goegan, D. Nadeau, S. Karthikeyan, J. R. Brook, and R. Vincent.** 2004. Effects of ambient air particles on nitric oxide production in macrophage cell lines. *Cell Biol Toxicol* **20**:221-239.
10. **Connelly, L., M. Palacios-Callender, C. Ameixa, S. Moncada, and A. J. Hobbs.** 2001. Biphasic regulation of NF-kappa B activity underlies the pro- and anti-inflammatory actions of nitric oxide. *J Immunol* **166**:3873-3881.
11. **Dlaska, M., and G. Weiss.** 1999. Central role of transcription factor NF-IL6 for cytokine and iron-mediated regulation of murine inducible nitric oxide synthase expression. *J Immunol* **162**:6171-6177.

12. **Ganster, R. W., B. S. Taylor, L. Shao, and D. A. Geller.** 2001. Complex regulation of human inducible nitric oxide synthase gene transcription by Stat 1 and NF-kappa B. *Proc Natl Acad Sci U S A* **98**:8638-8643.
13. **Gao, J., D. C. Morrison, T. J. Parmely, S. W. Russell, and W. J. Murphy.** 1997. An interferon-gamma-activated site (GAS) is necessary for full expression of the mouse iNOS gene in response to interferon-gamma and lipopolysaccharide. *J Biol Chem* **272**:1226-1230.
14. **Ghosh, D. K., H. M. Abu-Soud, and D. J. Stuehr.** 1995. Reconstitution of the second step in NO synthesis using the isolated oxygenase and reductase domains of macrophage NO synthase. *Biochemistry* **34**:11316-11320.
15. **Gordon, S.** 2003. Alternative activation of macrophages. *Nat Rev Immunol* **3**:23-35.
16. **Groves, J. T., and C. C. Wang.** 2000. Nitric oxide synthase: models and mechanisms. *Curr Opin Chem Biol* **4**:687-695.
17. **Guo, Z., L. Shao, X. Feng, K. Reid, E. Marderstein, A. Nakao, and D. A. Geller.** 2003. A critical role for C/EBPbeta binding to the AABS promoter response element in the human iNOS gene. *FASEB J* **17**:1718-1720.
18. **Harhaji, L., O. Vuckovic, D. Miljkovic, S. Stosic-Grujicic, and V. Trajkovic.** 2004. Iron down-regulates macrophage anti-tumour activity by blocking nitric oxide production. *Clin Exp Immunol* **137(1)**:109-116.
19. **Harrison, P. M., and P. Arosio.** 1996. The ferritins: molecular properties, iron storage function and cellular regulation. *Biochim Biophys Acta* **1275**:161-203.
20. **Haspel, R. L., and J. E. D. Jr.** 1999. A nuclear protein tyrosine phosphatase is required for the inactivation of Stat1. *Proc Natl Acad Sci U S A* **96**:10188-10193.
21. **Haspel, R. L., M. Salditt-Georgieff, and J. E. Darnell Jr.** 1996. The rapid inactivation of nuclear tyrosine phosphorylated Stat1 depends upon a protein tyrosine phosphatase. *EMBO J* **15**:6262-6268.
22. **Helton, J. C., F. J. Davis, A. Saltelli, K. Chan, and E. M. Scott.** 2000. *Sampling-Based Methods*, p. 101-153. *Sensitivity Analysis*. John.
23. **Hentze, M. W., and L. C. Kuhn.** 1996. Molecular control of vertebrate iron metabolism: mRNA-based regulatory circuits operated by iron, nitric oxide, and oxidative stress. *Proc Natl Acad Sci U S A* **93**:8175-8182.
24. **Herynek, V., J. W. Bulte, T. Douglas, and R. A. Brooks.** 2000. Dynamic relaxometry: application to iron uptake by ferritin. *J Biol Inorg Chem* **5**:51-56.

25. **Hess, D. T., A. Matsumoto, S. O. Kim, H. E. Marshall, and J. S. Stamler.** 2005. Protein S-nitrosylation: purview and parameters. *Nat Rev Mol Cell Biol* **6**:150-166.
26. **Hlavacek, W. S., and M. A. Savageau.** 1995. Subunit structure of regulator proteins influences the design of gene circuitry: analysis of perfectly coupled and completely uncoupled circuits. *J Mol Biol* **248**:739-755.
27. **Howell, D.** 1987. *Statistical Methods for Psychology*. Duxbury Press, Boston.
28. **Huang, H., J. L. Rose, and D. G. Hoyt.** 2004. p38 Mitogen-activated protein kinase mediates synergistic induction of inducible nitric-oxide synthase by lipopolysaccharide and interferon-gamma through signal transducer and activator of transcription 1 Ser727 phosphorylation in murine aortic endothelial cells. *Mol Pharmacol* **66**:302-311.
29. **Irvine, D.** 1991. The Method of Controlled Mathematical Comparison, p. 90-109. *In* E. Voit (ed.), *Canonical Nonlinear Modeling. S-System Approach to Understanding Complexity*. Van Nostrand Reinhold, New York.
30. **Kakhlon, O., and Z. I. Cabantchik.** 2002. The labile iron pool: characterization, measurement, and participation in cellular processes. *Free Radic Biol Med* **33**:1037-1046.
31. **Kim, S., and P. Ponka.** 2002. Nitrogen monoxide-mediated control of ferritin synthesis: implications for macrophage iron homeostasis. *Proc Natl Acad Sci U S A* **99**:12214-12219.
32. **Kim, S., and P. Ponka.** 2003. Role of nitric oxide in cellular iron metabolism. *Biometals* **16**:125-135.
33. **Kim, S., S. S. Wing, and P. Ponka.** 2004. S-nitrosylation of IRP2 regulates its stability via the ubiquitin-proteasome pathway. *Mol Cell Biol* **24**:330-337.
34. **Konijn, A. M., H. Glickstein, B. Vaisman, E. G. Meyron-Holtz, I. N. Slotki, and Z. I. Cabantchik.** 1999. The cellular labile iron pool and intracellular ferritin in K562 cells. *Blood* **94**:2128-2134.
35. **Kosaka, H., and T. Shiga.** 1996. *Methods in nitric oxide research*. 373.
36. **Krombach, F., S. Munzing, A. M. Allmeling, J. T. Gerlach, J. Behr, and M. Dorger.** 1997. Cell size of alveolar macrophages: an interspecies comparison. *Environ Health Perspect* **105 Suppl 5**:1261-1263.
37. **Kwon, S., R. L. Newcomb, and S. C. George.** 2001. Mechanisms of synergistic cytokine-induced nitric oxide production in human alveolar epithelial cells. *Nitric*

Oxide **5(6)**:534-546.

38. **Lewis, R. S., and W. M. Deen.** 1994. Kinetics of the reaction of nitric oxide with oxygen in aqueous solutions. *Chem Res Toxicol* **7**:568-574.
39. **Llovera, M., J. D. Pearson, C. Moreno, and V. Riveros-Moreno.** 2001. Impaired response to interferon-gamma in activated macrophages due to tyrosine nitration of STAT1 by endogenous nitric oxide. *Br J Pharmacol* **132**:419-426.
40. **Lorsbach, R. B., W. J. Murphy, C. J. Lowenstein, S. H. Snyder, and S. W. Russell.** 1993. Expression of the nitric oxide synthase gene in mouse macrophages activated for tumor cell killing. Molecular basis for the synergy between interferon-gamma and lipopolysaccharide. *J Biol Chem* **268**:1908-1913.
41. **Marletta, M. A., P. S. Yoon, R. Iyengar, C. D. Leaf, and J. S. Wishnok.** 1988. Macrophage oxidation of L-arginine to nitrite and nitrate: nitric oxide is an intermediate. *Biochemistry* **27**:8706-8711.
42. **Marshall, H. E., K. Merchant, and J. S. Stamler.** 2000. Nitrosation and oxidation in the regulation of gene expression. *FASEB J* **14**:1889-1900.
43. **Marshall, H. E., and J. S. Stamler.** 2001. Inhibition of NF-kappa B by S-nitrosylation. *Biochemistry* **40**:1688-1693.
44. **Mateos, F., J. H. Brock, and J. L. Perez-Arellano.** 1998. Iron metabolism in the lower respiratory tract. *Thorax* **53**:594-600.
45. **McKay, M. D., W. J. Conover, and R. J. Beckman.** 1979. A comparison of three methods of selecting values of input variables in the analysis of output from a computer code. *Technometrics* **21**:239-245.
46. **McKinney, L. C., E. M. Aquilla, D. Coffin, D. A. Wink, and Y. Vodovotz.** 1999. Ionizing radiation potentiates the induction of nitric oxide synthase by IFN-gamma and/or LPS in murine macrophage cell lines: role of TNF-alpha. *J Leukoc Biol* **64(4)**:459-466.
47. **Meyer, J., N. Richter, and M. Hecker.** 1997. High-performance liquid chromatographic determination of nitric oxide synthase-related arginine derivatives in vitro and in vivo. *Anal Biochem* **247**:11-16.
48. **Miller, B. H., R. A. Fratti, J. F. Poschet, G. S. Timmins, S. S. Master, M. Burgos, M. A. Marletta, and V. Deretic.** 2004. Mycobacteria inhibit nitric oxide synthase recruitment to phagosomes during macrophage infection. *Infect Immun* **72**:2872-2878.
49. **Muijsers, R. B., N. H. t. Hacken, I. V. Ark, G. Folkerts, F. P. Nijkamp, and**

- D. S. Postma.** 2001. L-Arginine is not the limiting factor for nitric oxide synthesis by human alveolar macrophages in vitro. *Eur Respir J* **18**:667-671.
50. **Myers, J. T., A. W. Tsang, and J. A. Swanson.** 2003. Localized reactive oxygen and nitrogen intermediates inhibit escape of *Listeria monocytogenes* from vacuoles in activated macrophages. *J Immunol* **171**:5447-5453.
51. **Nathan, C., and M. U. Shiloh.** 2000. Reactive oxygen and nitrogen intermediates in the relationship between mammalian hosts and microbial pathogens. *Proc Natl Acad Sci U S A* **97**:8841-8848.
52. **Nelson, G., L. Paraoan, D. G. Spiller, G. J. Wilde, M. A. Browne, P. K. Djali, J. F. Unitt, E. Sullivan, E. Floettmann, and M. R. White.** 2002. Multi-parameter analysis of the kinetics of NF-kappaB signalling and transcription in single living cells. *J Cell Sci* **115**:1137-1148.
53. **Petrat, F., H. de Groot, R. Sustmann, and U. Rauen.** 2002. The chelatable iron pool in living cells: a methodically defined quantity. *Biol Chem* **383**:489-502.
54. **Recalcati, S., D. Conte, and G. Cairo.** 1999. Preferential activation of iron regulatory protein-2 in cell lines as a result of higher sensitivity to iron. *Eur J Biochem* **259**:304-309.
55. **Salimuddin, A. Nagasaki, T. Gotoh, H. Isobe, and M. Mori.** 1999. Regulation of the genes for arginase isoforms and related enzymes in mouse macrophages by lipopolysaccharide. *Am J Physiol* **277**:E110-117.
56. **Savageau, M. A.** 2002. Alternative designs for a genetic switch: analysis of switching times using the piecewise power-law representation. *Math Biosci* **180**:237-253.
57. **Savageau, M. A.** 2001. Design principles for elementary gene circuits: Elements, methods, and examples. *Chaos* **11**:142-159.
58. **Savageau, M. A.** 1996. Power-law formalism: A canonical nonlinear approach to modeling and analysis in World Congress of Nonlinear Analysts 92. **4 pp. 3323-3334.**
59. **Schaible, U., and S. Kaufmann.** 2004. Iron and microbial infection. *Nature Reviews Microbiology* **2**:946-953.
60. **Smith, J. J., A. R. O'Brien-Ladner, C. R. Kaiser, and L. J. Wesselius.** 2003. Effects of hypoxia and nitric oxide on ferritin content of alveolar cells. *J Lab Clin Med* **141**:309-317.
61. **Theil, E. C.** 2003. Ferritin: at the crossroads of iron and oxygen metabolism. *J*

Nutr **133**:1549S-1553S.

62. **Thomas, D. D., X. Liu, S. P. Kantrow, and J. R. L. Jr.** 2001. The biological lifetime of nitric oxide: implications for the perivascular dynamics of NO and O₂. *Proc Natl Acad Sci U S A* **98**:355-360.
63. **Thomson, A. M., J. T. Rogers, and P. J. Leedman.** 1999. Iron-regulatory proteins, iron-responsive elements and ferritin mRNA translation. *Int J Biochem Cell Biol* **31**:1139-1152.
64. **Voit, E.** 2000. *Computational Analysis of Biochemical Systems : A Practical Guide for Biochemists and Molecular Biologists.* Cambridge University Press.
65. **Wang, J., G. Chen, and K. Pantopoulos.** 2005. Nitric oxide inhibits the degradation of IRP2. *Mol Cell Biol* **25**:1347-1353.
66. **Weiss, G.** 2005. Modification of iron regulation by the inflammatory response. *Best Pract Res Clin Haematol* **18(2)**:183-201.
67. **Weiss, G., G. Werner-Felmayer, E. R. Werner, K. Grunewald, H. Wachter, and M. W. Hentze.** 1994. Iron regulates nitric oxide synthase activity by controlling nuclear transcription. *J Exp Med* **180**:969-976.
68. **Wesselius, L., W. Williams, K. Bailey, S. Vamos, A. O'Brien-Ladner, and T. Wiegmann.** 1999. Iron uptake promotes hyperoxic injury to alveolar macrophages. *Am J Respir Crit Care Med* **159**:100-106.
69. **Xie, Q. W., H. J. Cho, J. Calaycay, R. A. Mumford, K. M. Swiderek, T. D. Lee, A. Ding, T. Troso, and C. Nathan.** 1992. Cloning and characterization of inducible nitric oxide synthase from mouse macrophages. *Science* **256**:225-228.
70. **Ying, W. Z., H. Xia, and P. W. Sanders.** 2001. Nitric oxide synthase (NOS2) mutation in Dahl/Rapp rats decreases enzyme stability. *Circ Res* **89**:317-322.

Chapter 3

The Timing of TNF and IFN- γ Signaling Affects Macrophage Activation Strategies During *Mycobacterium tuberculosis* Infection

3.1 Introduction

During most bacterial infections, the population of host immune cells known as macrophages (M ϕ s) internalize and kill bacteria as an integral part of the innate immune response. However, during infection with *Mycobacterium tuberculosis* (Mtb), M ϕ s are both the preferred environment for growth (11) and the primary immune cell responsible for its control (reviewed in 9). Killing of Mtb by M ϕ s is impaired except under conditions of appropriate activation that occurs during adaptive immunity. In previous work we predicted that the evolution of M ϕ activation has favored a robust quiescent state to prevent excessive activation in most situations (41); however, this design may benefit Mtb infection.

In mouse models of Mtb infection, M ϕ s require at least two complementary activation signals to become effective at killing Mtb (12, 24). One of the signals, interferon (IFN)- γ , is secreted by activated T cells directly to the immunological synapse (28), which forms at the interface with antigen presenting cells such as M ϕ s. In contrast, tumor necrosis factor- α (TNF), a complementary signal to IFN- γ for effective Mtb killing by M ϕ s, was shown to be secreted multi-directionally from T cells (28), and is also produced by activated M ϕ s (17). Concentrations and distributions of cytokines at the site

of Mtb infection in the lungs are difficult or impossible to determine. Due to possible different spatial distributions of TNF and IFN- γ arising from their production pathways, timing of different activation signals received by the M ϕ may alter the kinetics of M ϕ activation and the success of responses to Mtb.

To test this hypothesis, we examined differences between three relevant M ϕ activation scenarios based on timing of receipt of the activating cytokine signals TNF and IFN- γ (Figure 3.1). The scenarios each posit a distinct possibility for when M ϕ s encounter these two cytokine signals in the course of an ongoing infection with adaptive immunity relative to when infection occurs. In Scenario 1, IFN- γ and TNF signals both precede infection of M ϕ s (i.e. when M ϕ s internalize Mtb). This case may occur during very strong immune responses with high systemic cytokine levels. In Scenario 2, M ϕ s receive a TNF signal before infection while targeted secretion of IFN- γ occurs concurrent with Mtb infection. This case represents activation from M ϕ -derived TNF flanking the infection site and/or targeted secretion preventing wide IFN- γ distribution. M ϕ s may also receive both TNF and IFN- γ at the time of infection (i.e. at the time of Mtb uptake; Scenario 3). This represents recruitment of monocytes (which become M ϕ s) directly to the site of infection without prior cytokine exposure. A fourth scenario, where IFN- γ is received before TNF, is omitted since targeted IFN- γ secretion combined with TNF derived from M ϕ s make this scenario unlikely. These scenarios may occur simultaneously in the same infection, but preferentially allowing favorable scenarios may represent an activation strategy for the host. A scenario without TNF and IFN- γ serves as a negative control (labeled Control in Figure 3.1). We use a simple mathematical model

describing M ϕ -Mtb interactions at the cellular level that is analogous to a M ϕ cell-culture system. Each scenario is determined by experimenter-controlled variables in the model. We measure the effectiveness of the scenarios by the number of Mtb within M ϕ s 100 hours post-infection in the model.

In mouse models, TNF and IFN- γ induce production of nitric oxide (NO), which is necessary for killing of Mtb (35). NO and some reactive nitrogen intermediates (RNIs) derived from it are effective at killing Mtb *in vitro* (55), but other anti-microbial molecules are not (7, 16, 35, 43, 52). NO or RNIs may also induce a latent phase of the Mtb growth cycle (13, 37). As previously described (41), nitric oxide production primarily involves three main functional activities in M ϕ s: activation signaling, transcriptional regulation of killing, and intracellular iron regulation. These M ϕ activities are connected by regulatory interactions that result in feedback (Figure 3.2).

Two intracellular signaling mechanisms are primarily involved in activation of NO production in M ϕ s: NF- κ B and Stat1. The NF- κ B pathway is induced by bacterial antigens (such as LPS or LAM; 20, such as LPS or LAM; 24, 33) or TNF (15, 36, 44) while Stat1 is activated by IFN- γ (1, 12, 18, 42). These two signal pathways synergistically activate inducible nitric oxide synthase (iNOS) (31), the enzymatic producer of NO.

Intracellular iron homeostasis is co-regulated with NO production (30, 54). This allows internalization of extracellular (transferrin-bound) iron into the intracellular labile iron pool (LIP), where it ultimately becomes chelated into ferritin (22). The LIP regulates C/EBP- β (NF-IL6), which is necessary, but not sufficient, for iNOS transcription (25).

Iron is also a limiting nutrient for growth of Mtb and other intracellular pathogens (48) and intracellular mycobacteria remove iron from the LIP (38).

Clearly, NO regulates many components of the M ϕ network. However, it is not clear from the literature whether regulation by NO and RNIs is inherently stimulatory or inhibitory (e.g.23). Previous analysis by our group suggests that feedback regulation of iNOS transcription by NO is primarily negative, occurring via three pathways: NF- κ B, Stat1, and iron regulation. One effect of the proposed negative feedback is optimization of several system properties when compared to positive feedback in the same pathway (41). Since the timing of M ϕ activation reflects possible host activation strategies, the kinetic effects of NO feedback may be important in Mtb infection.

The model we develop here expands our previous work (41). In that model we assumed general endotoxin (LPS) stimulation of the NF- κ B pathway. Here, we focus on Mtb-specific factors to study the parameters that determine clearance versus persistence in the interaction between macrophages and Mtb. To this end, we introduce a dynamic intracellular population of Mtb into the existing model (Figure 3.2). The ability of M ϕ s to kill Mtb via NO-mediated mechanisms may depend on timing of TNF and IFN- γ signaling. In addition to TNF and IFN- γ , Mtb-derived signals also contribute to M ϕ activation. We assume this to occur due to ManLAM, a complex glycolipid of Mtb, including the virulent H37Rv strain (6, 8). Lack of quantitative data for M ϕ responses to ManLAM prompted dose-response experiments performed herein for calibration of the model to M ϕ activation kinetics.

3.2 Materials and Methods

3.2.1 Dose-response experiments

In the mathematical model we assume that Mtb-derived signals contribute to activation via ManLAM-mediated NF- κ B induction (6, 8). In order to calibrate the M ϕ model response to ManLAM of virulent Mtb strains and to establish a cooperative NO response with IFN- γ , we performed dose-response experiments with the J774.16 M ϕ cell line (ATCC; Figures 3.2 and 3.A1). Doses of 0, 0.01, 0.1, 1, 10, and 100 μ g/ml ManLAM (Colorado State University, Fort Collins, CO) were treated along with 0, 0.01, 0.1, 1, 10, and 100 U/ml IFN- γ (Sigma) in triplicate for 96 hours in 96-well plates (Becton Dickinson) seeded with 1.5×10^5 M ϕ s/well. At appropriate times we used the Griess reagent assay to measure nitrite output as a proxy for NO production (10).

3.2.2 A macrophage network model with mycobacterial infection

We previously developed a mathematical model of the M ϕ response to activation signals (IFN- γ and the general endotoxin LPS) inducing killing mechanisms (iNOS/NO in the model) co-regulated with iron homeostasis apparatus (41). This model did not include a representation of infection. Here we introduce a population of Mtb that interacts with the existing M ϕ model framework to study how effectively this system kills Mtb under different signaling conditions, with ManLAM/TNF replacing LPS as the complementary signal to IFN- γ .

We represent each component of the model as a continuous entity in an ordinary differential equation. It is useful to think of this model as being analogous to a M ϕ cell culture system, with the results averaged over a large population of M ϕ s. The model is built with a non-dimensionalized form of the local and piecewise S-system

representations of the power law formalism (45, 47). Each of n molecular components of the system is described by a differential equation

$$\frac{dx_i}{dt} = a_i \underbrace{\prod_{j=1}^{n+m} x_j^{g_{ij}}}_{v_i^+} - a_i \underbrace{\prod_{j=1}^{n+m} x_j^{h_{ij}}}_{v_i^-}. \quad (1)$$

v_i^+ and v_i^- are aggregate power law fluxes describing the production and consumption of molecule x_i that may be affected by any of m independent variables. Parameter a_i is a turnover rate, always positive, that sets the speed of production and consumption.

Parameters g_{ij} and h_{ij} are kinetic orders (regulatory parameters) quantifying the effect of the variable x_j on the rate of x_i production and consumption, respectively. How a model component (variable) regulates a given flux is determined by the kinetic order: if $g_{ij} > 0$, x_j has a stimulatory effect on the flux v_i^+ ; if $g_{ij} < 0$ the effect is inhibitory; if $g_{ij} = 0$ then x_j does not regulate v_i^+ . Figure 3.2 illustrates the biochemical network with numerical indices for each variable and important parameters. We present the complete set of equations and parameter values in the Appendix. With the model in non-dimensional form, we report [NO], [LIP] and other molecular species as fold-induction above the basal steady state: $x_j = X_j/X_{j,0}$ (where X_j is the absolute concentration and $X_{j,0}$ is the quiescent steady state level).

Some terms in the model (i.e. production rates of NF- κ B, Stat1 and iNOS mRNA) require a piecewise representation due to a biphasic response in the data (c.f. two response phases in Figure 3.3), where we quantify the effects of LAM and IFN- γ on activation signaling over the entire range of experimentally determined nitrite outputs. In this case the rate terms have the same mathematical form but the parameters depend on

which IFN- γ dose range is used (Figure 3.3 shows the phases with model fit; Table 3.A2 gives parameter estimates of the fit).

3.2.3 Simulated *M. tuberculosis* infection

We represent Mtb infection as a single variable: an intracellular bacterial population subject to the effects of NO and iron levels in the M ϕ network. The equation representing bacterial kinetics has growth and death rates parameterized as power laws:

$$\frac{db}{dt} = \begin{cases} \alpha_b b x_6^{g_{bNO}} x_7^{g_{bLIP}} \left(1 - \frac{b}{b_{\max}}\right) - \beta_b b x_6^{h_{bNO}}, & x_7 \geq k_{bLIP} \\ \alpha_b b x_6^{g_{bNO}} \left(1 - \frac{b}{b_{\max}}\right) - \beta_b b x_6^{h_{bNO}}, & x_7 < k_{bLIP} \end{cases} \quad (2)$$

This representation is mathematically equivalent to a piecewise Generalized Mass Action representation of the power law formalism (46). The Mtb load is sensitive to NO levels due to growth rate inhibition (represented by the parameter g_{bNO}) and enhancement of the rate of death (represented by h_{bNO} ; Figure 3.2). This model phenomenologically captures several effects of NO/RNIs; for example, g_{bNO} captures a possible dormancy program in Mtb induced by NO (37, 53). The relative insensitivity of Mtb to superoxide and other non-RNI killing mechanisms (7, 16, 35, 43, 52) allows us to omit these effectors, which are more important against other pathogens (34). The effect of elevated intracellular iron (represented by g_{bLIP}) is stimulatory, capturing the effects of iron-gathering siderophores produced by Mtb (14). This effect saturates when iron is no longer the rate-limiting nutrient (40) at a level given by k_{bLIP} .

The variables representing NO (x_6) and the LIP (x_7) are scaled to accurately represent how these quantities affect Mtb growth. For simplicity, mycobacteria are

presumed to grow best in the absence of NO and to be sensitive to relatively small levels of it. Then $x_6 = 1$ (non-dimensional [NO] at the quiescent steady state) is the threshold for sensitivity of Mtb growth and death rates to NO. The LIP concentration giving the fastest growth defines the LIP saturation threshold, k_{bLIP} . The parameter g_{bLIP} scales the effect of the iron pool (in the sub-saturation range) on the rate of bacterial growth. The logistic term $\left(1 - \frac{b}{b_{\text{max}}}\right)$ ensures that the population does not exceed a plausible MOI, above a maximal population we set at 50 bacteria per cell (39, 56).

Iron is removed from the cellular LIP at a rate proportional to the number of bacteria. When bacterial levels drop below detectable levels (set by k_{LIPb}), this effect is absent. Sensitivity of iron pool levels to bacterial number is scaled by h_{LIPb} . We expect this parameter to be small (estimated at 0.05) to approximate the level of iron loss from Mφs (approximately 30%; 38). The resulting iron loss rate in the Mφ network is:

$$v_7^- = \begin{cases} a_7 x_7^{h_{77}} x_8^{h_{78}} (k_{\text{LIPb}} b)^{h_{\text{LIPb}}} & b > 1/k_{\text{LIPb}} \\ a_7 x_7^{h_{77}} x_8^{h_{78}} & b \leq 1/k_{\text{LIPb}} \end{cases} \quad (3)$$

3.2.4 Activation Signals

We introduce exogenous concentrations of TNF and IFN- γ into the model as independent variables (x_{11} and x_{12} , respectively). Each independent variable is scaled by a parameter d to interface with the non-dimensional network model. Intracellular Mtb also contributes to Mφ activation, assumed to be from stimulation by sloughed ManLAM. Since it is derived from the intracellular Mtb population, it is a function of the number of bacteria present. σ scales the Mtb population to capture the effect of ManLAM for

compatibility with the M ϕ model. The resulting terms for production of active NF- κ B (v_1^+) and Stat1 (v_2^+), which go into equations for x_1 and x_2 , are

$$\begin{aligned} v_1^+ &= a_1(\sigma b)^{g_{sb}} (d_{\text{TNF}}x_{11})^{g_{111}} x_6^{g_{16}} \\ v_2^+ &= a_2(d_{\text{IFN-}\gamma}x_{12})^{g_{212}} x_6^{g_{26}}. \end{aligned} \quad (4)$$

3.2.5 Parameter estimation

Specific choices of parameter values give the system quantitative characteristics and are required to solve the system on a computer (Table 3.A1). To calibrate the model and estimate unknown parameters, we modified the M ϕ network model (without Mtb) to include a variable representing nitrite accumulation from NO production, a modification to capture experiments performed herein. We also account for degradation of ManLAM and IFN- γ in cell culture. This allowed us to directly fit simulated nitrite dynamics to our dose-response experiments (Figure 3.A1). We account for the biphasic response in the model using a piecewise function for Stat1 and NF- κ B activation rate laws (described above). The fitted parameters (listed in Table 3.A2) were assigned an initial value based on previous work (41) and systematically adjusted by hand to achieve the fit¹ (Figure 3.3).

¹Two of the dose combinations (1 U/ml IFN- γ with 10 or 100 μ g/ml ManLAM) give model predictions lower than the experimental data. These data appear to be anomalously high in comparison to nitrite output at other doses (Figures 2 and A1 starred), and we attribute the discrepancy to experimental error.

3.2.6 Simulated infection and treatment protocols

Simulations employed a protocol where M ϕ s were treated with constant concentrations of TNF and/or IFN- γ as described in the 3 scenarios with infection of 1.5×10^5 bacteria at $t = 0$ hrs, (i.e. MOI = 1, or one bacillus per M ϕ , in analogy to a cell culture system; Figure 3.1). As a reference threshold of activation, TNF concentrations of 22 ng/ml and IFN- γ concentrations of 1 U/ml were simulated. We increased IFN- γ to 100 U/ml and/or TNF to 220 ng/ml in some simulations to determine the effects of variable cytokine doses. The concentrations of IFN- γ were chosen to represent a range from phase 2 of the dose response studies (Figure 3.3), where activation levels are likely bactericidal. TNF concentrations are known to be in the ng/ml range in tuberculosis patients (21). We chose the reference TNF dose to represent a high level of activation without dominating the response to IFN- γ .

For scenarios with TNF and/or IFN- γ stimuli preceding infection (c.f. Figure 3.1), the M ϕ system was brought to steady state before infection. We use the intracellular population of Mtb at $t = 100$ hrs post-infection as a measure of the effectiveness of M ϕ s at killing Mtb (i.e. the *infection outcome*). This time frame is similar to longer co-culture experiments here and elsewhere (5, 44).

3.2.7 Numerical simulations

After deriving the model, we solved the nonlinear ordinary differential equation S-system to obtain temporal dynamics for each element of the model. We used Mathematica (Wolfram Research) for most calculations, including an algorithm for uncertainty and sensitivity analysis and mathematically controlled comparisons (both

described below). Results derived with these algorithms were confirmed with a second differential equation solver in C++ implementing Runge-Kutta adaptive step-size solvers and appropriate finite difference methods. A Systems Biology Markup Language file of the model is available at <http://malthus.micro.med.umich.edu/lab/sbml.html>.

3.2.8 Uncertainty and sensitivity analysis

Parameters measured from experimental studies likely vary by experiment due to intrinsic errors of measurement and differences in experimental protocol. To explore the effects of uncertainty in the model, we evaluated it with a range of specific parameter values using *Latin hypercube sampling* (32). For this scheme, each parameter range was divided into 1000 equiprobable subintervals of a uniform distribution, randomly combined from each parameter to give 1000 parameter sets. Parameters g_{111} , g_{212} , b_{TNF} and $b_{\text{IFN-}\gamma}$ were held constant during this analysis to preserve relative levels of activation of Stat1 and NF- κ B pathways. Computing the numerical solution to these 1000 specific cases gives a statistical description of each model component at any time point, here using Mtb population at $t = 100$ hrs post-infection as the outcome measure. We determine statistical sensitivity by computing partial rank correlations (PRCs) between the outcome Mtb population and each varied parameter (4). These correlations vary between -1 and 1, with a significance test approximating a Student's T (4) to determine if the PRC is significantly different from zero. Each sampled parameter has its own correlation that we interpret to represent the sensitivity of the Mtb population to that parameter. A separate Z test (27) compares the relative correlations between different parameters and between the same parameter examined under different experimental conditions. To account for the

large number of varied parameters we corrected significance levels using the Bonferroni method (50).

3.2.9 Macrophage network characteristics and effective reduction of Mtb numbers

We previously used *mathematically controlled comparisons* (29) to predict the type of regulation (i.e. positive or negative) between important M ϕ network interactions (represented by the boldfaced regulatory parameters in Table 3.A1; see Figure 3.2).

These are based on evolutionary pressures represented by criteria for functional effectiveness (described below). This approach has been applied before with statistical techniques to study S-system behavior (3, 49).

With this method we compare the effect of positive regulation (+) versus no regulation (0) versus negative regulation (-) for each interaction in the M ϕ model to meet criteria for how the system best operates. It also allows comparisons for quantitative changes in each interaction constrained to one type of regulation (i.e. +/0/-). We previously analyzed the model without Mtb (41) using three criteria established for other inducible genetic circuits (26): *stability, robustness and responsiveness*. Stability refers to the ability of a system to return to steady state after a small change in component levels. Robustness means a relative insensitivity of model variables and production/consumption rates to perturbations in parameters and other external components. Finally, responsiveness in this case represents a fast temporal change in NO levels after activation signals, reaching an activated steady state as quickly as possible after induction.

For this study we define *response time* as the time for NO concentrations to reach half way to the activated steady state level (approximated by the level of NO 100 hours

post-infection). This definition captures the speed of response without penalizing for overshoot (of NO).

Mathematically controlled comparisons require *internal* and *external* equivalence of the system across changes in the parameter of interest (Schwacke & Voit, 2004 discuss these equivalence requirements in more detail). Internal equivalence is ensured by requiring that all terms in the mathematical model that are not involved in the interaction under study must have identical values. Meeting external equivalence requires correction of parameters in the rate term (V) containing the parameter of interest (p) as p is altered to ensure some equivalent external behavior of the system. To meet this requirement, the gain of iNOS from changes in TNF, IFN- γ and exogenous iron are held constant as the strength of the interaction changes. That is, the sum $L_s = L(X_4, X_{11}) + L(X_4, X_{12}) + L(X_4,$

$X_{17})$ must be constant, where $L(X_i, X_j) = \frac{\partial \ln \hat{X}_i}{\partial \ln \hat{X}_j}$ (the mathematical definition of gain in

this type of system, which may be positive or negative; \hat{X}_i denotes a quiescent or activated steady state level of X_i). For each interaction, we deduce a constrained, two-dimensional parameter space (41) with the interaction parameter under study and one other parameter in the same rate term V corrected for external equivalence. There is a line of equivalent gain in this parameter space found from L_s along which the parameters are varied for the comparison.

We now extend the analysis described above to include one further functional criterion, *bacterial control*: optimizing the reduction or killing of Mtb. We calculated bacterial load in the system at $t = 100$ hrs after infection for two kinds of changes in the parameters of interest. In some cases, we changed the interaction type ($-/0/+$) while for

others we changed the intensity of regulation for a specific interaction type. The type or level of regulation for each interaction that resulted in the lowest bacterial numbers represents the parameter value that optimally leads to a reduction in bacterial loads for that parameter.

3.3 Results

While macrophages are capable of effectively killing most pathogens, Mtb preferentially survives within them under certain conditions. Our goal is to determine why M ϕ s are poor at killing Mtb, and to predict conditions that optimize killing/reducing Mtb levels. Here we use a mathematical model to determine the effects of timing of the activation signals TNF and IFN- γ in achieving this goal.

3.3.1 Macrophage network characteristics that prevent effective Mtb killing

While negative regulation by NO optimizes stability, robustness and responsiveness of the M ϕ network, it does so by down-regulating iNOS transcription (41). To determine the effects of negative feedback on Mtb killing, we computed the predicted infection outcome (Mtb numbers 100 hours post-infection) under different feedback conditions. Parameters representing regulation of NF- κ B, Stat1 and iron regulatory apparatus were varied between positive, negative and lack of feedback using mathematically controlled comparisons. We then simulated each scenario (Figure 3.1) at the reference cytokine dosage (22 ng/ml TNF and 1 U/ml IFN- γ) for each type of regulation. We also performed this analysis for transcriptional signals to confirm that this method gives results in agreement with known types of iNOS regulation. We present one

interaction in detail (NO feedback to NF- κ B: g_{16} ; Figure 3.4) to show our methodology and summarize the other results in Table 3.1.

Table 3.1 shows that the predicted type of regulation that minimizes Mtb numbers for NO feedback to NF- κ B is positive, which suggests that positive feedback optimizes Mtb killing. This is also true for another case regarding NO regulation of iron regulatory apparatus (parameter h_{96}), while NO feedback to Stat1 (g_{26}) is neutral to infection outcome (Table 3.1). These results contradict our previous predictions that negative feedback is optimal in each case for the other criteria for M ϕ function in the uninfected form of the model (c.f. Table 3.1 and Ray & Kirschner (41)). Therefore, the type of regulation by NO in the M ϕ network that optimizes other functional criteria does not improve bacterial control (Mtb killing) in comparison to other types of regulation, and in some cases is antagonistic toward killing. We now show how the timing of activation, signals relative to when infection occurs, can compensate for this effect.

3.3.2 Activation signals concurrent with infection counteract the antagonistic effects of negative feedback

While the previous results suggest that negative feedback regulation by NO in M ϕ s reduces the effectiveness of killing, the sensitivity of Mtb to this effect may depend on the timing of activation signals. Since feedback likely affects kinetics of activation, we hypothesized that the timing of activation signals may benefit from the kinetic advantages of negative feedback. To test this, we performed sensitivity analysis that correlates the number of Mtb 100 hours post-infection (the infection outcome) with changes in the strength of each parameter in the model, preserving the qualitative type of regulation (+ or -) for all parameters. The resulting correlations indicate the sensitivity of Mtb to each

varied interaction (see Section 3.2.8 for details). We calculated these correlations separately for each activation scenario (Figure 3.1).

The total number of parameters that significantly correlate with the infection outcome is reduced from 9 for Scenario 1 (i.e. TNF and IFN- γ introduction preceding infection; the significant parameters are β_b , g_{16} , g_{26} , g_{31} , g_{32} , g_{37} , h_{96} , h_{97} and h_{bNO} as defined in Table 3.A1) to 6 of these 9 for Scenario 2 (i.e. TNF introduction preceding infection; the significant parameters are β_b , g_{26} , g_{31} , g_{32} , h_{96} , and h_{bNO}) and 4 of the 9 for Scenario 3 (i.e. TNF and IFN- γ introduction concurrent with infection; the significant parameters are β_b , g_{31} , g_{32} , and h_{bNO}). Since the only difference between these scenarios is the timing of TNF and IFN- γ , competing effects may ‘cancel out’ the sensitivity of some parameters in Scenario 2 and 3 due to activation kinetics. To test this, we examined the effect of each scenario on sensitivities to NO feedback parameters.

Table 3.2 shows statistical sensitivities of Mtb infection outcome to each NO feedback parameter. Each non-zero sensitivity is negative. Since the parameters are negative (representing negative feedback), a negative sensitivity here represents an effect that reduces the effectiveness of Mtb killing. Each of the sensitivities is significantly smaller than zero in Scenario 1. Scenario 2 shows a reduced effect for two of the parameters (feedback to Stat1 and IRP; $p < 0.01$ in a Z test versus Scenario 1 sensitivities) and no sensitivity to feedback to NF- κ B. In Scenario 3, none of the three sensitivities is significantly different from zero. These changes in sensitivity between the three scenarios suggest that the timing of activation signals has an effect on the role of NO regulatory effects in Mtb killing, where activation concurrent with infection relaxes the undermining effects of these signals.

3.3.3 Dynamics that benefit cytokine signals concurrent with infection

While negative feedback speeds response times in all the tested scenarios, NO production by M ϕ s is initially lower in Scenarios 2 and 3 as compared to Scenario 1. Therefore the effects of NO in the M ϕ system do not consistently favor Mtb killing. This may create a dependency on fast response times that favors strong negative feedback. We hypothesized that the dynamics of M ϕ activation in the initial hours post-infection may neutralize the effects of negative feedback that reduces the effectiveness of Mtb killing.

To test this hypothesis, we investigate the effects of the parameter representing NO feedback to NF- κ B (g_{16}) using mathematically controlled comparisons. For brevity we explore only this parameter, but the effects hold qualitatively for NO feedback to Stat1 (g_{26}) and iron regulation (h_{96}) as well. To determine the specific effect of feedback to NF- κ B in each scenario, we varied g_{16} using mathematically controlled comparisons as described in Methods (Figure 3.5). As the feedback becomes more strongly negative (i.e. g_{16} from -0.5 to -2.0), the response time of NO levels (measured here as the time, in hours, required to reach half [NO] at $t = 100$) is unchanged for the scenario with no exogenous cytokine signals (Control). Scenario 1 improves on this response time only for very strong negative feedback (Figure 3.5A), while response times readily improve for Scenarios 2 and 3 (Figures 3.5B and 3.5C, respectively)². This result suggests that strong negative feedback preferentially benefits M ϕ activation in scenarios with delayed activation signals (Scenario 3).

² We also found response times to be improved for stronger negative feedback in parameter sets not exhibiting the overshoot effect seen in Figure 3.5 (not shown).

3.3.4 Strong negative feedback improves relative bacterial killing with activation concurrent with Mtb infection compared to other scenarios

Due to the combination of costs and benefits of negative feedback, we hypothesized that higher cytokine concentrations received concurrent with infection can compensate for antagonistic effects of feedback on Mtb killing by M ϕ s.

To test this hypothesis, we examined Mtb numbers at 100 hours post-infection for each activation scenario as we varied levels of feedback to NF- κ B using mathematically controlled comparisons (Figure 3.6). This was done at two simulated cytokine concentrations, representative of the reference dose used throughout (1 U/ml IFN- γ and 22 ng/ml TNF; Figure 3.6A) and a case with IFN- γ concentration elevated to 100 U/ml (Figure 3.6B). We repeated this analysis for elevated TNF concentrations with each IFN- γ concentration with similar results (not shown).

For a given level of feedback, Mtb killing is nearly identical between all three activation scenarios at the lower cytokine dose (Figure 3.6A). For elevated IFN- γ dosing and strongly negative feedback (Figure 3.6B), IFN- γ concurrent with infection (Scenario 2) shows somewhat enhanced killing over IFN- γ preceding infection (Scenario 1). Scenario 3 shows a much larger improvement in killing, with higher levels of negative feedback becoming beneficial to killing beyond a certain level (Figure 3.6B). This coincides with high levels of NO overshoot beyond the activated steady state level for this activation scenario (e.g. Figure 3.5C), suggesting a mechanism for this effect.

Therefore, in scenarios with cytokine signaling that is timed to coincide with infection, M ϕ s perform at least as well at Mtb killing as scenarios with signaling preceding infection at equal concentrations. High cytokine doses can improve killing in

Scenarios 2 and 3 under strong negative feedback, with sufficient overshoot of NO reversing the antagonistic effects of NO on Mtb killing.

3.4 Discussion

M ϕ s require complementary activation signals (TNF or bacterial antigens and IFN- γ) to achieve a bactericidal state during infection with Mtb. Different sources for TNF (produced by M ϕ s and T cells) and IFN- γ (which undergoes targeted secretion by T cells) may reflect a host strategy to prevent superfluous perturbation of surrounding tissues. However, the timing of these activation signals may affect the outcome of Mtb infection.

We simplified a range of possible activation kinetics into three scenarios based on timing of TNF and IFN- γ signals that M ϕ s receive relative to when they become infected (i.e. take up Mtb; Figure 3.1). The effects of these scenarios were tested with a mathematical model representing important M ϕ activities known to interact with intracellular Mtb in mouse models (Figure 3.2). This model was calibrated to extensive dose-response experiments (Figures 3.3 and 3.A1) to establish a reasonable kinetic response for production of NO, a major anti-mycobacterial effector molecule.

To prevent excessive activation while still allowing high NO levels when necessary, the M ϕ network must balance a quiescent state with the rare need to reach high levels of activation. To this end a series of negative feedback loops modulate NO production (Figure 3.2). However, one possible effect of negative feedback is that effective Mtb killing by M ϕ s is reduced when compared to positive feedback (Table 3.1 and Figure 3.4).

The mathematical model predicts a reduced effect of negative feedback by NO in scenarios where TNF and/or IFN- γ signals are introduced concurrent with Mtb infection (Table 3.2). Strengthening the feedback (i.e. making NO regulation of NF- κ B more negative by making the parameter g_{16} more negative) also speeds M ϕ responses after infection in scenarios where receipt of TNF and/or IFN- γ signals coincides with infection (Figure 3.5). This suggests the importance of improved response times allowed by negative feedback in Scenarios 2 and 3.

This result depends on the interpretation of response times as rise times of NO, which permits the system to be capable of high overshoots that may be detrimental to overall system function. Our previous results suggest that this system allows high NO production if the appropriate signals are present (41). Based on this activation model, we suggest that overproduction of NO is acceptable in circumstances with multiple activation signals.

We also find a possible advantage of this overshoot. Under conditions of strengthened feedback to NF- κ B (i.e. parameter $g_{16} < -1.25$), the model predicts enhanced killing of Mtb by M ϕ s at high cytokine concentrations for Scenarios 2 and 3 compared to Scenario 1. This effect is particularly apparent for Scenario 3, where TNF and IFN- γ signals occur concurrent with infection of M ϕ s (Figure 3.6), and coincides with the predicted overshoot of NO production. This indicates an advantage of the initial burst of NO levels permitted by negative feedback after infection.

During the course of pulmonary infection with Mtb, multiple signals from cell-mediated adaptive immunity induce migration of M ϕ s along with T cells to the lung leading to the formation of immune structures called granulomas (2). M ϕ s that have

ingested Mtb at the site of infection can present antigen to T cells, which, upon activation constitute a rich source of TNF and IFN- γ (reviewed in 19). The most frequent clinical outcome of pulmonary Mtb infection is a latent infection that represents a stable co-existence of host and pathogen. We have emphasized the functional consequences of host M ϕ activation strategies from the perspective of optimizing Mtb killing, but our results also suggest a mechanism for establishing latent infections. The most effective host activation strategy may be recruitment of M ϕ s directly into the granuloma (with cytokine signaling as in Scenario 3 in Figure 3.1), and prevention of this strategy may favor Mtb growth (for instance, via loss of vascular points of M ϕ entry in regions of Mtb-induced necrosis). An ongoing immune response at the periphery of a granuloma prevents bacterial dissemination in most cases. However, M ϕ s migrating to the site of infection from flanking lung tissues (possibly encountering cytokines as in Scenarios 1 and 2 in Figure 3.1) are more likely to permit some Mtb growth, thus striking a balance favorable to a latent infection state (Figure 3.7).

A role for the timing of events from M ϕ activation has been proposed to tip the balance between host-pathogen interactions in different contexts (e.g. 51). In the case of Mtb infection, our model suggests that late activation is an optimal pathogen killing strategy. Experimental Mtb infection of M ϕ s with cytokine signals timed as in each of the scenarios here can test our predictions. These results also call for the integration of theoretical and experimental approaches to understand the temporal and spatial roles of signaling and macrophage migration in Mtb granuloma formation.

Figures

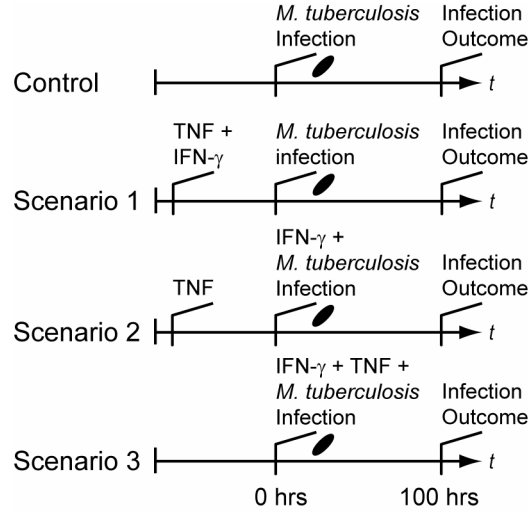


Figure 3.1. Simulated experimental scenarios for macrophage activation that depend on the timing of IFN- γ and TNF signaling relative to infection. “Infection Outcome” refers to the success or failure of macrophage responses, measured by the number of intracellular bacteria. In Scenario 1, TNF and IFN- γ signaling precedes infection. Scenario 2 represents targeted secretion of IFN- γ at the time of infection with TNF stimulation preceding. Scenario 3 represents TNF and IFN- γ signaling both concurrent with infection. The control scenario represents no cytokines present as is the case during an innate response. In this case the only activation signal is derived from mycobacteria during infection. After macrophages initially receive a given signal, we assume that signal is persistent.

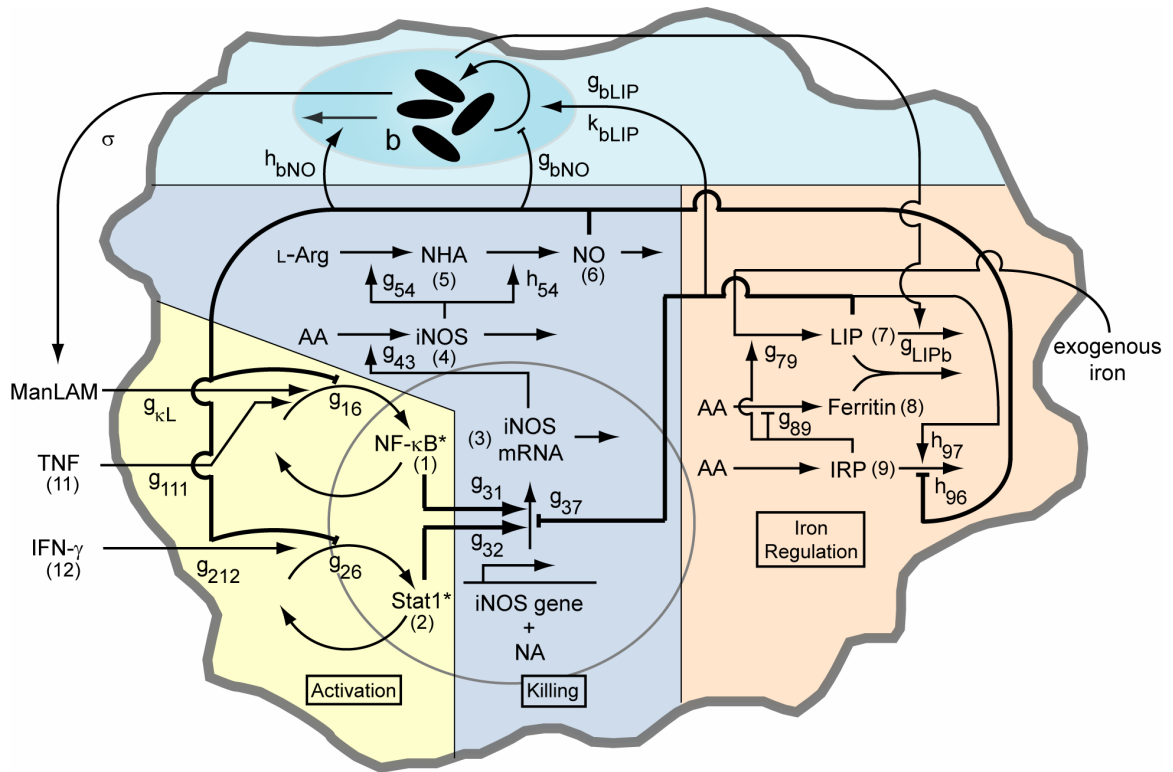


Figure 3.2. Macrophage network schematic including interactions with an intracellular population of *Mycobacterium tuberculosis* (b) with parameter names and variable numbers depicted. Numbers in parentheses refer to the variable number of the component (e.g. (1) refers to x_1 , (11) refers to x_{11} , etc). Parameters g_{ij} and h_{ij} quantify network interaction types (stimulation or inhibition of a process by a cellular component) and interactions with the bacterial population. See Table 3.A1 for parameter definitions and values. The model is analogous to a cell culture experiment, with these interactions averaged over a large population of macrophages. The biochemical model (Activation, Killing and Iron Regulation) was previously analyzed without a representation of bacteria in (41).

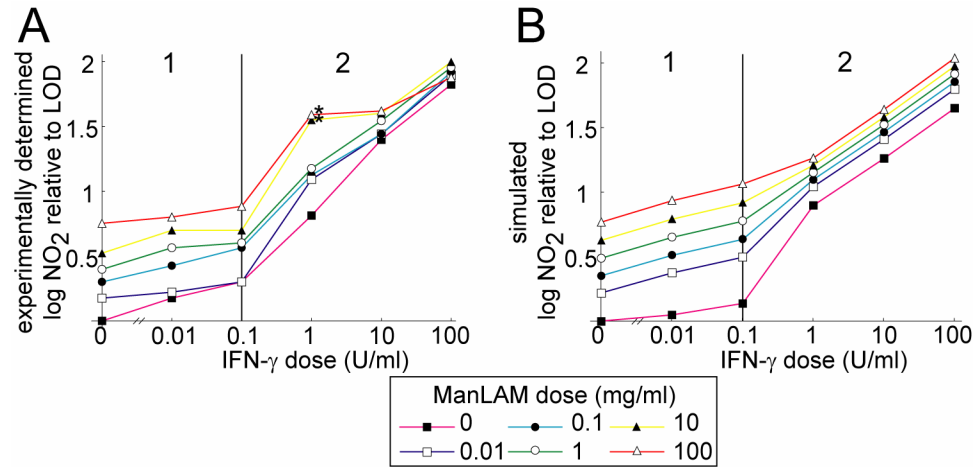


Figure 3.3. Calibration of the model to dose-response of ManLAM and IFN- γ . A. Cumulative nitrite output of J774.16 macrophages at 96 h after treatment with a wide range of ManLAM and IFN- γ doses. Note two distinct response phases based on the dose of IFN- γ , marked 1 and 2. B. Simulated cumulative nitrite production at 96 h after treatment reproduces experimental trends. A version of the mathematical model without *M. tuberculosis* infection simulated the cell culture experiment. LOD: limit of detection for nitrite. The two asterisks denote dose levels excluded from the fitting (see Footnote 1 in the text).

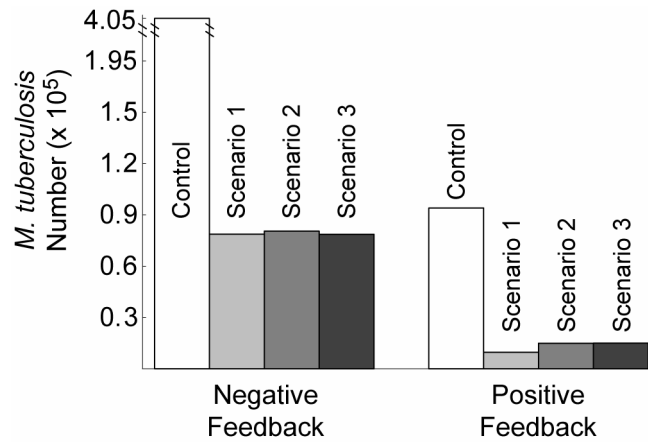


Figure 3.4. Greater survival of *M. tuberculosis* in macrophages with negative feedback to NF- κ B by NO compared to positive feedback. The feedback parameter (g_{16}) was changed between negative (-0.75) and positive (0.75) using mathematically controlled comparisons. *M. tuberculosis* numbers represent the population of Mtb in 1.5×10^5 M ϕ s at 100 hours post-infection. Control: no cell-mediated immunity. In Scenario 1, TNF and IFN- γ signaling precedes infection. Scenario 2 represents targeted secretion of IFN- γ at the time of infection with TNF stimulation preceding. Scenario 3 represents TNF and IFN- γ signaling both concurrent with infection. See Figure 3.1 for details of the scenarios.

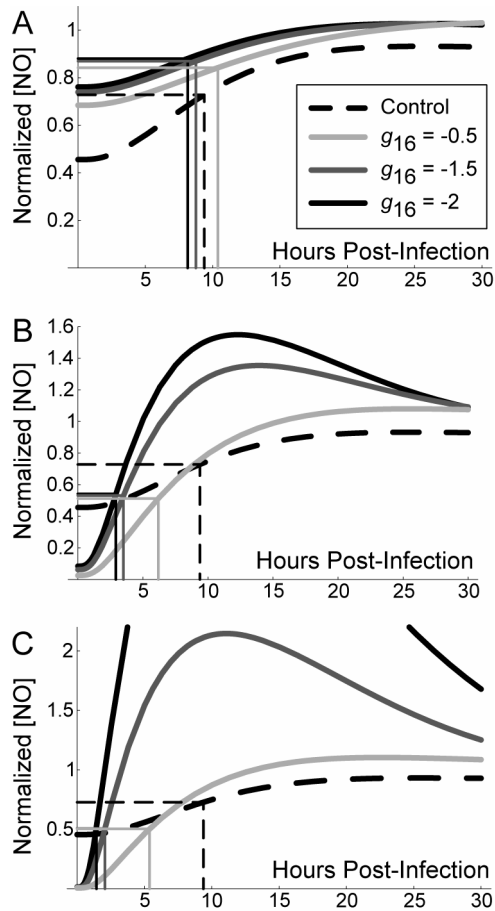


Figure 3.5. Stronger negative feedback improves macrophage activation time during infection with *M. tuberculosis*. Graphs depict the first 30 hours post-infection to show initial kinetics. The level of negative feedback to NF- κ B by nitric oxide (represented in the model by parameter g_{16}) was varied using mathematically controlled comparisons. A. TNF and IFN- γ signals preceding infection (Scenario 1). B. Targeted secretion of IFN- γ restricting it to the site of infection (Scenario 2). C. Initial cytokine stimulus concurrent with infection time (Scenario 3). We found the control scenario (without cell-mediated immunity; dashed line in A, B and C) to be constant over variations in the level of feedback; we therefore use it as a reference point between scenarios. Rectangles depict the response time (number of hours for nitric oxide concentration to reach half the level at 100 hours post-infection) for each case. Nitric oxide levels are normalized in each scenario by the level at 100 hours post-infection. See Figure 3.1 for scenarios.

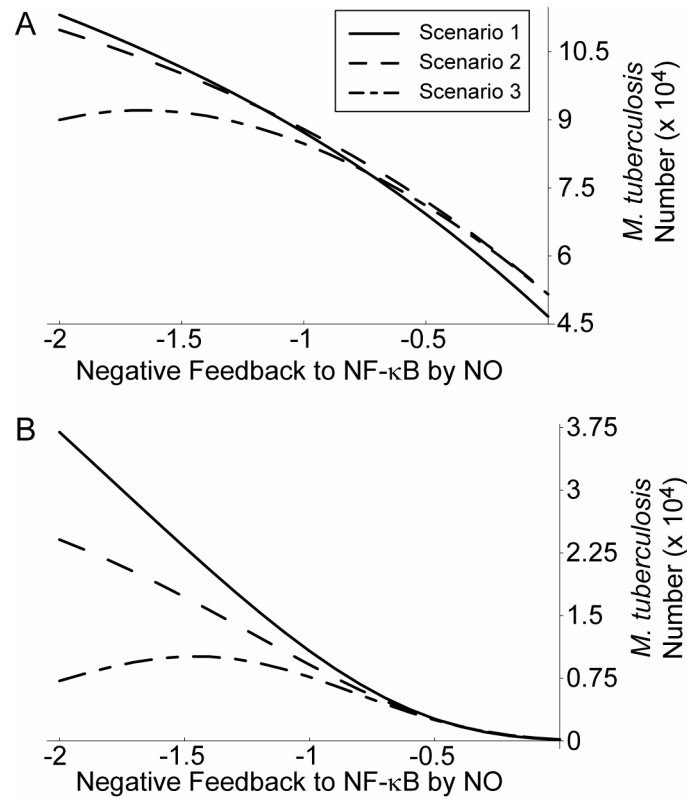


Figure 3.6. High cytokine concentrations that do not precede infection enhance killing under strong negative feedback. A. Level of Mtb killing for three macrophage activation scenarios with cytokine concentrations of 22 ng/ml TNF and 1 U/ml IFN- γ . B. Mtb killing for three activation scenarios with 22 ng/ml TNF and 100 U/ml IFN- γ . Scenario 1: TNF and IFN- γ signaling precedes infection. Scenario 2: targeted secretion of IFN- γ at the time of infection with TNF stimulation preceding. Scenario 3: TNF and IFN- γ signaling both concurrent with infection. See Figure 3.1 for details of the scenarios.

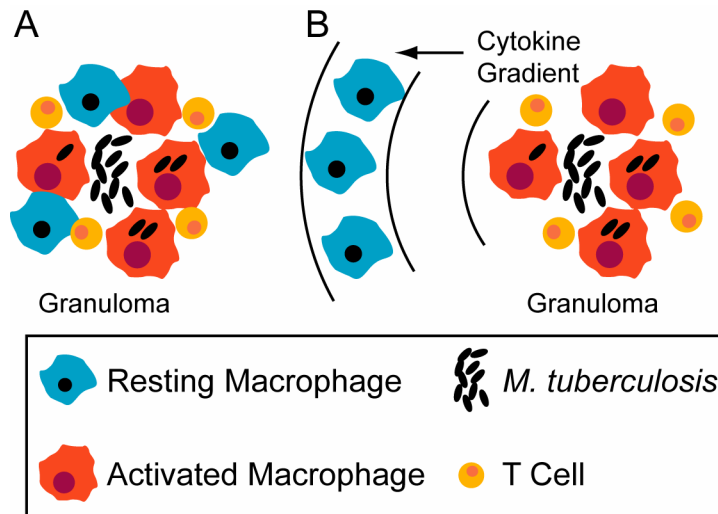


Figure 3.7. Recruitment scenarios that tip the balance between bacterial killing and persistence based on timing of activation signals. A. Recruitment of blood monocytes (that become macrophages) directly to a granuloma from localized vascular sources may favor effective bacterial killing. B. Recruitment of macrophages from surrounding lung tissue may result in some level of activation preceding infection, favoring latent infection.

Tables

Table 3.1. Macrophage regulatory interactions optimizing killing of *M. tuberculosis* and temporal responsiveness

	Transcriptional regulation of iNOS by:			Nitric oxide feedback to:		
	NF- κ B (<i>g</i> ₃₁)	Stat1 (<i>g</i> ₃₂)	LIP ¹ (<i>g</i> ₃₇)	NF- κ B (<i>g</i> ₁₆)	Stat1 (<i>g</i> ₂₆)	IRP ² (<i>h</i> ₉₆)
Optimal Killing ³	+	+	–	+	≈ ⁴	+
Optimal Response Time ⁵	+	+	–	–	–	–

¹ Regulation occurs indirectly via C/EBP- β *in vivo*.

² IRP: Iron response protein. See Figure 3.2.

³ In all scenarios with cell-mediated immunity.

⁴ All Mtb numbers within 5% for positive (+), null (0) and negative (–) feedback.

⁵ Other criteria for macrophage function also conform to this result (48).

Table 3.2. Sensitivity of *M. tuberculosis* numbers (100 hours post-infection) to quantitative variations in regulatory interactions

Partial Rank Correlations with Mtb #	NO regulation of: ¹		
	NF- κ B	Stat1	IRP ²
Control	-0.214	-0.146	-0.330
Scenario 1	-0.236	-0.300	-0.347
Scenario 2	NS	-0.134	-0.154
Scenario 3	NS	NS	NS

* $p < 0.01$. The far right bracket for each parameter denotes significant differences between Control and each numbered scenario. The remaining two brackets denote significant changes between the three numbered scenarios. NS: not significantly different from zero ($p > 0.01$).

¹Due to *negative* regulation by these interactions, correlations with negative signs are interpreted to mean that stronger negative regulation reduces the effectiveness of *M. tuberculosis* killing.

²IRP: Iron response protein. See Figure 3.2.

3.5 Appendix

Complete specification of the mathematical model. The definition of each variable and parameter can be found in Section 3.2, Figures 2 and A1, and Tables A1 and A2. The effects of some precursors (e.g. amino acids) are omitted for clarity.

$$\frac{dx_1}{dt} = a_1[(\sigma b)^{g_{\kappa B}} (d_{\text{TNF}} x_{11})^{g_{111}} x_6^{g_{16}} - x_1]$$

$$\frac{dx_2}{dt} = a_2[(d_{\text{IFN-}\gamma} x_{12})^{g_{212}} x_6^{g_{26}} - x_2]$$

$$\frac{dx_3}{dt} = a_3[x_1^{g_{31}} x_2^{g_{32}} x_3^{g_{37}} - x_3]$$

$$\frac{dx_4}{dt} = a_4[x_3^{g_{43}} - x_4]$$

$$\frac{dx_5}{dt} = a_5[x_3^{g_{54}} - x_4^{h_{54}} x_5]$$

$$\frac{dx_6}{dt} = a_6[x_4^{h_{64}} x_5 - x_6]$$

$$\frac{dx_7}{dt} = a_7 x_{17}^{g_{717}} x_9^{g_{79}} - \begin{cases} a_7 x_7 x_8^{h_{78}} (k_{\text{LIP}b} b)^{h_{\text{LIP}b}} & b > 1/k_{\text{LIP}b} \\ a_7 x_7 x_8^{h_{78}} & b \leq 1/k_{\text{LIP}b} \end{cases}$$

$$\frac{dx_8}{dt} = a_8[x_9^{g_{89}} - x_7 x_8]$$

$$\frac{dx_9}{dt} = a_9[1 - x_6^{h_{96}} x_7^{h_{97}} x_9]$$

$$\frac{db}{dt} = \begin{cases} \alpha_b b x_6^{g_{b\text{NO}}} x_7^{g_{b\text{LIP}}} \left(1 - \frac{b}{b_{\text{max}}}\right) - \beta_b b x_6^{h_{b\text{NO}}}, & x_7 \geq k_{b\text{LIP}} \\ \alpha_b b x_6^{g_{b\text{NO}}} \left(1 - \frac{b}{b_{\text{max}}}\right) - \beta_b b x_6^{h_{b\text{NO}}}, & x_7 < k_{b\text{LIP}} \end{cases}$$

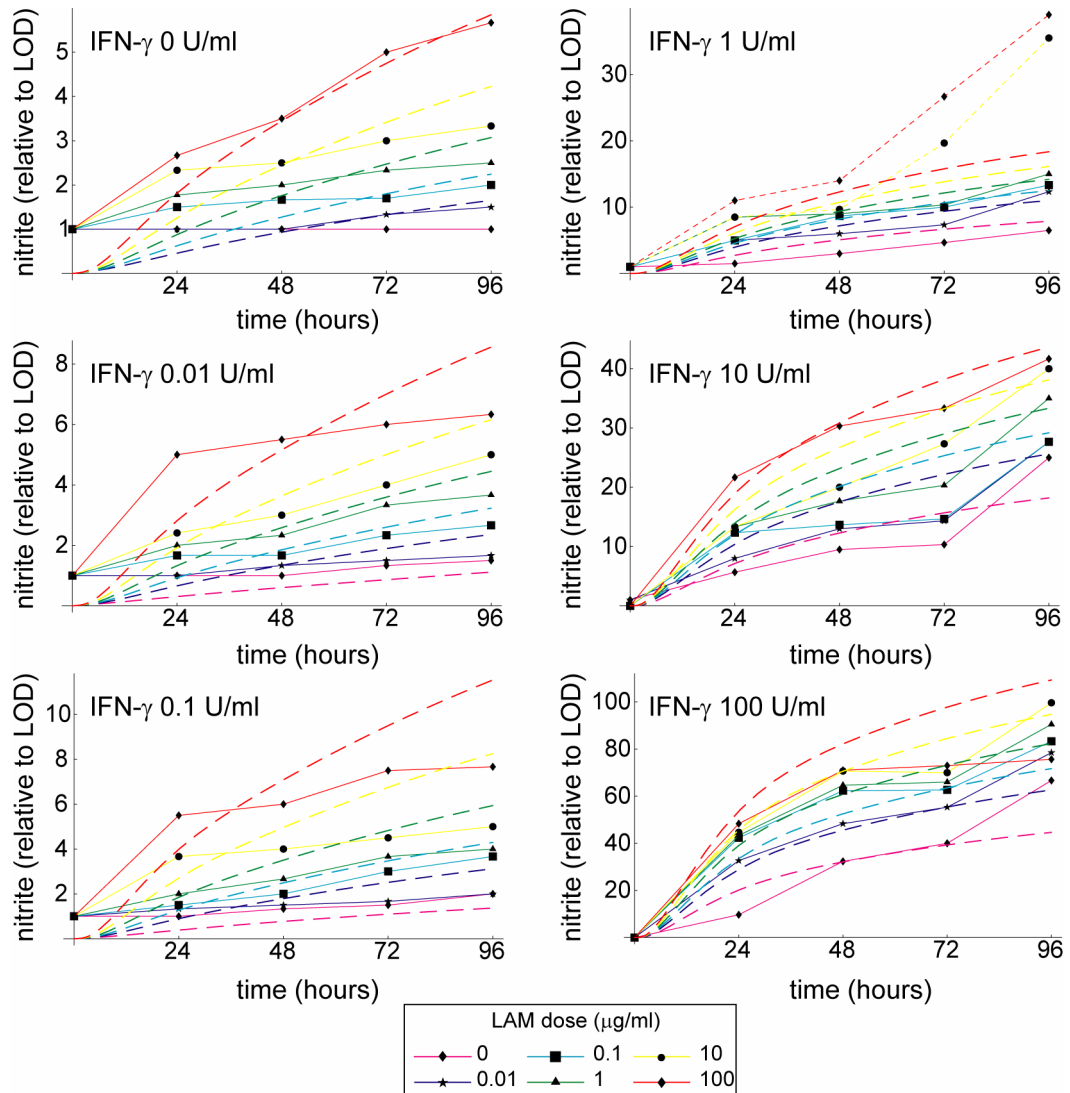


Figure 3.A1. Simulations and experimental data shown as time series over 96 hours. The mathematical model reproduces experimental trends over the entire 96 hour time frame. Dashed lines represent simulated nitrite output for various LAM doses, while solid lines with data squares represent experimental data. The two dotted lines represent dose levels excluded from the fitting (see Footnote 1 in the main text).

Table 3.A1. Definitions and estimates of model parameters. Boldfaced parameters are the focus of the analysis.

Effect	Parameter	Est'd Value	LHS Range ^a	References
NF-κB turnover	a_1	2.4 h ⁻¹	[0.01, 50]	(30)
Stat1 turnover	a_2	2.77 h ⁻¹	[0.01, 50]	(25)
iNOS mRNA turnover	a_3	0.173 h ⁻¹	[0.116, 0.347]	(48)
iNOS turnover	a_4	0.0693 h ⁻¹	[0.0365, 0.693]	(48)
NHA turnover	a_5	5.545 μmol/h	[5.454, 332.711]	(48)
NO turnover	a_6	2.773 h ⁻¹	[2.727, 166.355]	(48)
LIP turnover	a_7	32.201 μmol/h	[2.565, 61.820]	(48)
Ferritin turnover	a_8	40.0 μmol/h	[4, 89]	(48)
IRP turnover	a_9	35.0 μmol ⁻¹ h ⁻¹	[29.17, 44.06]	(48)
NF-κB reg. by TNF	g_{111}	1.18	Not Varied	(23)
TNF conc. scaling	b_{TNF}	117.4	Not Varied	(23)
Stat1 reg. by IFN-γ	g_{212}	cf. Table 3.2	Not Varied	cf. Table 3.2
IFN-γ conc. scaling	$b_{IFN-γ}$	20	Not Varied	cf. Table 3.2
NF-κB txn reg.	g_{31}	1.46	[0.1, 1.5]	cf. Table 3.2
Stat1 txn reg.	g_{32}	0.26	[0.1, 1]	cf. Table 3.2
LIP txn reg.	g_{37}	-0.177	[-0.1, -2]	(48)
NO feedback to NF-κB	g_{16}	-0.672	[-0.3, -1.5]	(26); cf. Table 3.2
NO feedback to Stat1	g_{26}	-0.5	[-0.3, -1.5]	(48)
Translation	g_{43}	1	Not Varied	(48)
Arg→NHA reg.	g_{54}	1	Not Varied	(48)
NHA→NO reg.	h_{54}	1	Not Varied	(48)
reg. of iron influx	g_{79}	0.5	[0.1, 1.5]	(48)
LIP sequestration	h_{78}	0.74	Not Varied	(34)
IRP reg. of ferritin	g_{89}	-0.645	[-0.1, -2]	(48)
LIP → Ferritin	h_{87}	1	Not Varied	(48)
NO reg. of IRP	h_{96}	-0.5	[-0.1, -1]	(48)
LIP reg. of IRP	h_{97}	0.5	[0.4, 2]	(48)
Mtb growth rate	α_b	0.0250 Mtb/h	[0.0191, 0.0385]	Avg. of (21, 37, 59, 64)
NO reg. of Mtb growth	g_{bNO}	-0.5	[-0.3, -1.5]	Initial guess
Iron enhancement of Mtb growth	g_{bLIP}	1	[0.3, 1.0]	Initial guess
Iron effect saturation	k_{bLIP}	1	[0.1, 2]	Initial guess
Intrinsic Mtb death rate	β_b	2.5×10^{-4} Mtb/h	[2.5×10^{-5} , 2.5×10^{-4}]	1 % of α_b
Killing by NO	h_{bNO}	0.75	[0.1, 2]	Initial guess ^b
NF-κB reg. by LAM	$g_{κL}$	cf. Table 3.2	Not Varied	cf. Table 3.2
Sloughed LAM	σ	120 Mtb ⁻¹	[10, 10000]	(43)
Scaling of Mtb on LIP	k_{LIPb}	10^6 Mtb ⁻¹	Not Varied	Initial guess
Effect of Mtb on LIP	h_{LIPb}	0.05	[0.1, 0.001]	Initial guess
Maximum Mtb per Mφ	b_{max}	50 Mtb/Mφ	Not Varied	Guess from (46, 64)

^aLHS: Latin hypercube sampling.

^bCalibrated to achieve approximately 50% killing at the default cytokine dose for default parameter values.

Table 3.A2. Parameter estimates from dose response experiments

Phase	IFN- γ dose	NF- κ B activation by LAM ($g_{\kappa L}$)	Stat1 activation by IFN- γ (g_{212})	iNOS activation by NF- κ B (g_{31})	iNOS activation by Stat1 (g_{32})	NO feedback to NF- κ B (g_{16})
A	≤ 0.1 U/ml	0.2	1.0	1.46	0.26	-0.672
B	> 0.1 U/ml	0.2	2.5	0.5	0.26	-1.5
Phase	IFN- γ dose	LAM half-life in culture (k_{LAM}) ¹	IFN- γ half-life in culture ($k_{IFN-\gamma}$) ¹	Scaling constant for LAM (d_{LAM}) ¹	Scaling constant for IFN- γ ($d_{IFN-\gamma}$)	
A	≤ 0.1 U/ml	0.025	0.035	500	20	
B	> 1 U/ml	0.025	0.035	500	20	

¹Parameter required to accurately fit the model to the data, but not needed for simulations in the main text.

3.6 References

1. **Aaronson, D. S., and C. M. Horvath.** 2002. A road map for those who know JAK-STAT. *Science* **296**:1653-1655.
2. **Algood, H., J. Chan, and J. Flynn.** 2003. Chemokines and tuberculosis. *Cytokine & Growth Factor Reviews* **14**:467-477.
3. **Alves, R., and M. A. Savageau.** 2000. Extending the method of mathematically controlled comparison to include numerical comparisons. *Bioinformatics* **16**:786-798.
4. **Blower, S. M., and H. Dowlatabadi.** 1994. Sensitivity and Uncertainty Analysis of Complex Models of Disease Transmission: an HIV Model, as an Example. *Int Stat Rev* **62**:229-243.
5. **Bonecini-Almeida, M. G., S. Chitale, I. Boutsikakis, J. Geng, H. Doo, S. He, and J. L. Ho.** 1998. Induction of in vitro human macrophage anti-*Mycobacterium tuberculosis* activity: requirement for IFN-gamma and primed lymphocytes. *J Immunol* **160**:4490-4499.
6. **Brown, M. C., and S. M. Taffet.** 1995. Lipoarabinomannans derived from different strains of *Mycobacterium tuberculosis* differentially stimulate the activation of NF- κ B and KBF1 in murine macrophages. *Infect Immun* **63**:1960-1968.
7. **Bryk, R., P. Griffin, and C. Nathan.** 2000. Peroxynitrite reductase activity of bacterial peroxiredoxins. *Nature* **407**:211-215.
8. **Chan, E. D., K. R. Morris, J. T. Belisle, P. Hill, L. K. Remigio, P. J. Brennan, and D. W. Riches.** 2001. Induction of Inducible Nitric Oxide Synthase-NO[•] by Lipoarabinomannan of *Mycobacterium tuberculosis* Is Mediated by MEK1-ERK, MKK7-JNK, and NF- κ B Signaling Pathways. *Infect Immun* **69**:2001-2010.
9. **Chan, J., and J. Flynn.** 2004. The immunological aspects of latency in tuberculosis. *Clin Immunol* **110**:2-12.
10. **Chan, J., Y. Xing, R. S. Magliozzo, and B. R. Bloom.** 1992. Killing of virulent *Mycobacterium tuberculosis* by reactive nitrogen intermediates produced by activated murine macrophages. *J Exp Med* **175**:1111-1122.
11. **Collins, H. L., and S. H. Kaufmann.** 2001. The many faces of host responses to tuberculosis. *Immunology* **103**:1-9.

12. **Cooper, A., D. Dalton, T. Stewart, J. Griffin, D. Russell, and I. Orme.** 1993. Disseminated tuberculosis in interferon gamma gene-disrupted mice. *J Exp Med* **178**:2243-2247.
13. **Couture, M., S. Yeh, B. Wittenberg, J. Wittenberg, Y. Ouellet, D. Rousseau, and M. Guertin.** 1999. A cooperative oxygen-binding hemoglobin from *Mycobacterium tuberculosis*. *Proc Natl Acad Sci U S A* **96**:11223-11228.
14. **DeVoss, J. J., K. Rutter, B. G. Schroeder, H. Su, Y. Zhu, and C. E. Barry3rd.** 2000. The salicylate-derived mycobactin siderophores of *Mycobacterium tuberculosis* are essential for growth in macrophages. *Proc Natl Acad Sci U S A* **97**:1252-1257.
15. **Ding, A., C. Nathan, and D. Stuehr.** 1988. Release of reactive nitrogen intermediates and reactive oxygen intermediates from mouse peritoneal macrophages. Comparison of activating cytokines and evidence for independent production. *J Immunol* **141**:2407-2412.
16. **Ehrt, S., M. U. Shiloh, J. Ruan, M. Choi, S. Gunzburg, C. Nathan, Q. Xie, and L. W. Riley.** 1997. A novel antioxidant gene from *Mycobacterium tuberculosis*. *J Exp Med* **186**:1885-1896.
17. **Eilers, A., and T. Decker.** 1995. Activity of Stat family transcription factors is developmentally controlled in cells of the macrophage lineage. *Immunobiology* **193**:328-333.
18. **Flesch, I., and S. Kaufmann.** 1987. Mycobacterial growth inhibition by interferon-gamma-activated bone marrow macrophages and differential susceptibility among strains of *Mycobacterium tuberculosis*. *J Immunol* **138**:4408-4413.
19. **Flynn, J. L., and J. Chan.** 2001. Immunology of tuberculosis. *Annu Rev Immunol* **19**:93-129.
20. **Fujihara, M., M. Muroi, K. Tanamoto, T. Suzuki, H. Azuma, and H. Ikeda.** 2003. Molecular mechanisms of macrophage activation and deactivation by lipopolysaccharide: roles of the receptor complex. *Pharmacol Ther* **100**:171-194.
21. **Grebenchtchikov, N., J. van der Ven-Jongekrijg, G. J. Pesman, A. Geurts-Moespot, J. W. van der Meer, and F. C. Sweep.** 2005. Development of a sensitive ELISA for the quantification of human tumour necrosis factor-alpha using 4 polyclonal antibodies. *Eur Cytokine Netw* **16**:215-222.
22. **Harrison, P. M., and P. Arosio.** 1996. The ferritins: molecular properties, iron storage function and cellular regulation. *Biochim Biophys Acta* **1275**:161-203.

23. **Hattori, Y., K. Kasai, and S. Gross.** 2004. NO suppresses while peroxynitrite sustains NF-[kappa]B: a paradigm to rationalize cytoprotective and cytotoxic actions attributed to NO. *Cardiovascular Research* **63**:31-40.
24. **Heldwein, K. A., and M. J. Fenton.** 2002. The role of Toll-like receptors in immunity against mycobacterial infection. *Microbes Infect* **4**:937-944.
25. **Hentze, M. W., and L. C. Kuhn.** 1996. Molecular control of vertebrate iron metabolism: mRNA-based regulatory circuits operated by iron, nitric oxide, and oxidative stress. *Proc Natl Acad Sci U S A* **93**:8175-8182.
26. **Hlavacek, W. S., and M. A. Savageau.** 1995. Subunit structure of regulator proteins influences the design of gene circuitry: analysis of perfectly coupled and completely uncoupled circuits. *J Mol Biol* **248**:739-755.
27. **Howell, D.** 1987. *Statistical Methods for Psychology*. Duxbury Press, Boston.
28. **Huse, M., B. r. Lillemeier, M. Kuhns, D. Chen, and M. Davis.** 2006. T cells use two directionally distinct pathways for cytokine secretion. *Nature Immunology* **7**:247-255.
29. **Irvine, D.** 1991. The Method of Controlled Mathematical Comparison, p. 90-109. *In* E. Voit (ed.), *Canonical Nonlinear Modeling. S-System Approach to Understanding Complexity*. Van Nostrand Reinhold, New York.
30. **Kim, S., and P. Ponka.** 2003. Role of nitric oxide in cellular iron metabolism. *Biomaterials* **16**:125-135.
31. **Lorsbach, R. B., W. J. Murphy, C. J. Lowenstein, S. H. Snyder, and S. W. Russell.** 1993. Expression of the nitric oxide synthase gene in mouse macrophages activated for tumor cell killing. Molecular basis for the synergy between interferon-gamma and lipopolysaccharide. *J Biol Chem* **268**:1908-1913.
32. **McKay, M. D., W. J. Conover, and R. J. Beckman.** 1979. A comparison of three methods of selecting values of input variables in the analysis of output from a computer code. *Technometrics* **21**:239-245.
33. **Means, T. K., S. Wang, E. Lien, A. Yoshimura, D. T. Golenbock, and M. J. Fenton.** 1999. Human toll-like receptors mediate cellular activation by *Mycobacterium tuberculosis*. *J Immunol* **163**:3920-3927.
34. **Miller, R., and B. Britigan.** 1997. Role of oxidants in microbial pathophysiology. *Clin Microbiol Rev* **10**:1-18.

35. **Nathan, C., and M. U. Shiloh.** 2000. Reactive oxygen and nitrogen intermediates in the relationship between mammalian hosts and microbial pathogens. *Proc Natl Acad Sci U S A* **97**:8841-8848.
36. **Nathan, C. F., H. W. Murray, M. E. Wiebe, and B. Y. Rubin.** 1983. Identification of interferon-gamma as the lymphokine that activates human macrophage oxidative metabolism and antimicrobial activity. *J Exp Med* **158**:670-689.
37. **Ohno, H., G. Zhu, V. Mohan, D. Chu, S. Kohno, W. Jacobs, and J. Chan.** 2003. The effects of reactive nitrogen intermediates on gene expression in *Mycobacterium tuberculosis*. *Cell Microbiol* **5**:637-648.
38. **Olakanmi, O., L. S. Schlesinger, A. Ahmed, and B. E. Britigan.** 2002. Intraphagosomal *Mycobacterium tuberculosis* acquires iron from both extracellular transferrin and intracellular iron pools. Impact of interferon-gamma and hemochromatosis. *J Biol Chem* **277**:49727-49734.
39. **Paul, S., P. Laochumroonvoranpong, and G. Kaplan.** 1996. Comparable growth rates of virulent and avirulent *Mycobacterium tuberculosis* in human macrophages *in vitro*. *J Infect Dis* **177**:1723.
40. **Raghu, B., G. R. Sarma, and P. Venkatesan.** 1993. Effect of iron on the growth and siderophore production of mycobacteria. *Biochem Mol Biol Int* **31**:341-348.
41. **Ray, J. C. J., and D. E. Kirschner.** 2006. Requirement for multiple activation signals by anti-inflammatory feedback in macrophages. *J Theor Biol* **241**:276-294.
42. **Rook, G., J. Steele, M. Ainsworth, and B. Champion.** 1986. Activation of macrophages to inhibit proliferation of *Mycobacterium tuberculosis*: comparison of the effects of recombinant gamma-interferon on human monocytes and murine peritoneal macrophages. *Immunology* **59**:333-338.
43. **Ruan, J., G. S. John, S. Ehrt, L. Riley, and C. Nathan.** 1999. noxR3, a novel gene from *Mycobacterium tuberculosis*, protects *Salmonella typhimurium* from nitrosative and oxidative stress. *Infect Immun* **67**:3276-3283.
44. **Sato, K., T. Akaki, and H. Tomioka.** 1998. Differential potentiation of anti-mycobacterial activity and reactive nitrogen intermediate-producing ability of murine peritoneal macrophages activated by interferon-gamma (IFN-gamma) and tumour necrosis factor-alpha (TNF-alpha). *Clin Exp Immunol* **112**:63-68.
45. **Savageau, M. A.** 2002. Alternative designs for a genetic switch: analysis of switching times using the piecewise power-law representation. *Math Biosci* **180**:237-253.

46. **Savageau, M. A.** 2001. Design principles for elementary gene circuits: Elements, methods, and examples. *Chaos* **11**:142-159.
47. **Savageau, M. A.** 1996. Power-law formalism: A canonical nonlinear approach to modeling and analysis in World Congress of Nonlinear Analysts 92. **4 pp. 3323-3334.**
48. **Schaible, U. E., and S. H. E. Kaufmann.** 2004. Iron and microbial infection. *Nature Reviews Microbiology* **2**:946-953.
49. **Schwacke, J., and E. Voit.** 2004. Improved methods for the mathematically controlled comparison of biochemical systems. *Theor Biol Med Model* **1**.
50. **Shaffer, J. P.** 1995. Multiple Hypothesis Testing. *Ann. Rev. Psych.* **46**:561-584.
51. **Shaughnessy, L. M., and J. A. Swanson.** 2007. The role of the activated macrophage in clearing *Listeria monocytogenes* infection. *Front Biosci* **12**:2683-2692.
52. **Springer, B., S. Master, P. Sander, T. Zahrt, M. McFalone, J. Song, K. G. Papavinasasundaram, M. J. Colston, E. Boettger, and V. Deretic.** 2001. Silencing of oxidative stress response in *Mycobacterium tuberculosis*: expression patterns of *ahpC* in virulent and avirulent strains and effect of *ahpC* inactivation. *Infect Immun* **69**:5967-5973.
53. **Voskuil, M., K. Visconti, and G. Schoolnik.** 2004. *Mycobacterium tuberculosis* gene expression during adaptation to stationary phase and low-oxygen dormancy. *Tuberculosis (Edinb)* **84**:218-227.
54. **Weiss, G., G. Werner-Felmayer, E. R. Werner, K. Grunewald, H. Wachter, and M. W. Hentze.** 1994. Iron regulates nitric oxide synthase activity by controlling nuclear transcription. *J Exp Med* **180**:969-976.
55. **Yu, K., C. Mitchell, Y. Xing, R. S. Magliozzo, B. R. Bloom, and J. Chan.** 1999. Toxicity of nitrogen oxides and related oxidants on mycobacteria: *M. tuberculosis* is resistant to peroxynitrite anion. *Tuber Lung Dis* **79**:191-198.
56. **Zhang, M., J. Gong, Y. Lin, and P. Barnes.** 1998. Growth of Virulent and Avirulent *Mycobacterium tuberculosis* Strains in Human Macrophages. *Infect Immun* **66**:794-799.

Chapter 4

Roles of Tumor Necrosis Factor Signaling in Granuloma Formation During *Mycobacterium tuberculosis* Infection

4.1 Introduction

Tuberculosis (TB) kills more people per year than any other infectious disease. Infection by its causative agent, *Mycobacterium tuberculosis* (Mtb), results in active disease in only a minority of cases (~10%) –the majority of cases result in control of infection, where the host remains infected indefinitely, but clinically silent (reviewed in 10). Latently infected hosts are a reservoir of Mtb, sustaining epidemics through reactivation of latent infection that results in active and contagious TB.

The classic feature of pulmonary Mtb infection arises during the immune response where aggregates of immune cells and bacteria, called granulomas, form in the lungs. In humans and non-human primates with latent pulmonary infection, granulomas form as well-circumscribed masses in the lung parenchyma comprised of resting, infected and activated macrophages with a characteristic cuff of T cells on the periphery (e.g. 6, 35) and a caseous necrotic center (25). Macrophages within a granuloma have dual roles in Mtb infection: they are the primary mechanism for Mtb containment and the preferred location for bacterial growth. At the level of a single granuloma, macrophages may fail to control infection, leading to necrotic granulomas harboring large numbers of bacteria within macrophages (7). However, the relationship between bacterial control in a single

granuloma and the outcome of infection at the level of the entire host is not well established (7).

Type-1 adaptive immunity is required to control infection at the host level. In this type of response, activated T cells migrate to the site of infection and act as immune effectors. We distinguish three primary T cell types based on their effector function (c.f. 17). Pro-inflammatory T cells (which may be CD4⁺ or CD8⁺) provide macrophage-activating cytokines (e.g. IFN- γ) while cytotoxic T cells (predominantly CD8⁺) provide cytolytic functions to control infection (reviewed in 10). A third T cell class, regulatory T cells (T_{reg}), are also present in mouse (28) and human (14) Mtb infections, and may prevent efficient Mtb clearance by immune responses (31, 38). T_{reg} are CD4⁺Foxp3⁺ cells that comprise approximately 5-10% of all CD4⁺ T cells (2, 40). They suppress the action of pro-inflammatory T cells (45) through poorly understood mechanisms that may occur by cell-contact, secretion of immunosuppressive cytokines (3), or both.

The pro-inflammatory cytokine tumor necrosis factor- α (TNF) is a central, multi-faceted contributor to the immune response in Mtb infection (4, 5, 11, 27, 30) that is produced by activated macrophages and pro-inflammatory T cells. The role of TNF is of great clinical interest due to the association of anti-inflammatory TNF-blocking drugs with reactivation of latent TB in humans (19, 50). TNF is also necessary for Mtb containment in mouse models (11). TNF gene-disrupted mice have disorganized granulomas in Mtb infections (4), underscoring the link between granuloma structure and effective containment of infection.

TNF has multiple known immunological functions during infection with Mtb (Figure 4.1A). First, TNF has a direct role in cell recruitment via up-regulation of

endothelial adhesion molecules (54), facilitating trans-endothelial migration of immune cells to the site of infection. Second, TNF also upregulates production of chemokines by macrophages (1, 37) that further induce trans-endothelial migration (reviewed in 47) and coordinate recruitment (reviewed in 42) of immune cells. Third, TNF activates macrophages in a manner complementary to the type-1 cytokine IFN- γ (8, 9, 39); such activated macrophages can kill intracellular mycobacteria. Fourth, TNF induces necrotic and apoptotic cell death in macrophages (24) that is promoted by Mtb infection (18). Figure 4.1A summarizes these effects.

The effects of TNF in Mtb granuloma formation therefore are likely intimately related to the chemokine network induced during infection. We have identified a simplified model of chemokines based on three classes that affect recruitment of macrophages and T cells to the granuloma via binding of appropriate chemokine receptors on the cell surface (Figure 4.1B). The α -chemoattractant class (CXCL9,10, and 11; formerly Mig, IP-10 and I-TAC, respectively) binds chemokine receptor CXCR3 on pro-inflammatory CD4⁺ and CD8⁺ T cells (29), but not regulatory T cells (22). CCL2 (formerly MCP-1) binds CCR2 on macrophages (46) and proportions of pro-inflammatory T cell populations (34). CCL5 (formerly RANTES) binds CCR5 on macrophages and T cells, and is necessary for migration of regulatory T cells to the site of other infections (52), although this has not been demonstrated for Mtb.

The multiple roles of the pro-inflammatory cytokine TNF in granuloma formation raises the question of how competing factors act to affect control of infection. Each of the four roles of TNF (cellular migration, induction of chemokine/TNF secretion, macrophage activation and apoptosis) may contribute separately to establishing and

maintaining control of Mtb infection at the level of a single granuloma. Currently, it is impossible to experimentally study these separate TNF functions at this level of detail.

Here we use a specific type of computer model known as an agent-based model (ABM) to study the contributions of these immune effectors on granuloma formation. The model used here is based on one developed previously by Segovia-Juarez et al (41), which we have extended to include relevant effects of TNF, different T cell classes and a simple chemokine network. The usefulness of a computational approach for this type of system lies in its ability to capture multiple spatial and temporal scales of dynamics, with appropriate representations of immune cells (discrete entities), bacteria and molecules (continuous entities) in a spatial coordinate system (Figure 4.2). This allows us to manipulate and study specific factors in a way that is not currently attainable with experiments.

We used the model to assess the specific effects of individual TNF activities on Mtb infection at the level of a single granuloma, distinguishing which mechanisms in the system lead to control of Mtb growth versus uncontrolled bacterial growth within a granuloma. We also attempt to distinguish the roles of TNF in the initial granuloma formation versus maintenance (i.e. long-term control) of established granulomas.

4.2 Methods

4.2.1 Hybrid agent-based model

The model presented here is an extension of a previous ABM simulating cellular interactions leading to granuloma formation during infection with Mtb (41). The model is considered hybrid since it utilizes both discrete entities (cells) and continuous entities (chemokines, TNF and Mtb) simultaneously. ABMs are developed based on four considerations: an environment, agents that reside there, the rules that describe the agents and their interactions, and the timescales on which events are defined. We give an overview of these areas below with the complete list of rules in Appendix 4.5.

As in the previous model (41), the *environment* represents a 2 mm x 2 mm slice of lung parenchyma as a 100 x 100 square 2-dimensional lattice with individual micro-compartments scaled to the approximate size of a single macrophage: 20 μm in diameter (23). Discrete agents move on the lattice and respond to their environment based on rules representing their individual biological activities. Bacteria and effector molecules can reside anywhere on the lattice and undergo diffusion when appropriate.

We include two types of discrete *agents* in the model: macrophages and T cells. As previously (41), macrophage agents assume different states as follows: resting (M_r), infected (M_i ; have taken up bacteria), chronically infected (M_{ci} ; are unable to clear their intracellular bacterial load), and activated (M_a ; can effectively kill bacteria). In contrast to our previous study (41), where a single T cell class phenomenologically captured all cell behaviors, here we represent three distinct T cell subpopulations as defined in the introduction: the T_γ class captures $CD4^+$ and $CD8^+$ pro-inflammatory T cells; T_c represent cytotoxic T cells; and T_{reg} represent regulatory T cells.

In addition to movement and placement of cells on the grid, each micro-compartment also contains environmental variables that are affected by local conditions. These include the number of extracellular bacteria, levels of diffusing effector molecules (CCL2, CCL5, CXCL9/10/11 and TNF), the number of activated or infected macrophage deaths that occur in a micro-compartment, if that space is designated a vascular source, and whether or not the micro-compartment has become caseous.

Caseation represents inflammation of, and damage to, the lung parenchyma from macrophage cell death. We note a change of terminology to “caseation” from “necrosis” in previous work (41), as strict necrosis within the granuloma is now believed to be caused by substantial neutrophil infiltration and death while caseation is likely initiated by macrophage death (unpublished data, JoAnne L. Flynn).

Cells respond to local conditions according to *rules* that represent known activities *in vivo*. During simulations, each agent responds depending on its state. Examples of rules include uptake of bacteria, macrophage activation by T cells, secretion of cytokines and chemokines, etc. For a full list of rules, see Appendix 4.5.

4.2.2 Initial conditions and timescales

At the beginning of a simulation, the grid has 105 randomly placed resident resting macrophages (M_r) moving randomly with no chemokine or cytokine present. Infection is initiated with one infected macrophage (M_i), containing 15 bacteria, placed at the center. Every 10 minutes of simulation time, positions and interactions between T cells and macrophages are updated, including recruitment from vascular sources and secretion of TNF and chemokines if appropriate. The resulting landscape of molecular

concentrations serves as the initial condition for computing cytokine and chemokine diffusion for 10 minutes of simulation time. Cell states and interactions are then updated again, in the beginning of the next 10-minute timestep in an asynchronous fashion, and continues in this way for 200 days (2,880,000 6s timesteps) of simulation time.

4.2.3 Uncertainty and sensitivity analyses

The lung environment presents a difficult system for accurate estimation of rate and probability parameters, leading to a high level of *epistemic* uncertainty; that is, the relevant probabilities and rates are not well-established. Simultaneously, randomness from probabilities in the model results in uncertainty in the outcome for a given parameter set (*aleatory* uncertainty). Due to the high number of model parameters (rates and probabilities) and uncertainty with the model, exhaustive exploration of parameter space is impractical. However, the technique of Latin hypercube sampling (LHS) allows high-efficiency variation of all relevant parameters, which allows model outputs (such as immune cell and bacterial numbers, granuloma size, etc) to be described statistically.

Statistical sensitivity analysis allows the quantification of each uncertain parameter by correlating several outcome variables (c.f. Tables 4.A1-4.A2) with variations in each parameter, to compute a partial rank correlation (PRC). One PRC exists for each parameter-variable pair, varies between -1 and 1 , and represents the strength of relationship between the parameter and outcome variable of interest. Details of these methods are outlined in Appendix 4.6.

4.2.4 Simulated deletion and depletion of TNF activities

In order to examine the effect of individual TNF activities on granuloma formation and maintenance, we performed deletions and depletions of relevant parameters using a baseline parameter set that leads to control of infection (Tables 4.1-4.3). *Deletion* refers to loss of the activity from the beginning the simulation at the onset of infection. *Depletion* refers to the loss of the activity after the establishment of a stable granuloma, 100 days post-infection. The timing of the depletion was determined by examining the results of sensitivity analysis and the baseline control scenario. Parameter sensitivities in the model stabilize by day 50 (c.f. Results), suggesting that 100 days post-infection represents a reasonable time for an established, stable granuloma. Significant differences between outcome variables were determined with a mean difference test (Welch's approximate t test) for 15 repeated simulations of each single deletion or depletion, and for 10 repeated simulations in deletion or depletion of two or more TNF activities simultaneously. We present more details on this procedure in Appendix 4.6.

4.2.5 Programming and simulations

The model was written in C++, with the code based on (41) and (36). Simulations were run on a computer with dual Intel Xeon quad-core processors, each 200 day simulation taking about one hour, with simulations terminated if/when complete bacterial elimination was reached. Sensitivity analysis of resulting simulations was performed using Matlab (The MathWorks, Inc). Time-lapse movies and data visualizations were programmed in Java or created using Mathematica (Wolfram Research).

4.3 Results

4.3.1 Simulated infections and granuloma formation

The agent-based model presented here predicts the dynamics of Mtb infection on the level of a single granuloma. To establish baseline behavior of the model, we identified a reference parameter set (Tables 4.1-4.3; see Methods) that leads to a controlled bacterial population (Figure 4.3A, white bars). This scenario results in a granuloma that has a tightly packed mass of cells, predominantly resting macrophages (green agents in Figure 4.3B), with T cell localization at the periphery of the granuloma (pink, purple, and light blue agents in Figure 4.3B). The model is robust in that for 15 repeated runs of the ABM using the reference parameter set, each individual simulation led to controlled infection, with none of the simulations predicting uncontrolled bacterial growth.

A simulated infection with all parameters set to the control scenario but lacking TNF (i.e. a TNF deletion; see Methods) shows the effect of TNF on granuloma formation in the model and serves as an example of a granuloma that is unable to contain bacterial growth. Numbers of extracellular Mtb in this scenario are significantly higher than the bacterial control scenario 20 days post-infection ($p < 0.01$) and all time points thereafter (Figure 4.3A, gray bars). Simulations result in an irregular, larger granuloma with widespread caseation (Figure 4.3C). Numbers of all macrophage and T cell populations in the model are significantly elevated in comparison to the control scenario within the first 20 days after infection as well (not shown). Therefore, loss of TNF may impair early control of infection, resulting in more extensive immune cell infiltration; this matches data from

murine models of Mtb infection (1), and provides a positive control for the model with respect to the requirement for TNF to control infection.

4.3.2 Attainable granuloma outcomes in the agent-based model

To determine the attainable types of granuloma outcomes in the model, we used uncertainty analysis to explore different parameter combinations. A sampling of 250 parameter sets from Table 4.1 (each replicated 4 times for 1000 total simulations; see Methods) yielded a distribution of extracellular Mtb numbers at day 200 as shown in Figure 4.4. Approximately half the parameter sets predict complete elimination of bacteria. This outcome is intuitive: most (~70%) humans exposed to Mtb do not become infected (43). The remaining simulation outcomes are distributed across nearly the entire range of attainable bacterial populations, which has an upper limit of 2.2×10^6 if every micro-compartment in the simulation carries the maximum number of bacteria. This range of extracellular Mtb numbers suggests a fair sampling of attainable simulation outcomes from the uncertainty analysis. Spatially, we observe a wide range of granuloma structures attainable for different bacterial levels (Figure 4.A1).

4.3.3 Timing of bacterial elimination is concurrent with changes in parameter sensitivity

The model predicts that two waves of bacterial elimination can occur (i.e. both $\bar{B}_e = 0$ and $\bar{B}_i = 0$; Figure 4.5B), one after the start of infection and the other immediately following the onset of T cell recruitment (after day 20). Elimination of bacteria occurred before day 100 for 97 percent of parameter sets that lead to elimination, with 87 percent of parameter sets leading to elimination before day 50. This supports the hypothesis that

early host-pathogen events can determine long term outcomes of infection. Further, in many cases, early elimination occurs due to the innate immune response before adaptive immunity is established (i.e. before T cells arrived at the infection site on day 20), suggesting that bacterial elimination by innate factors is attainable at the level of a single granuloma *in vivo*.

To explore the role of T cell arrival times in a second wave of bacterial elimination, we repeated the global uncertainty analysis with initial T cell recruitment occurring on day 10 and day 30 to compare with the results obtained with arrival on day 20 (Figure 4.5). When adaptive immunity begins on day 10, the second peak of bacterial elimination occurs before 20 days post-infection (Figure 4.5A), while delaying adaptive immunity to 30 days delays the second elimination peak (Figure 4.5C), strongly suggesting that initial T cell recruitment induces the second wave of elimination.

4.3.4 T cell, bacterial growth and TNF parameters control granuloma formation

Using the outcomes of the global uncertainty analysis, we performed a sensitivity analysis to determine which factors control granuloma formation and bacterial growth. Dominant sensitivities in the analysis relate to three areas: bacterial growth rates, T cell movement, and TNF levels.

4.3.4.1 Intracellular and extracellular bacterial growth rates drive infection

Statistical sensitivity analysis indicates that growth rates of intracellular and extracellular Mtb (α_{Bi} and α_{Be} , respectively) have dominant effects on the number of bacteria, showing a significantly positive correlation with bacterial numbers throughout

simulations¹ (Figure 4.6A; Table 4.4). This result suggests that the growth rate of mycobacteria serves as a virulence factor that can determine the success or failure of host responses, consistent with the fact that virulent clinical strains of Mtb grow more quickly in macrophages (e.g. 44). The intracellular growth rate also strongly affects other measured outcome variables in the model, promoting T cell recruitment and chemokine/TNF production (α_{Bi} in Table 4.4).

The significant role of both intracellular and extracellular growth rates in determining the number of bacteria suggests an evolutionary advantage for successful growth of both intracellular and extracellular Mtb populations. We therefore performed additional simulations to examine the effect of bacteria losing the ability to grow either intracellularly or extracellularly using the baseline parameter set for all other parameters (Tables 4.1-4.3). For the loss of intracellular growth (i.e. $\alpha_{Bi} = 0$) all simulations resulted in bacterial elimination as soon as T cells arrived after day 20. Loss of extracellular bacterial growth (achieved by setting $\alpha_{Be} = 0$) resulted in significantly lower but robust extracellular Mtb populations: $\bar{B}_e(200) = 163.35$ versus 578.54 for the baseline control scenario ($p < 0.01$). Therefore, while intracellular growth is essential for establishing a stable infection, our model predicts that extracellular growth acts to augment bacterial numbers.

4.3.4.2 Crowding of T cells has global effects on granuloma formation

¹ This result differs slightly from our previous results in Segovia-Juarez et al (42), which predicted that intracellular growth rates are transiently negatively correlated with extracellular Mtb numbers between days 30 and 150 post-infection. This discrepancy is due to a peak in chronically infected macrophage bursting in that model that is not reproduced here since we hold the initial number of macrophages constant. This allows uncertainty analysis to have identical initial conditions between different parameter sets.

The probability of the three T cell classes (T_γ , T_c and T_{reg}) moving to a location where a cell already resides (T_{move}) is significantly negatively correlated with bacterial levels starting shortly after T cells infiltrate the site of infection (T_{move} in Figure 4.6A), and has significant effects on nearly all measured outcome variables (Table 4.A1). Therefore, if T cells are more likely to penetrate the crowded group of macrophages in the granuloma, bactericidal macrophage activation can more effectively reduce bacterial numbers. This follows from the cell contact-mediated T cell hypothesis (16) used here. If this assumption is approximately correct, this result suggests an important role for cell crowding toward T cell-mediated immune function in a granuloma, and is consistent with our previous results (41).

4.3.4.3 Multifaceted TNF effects on granuloma outcomes

Statistical sensitivity analysis confirms the central role of TNF in granuloma formation: For most of the simulated infection time, faster TNF production is correlated with lower bacterial numbers (s_{TNF} in Figure 4.6A). The effects of TNF on many other outcome variables (Tables 4.4, 4.A1 and 4.A2) suggest that the rate of TNF secretion from macrophages and T_γ cells (s_{TNF}) has a global regulatory role in the system, strongly determining immune cell and bacterial populations as well as molecular secretion.

The secretion rate of TNF (s_{TNF}) maintains a strong and consistent effect on bacterial and immune cell numbers throughout infection, but no parameters reflecting specific TNF effector mechanisms show significant correlations after the first day of infection. One explanation for this is that the most significant parameters may have drowned out effects of TNF-specific parameters when varying many parameters using

global statistical sensitivity analysis. To further explore the specific roles of TNF leading to different infection outcomes, we performed a focused sensitivity analysis, examining only the effect of TNF-related parameters on mean extracellular Mtb numbers (\bar{B}_e). The rest of the parameters were set equal to the reference parameter set that leads to a scenario with controlled bacterial numbers (Tables 4.1, 4.2 and 4.3).

This analysis (Figure 4.6B) reveals steady, small positive correlations between extracellular Mtb numbers and four TNF-related parameters: τ_{TNFact} (threshold for TNF-induced activation by macrophages); τ_{TNFapopt} (threshold for TNF-induced apoptosis by macrophages); δ_{TNF} (rate of TNF degradation); and r_{MTNF} (effect of TNF on trans-endothelial migration). Therefore, multiple specific TNF mechanisms appear to contribute to the overall effect of TNF after T cell infiltration with no one mechanism dominant.

4.3.5 Distinct effects of individual TNF mechanisms on granuloma structure

To directly explore the roles of TNF effector mechanisms in granuloma formation versus maintenance (i.e. long-term control), we used the reference parameter set (Tables 4.1-4.3) to perform deletions and depletions of the four individual TNF activities (Figure 4.1A). Deletion refers to loss of a TNF activity from day 0, to reveal the role of TNF activities from the onset of infection. Depletion refers to loss of a TNF activity only after the establishment of controlled infection (here, 100 days post-infection; see Methods), which shows the role of TNF activities in maintaining infection control and granuloma formation. Data are presented as significant changes in each outcome variable (cell and molecule numbers, granuloma sizes, etc) from the baseline control scenario.

4.3.5.1 Effects of TNF-induced apoptosis activity

One trend that is evident from these simulations is that TNF has a role in sustaining infection. Deletion or depletion of TNF-induced apoptosis activity (“Apoptosis” in Table 4.5) results in complete elimination of bacteria in nearly all replicates (all deletions and 14 of 15 depletions).

There are two possible mechanisms for the effects of TNF losing the ability to induce apoptosis in macrophages. One is that intracellular bacteria surviving the apoptosis event play a central role in sustaining infection. Another possibility is that apoptosis regulates inflammation by preferentially targeting cells that are producing chemokines and TNF, and thereby contributes to the propagation of infection by lowering the number of immune cells during the host response. To test the first hypothesis, we simulated infections with the baseline parameter set, varying the survival rate of bacteria within a macrophage undergoing apoptosis from zero to 100 percent; the results show no significant change in bacterial numbers or other outcome measures (not shown).

To test the other possibility, we examined the transient kinetics of bacteria, immune cells, TNF, and chemokines that occur during the apoptosis activity depletion (representative graphs are shown in Figure 4.7). Immediately after depletion, T cell and effector molecule levels permanently increase and numbers of activated macrophages transiently increase. The single sustained infection that occurred during the simulated depletion of apoptosis activity shows extensive macrophage infiltration, with no discernable granuloma structure (Table 4.5F). Taken together, this strongly supports the explanation that TNF-induced apoptosis modulates production of effector molecules and recruitment of immune cells in this model.

In contrast to the results presented here, some virulent strains of *M. tuberculosis* promote bacterial growth via inhibition of TNF-induced apoptosis of infected macrophages (12, 20, 48). To further explore this issue, we performed depletions of TNF-induced apoptosis effects on infected versus uninfected macrophages separately. Depletion of TNF-induced apoptosis of uninfected macrophages resulted in clearance and high immune cell infiltration, while the effect targeting infected macrophages was more subtle (Figure 4.8). Therefore, the effects of losing TNF-induced apoptosis in the model are likely driven by secretion of chemokines and TNF by uninfected macrophages.

Gradual reduction of the probability that TNF induces apoptosis (p_{apopt}) in all macrophage types predicts lower bacterial loads, but with granuloma structures largely unchanged (Figure 4.9). This is consistent with a scenario where loss of TNF-induced apoptosis results in “runaway” recruitment of immune cells. It may also point to an important role for anti-inflammatory cytokines such as IL-10 (10) that were omitted from this model but may buffer this effect *in vivo*.

4.3.5.2 Effects of TNF-induced activation, effector molecule production and recruitment

Deletion and depletion of TNF-related macrophage activation shows significantly higher levels of caseation and extracellular bacteria, with lower overall macrophage numbers and unchanged granuloma size (Table 4.5). The granuloma structures resemble an intermediate between the solid form of the baseline scenario and the caseous core observed with complete TNF deletion or depletion (c.f. Figure 4.A2F-G). Therefore, the efficacy of TNF as part of the macrophage activation pathway may partially determine levels of caseation at the core without affecting overall granuloma integrity.

Deletion and depletion of TNF-induced recruitment and secretion activities (Table 4.6) suggests different roles for TNF before and after T cell infiltration. In both cases, the effects are more pronounced in deletion. Loss of secretion activity (that is, the activity of TNF inducing TNF and chemokine production from macrophages) has particularly divergent effects between deletion and depletion, with larger granuloma size and higher levels of caseation, bacteria, and most cell types in the deletion but no significant effects in the depletion (compare Table 4.6E and F). This suggests that this role of TNF is key to formation of granulomas but not involved in maintenance.

4.3.6 Synergism and competition between TNF activities

In order to determine the effects of interactions between specific TNF activities on granuloma structure, we repeated deletions and depletions of pairs and triplets of individual activities. Figure 4.10 depicts representative granulomas for some deletions (Figure 4.A3 shows all simulated granulomas still containing infection at day 200 for all combinations of deletions and depletions). The structures reveal that TNF-induced apoptosis, activation, and TNF/chemokine secretion each make distinct contributions to granuloma structure.

Deletion of both TNF-induced apoptosis activity and TNF-mediated activation activity results in high immune cell infiltration, but no effective control of infection (Figure 4.10A). However, loss of TNF-induced TNF/chemokine secretion activity and apoptosis activity results in a small, well-controlled granuloma (Figure 4.10B). This confirms that TNF/chemokine secretion activity from macrophages drives the hyper-inflammatory state observed with loss of TNF-induced apoptosis.

Simultaneous deletion of both TNF-mediated TNF/chemokine secretion activity and activation activity results in a granuloma structure reminiscent of deletion or depletion of all TNF activity (compare Figure 4.10C with 4.3C). Granuloma structures in a 3-way deletion (loss of TNF-induced apoptosis, activation and effector molecule secretion activities) are similar as well, but with higher levels of macrophages, TNF and chemokines (Tables 4.A3-4.A4). This confirms a distinct role for each TNF-mediated activity contributing to the granuloma structure.

4.4 Discussion

Granuloma formation in Mtb infection is complex, involving multiple scales of interactions including molecular, cellular, and tissue-scale processes. Our agent-based model of granuloma formation reproduces major features of infection by representing interactions of individual cell agents and molecular effectors with a representation of a growing mycobacterial population. This work was based on a previous model (41) with major extensions that include representations of TNF, a simple chemokine network, and distinct T cell sub-populations (Figure 4.1). A baseline parameter set demonstrates bacterial control (Figures 4.3A and B), which is disrupted by simulated deletion of TNF (Figure 4.3C).

Granulomas in human TB are highly variable, and the relative effectiveness of each type of granuloma in containing infection is not known. Global uncertainty analysis revealed a wide range of possible granuloma types (Figure 4.A1) representing a range of associated bacterial loads from controlled to uncontrolled growth (Figure 4.4).

4.4.1 Onset of adaptive immunity

Global uncertainty analysis predicts that there is an important role for both innate and adaptive immunity in granuloma formation: bacterial elimination occurs in two waves, one during innate immunity and the second following soon after the first T cells arrive at day 20 post-infection (Figure 4.5A and B). With initial T cell entry set to day 10 post-infection, an immediate wave of elimination follows before day 20 (Figure 4.5C). This suggests the importance of adaptive immunity in mounting responses that may prevent bacteria gaining a foothold in the lung, preventing latent or active disease. This conclusion is reinforced by simulations with T cell entry delayed to day 30, which predicts a delayed second wave of bacterial clearance (Figure 4.5D). A long period of time before the onset of adaptive immunity allows establishment of persistent infection. This can be prevented by earlier T cell arrival at the site of infection. One possible implication of this result is that a vaccine to Mtb generating a fast T cell response at the infection site can favor complete elimination of bacteria.

4.4.2 Effects of TNF pleiotropy

TNF is clearly a central factor in granuloma formation and maintenance as observed in experiments (4) as well as in this model (s_{TNF} in Figure 4.6). However, the relative importance of its primary activities (Figure 4.1A) has not been elucidated.

Our model can shed light on this issue and predicts that loss of any one individual TNF activity is not sufficient to account for the type of granulomas observed under total loss of TNF activity with quantitative or qualitative measures (Tables 4.5, 4.6). Hence, each activity has a role that synergizes to accomplish the overall function of TNF.

Focused sensitivity analysis predicts similar effects of several TNF activities on extracellular Mtb numbers (Figure 4.6), but deletions and depletions of specific TNF activities show the overall effect of each activity to be distinct.

First, deletion and depletion of TNF-induced apoptosis nearly always results in effective clearance of bacteria (“Apoptosis” in Table 4.5). Out of 15 deletion and 15 depletion replicates, one depletion simulation predicted bacterial persistence to day 200 with disrupted granuloma structure and a heavy increase of cell infiltration and TNF/chemokine production after depletion compared to preceding depletion (Figure 4.10). Separate depletion of TNF-induced apoptosis activity from infected and uninfected macrophages shows that this phenomenon is primarily driven by uninfected macrophages (Figure 4.8). Therefore, TNF-induced apoptosis may play a role in maintaining granuloma integrity by preventing excessive inflammation, promoting sustained Mtb infection as an unfortunate side-effect. This result also points to an important role for anti-inflammatory cytokines such as IL-10, which are omitted from the model but may modulate the effects of TNF in the face of natural variation in apoptosis rates.

This result also appears in contrast to two lines of experimental evidence. First, virulent Mtb strains prevent apoptosis of infected macrophages in order to promote infection (12, 20, 48), while strains that promote apoptosis may enhance the immune response (15). One mechanism accounting for this effect may be enhancement of antigen presentation as a result of apoptosis (13, 15), a mechanism absent from the agent based model. However, the result of TNF-induced apoptosis deletion and depletion is clearly being driven by resting macrophages in the granuloma, not infected macrophages (Figure 4.8). Therefore, our result is not directly contradictory of this work.

A second line of evidence lies in the *sstI* mutant mouse (21), which does not undergo apoptosis of infected macrophages and results in impairment of innate immune responses, leading to uncontrolled Mtb infection (32, 51). Macrophages carrying this mutation also show higher rates of intracellular bacterial growth rate, and production of necrotic foci may allow enhanced extracellular Mtb growth (51). In an interesting parallel, our model predicts uncontrolled bacterial growth in simulations lacking both TNF-induced apoptosis and activation activities. While the factors affected by the *sstI* mutation are not fully understood, our model predicts that impairment of TNF-mediated macrophage activation would contribute to the phenotype observed in the *sstI* mutant.

Deletion and depletion of TNF-induced macrophage activation has the effect of significantly enhancing extracellular Mtb populations while reducing macrophage numbers compared to baseline (“Activation” in Table 4.5). A caseous core is visible in sample granulomas that lack TNF-induced activation (Table 4.5 C-D), suggesting that lowered macrophage activation is a mechanism for this type of granuloma. Deletion of other TNF-mediated activities in addition to activation results in more irregular granulomas with more extracellular bacteria (Figure 4.10), suggesting that several individual TNF activities (particularly regulation of activation, apoptosis, and effector molecule secretion) contribute to the type of structure observed. Finally, the effects of deletion of TNF-induced chemokine/TNF secretion activity on several variables are strong, but not so for depletions (“Secretion” in Table 4.6). This result suggests that the positive feedback effect of TNF inducing itself is an important mechanism for establishment of a granuloma.

4.4.3 Conclusions

The model presented here raises several possibilities for future work. Since the probabilities of cell-cell interactions are of high importance, a three-dimensional spatial representation may be an important step to capturing these interactions more naturally. Consideration of anti-inflammatory cytokines are also necessary. Linked to a sophisticated model for antigen presentation in the lymph node (36), adaptive immunity may be represented in a mechanistic manner, capturing a simplified multi-tissue system. This approach represents a step toward determining the consequences of Mtb infection on a larger scale, with the goal of predicting bacterial dissemination or containment on the organism level.

Figures

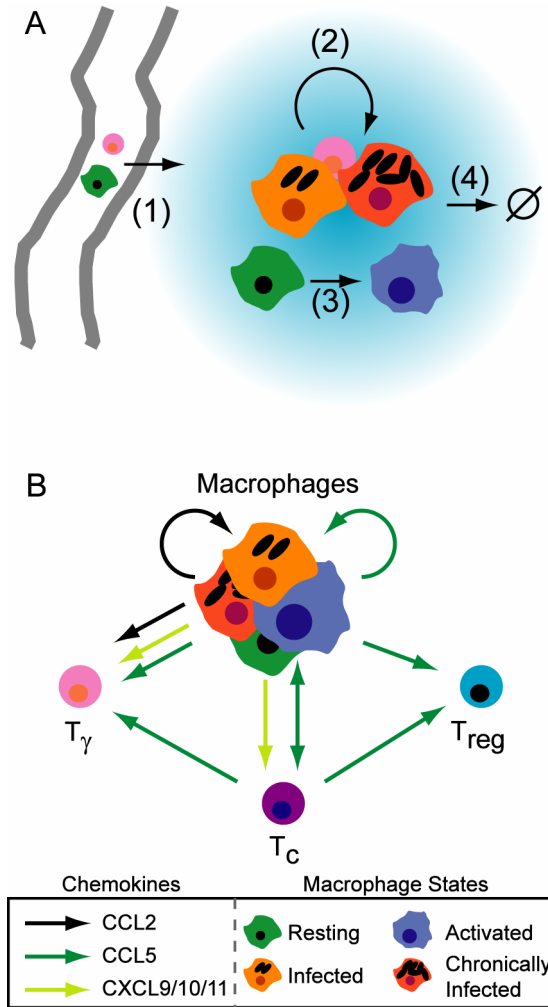


Figure 4.1. Models of molecular signaling networks that affect granuloma formation during infection with *Mycobacterium tuberculosis*. A. TNF (blue gradient) is an immunological effector with multiple roles. (1) TNF-dependent enhancement of transendothelial migration of monocytes and T cells to the lung parenchyma occurs via upregulation of endothelial adhesion molecules. (2) TNF-dependent activation of macrophages in concert with IFN- γ stimulates chemokine production and bacterial killing. (3) TNF-dependent apoptosis, a second pathway for mycobacterial killing. B. Model of the chemokine network induced during infection with *Mycobacterium tuberculosis*. CXCL9/10/11 are α -chemoattractants that bind the same chemokine receptor (CXCR3); CCL2 binds CCR2; CCL5 binds CCR5. T_γ are pro-inflammatory Th1 cells. T_c are cytotoxic T cells. T_{reg} are regulatory T cells.

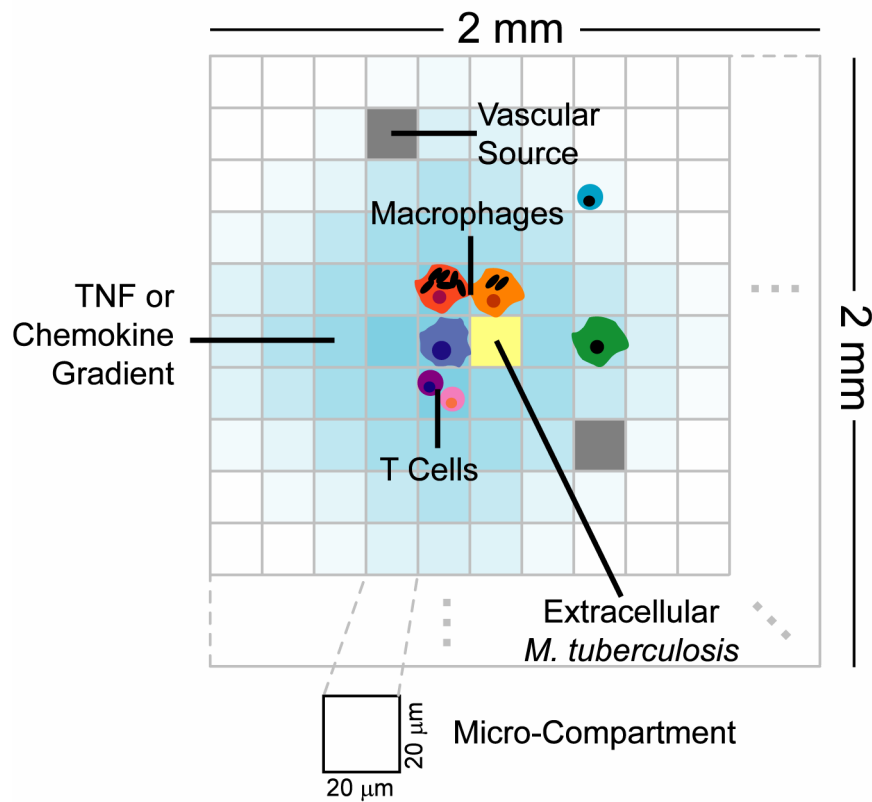


Figure 4.2. Structure of the agent-based model environment. A 100 x 100 grid of micro-compartments represents a 2 mm x 2 mm section of lung tissue. Discrete entities include macrophages and T cells. TNF, chemokines and extracellular *M. tuberculosis* are represented as continuous entities. Each micro-compartments can contain either one macrophage or up to two T cells along with extracellular bacteria, TNF and chemokines. A percentage of randomly chosen micro-compartments are designated as vascular sources that allow new macrophages and T cells to be recruited to the grid by chemokines and TNF.

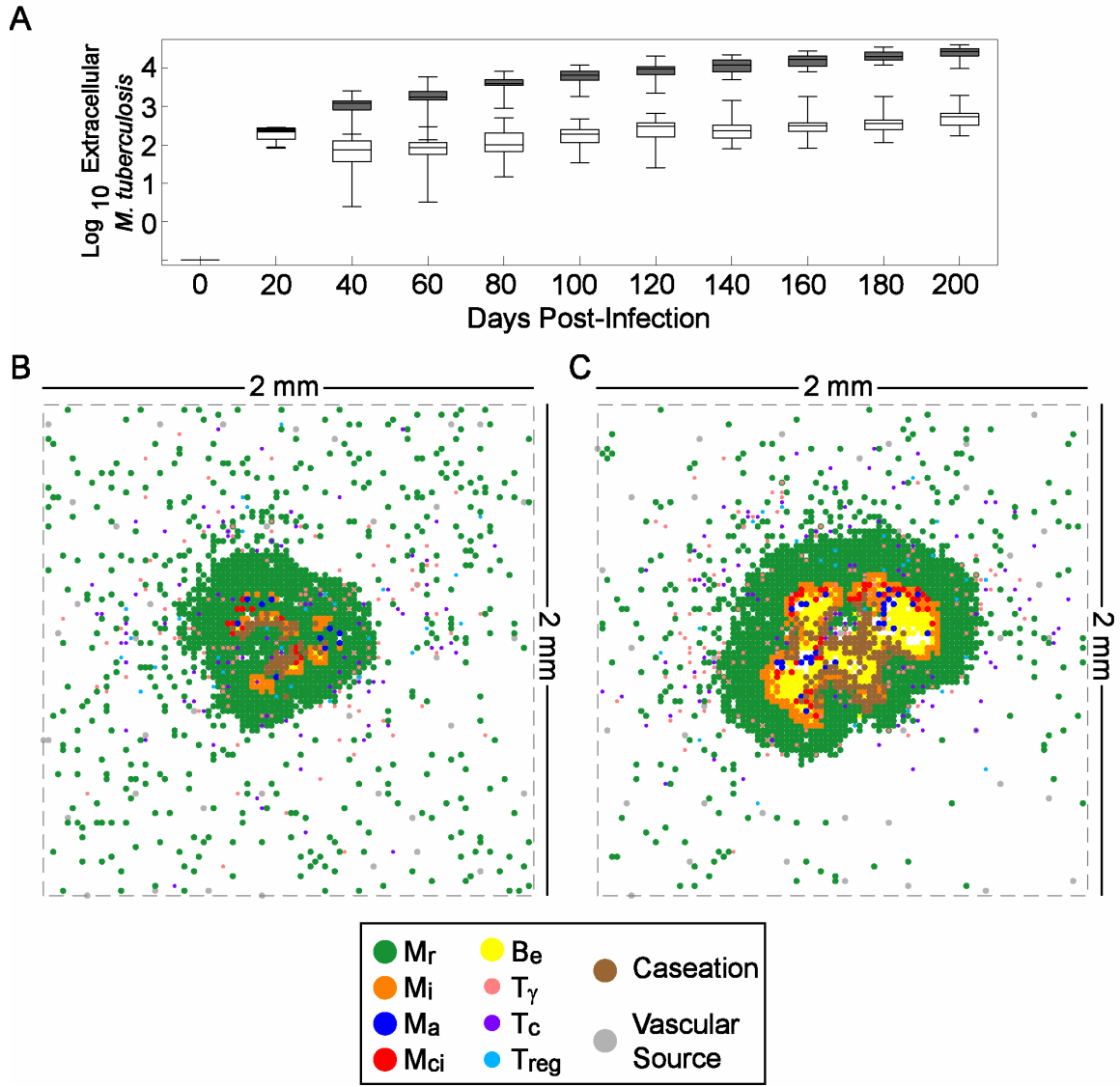


Figure 4.3. Simulated kinetics of extracellular *M. tuberculosis* and typical granuloma structures at 200 days post-infection in baseline control and TNF deletion scenarios. A. Box-whisker plots represent minimum, median, maximum and interquartile range of bacterial numbers for 15 simulations each for the containment scenario (white bars) and lacking TNF (gray bars). B. Containment granuloma using the baseline set of parameters (Tables 4.1-4.3). C. Irregular granuloma with uncontrolled bacterial growth resulting from lack of TNF in the simulation. M_r , M_i , M_a , and M_{ci} are resting, infected, activated and chronically infected macrophages, respectively. B_e is extracellular mycobacteria. T_γ , T_c , and T_{reg} are pro-inflammatory, cytotoxic and regulatory T cells, respectively. Parameters are as in Table 4.1-3 except for TNF deletion (where parameter $s_{TNF} = 0$).

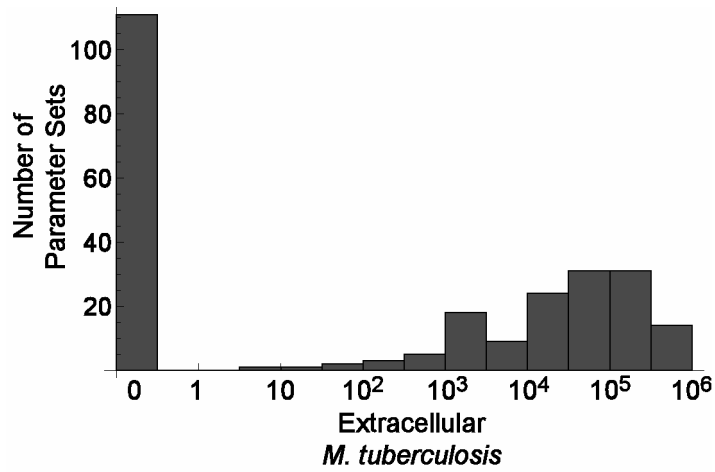


Figure 4.4. Distribution of average extracellular *M. tuberculosis* numbers at 200 days post-infection using parameter ranges in Table 4.1. 250 parameter sets were selected with Latin hypercube sampling (global uncertainty analysis). Simulations with each parameter set were replicated four times and averaged.

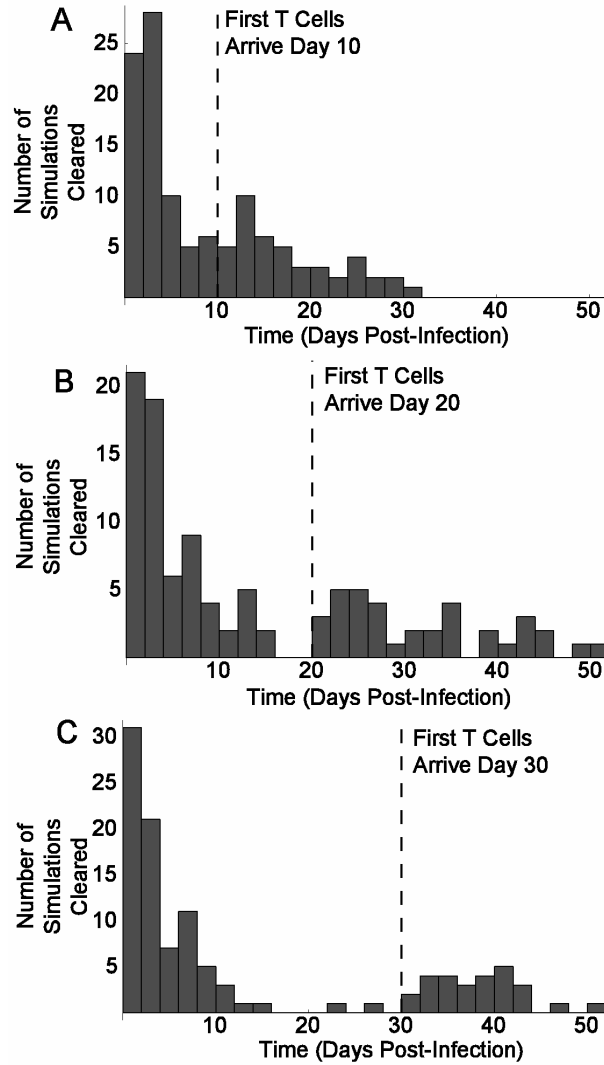


Figure 4.5. Time of bacterial clearance for simulations that predict complete elimination of bacteria depends on timing of innate and adaptive immune response. Shown are the number of simulations that clear all bacteria (y-axis) by day post-infection (x-axis). Two waves of elimination occur, the first with the innate immune response and the second following the onset of T cell arrival. A. Early second peak in bacterial elimination when T cell recruitment begins 10 days post-infection. C. Two waves of elimination with the default day 20 arrival time. D. The second peak of bacterial elimination is delayed and less pronounced when T cell recruitment begins on day 30 post-infection. Histograms depict averages of 3 (A and C) or 4 (B) simulation replicates for 250 separate parameter sets. Dashed lines depict the initiation of T cell recruitment.

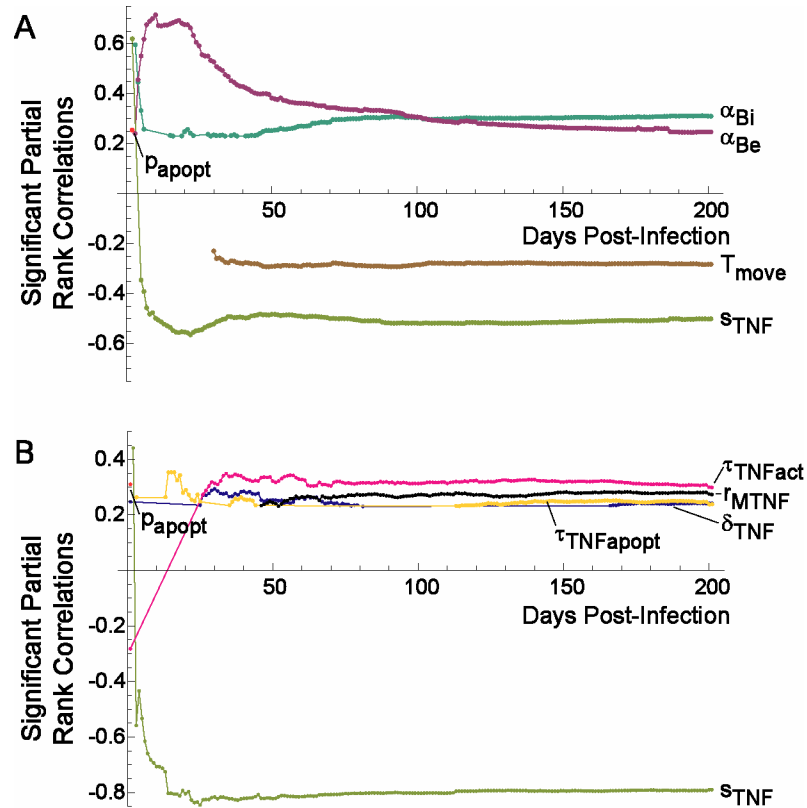


Figure 4.6. Sensitivity analysis of granuloma simulations. Graphs depict significant partial rank correlations ($p < 0.01$) between extracellular *M. tuberculosis* numbers and parameters that affect their levels in the agent-based model. A. Global sensitivity analysis reveals four dominant parameters. B. TNF-focused sensitivity analysis predicts the contribution of individual TNF-related mechanisms over time. Non-TNF parameters are set equal to the baseline control scenario (Tables 4.1-4.3) in panel B. α_{Be} : extracellular Mtb growth rate; α_{Bi} : intracellular Mtb growth rate; p_{apopt} : probability of TNF-induced apoptosis in one ten-minute interval; T_{move} : probability of T cell movement onto an occupied location; s_{TNF} : rate of TNF secretion by macrophages; τ_{TNFact} : threshold for TNF-induced activation by macrophages; r_{MTNF} : effect of TNF on trans-endothelial migration; δ_{TNF} : rate of TNF degradation; $\tau_{TNFapopt}$: threshold for TNF-induced apoptosis by macrophages.

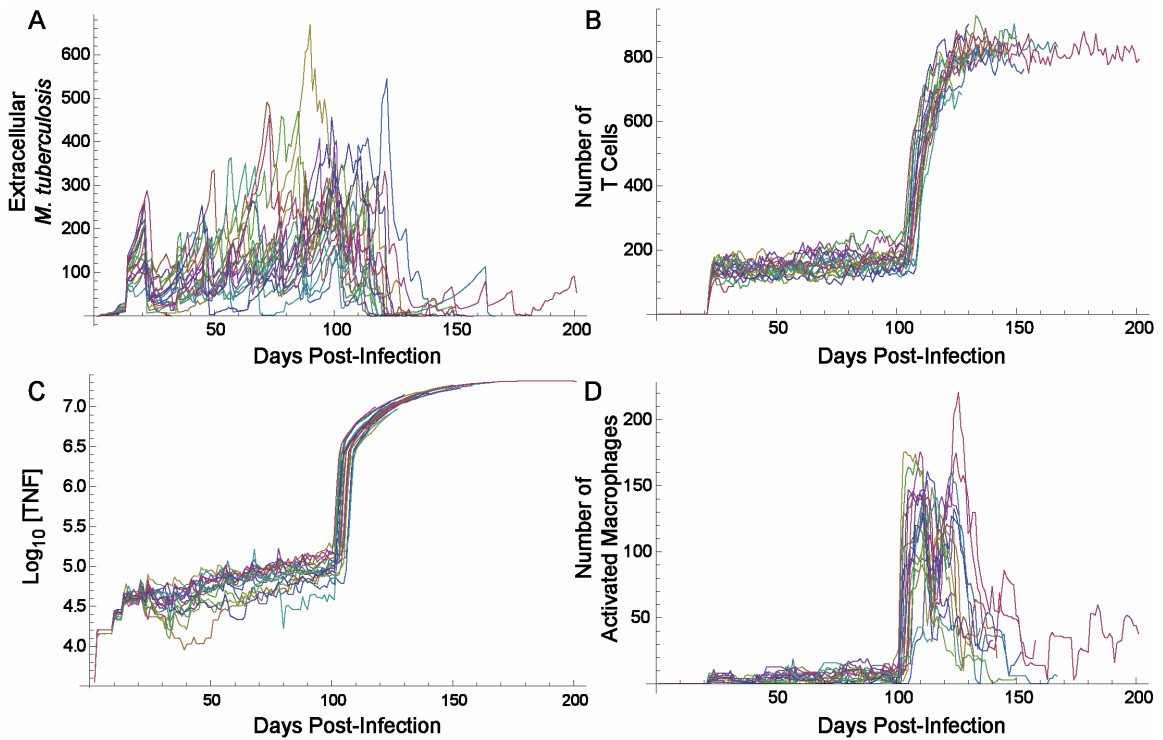


Figure 4.7. Depletion of TNF-induced apoptosis activity. Granuloma kinetics suggest a hyper-inflammatory state upon targeted depletion of TNF-induced apoptosis activity. Plots depict tracings of ten individual simulations with targeted depletion of TNF-induced apoptosis activity at day 100. A. Extracellular bacterial numbers decrease after depletion, leading to complete elimination for 9 of the 10 simulations. B, C. Total T cell numbers and TNF concentrations rapidly and permanently increase after depletion. D. Activated macrophage levels transiently increase after depletion.

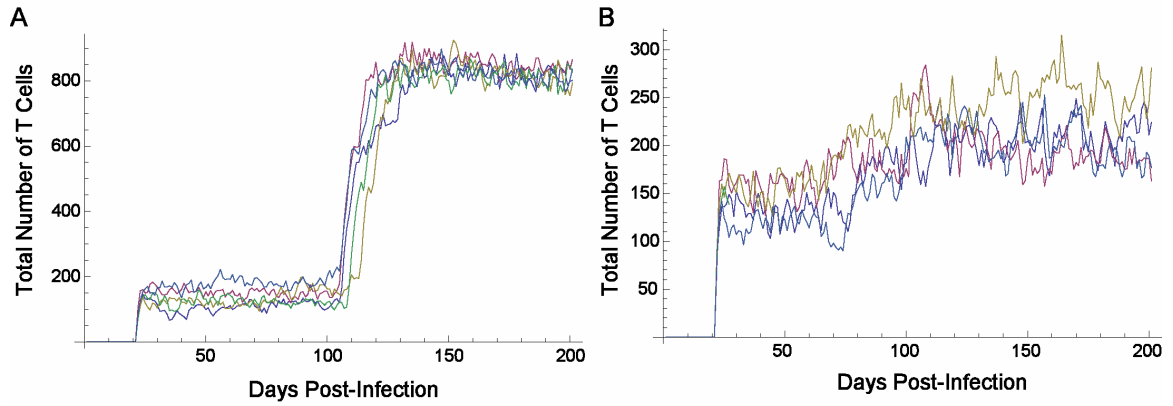


Figure 4.8. T cell kinetics for depletion of TNF-induced apoptosis activity in subsets of the macrophage population. A. Depletion of apoptosis activity from resting and activated, but not infected, macrophages. B. Depletion of apoptosis activity from infected macrophages only. Each plot depicts individual tracings of 5 replicates. Note difference of scale on y-axis.

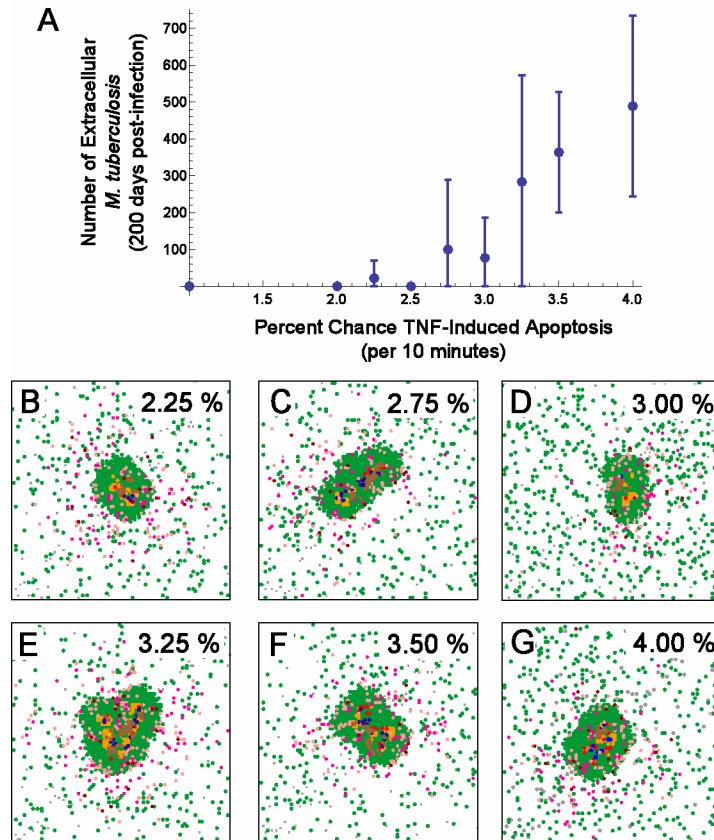


Figure 4.9. Effects of changing the probability of TNF-induced apoptosis activity on extracellular *M. tuberculosis* numbers and granuloma structures in the agent-based model. A. Reductions in the probability of apoptosis activity (parameter p_{apopt}) lower mean bacterial loads. In the baseline control scenario, the probability of apoptosis is set to 4 percent ($N = 15$ replicates). Tested reductions in the probability were performed with 5 replicates each. B-G. Typical granulomas for persistent infection the agent-based model with reduced chance of TNF-induced apoptosis activity.

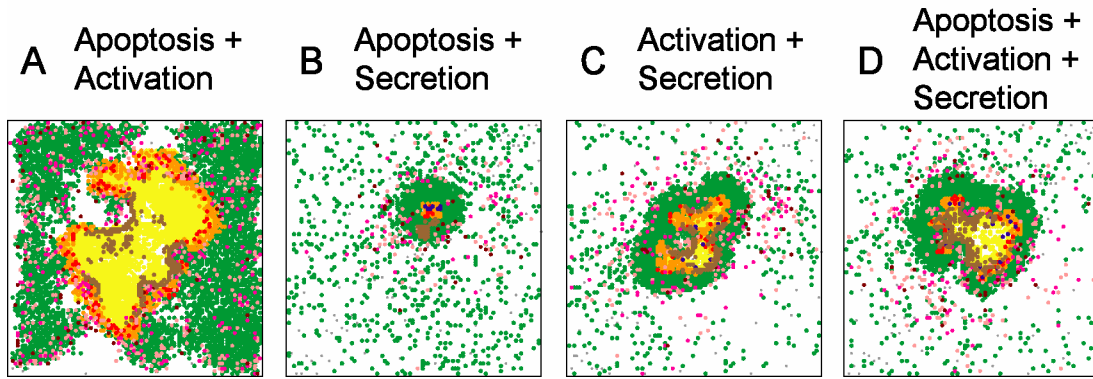


Figure 4.10. Double and triple deletions of TNF-activities. Representative granuloma structures for deletions of different TNF activity combinations. Structures for multiple replicates of each simulation, and for depletions of each combination at 100 days post-infection, are given in Figure 4.A2.

Table 4.1. Parameters varied for Latin hypercube sampling

Parameter	Description ¹	Default	Range	Distribution	Varied in focused analysis?
α_{Bi}	Intracellular Mtb growth rate (per 10 minutes)	0.002	[0.0002, 0.002]	Uniform	No
α_{Be}	Extracellular Mtb growth rate (per 10 minutes)	0.001	[0.00015, 0.015]	Log-Uniform	No
p_k	Probability of M_r killing bacteria	0.015	[0.01, 0.1]	Uniform	No
T_{actm}	Probability of M_i activation by T_γ	0.05	[0.0001, 0.1]	Log-Uniform	No
M_{recr}	Probability of macrophage recruitment	0.075	[0.01, 0.1]	Uniform	No
T_{recr}	Probability of T cell recruitment	0.075	[0.01, 0.1]	Uniform	No
T_{move}	Prob of a T cell moving onto an occupied micro-compartment	0.01	[0.00001, 0.1]	Log-Uniform	No
T_{rrecr}	Proportion of T_{reg} cells out of all T cells recruited	0.1	[0.01, 0.2]	Uniform	No
λ_c	Chemokine diffusion rate (per 0.1 minutes)	0.3734	[0.1, 0.7]	Uniform	No
δ_c	Chemokine degradation rate (per 0.1 minutes)	0.00123	[0.0005, 0.0015]	Uniform	No
r_T	Combined TNF/chemokine threshold for T cell recruitment at a vascular source ²	1,000	$[0.1, 10] \times 10^4$	Log-Uniform	No
r_M	Combined TNF/chemokine threshold for M_r recruitment at a vascular source ²	1,000	$[0.1, 10] \times 10^4$	Log-Uniform	No
s_{c5}	CCL5 production rate (molecules per 10 minutes) ⁺	7.5×10^6	$[1, 10] \times 10^6$	Uniform	No
s_{5m}	Macrophage CCL5 saturation threshold (molecules)	1.413×10^6	$[1, 100] \times 10^6$	Log-Uniform	No
τ_{5m}	Macrophage CCL5 threshold (molecules)	2×10^4	$[1, 100] \times 10^4$	Log-Uniform	No

Table 4.1. (continued) Parameters varied for Latin hypercube sampling

Parameter	Description ¹	Default	Range	Distribution	Varied in focused analysis?
λ_{TNF}	TNF diffusion rate (per 0.1 minutes)	0.7	[0.1, 0.7]	Uniform	Yes
δ_{TNF}	TNF degradation rate (per 0.1 minutes)	0.0006	[0.0001, 0.001]	Uniform	Yes
s_{TNF}	TNF production rate (molecules per 10 minutes)	2.25×10^5	$[1, 100] \times 10^4$	Log-Uniform	Yes
p_{apopt}	Probability of TNF-induced apopt per 10 minute interval	0.1	[0.001, 0.2]	Uniform	Yes
τ_{TNF}	Macrophage TNF detection threshold (molecules)	7×10^5	$[1, 15] \times 10^5$	Uniform	Yes
r_{MTNF}	Effect of TNF on M _i recruitment ²	150	[10, 1000]	Log-Uniform	Yes

¹All probabilities are per 10 minute interval.

²Non-dimensional; c.f. II.3.iv-v. of the Agent-Based Model Rules (Appendix)

Table 4.2. Parameter relationships constrained for analyses

Parameter	Description	Value
s_{c2}	CCL2 production rate (molecules per 10 minutes)	s_{c5}
s_{c9}	CXCL9/10/11 production rate (molecules per 10 minutes)	$2*s_{c5}$
s_{2m}	Macrophage CCL2 saturation (molecules)	$10*s_{5m}$
τ_{2m}	Macrophage CCL2 threshold (molecules)	$0.1*\tau_{5m}$
$s_{2T\gamma}$	T_{γ} CCL2 saturation (molecules)	$10*s_{5m}$
$\tau_{2T\gamma}$	T_{γ} CCL2 threshold (molecules)	$0.1*\tau_{5m}$
$s_{5T\gamma}$	T_{γ} CCL5 saturation (molecules)	s_{5m}
$\tau_{5T\gamma}$	T_{γ} CCL5 threshold (molecules)	τ_{5m}
$s_{9T\gamma}$	T_{γ} CXCL9 saturation (molecules)	$10*s_{5m}$
$\tau_{9T\gamma}$	T_{γ} CXCL9 threshold (molecules)	τ_{5m}
s_{5Tc}	T_c CCL5 saturation (molecules)	s_{5m}
τ_{5Tc}	T_c CCL5 threshold (molecules)	τ_{5m}
s_{9Tc}	T_c CXCL9 saturation (molecules)	$10*s_{5m}$
τ_{9Tc}	T_c CXCL9 threshold (molecules)	τ_{5m}
s_{5Tr}	T_{reg} CCL5 saturation (molecules)	s_{5m}
τ_{5Tr}	T_{reg} CCL5 threshold (molecules)	$0.1*\tau_{5m}$
r_{M2}	Effect of CCL2 on M_r recr ^{1,2}	r_{MTNF}
r_{M5}	Effect of CCL5 on M_r recr ^{1,2}	$0.1*r_{MTNF}$
r_{TNF}	Effect of TNF on T cell recr ¹	r_{MTNF}
r_{T9}	Effect of CXCL9 on T_{γ} , T_c cell recr ^{1,2}	$0.1*r_{MTNF}$
$r_{T\gamma 2}$	Effect of CCL2 on T_{γ} cell recr ^{1,2}	r_{MTNF}
r_{T5}	Effect of CCL5 on T_{γ} , T_c cell recr ^{1,2}	$0.1*r_{MTNF}$
r_{Tr5}	Effect of CCL5 on T_{reg} cell recr ^{1,2}	r_{MTNF}
$T_{\gamma recr}$	Proportion of T_{γ} cells recruited	$0.6*(1 - T_{rrecr})$
T_{crecr}	Proportion of T_c cells recruited	$0.4*(1 - T_{rrecr})$

¹Non-dimensional; c.f. II.3.iv-v. of the Agent-Based Model Rules (Appendix).

²These parameters were held constant in the focused sensitivity analysis at the default value of r_{MTNF} given in Table 4.1.

Table 4.3. Parameters not varied in uncertainty analysis

Parameter	Description	Value	Reasoning
M_{init}	Number of resident macrophages	105	1
K_{be}	Carrying capacity of micro-compartment for extracellular Mtb	220	2, 3
N_{rk}	Number of Mtb engulfed/killed by M_r	2	3
N_{phag}	Number of Mtb killed by M_a every 10 minutes	10	3
N_{tact}	Maximum T_γ number in Moore of M_i having effect	4	3
N_{caseum}	Number of M_a , M_i and M_{ci} deaths for caseation	6	3
$t_{regT\gamma}$	T_γ inactivity time after T_{reg} interactions (min)	110	3
N_c	Number of Mtb for $M_i \rightarrow M_{ci}$ transition	10	3, 4
K_{bi}	Number of bacteria causing bursting	20	3, 4
M_{als}	Lifespan of M_a in days	10	5
T_{ls}	Lifespan of T cells in days	3	5
M_{rls}	Lifespan of M_r in days	100	5
T_{delay}	T cell recruitment delay in days	20	6
P_{kill}	Fraction Mtb killed by Fas/FasL apoptosis	0.5	7
p_{Tk}	Prob of Fas/FasL (TNF-independent) apoptosis by T cells	0.006	7
T_{ckmtb}	Probability of T_c killing Mtb in M_{ci} death	0.75	7
T_{ckmci}	Probability of T_c killing M_{ci}	0.95	7

1. Set to the reference number for containment to have identical initial conditions.
2. Set ~10-fold larger than the amount causing macrophage bursting. There is physical space for approximately 450 bacilli in one micro-compartment (tightly packed), but lack of nutrients for growth limits this.
3. These parameters have integer values that cannot be continuously varied over at least 250 different values.
4. The same effect as varying this is captured by changing intracellular growth rate: the faster Mtb grow, the sooner the transition to chronic infection. If N_c is varied in say [5, 25] we should set $K_{bi} = 2*N_c$.
5. Relative lifespans are well known. Vary cell age between 0 and the maximum age, so changing these would have questionable relevance.
6. Many parameter sensitivities change before and after this time, so it was held constant but multiple uncertainty analyses were performed to show the effect of this parameter.
7. Preliminary analysis revealed little effect for reasonable ranges. Thus, this was not varied to reduce the number of parameters varied.

Table 4.4. Significant partial rank correlations between parameters and different granuloma outcome measures 20 and 200 days post-infection for several different outcome variables (column 1).¹ See Tables 4.A1 and 4.A2 for additional correlations.

Parameter Outcome Measure	α_{Bi}		α_{Be}		S_{TNF}	
	20	200	20	200	20	200
B _e	+++	+++	+++	+	---	---
B _i	+++	++			---	---
Total T cells		+				---
T _γ		+				---
“Secretor” T _γ ²		++				---
T _c		+				---
T _{reg}						---
Total Macs					---	---
M _r					---	---
M _i	+++	++			---	---
M _{ci}	+++	++			---	---
M _a						---
TNF	+++					
Chemokines	+++				--	---
Caseation		+++				---
B _e growth rate	++	++	+		---	---
Granuloma Size	ND ³	+	ND ³		ND ³	---

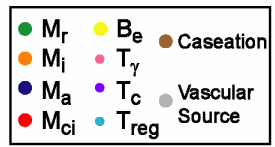
¹Parameter definitions are given in Tables 4.1-4.3. Significant positive correlations: +++ (p < 0.0001); ++ (p < 0.001); + (p < 0.01). Significant negative correlations: --- (p < 0.0001); -- (p < 0.001); - (p < 0.01).

²Number of T_γ cells actively secreting IFN-γ.

³ND: Not done due to relative lack of granuloma formation by day 20.

Table 4.5. Significant changes in granuloma variables at 200 days post-infection for deletion and depletion of all TNF activity (“Positive Control”), TNF-induced activation activity (“Activation”), and TNF-induced apoptosis activity (“Apoptosis”) versus the baseline control scenario¹. Sample granuloma structures for each deletion and depletion are shown.

	Positive Control		Activation		Apoptosis		All TNF Production	TNF-Induced Activation	TNF-Induced Apoptosis	
	Del (A)	Depl (B)	Del (C)	Depl (D)	Del (E)	Depl (F)				
B _e	+++	+++	+++	+++	---	---	A	C	E	Deletion
B _i	+++	++			---	---				
Total T cells					++	+++	B	D	F	Depletion
T _γ		-			++	+++				
“Secretor” T _γ ²	++					-	Baseline			
T _c					++	+++				
T _{reg}					+	+++				
Total Macrophages			---	--		+++				
M _r		--	---	--		+++				
M _i	+++	+		+	---	---				
M _{ci}	+++	+++			---	---				
M _a	+		---	---	+++	+				
TNF	---	---			+	+++				
Chemokines	+++	+			+	+++				
Caseation	+++	++	+++	+++	---	---				
Granuloma Size	+++	+++			ND ³	ND ³				

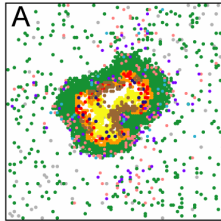
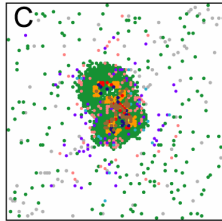
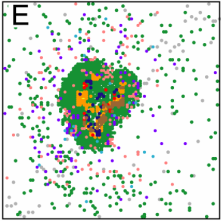
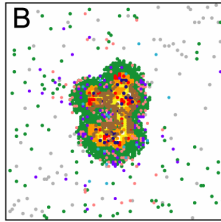
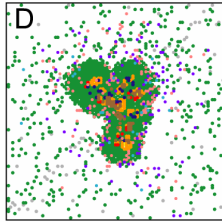
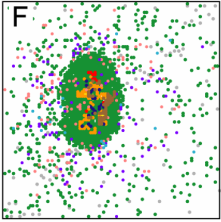
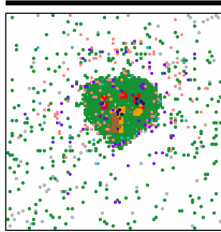


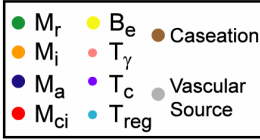
¹+ denotes a higher variable value for the deletion or depletion than the control scenario; - denotes a lower value. +++ (p < 0.0001); ++ (p < 0.001); + (p < 0.01). Significant negative correlations: --- (p < 0.0001); -- (p < 0.001); - (p < 0.01).

²Number of T_γ cells actively secreting IFN-γ.

³Nearly complete bacterial elimination prevented testing.

Table 4.6. Significant changes in granuloma variables at 200 days post-infection for deletion and depletion of all TNF activity activity (“Positive Control”), TNF effects on cellular transendothelial migration activity (“Recruitment”), and TNF-induced secretion of chemokines/TNF activity (“Secretion”) versus the baseline control scenario¹. Sample granuloma structures for each deletion and depletion are shown.

	Positive Control		Recruitment		Secretion		All TNF Production	TNF-Induced Recruitment	TNF-Induced Secretion	
	Del (A)	Depl (B)	Del (C)	Depl (D)	Del (E)	Depl (F)				
B _e	+++	+++			+					Deletion
B _i	+++	++			+++					
Total T cells			---	--	+++					
T _γ		-	---	--	+++					
“Secretor” T _γ ²	++									
T _c		-		---	+++					
T _{reg}					++					Depletion
Total Macrophages		-	---	-	+					
M _r		--	---	-	+					
M _i	+++	+	-		+++					
M _{ci}	+++	+++			++					
M _a	+				+					
TNF	---	---	-		+++					
Chemokines	+++	+	-		+++					
Caseation	+++	++			+++					
Granuloma Size	+++	+++			++					
										



¹+ denotes a higher variable value for the deletion or depletion than the control scenario; - denotes a lower value. +++ (p < 0.0001); ++ (p < 0.001); + (p < 0.01). Significant negative correlations: --- (p < 0.0001); -- (p < 0.001); - (p < 0.01).
²Number of T_γ cells actively secreting IFN-γ.

4.5 Appendix: Agent-Based Model Rules

4.5.1 Details of Agent-Based Model Rules

4.5.1.1 Bacteria and effector molecules in the model

Chemokines and TNF are modeled by partial differential equations (PDEs) representing diffusion on the grid. Each molecular effector type (CCL2, CCL5, CXCL9/10/11 and TNF) is defined separately. We assume simple first-order diffusion with a term for signal degradation. Due to the scale difference between diffusing molecular signals and cells, we assume that diffusion is unaffected by the presence of cells, and concentrations of different types of molecules may be overlapping. Diffusion is solved in $\Delta t = 6$ second timesteps.

Numbers of Mtb are continuously represented as well. Since Mtb is a non-motile bacterium, we assume that bacteria do not diffuse, so we capture their numbers with discretized ordinary differential equations. In a given $20 \mu\text{m}^2$ micro-compartment, bacteria grow according to a logistic growth law with a population capacity of $K_{be} = 220$: $B_e(t+1) = B_e(t) + \alpha_{be} B_e(t)(1 - B_e(t)/K_{be})$. The population limit of bacteria per micro-compartment is 10 times the number of Mtb contained within a macrophage before bursting. While the geometry of the micro-compartment allows up to approximately 450 individual bacilli in a single compartment due to the size of Mtb (a rod shape that is 2-5 μm long and 0.2-0.3 μm thick), we assume that there is a growth limitation due to competition for nutrient resources, preventing bacterial numbers from growing to this density.

4.5.1.2 Environment

The 2-dimensional grid representation of lung tissue is a major simplification that makes spatial considerations computationally tractable. However, the representation requires some considerations to permit a realistic model of cellular crowding. Due to the size difference between macrophages and T cells, we allow up to two T cells to enter the same micro-compartment (with probability $4 \times T_{move}$), but only if no macrophage is present. A T cell may also move into the same micro-compartment as a macrophage (with probability T_{move}). This model of cell spacing is a compromise between a realistic spatial representation and computational tractability since we capture crowding effects while saving the computational cost of a continuous spatial representation. A three-dimensional approach has been developed (49) that confirmed results obtained with our previous two-dimensional model (41), suggesting that a two-dimensional approach is sufficient to capture first order effects.

In addition to movement and placement of cells on the grid, each micro-compartment also contains environmental variables that are affected by local conditions. These include the number of extracellular bacteria, the number of activated or infected macrophage deaths that occur in a micro-compartment, whether or not the micro-compartment has become caseous, and if that space is designated a vascular source.

We assume that a set number ($N_{caseum} = 6$) of deaths of activated or infected macrophages occurring in a micro-compartment causes the onset of caseation (this number can be varied in the analysis). When the last macrophage death leading to caseation is reached (i.e. N_{caseum} deaths have occurred), any T cell present in the micro-compartment is killed and no further cells are permitted entry to the micro-compartment.

If TNF and/or chemokine concentrations exceed a set threshold, then micro-compartments defined to be vascular sources have a chance of recruiting a macrophage or T cell at each timestep. The thresholds are set by parameters labeled r in Tables 4.1-4.2 (r_{MTNF} , r_{TTNF} , etc.).

4.5.1.3 Rules for immune cells

Cells respond to local conditions according to rules that represent known activities *in vivo*. During simulations, each agent responds depending on its state. Several internal macrophage variables are set or altered by surrounding conditions: chemokine/TNF secretion (on/off), IFN- γ signal received (on/off), TNF or bacterial signal received (on/off), cell age, activation time, cell state (resting, activated, infected or chronically infected), and number of intracellular bacteria. Resting (M_r) and activated (M_a) macrophages can take up bacteria that are in the same micro-compartment. Resting macrophages may kill a small number of Mtb or become infected if the number of internalized bacteria exceeds 2. Production of chemokines and TNF by macrophages depends on activation by bacterial antigens and TNF; we therefore include a switch for chemokine secretion that is independent of the macrophage state (resting, infected, etc). If the macrophage detects sufficient TNF (above the threshold τ_{TNF}), it becomes capable of secreting TNF and chemokines, with a small probability of undergoing TNF-induced apoptosis (p_{apopt}). TNF and chemokine secretion is also induced by sufficient extracellular bacterial numbers in the same microcompartment ($B_{actM} = 100$). Infected macrophages secrete chemokines and TNF at half the rate in the absence of activation signals.

During each update interval, infected macrophages may be activated by pro-inflammatory T cells (T_γ) in their *Moore neighborhood*, the 9-micro-compartment area around the cell location. Each pro-inflammatory T cell in the Moore neighborhood has a chance (T_{actm}) of activating an infected macrophage. For macrophages to reach bactericidal levels of macrophage activation, IFN- γ must work in concert with one other activation signal (either TNF or bacterial products) (9). Mtb-derived products only effectively complement IFN- γ in the model if extracellular bacterial levels at that location exceed a threshold ($B_{actM} = 100$). The contribution of T cell-derived IFN- γ to macrophage activation is represented with cell-cell interactions. This is an acceptable model since IFN- γ signaling requires close proximity of macrophage to T cell, as it is known to be secreted from T cells in a directed manner to the immunological synapse (16). Activated macrophages (M_a) effectively kill all their intracellular bacteria. A pro-inflammatory T cell (T_γ) that has successfully activated a macrophage then secretes TNF in a non-directed fashion (16) and becomes an IFN- γ secretor, so that the cell is able to activate the IFN- γ pathway in macrophages encountered thereafter.

If a macrophage is infected (M_i), intracellular Mtb divide at a rate set by parameter α_{Bi} . In the absence of activation, the intracellular number of Mtb may exceed a threshold (N_c , set to 10, half the carrying capacity of a macrophage, given below) where the cell becomes chronically infected (M_{ci}) after which it is incapable of being activated. Beyond a further threshold for intracellular bacterial numbers per macrophage (K_{bi} , set to 20 based on (33, 53)) the chronically infected macrophage bursts, releasing bacteria uniformly into the Moore neighborhood. This bursting, along with death of activated macrophages (M_a), contributes to caseation.

Cytotoxic T cells (T_c) randomly check one space in their Moore neighborhood each 10-minute time interval for the presence of infected macrophages. If an infected macrophage is present, the cytotoxic T cell has a low probability of killing that macrophage, along with all its intracellular bacteria if it was not chronically infected (reviewed in (10)). When chronically infected macrophages are killed, there is a 75% chance of all intracellular Mtb being killed, a 20% chance of dispersal to the Moore neighborhood, and a 5% chance of nothing occurring. T cell interactions with infected macrophages can also result in TNF-independent Fas/FasL-induced apoptosis (reviewed in (10)), resulting in 50% killing of intracellular Mtb and dispersal of the rest to the Moore neighborhood.

The mechanism of regulatory T cell (T_{reg}) function in Mtb infection is not well established, but may involve cell-contact mediated or immunosuppressive cytokine mechanisms (3). We adopt a cell-contact-mediated model of T_{reg} cell activity. T_{reg} cells check one space in the Moore neighborhood for the presence of a pro-inflammatory T (T_γ) cell. If it is present, cell-cell interaction occurs and the T_γ cell becomes incapable of activating infected macrophages for a set time afterwards (t_{regT_γ} , 110 minutes by default). Since this time frame is not well established, we estimate it based on an approximate time to change the genetic program of the regulated cell while regaining activity.

4.5.2 Outline of Rules

- I. Initialization: conditions at the start of a simulation
 - a. 100 x 100 2-dimensional grid (representing 2 square mm)
 - i. Cellular boundary conditions:
periodic (toroidal)
 - ii. Molecular (chemokine and TNF) boundary conditions:
zero outside grid perimeter
 - b. 50 vascular source locations randomly distributed in 7 partitions of grid space
 - c. Microcompartment caseation counters set to 0
 - d. Distribute 105 resting macrophages randomly on grid
 - e. No chemokine or TNF present
 - f. 1 infected macrophage with 15 intracellular Mtb at the center of the grid
- II. Overview: Timing and Order of Events
 - a. Diffusion/degradation of chemokine and TNF (if present) according to $u_t = \lambda[\nabla^2 u] - \delta u$ for molecule u in $\Delta t = 6$ second increments (smallest timestep in model)²
 - b. Move macrophages based on CCL2/CCL5 (c.f. III.a.)
 - i. Move M_r on a 20-minute interval
 - ii. Move M_a on a ~13 hour interval
 - iii. Move M_i on a 24 hour interval

²Diffusion is solved in $\Delta t = 6$ second timesteps based on finding diffusion coefficients λ_c and λ_{TNF} from $\lambda = 4\delta\Delta t / \Delta x$, where δ is the molecular diffusion rate in m^2/s and $\Delta x = 10^{-5} m^2$ is the grid size (41).

c. Events on 10-minute intervals

- i. Move T_γ based on CCL2, CCL5, and CXCL9/10/11 (c.f. III.b.)
- ii. Move T_c based on CCL5, CXCL9/10/11 (c.f. III.b.)
- iii. Move T_{reg} based on CCL5 (c.f. III.b.)
- iv. Determine macrophage (M_r) recruitment from each source:³

$$\text{if } r_{MTNF} * TNF(x,y) + r_{M2} * CCL2(x,y) + r_{M5} * CCL5(x,y) > r_M,$$

there is a probability M_{recr} of M_r recruitment

- v. Determine T cell (T_γ , T_c and T_{reg}) recruitment:

1. Proportions are $\rho_\gamma * T_{\gamma recr} + \rho_c * T_{c recr} + \rho_r * T_{r recr}$

2. Pro-inflammatory T cell (T_γ) recruitment: if

$$r_{T\gamma TNF} * TNF(x,y) + r_{T\gamma 2} * CCL2(x,y) + r_{T\gamma 5} * CCL5(x,y) +$$

$$r_{T\gamma 9} * CXCL9/10/11(x,y) > r_{T\gamma}, \rho_\gamma = 1, \text{ otherwise } \rho_\gamma = 0$$

3. Cytotoxic T cell (T_c) recruitment: if $r_{T_c TNF} * TNF(x,y) +$

$$r_{T_c 5} * CCL5(x,y) + r_{T_c 9} * CXCL9/10/11(x,y) > r_{T_c}, \rho_c = 1,$$

otherwise $\rho_c = 0$

4. Regulatory T cell (T_{reg}) recruitment: if $r_{T_r TNF} * TNF(x,y) +$

$$r_{T_r 5} * CCL5(x,y) > r_{T_r}, \rho_r = 1, \text{ otherwise } \rho_r = 0$$

- vi. Determine cell-cell interactions, activation, chemokine production

1. M_r, M_i, M_{ci}, M_a (c.f. IV below)

2. T_γ, T_c, T_{reg} (c.f. V below)

³ For the source at the microcompartment denoted by coordinates (x,y) , $TNF(x,y)$ represents the amount of TNF at that point; likewise for chemokines.

- vii. Compute contribution of Mtb to chemotactic effects (Met-Leu-Phe, lipid antigens, etc.): modeled as contribution to CCL5 level
- viii. Remove dead cells from the grid
- ix. Calculate growth of extracellular Mtb according to

$$B_e(t+1) = B_e(t) + \alpha_{be} B_e(t)(1 - B_e(t)/(1.1 \cdot K_{be}))$$

- d. Increment counter by 6 seconds, return to II.a.

III. Movement Rules

- a. Each cell type has threshold (τ) and saturation (s) parameters for each chemokine it responds to.
- b. Movement is random if all chemokines are below threshold or above saturation.
- c. Macrophage chemotaxis:
 - i. Levels of CCL2 and CCL5 in surrounding microcompartments determine a probability distribution for movement
 - 1. CCL2 affects movement if $\tau_{2m} < [\text{CCL2}] < s_{2m}$
 - 2. CCL5 affects movement if $\tau_{5m} < [\text{CCL5}] < s_{5m}$
 - ii. Highest probability direction has further doubled probability
 - iii. Movement is blocked by
 - 1. Caseous microcompartment
 - 2. Macrophage presence
- d. T cell chemotaxis:
 - i. Pro-inflammatory T cells (T_γ) depend on CCL2, CCL5 and CXCL9/10/11 (with saturation and detection thresholds as above)

- ii. Cytotoxic T cells (T_c) depend on CCL5 and CXCL9/10/11 (with saturation and detection thresholds as above)
 - iii. Regulatory T cells (T_{reg}) depend on CCL5 (with saturation and detection thresholds as above)
 - iv. Movement is blocked/reduced by
 1. Caseation (blocked)
 2. Macrophage presence (probability of movement T_{moveM})
 3. T cell presence (probability of movement T_{moveT})
- IV. Rules for macrophages in each 10 minute interval
- a. Resting (M_r):
 - i. Response to TNF: If local [TNF] exceeds a detection threshold (τ_{TNF}),
 1. the cell becomes capable of secreting TNF and chemokines (CCL2, CCL5 and CCL9).
 2. there is a chance (p_{apopt}) that TNF induces apoptosis of M_r cells.
 - ii. Phagocytosis of Mtb may result in infection:
 1. If extracellular Mtb (b_e) $\leq N_{rk}$, the M_r kills them.
 2. If $b_e > N_{rk}$:
 - a. the M_r kills them with probability p_k
 - b. the M_r becomes infected (M_i) otherwise
 - iii. Death due to age at a time uniformly distributed between 0 and 100 days after arrival on the grid.

- b. Infected (M_i):
- i. TNF and chemokine secretion.
 - ii. There is a chance (p_{apopt}) that TNF induces apoptosis.
 1. If this occurs, half of the intracellular bacteria survive and are distributed to the surrounding environment.
 2. Death contributes to the caseation counter at the location of the cell (microcompartment becomes caseous if the counter exceeds N_{caseum}).
 - iii. Intracellular Mtb replicate according to

$$b_i(t) = b_i(t-1) + \alpha_{bi} b_i(t-1).$$
 - iv. If intracellular Mtb number exceeds a threshold ($B_i > N_c$), the M_i becomes chronically infected (M_{ci}).
 - v. Chance of activation by IFN- γ from pro-inflammatory T_γ cells not currently regulated by T_{reg} .
 1. With probability T_{actm} , any of the T cells may activate the macrophage; intracellular bacteria are killed and the cell becomes activated (M_a).
 2. The probability of activation saturates if the number of surrounding T_γ cells is above a certain number (N_{tact}).
 - vi. If the M_i dies due to age, disperse intracellular Mtb into the Moore neighborhood surrounding the cell.
 - vii. If the M_i dies due to age, increment the local caseation counter (the compartment becomes caseous if the counter exceeds N_{caseum}).

- c. Chronically Infected (M_{ci}):
 - i. The cell undergoes the same secretion, apoptotic and bacterial growth events as infected macrophages (M_i), but is incapable of becoming activated.
 - ii. If the number of intracellular Mtb exceeds a threshold (K_{bi}),
 - 1. The macrophage bursts
 - 2. Intracellular bacteria are evenly distributed to the Moore neighborhood surrounding the M_{ci} .
 - 3. Caseation counter is incremented
 - iii. The nominal lifespan is inherited from M_i predecessor
- d. Activated (M_a):
 - i. Macrophages secrete chemokines and TNF
 - ii. Probability p_{apopt} of TNF-dependent apoptosis
 - iii. Actively take up and kill extracellular bacteria at a rate of N_{phag} bacteria per ten minute interval.
 - iv. M_a have a shortened lifespan of M_{als} (= 10 days) after activation

V. Rules for T cells in each 10 minute interval

- a. Check for death due to age (uniformly distributed between 0 and 3 days after emergence from vascular source)
- b. Pro-inflammatory T_γ :
 - i. Chance of activating infected macrophages (M_i) via IFN- γ – detailed in section III.b.v.
 - ii. TNF secretion results from activation interaction

- iii. Probability of TNF-independent induction of apoptosis in infected or chronically infected macrophages in surrounding compartments
 - a. Kill half of intracellular Mtb
 - b. Remaining Mtb uniformly distributed in Moore neighborhood
 - c. Increments local caseation counter
- c. Cytotoxic T_c :
 - i. Chance of perforin/granulysin-mediated killing of M_i and M_{ci}
 - 1. If M_i is found, chance of M_i and Mtb death, CCL5 release
 - 2. If M_{ci} is found,
 - a. 75% chance of M_{ci} and Mtb death, CCL5 release
 - b. 20% chance of M_{ci} death, Mtb dispersal, CCL5 release
 - c. 5% chance nothing happens
 - 3. Probability of TNF-independent apoptosis induction in M_i or M_{ci}
 - a. Kill half of intracellular Mtb
 - b. Remaining Mtb uniformly distributed in Moore neighborhood
 - c. Increment local caseation counter
- d. Regulatory T_{reg} :
 - i. Chance of inactivating pro-inflammatory T cells (T_γ)
 - 1. Inactive T_γ state lasts for t_{regT_γ} timesteps.

4.6 Appendix: Detailed methods

4.6.1 Uncertainty and sensitivity analyses

With the Latin hypercube method we determine relevant ranges for each parameter (Tables 4.1 and 4.2), partition this range into M ($= 250$) intervals, and sample each interval once. We sample parameters from uniform or log-uniform distributions, depending on the size of the sampled parameter range (Table 4.1). These samples for each parameter are combined to form M total parameter sets.

Statistical sensitivity analysis allows the quantification of each uncertain parameter by correlating several outcome variables (c.f. Tables 4.A1-4.A4) with variations in each parameter, to compute a partial rank correlation (PRC). One PRC exists for each parameter-variable pair, varying between -1 and 1 , and representing the strength of relationship between the parameter and variable. We use a T test to determine if the correlations are significantly greater than zero, and a Z test to determine if two correlations significantly differ from each other. Due to the number of comparisons made, we use a false-detection correction method (FDR) to prevent spurious indications of significance. For a review of uncertainty and sensitivity analysis methods in systems biology, see (26).

One requirement of statistical sensitivity analysis used here is monotonicity between each parameter-variable relationship. Aleatory uncertainty may cause the model to violate this requirement. Based on recent work in our group (26), we use a modified methodology where each sampled parameter set is run X times, with the average of the outcomes used for the sensitivity analysis. Here X is chosen to be 4, which is sufficient to

reduce the level of uncertainty for this analysis. Thus the total number of simulation runs for each sensitivity analysis is $4M = 1000$.

4.6.2 Measurement of granuloma size

One benefit of an ABM is that it has a spatial representation. To take advantage of this, we developed an algorithm to determine granuloma size for use as an outcome variable in sensitivity analysis. The process was made as simple as possible, with the goal being a quantitative measure of a spatial characteristic for sensitivity analysis. First, a graph of each granuloma at 200 days post-infection (c.f. Figure 4.A1) was manually scored for a granuloma-like structure. Cases lacking a distinct mass or ring of macrophages were assigned a size of 0. For the remaining, we determined the granuloma size based on the median distance from the grid center (coordinate (50, 50)) of all macrophage types defined to be a part of the granuloma. To define the edge of a granuloma, a macrophage was counted as being in the granuloma if more than 6 other macrophages were in its Moore neighborhood.

4.6.3 Simulated deletion and depletion of TNF activities

Five separate parameters were changed to test alterations in specific TNF activities. In a total TNF deletion/depletion, total TNF secretion (parameter s_{TNF}) was set to 0. We removed the effect of TNF-induced trans-endothelial migration by setting TNF-related recruitment parameters (r_{MTNF} and r_{TTNF}) to 0, and the effect of TNF-induced apoptosis activity was removed by setting the probability of TNF-induced apoptosis (p_{apopt}) to 0. We removed macrophage sensitivity to TNF by setting the sensitivity

threshold (τ_{TNF}) to an unattainable level (10^6). To remove specific TNF-induced effects on macrophages, we introduced auxiliary parameters τ_{actTNF} representing the threshold for TNF-induced activation, $\tau_{secrTNF}$, representing the threshold for TNF-induced cytokine/chemokine secretion, and $\tau_{apoptTNF}$, representing the threshold for TNF-induced apoptosis. We then set each threshold to an unattainable level (10^6).

4.7 Appendix: Granuloma Structures

4.7.1 Granuloma structures in global uncertainty analysis

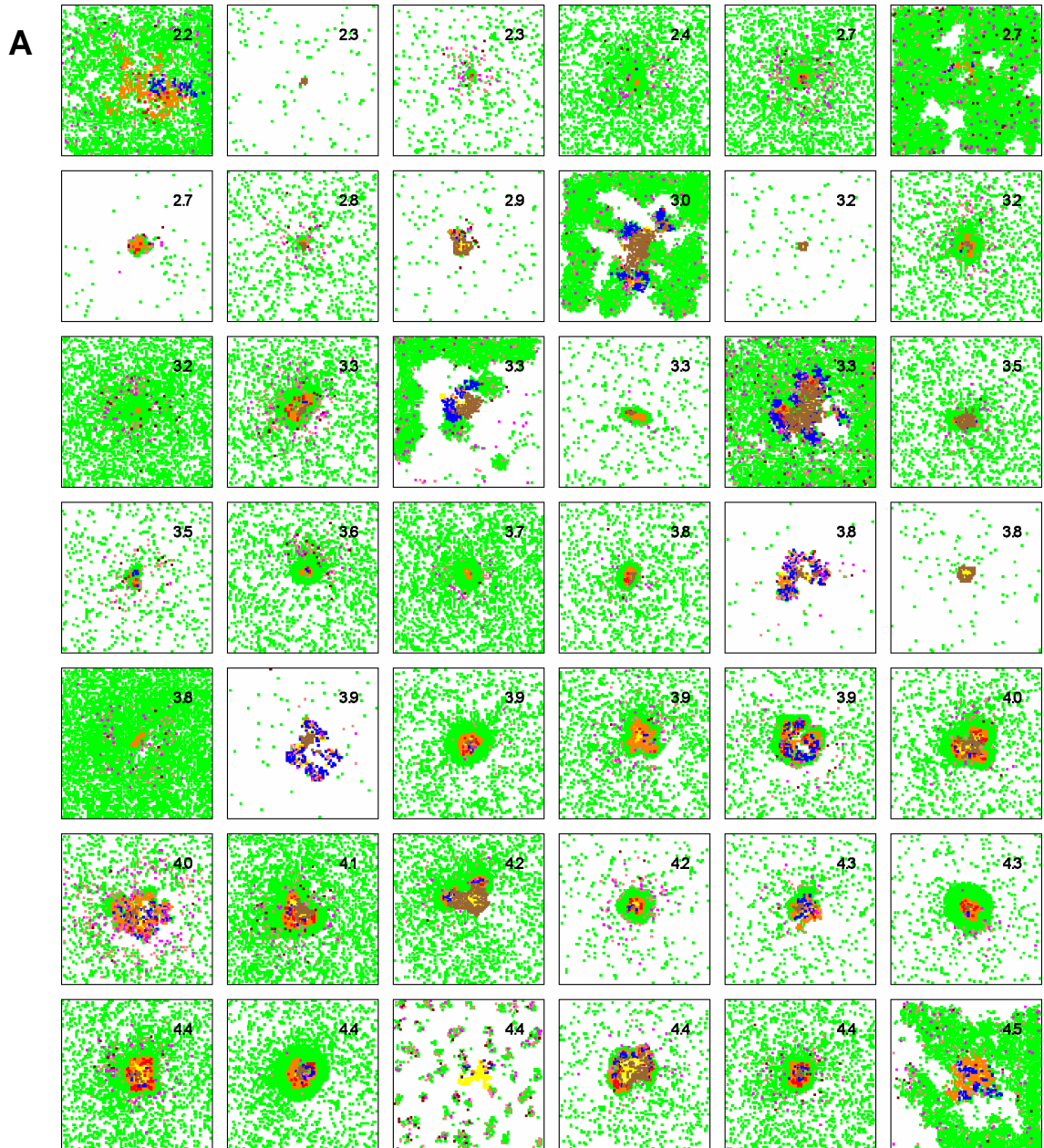


Figure 4.A1. (This figure is 3 pages long.) Attainable granuloma structures 200 days post-infection from one run of global uncertainty analysis. Slides are sorted by number of extracellular bacteria from left to right and top to bottom. 120 total simulations that did not predict complete bacterial elimination are shown. Numbers indicate \log_{10} extracellular *M. tuberculosis* number. Cells are colored as in Figure 4.3. Cell types are colored as follows: green, orange, red and blue are resting, infected, chronically infected and activated macrophages, respectively; yellow, extracellular bacteria; brown, caseation; pink, purple and light blue, pro-inflammatory, cytotoxic, and regulatory T cells, respectively.

B

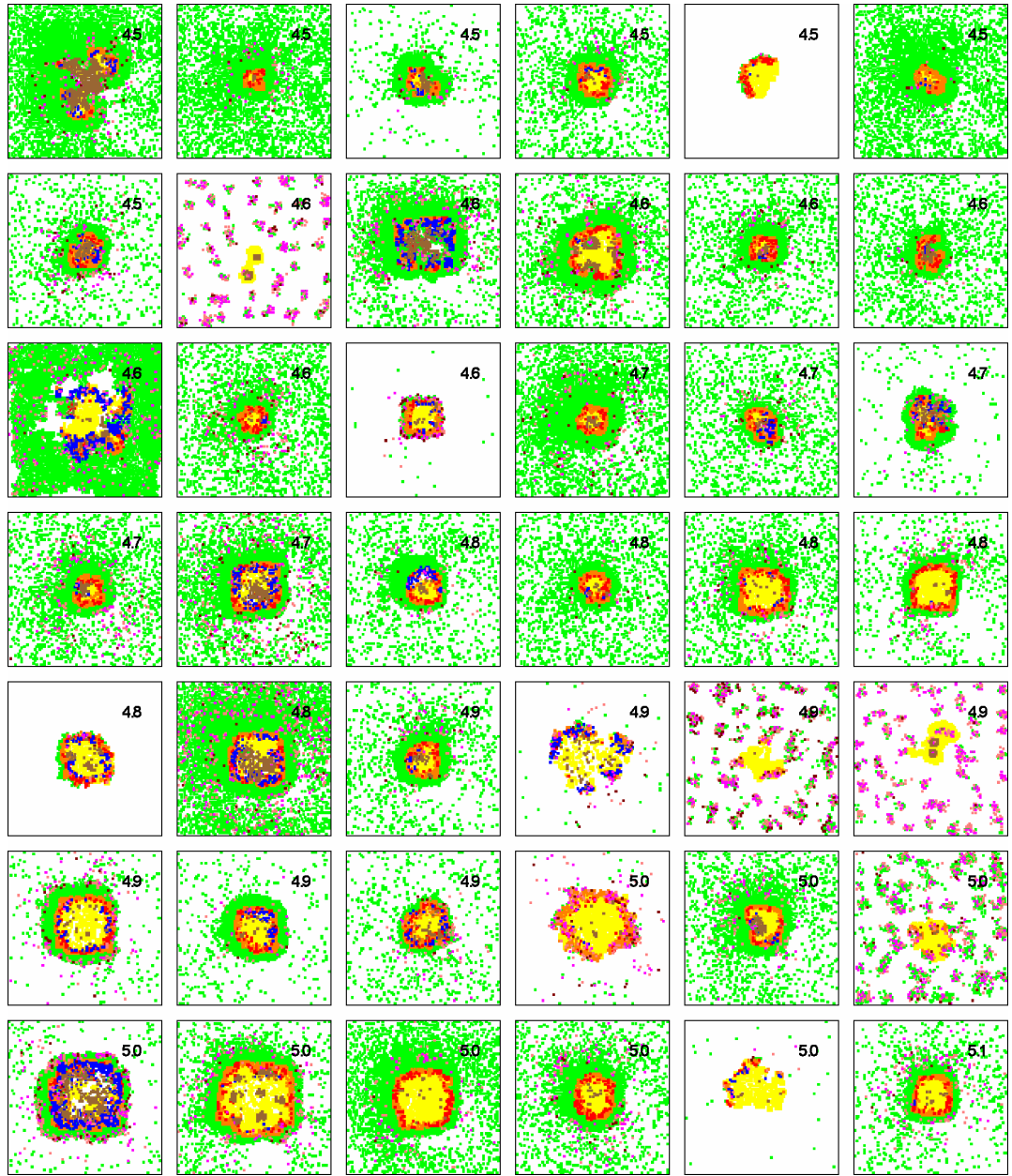


Figure 4.A1B. (continued from previous page)

C

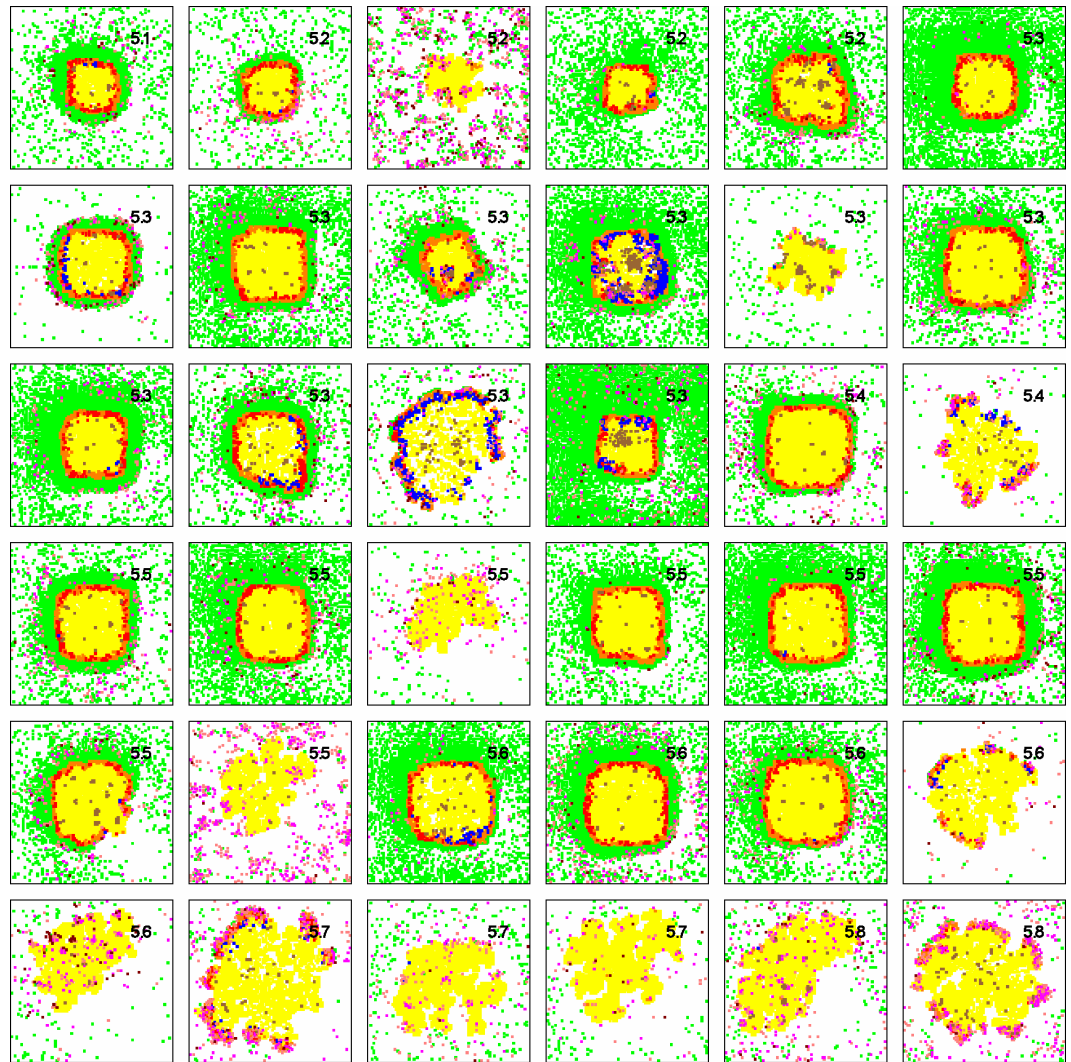


Figure 4.A1C. (continued from previous page)

4.7.2 Granuloma structures in targeted deletion and depletion of TNF activities

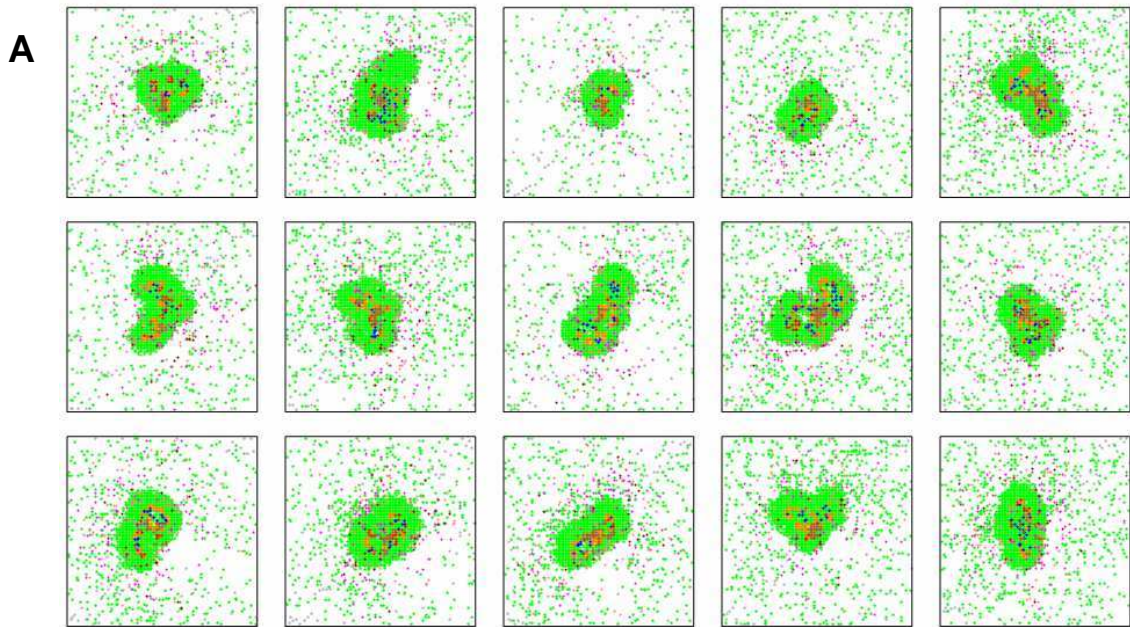


Figure 4.A2. (This figure is 5 pages long.) Granuloma structures predicted for deletion and depletion of each specific TNF activity. Replicates of structures containing infection at day 200 are shown. A. Baseline case with all TNF activities present. B-I. Deletion and depletion, respectively, of: all TNF activity (B, C); TNF-induced recruitment activity (D, E); TNF effects on macrophage activation activity (F, G); and TNF-induced chemokine and TNF secretion from macrophages activities (H, I). In D and F, less than 15 are shown due to complete bacterial elimination occurring before day 200 in some instances.

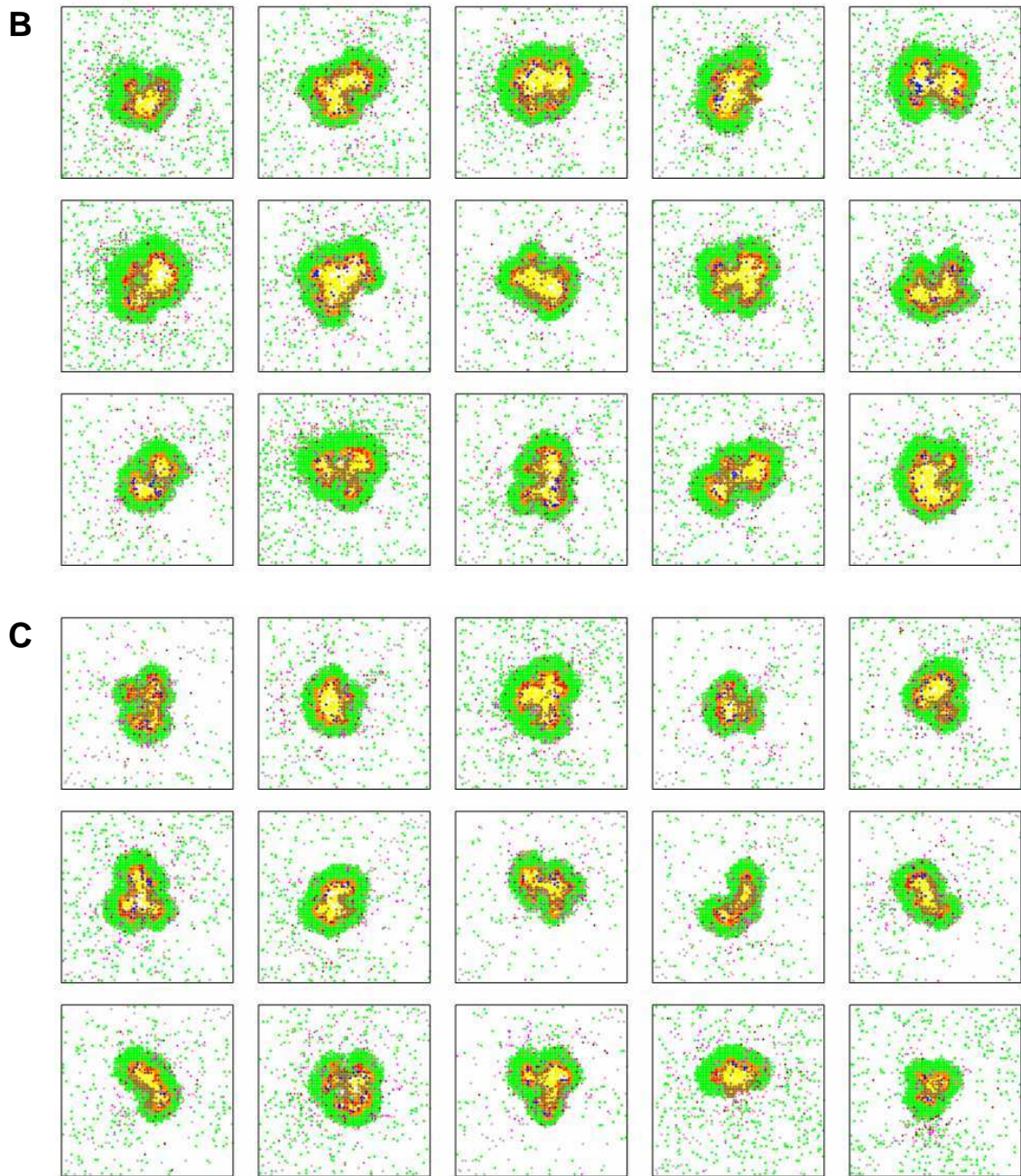


Figure 4.A2 B-C. Deletion (B) and depletion (C) of all TNF activity.

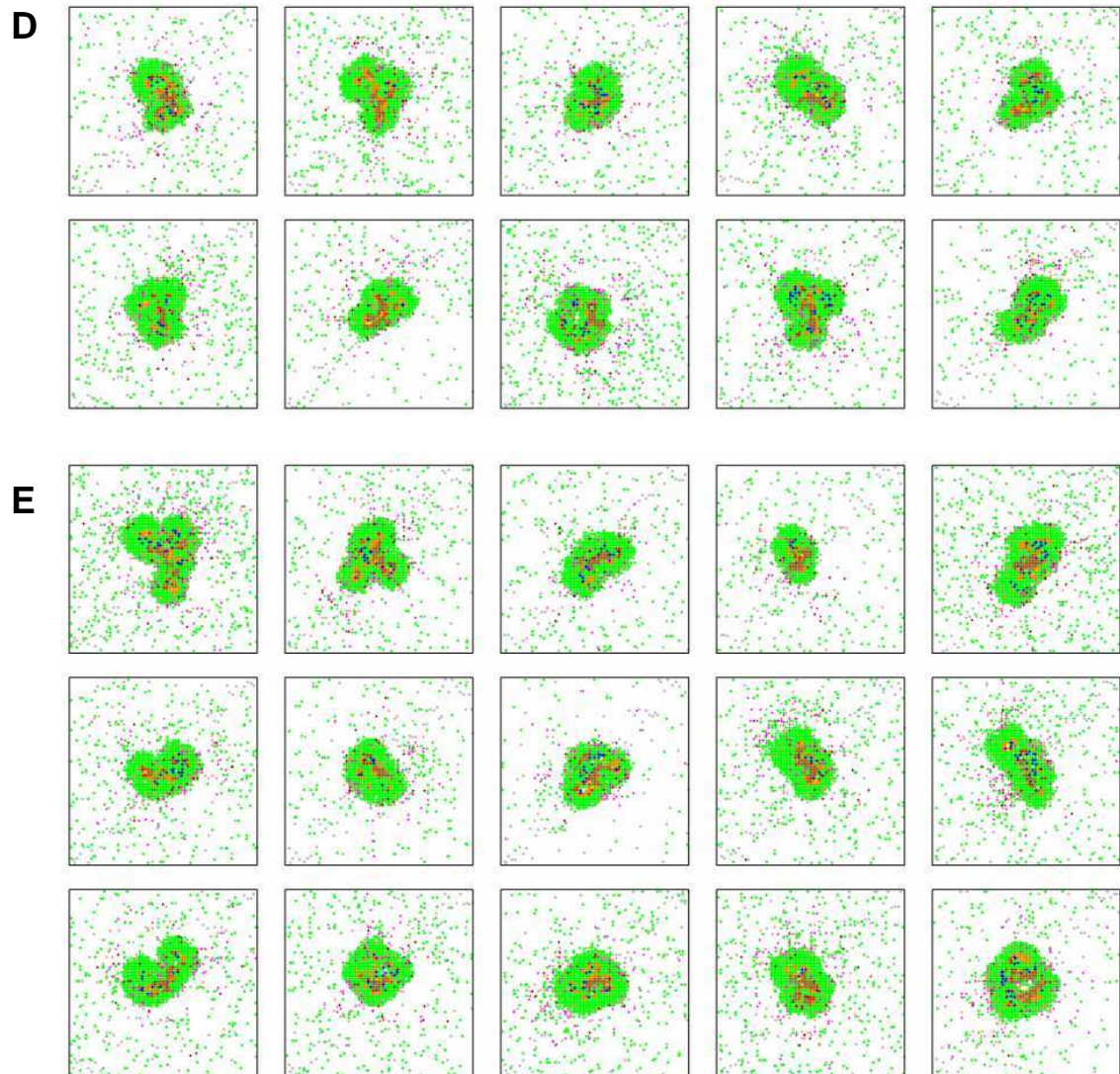


Figure 4.A2 D-E. Deletion (D) and depletion (E) of TNF-induced recruitment.

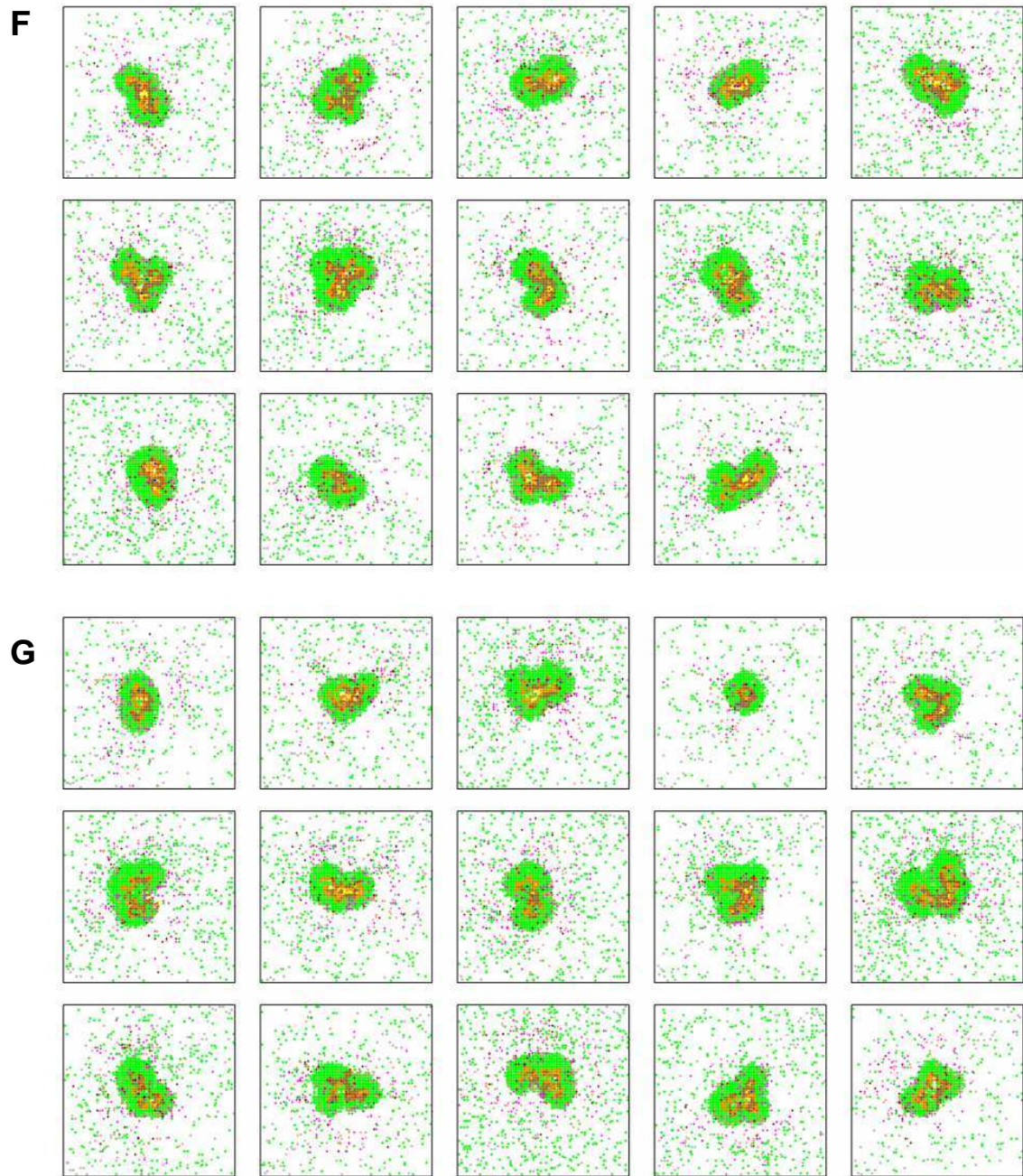


Figure 4.A2 F-G. Deletion (F) and depletion (G) of TNF effects on macrophage activation.

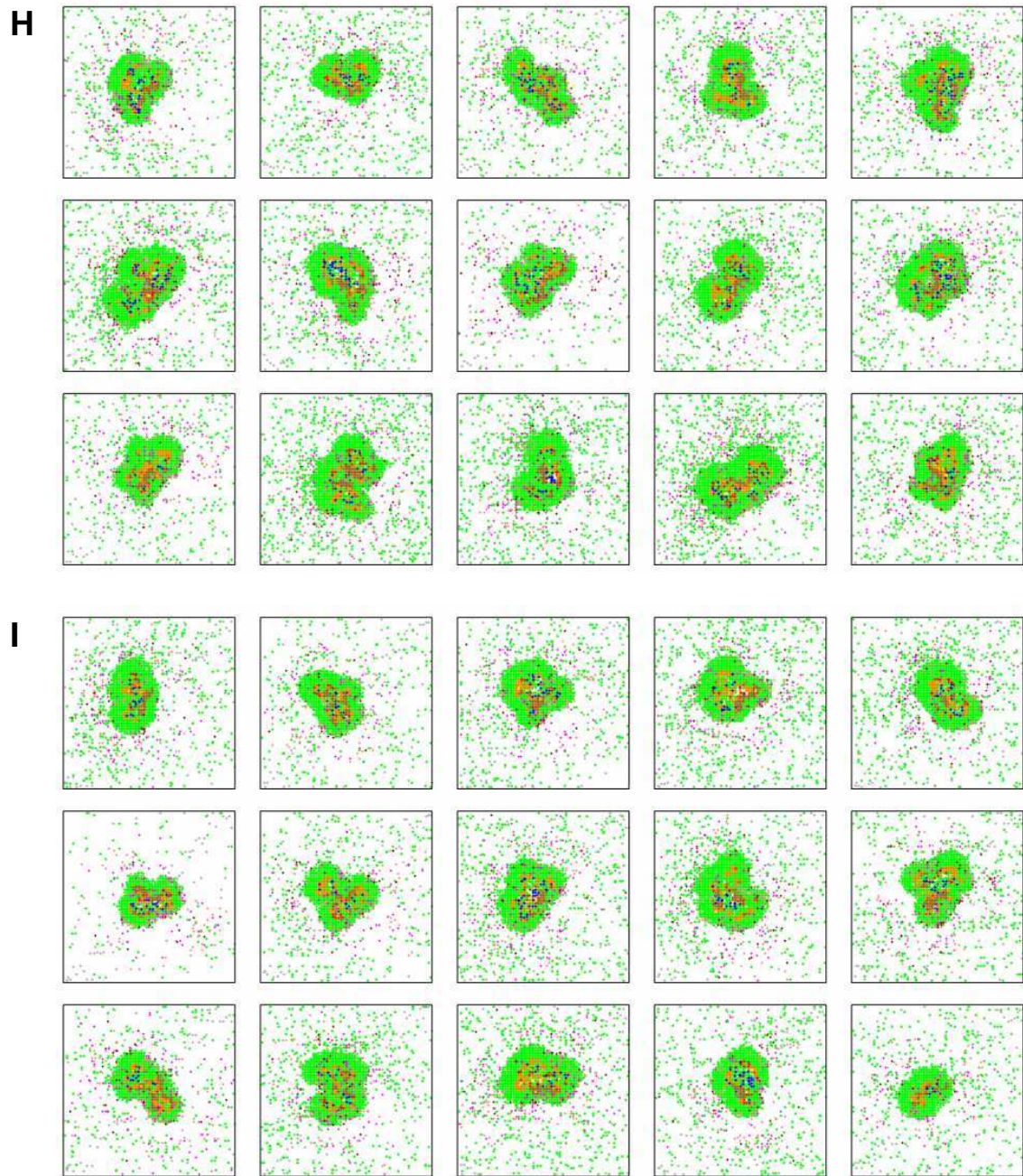


Figure 4.A2 H-I. Deletion (H) and depletion (I) of TNF-induced chemokine and TNF secretion from macrophages.

4.7.3 Granuloma structures in targeted deletion and depletion of TNF activities

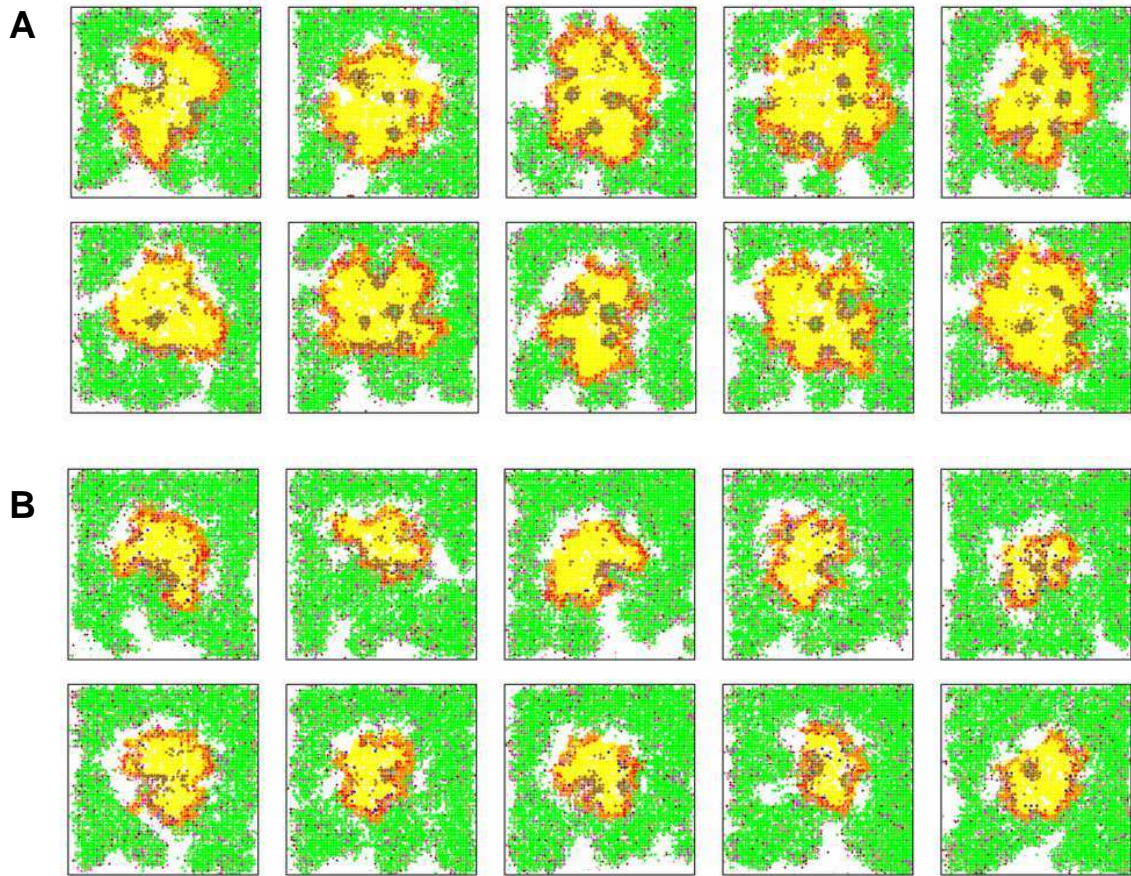


Figure 4.A3. (This figure is 9 pages long.) Granuloma structures predicted for ten replicates of deletion and depletion of specific TNF activity combinations. Replicates of structures containing infection at day 200 are shown. A-R. Deletion and depletion, respectively, of: apoptosis + activation (A, B); apoptosis + secretion activities (C, D); activation + recruitment activities (E, F); activation + secretion activities (G, H); recruitment + secretion activities (I, J); recruitment + activation + apoptosis activities (K, L), recruitment + activation + secretion activities (M, N); recruitment + apoptosis + secretion activities (O, P); activation + apoptosis + secretion activities (Q, R). Each activity refers to specific TNF-induced activities illustrated in Figure 4.1A. In some, less than 10 are shown due to complete bacterial elimination occurring before day 200 in those instances. The combination of apoptosis + recruitment deletion and depletion is omitted due to complete bacterial elimination predicted for all simulations.

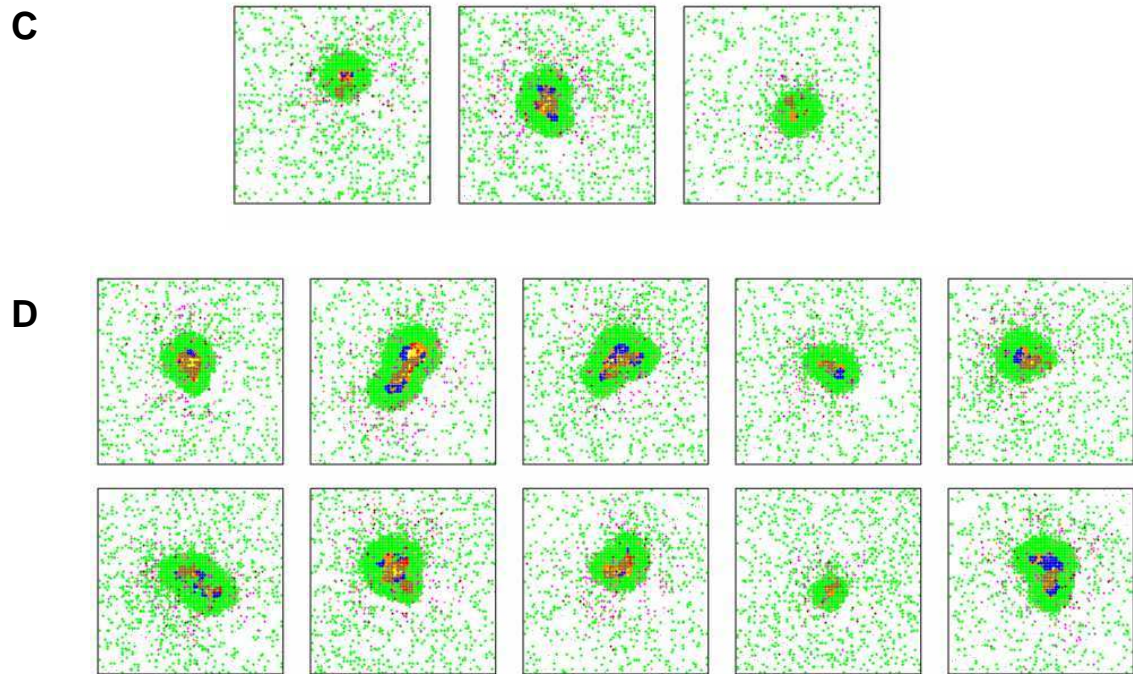


Figure 4.A3 C-D. Deletion (C) and depletion (D) of TNF-induced apoptosis and chemokine/TNF secretion from macrophages.

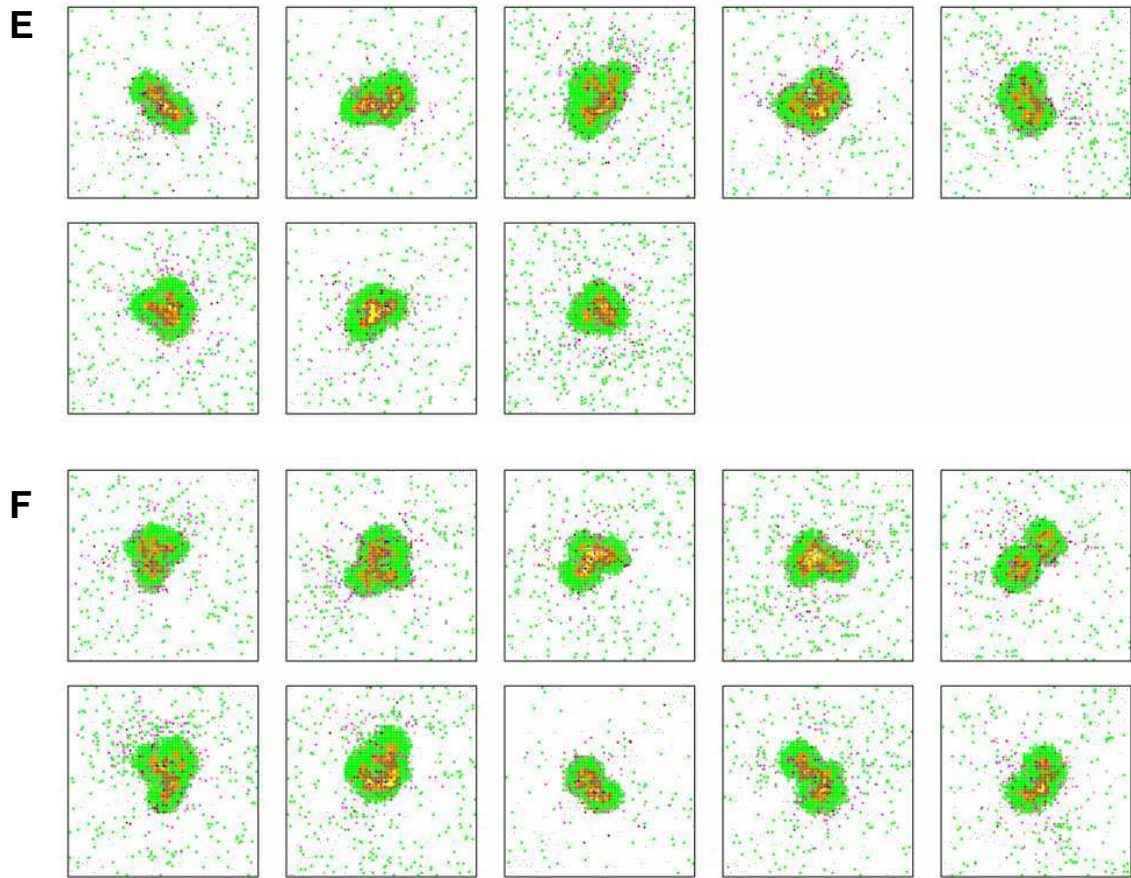


Figure 4.A3 E-F. Deletion (E) and depletion (F) of TNF-induced macrophage activation activity and recruitment of immune cells.

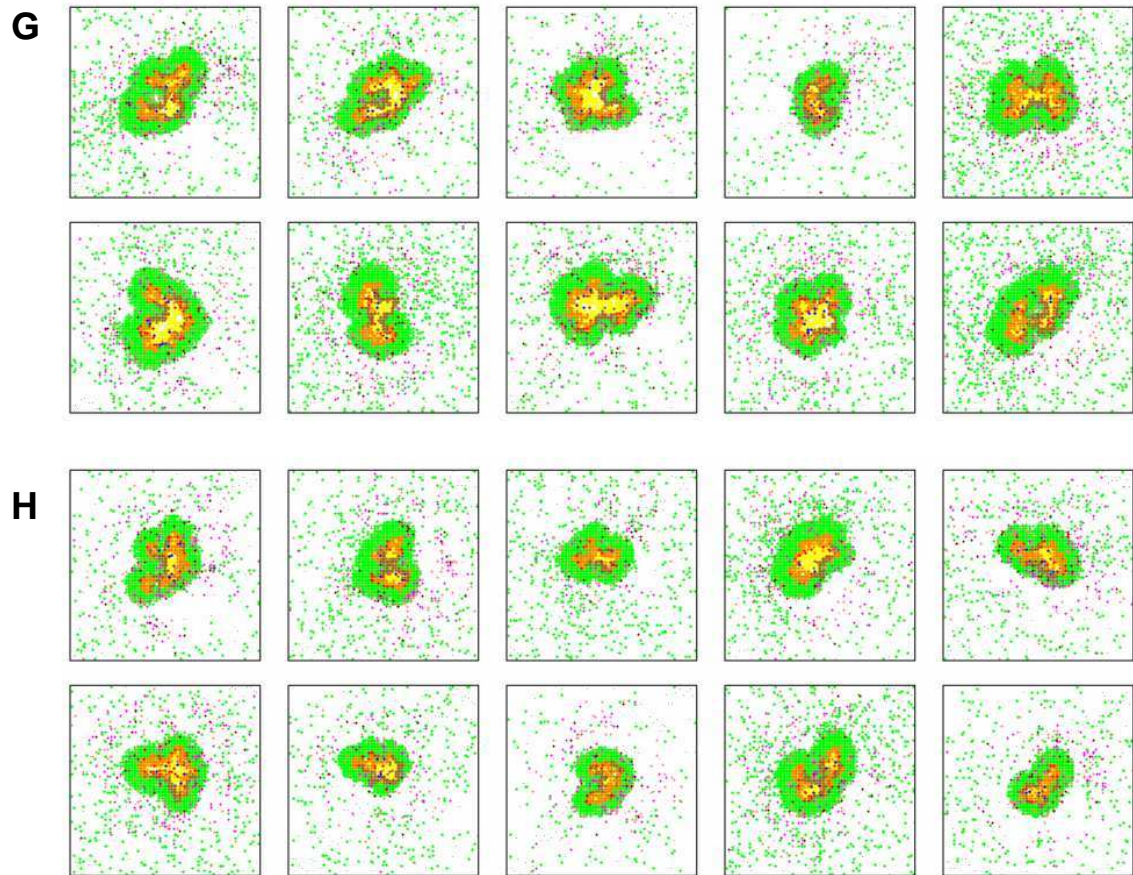


Figure 4.A3 G-H. Deletion (G) and depletion (H) of TNF-induced macrophage activation and chemokine/TNF secretion from macrophages.

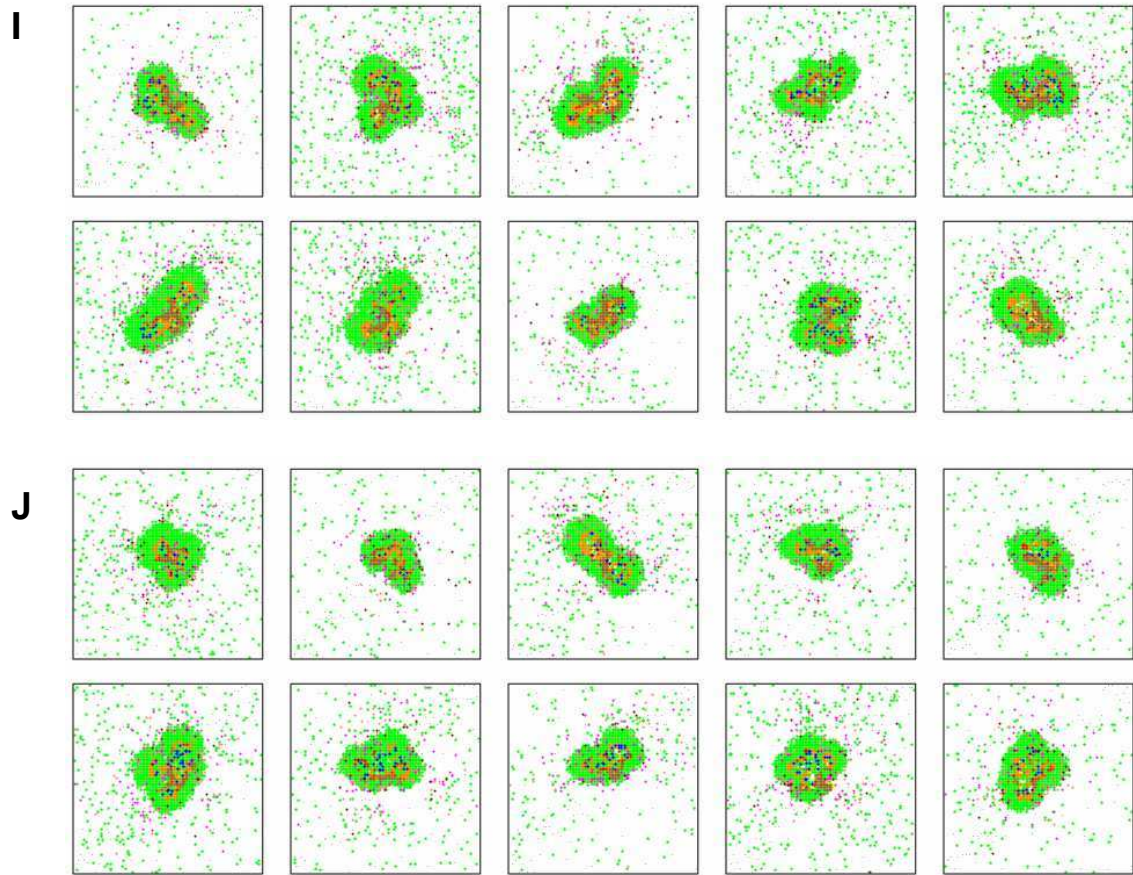


Figure 4.A3 I-J. Deletion (I) and depletion (J) of TNF-induced immune cell recruitment and chemokine/TNF secretion from macrophages.

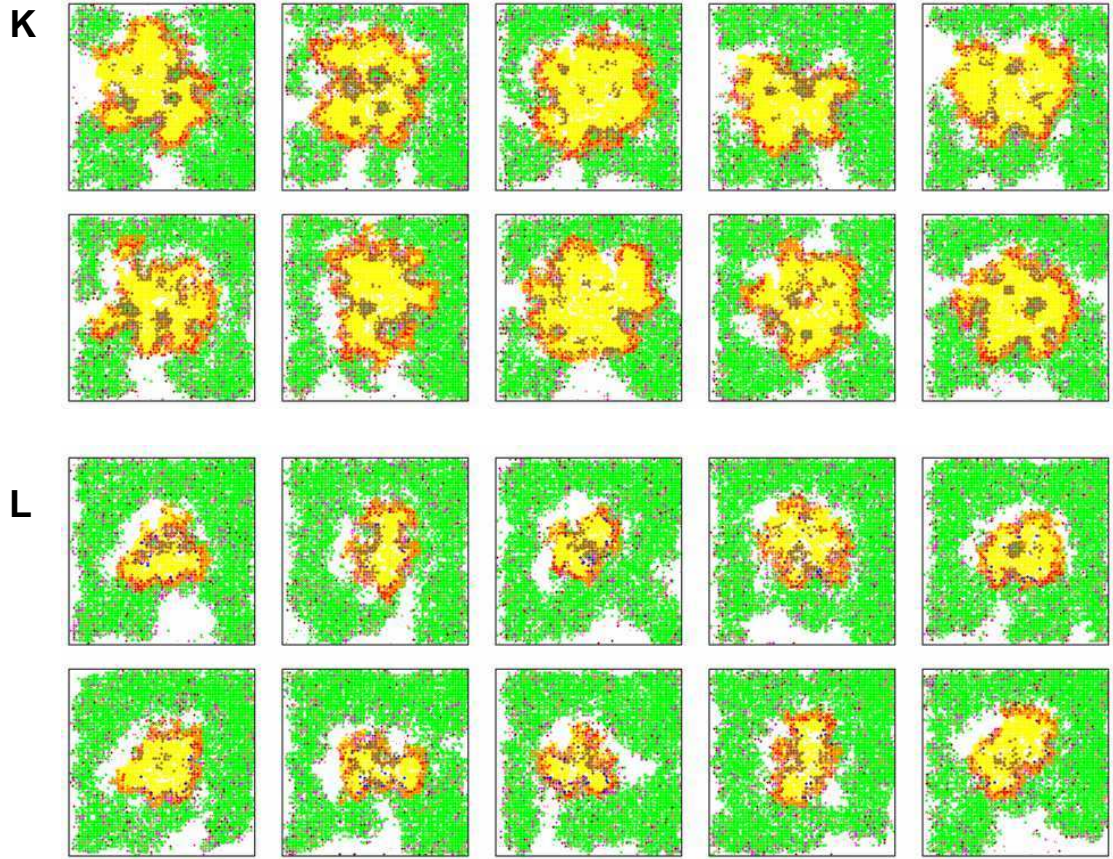


Figure 4.A3 K-L. Deletion (K) and depletion (L) of TNF-induced immune cell recruitment, apoptosis and chemokine/TNF secretion from macrophages.

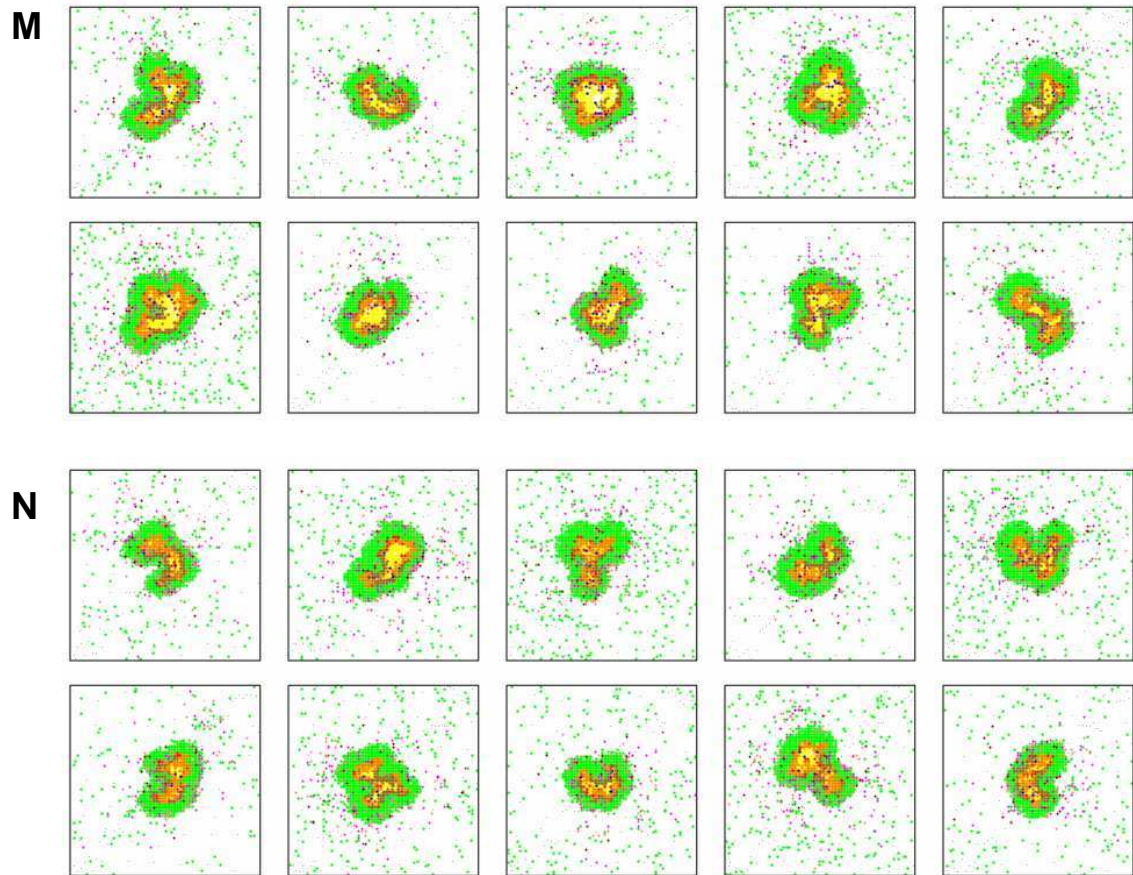


Figure 4.A3 M-N. Deletion (M) and depletion (N) of TNF-induced immune cell recruitment, macrophage activation, and chemokine/TNF secretion from macrophages.

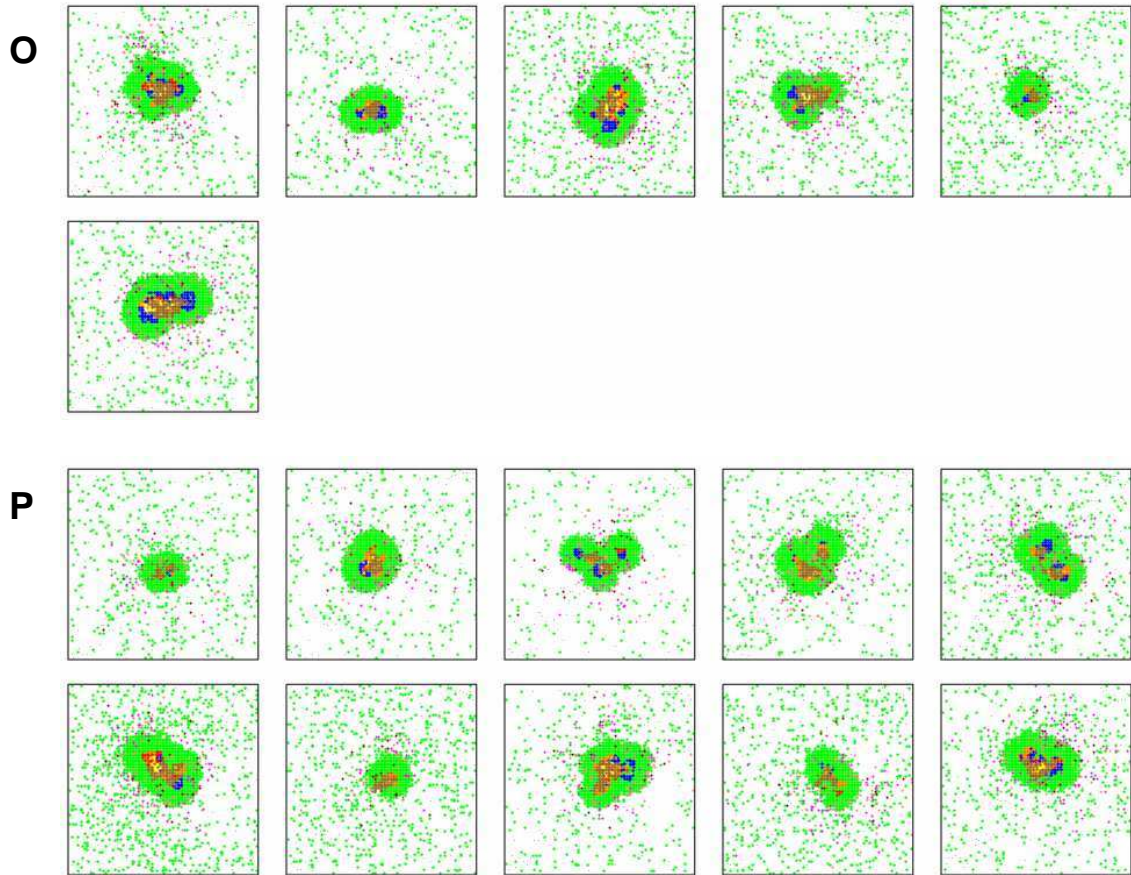


Figure 4.A3 O-P. Deletion (O) and depletion (P) of TNF-induced immune cell recruitment, apoptosis and chemokine/TNF secretion from macrophages.

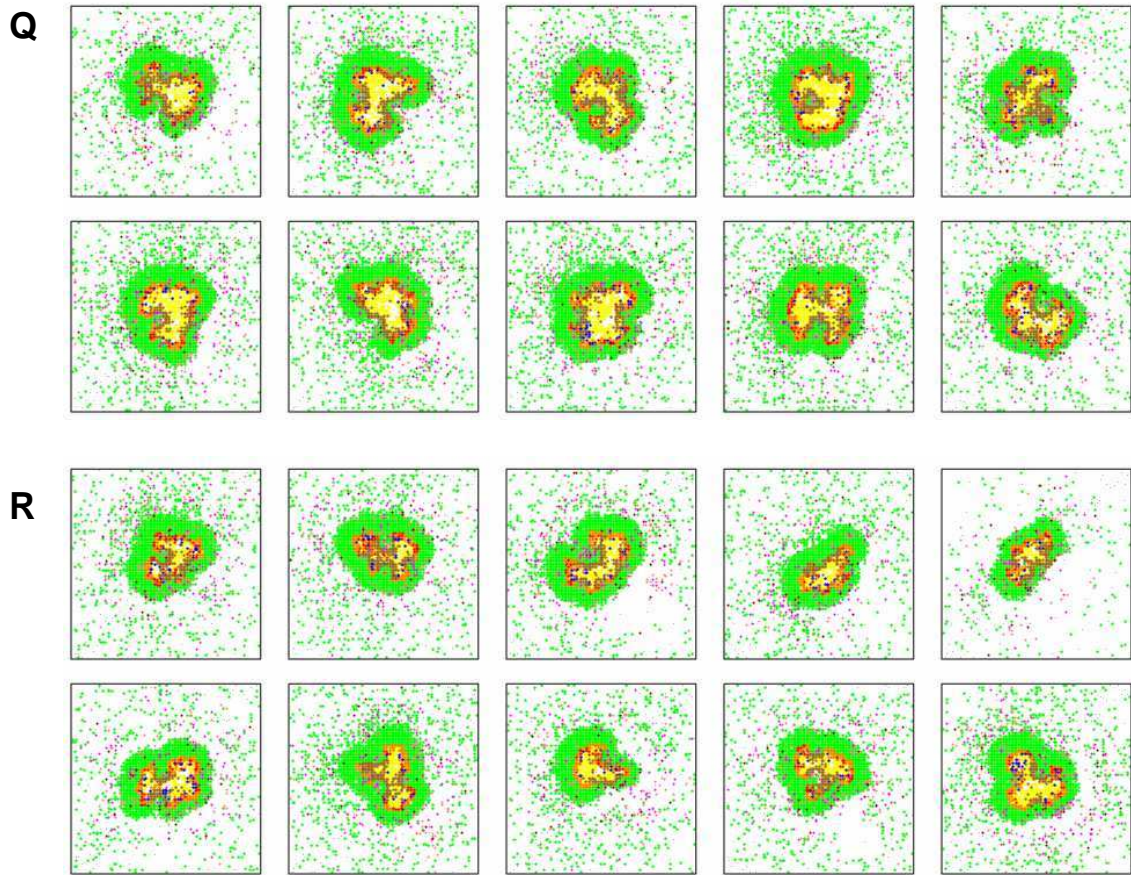


Figure 4.A3 Q-R. Deletion (Q) and depletion (R) of TNF-induced macrophage activation, apoptosis and chemokine/TNF secretion from macrophages.

4.8 Appendix: Global sensitivity analysis and multiple TNF deletions/depletions

Table 4.A1. Significant partial rank correlations between parameters and granuloma variables 200 days post-infection.¹

	α_{Bi}	α_{Be}	T_{actM}	M_{recr}	T_{move}	$STNF$	τ_{TNFsec}
B_e	+++	+			--	---	
B_i	++				---	---	
Total T cells	+				-	---	
T_γ	+				-	---	--
“Secretor” T_γ ²	++		+++			---	
T_c	+				-	---	--
T_{reg}					-	---	-
Total Macrophages				+	---	---	
M_r				+++	--	---	
M_i	++				---	---	
M_{ci}	++				---	---	
M_a					-	---	
TNF					-		-
Chemokines					-	---	-
Caseation	+++					---	
B_e growth rate	++				-	---	
Granuloma Size	+			+	---	---	+

¹Parameter definitions are given in Tables 4.1-4.3. Significant positive correlations: +++ ($p < 0.0001$); ++ ($p < 0.001$); + ($p < 0.01$). Significant negative correlations: --- ($p < 0.0001$); -- ($p < 0.001$); - ($p < 0.01$).

²Number of T_γ cells actively secreting IFN- γ .

Table 4.A2. Significant partial rank correlations between parameters and granuloma variables 20 days post-infection (immediately preceding adaptive immunity).¹

	α_{B_i}	α_{B_e}	M_{recr}	δ_{TNF}	S_c	S_{TNF}	τ_{TNFsec}	$\tau_{TNFapopt}$	ρ_{apopt}
B _e	+	+++				---			
B _i	+++					---		++	-
Total Macrophages			++			---			---
M _r			+++	-		---			--
M _i	+					---		+	-
M _{ci}	+++					---			
TNF				-				+	---
Chemokines	+	+			+	--	-	+	---
B _e growth rate	++	+				---			

¹Parameter definitions are given in Tables 4.1-4.3. Significant positive correlations: +++ (p < 0.0001); ++ (p < 0.001); + (p < 0.01). Significant negative correlations: --- (p < 0.0001); -- (p < 0.001); - (p < 0.01).

Table 4.A3. Significant changes in granuloma variables at 200 days post-infection for deletion and depletion of combinations of two individual TNF activities versus the baseline control scenario¹. Sample granuloma structures for each deletion and depletion are shown in Figures 4.9 and 4.A2. Apo: TNF-induced apoptosis; Rec: TNF-mediated recruitment; Act: TNF-mediated activation; Sec: TNF-induced chemokine/TNF secretion.

	Apo + Rec		Apo + Act		Apo + Sec		Act + Rec		Act + Sec		Rec + Sec	
	Del	Depl	Del	Depl	Del	Depl	Del	Depl	Del	Depl	Del	Depl
B _e	---	---	+++	+++			++	+++	+++	+++		
B _i	---	---	+++	+++	-				+++	+++	+++	
Total T cells	+	+++	+++	+++			-	--	++			-
T _γ	+	+++	+++	+++			-	--	++			-
“Secretor” T _γ ²	+	-	--		--			+		++	++	
T _c	+	++	+++	+++			-	-	+			--
T _{reg}	+	++	+++	+++				-				
Total Macrophages		+++	+++	+++			---	---				--
M _r		+++	+++	+++			---				-	
M _i	---	---	+++	+++	---	--			+++	+++	++	
M _{ci}	---	---	+++	+++					++	+		
M _a	++	+	---				---	---	---	---		
TNF	+	+++	+++	+++							++	
Chemokines	+	+++	+++	+++							++	
Caseation	---	---	+++	+++		+	++	++	+++	+	+++	+
Granuloma Size	ND ³	ND ³	ND ³	ND ³	-				+++			

¹+ denotes a higher variable value for the deletion or depletion than the control scenario; - denotes a lower value. +++ (p < 0.0001); ++ (p < 0.001); + (p < 0.01). Significant negative correlations: --- (p < 0.0001); -- (p < 0.001); - (p < 0.01).

²Number of T_γ cells actively secreting IFN-γ.

³Granuloma structures lack distinct bounds for quantification in these cases.

Table 4.A4. Significant changes in granuloma variables at 200 days post-infection for deletion and depletion of combinations of three individual TNF activities versus the baseline control scenario¹. Sample granuloma structures for each deletion and depletion are shown in Figures 4.9 and 4.A2. Apo: TNF-induced apoptosis; Rec: TNF-mediated recruitment; Act: TNF-mediated activation; Sec: TNF-induced chemokine/TNF secretion.

	Rec + Act + Apo		Rec + Act + Sec		Rec + Apo + Sec		Act + Apo + Sec	
	Del	Depl	Del	Depl	Del	Depl	Del	Depl
B _e	+++	+++	+++	+++			+++	+++
B _i	+++	+++	+++	+++			+++	+++
Total T cells	+++	+++	-		-	---	+++	+
T _γ	+++	+++	-		-	---	+++	
“Secretor” T _γ ²	--	+			-	-	+++	+
T _c	+++	+++			-	---	+++	+
T _{reg}	+++	+++					+++	+
Total Macrophages	+++	+++	--	--			+++	+
M _r	+++	+++	---	---			+++	
M _i	+++	+++	+++	+++	-	-	+++	+++
M _{ci}	+++	+++	++	++			+++	+++
M _a	---		--	---			+	
TNF	+++	+++	++	+++			+++	+++
Chemokines	+++	+++	++	+++			+++	+++
Caseation	+++	+++	+++	+++		+	+++	+++
Granuloma Size	ND ³	ND ³	++				+++	+++

¹+ denotes a higher variable value for the deletion or depletion than the control scenario; - denotes a lower value. +++ (p < 0.0001); ++ (p < 0.001); + (p < 0.01). Significant negative correlations: --- (p < 0.0001); -- (p < 0.001); - (p < 0.01).

²Number of T_γ cells actively secreting IFN-γ.

³Granuloma structures lack distinct bounds for quantification in these cases.

4.9 References

1. **Algood, H. M., P. L. Lin, and J. L. Flynn.** 2005. Tumor necrosis factor and chemokine interactions in the formation and maintenance of granulomas in tuberculosis. *Clin Infect Dis* **41 Suppl 3**.
2. **Asano, M., M. Toda, N. Sakaguchi, and S. Sakaguchi.** 1996. Autoimmune disease as a consequence of developmental abnormality of a T cell subpopulation. *J Exp Med* **184**:387-396.
3. **Baatar, D., P. Olkhanud, K. Sumitomo, D. Taub, R. Gress, and A. Biragyn.** 2007. Human Peripheral Blood T Regulatory Cells (Tregs), Functionally Primed CCR4+ Tregs and Unprimed CCR4- Tregs, Regulate Effector T Cells Using FasL. *J Immunol* **178**:4891-4900.
4. **Bean, A., D. Roach, H. Briscoe, M. France, H. Korner, J. Sedgwick, and W. Britton.** 1999. Structural Deficiencies in Granuloma Formation in TNF Gene-Targeted Mice Underlie the Heightened Susceptibility to Aerosol Mycobacterium tuberculosis Infection, Which Is Not Compensated for by Lymphotoxin. *J Immunol* **162**:3504-3511.
5. **Bekker, L. G., S. Freeman, P. J. Murray, B. Ryffel, and G. Kaplan.** 2001. TNF-alpha controls intracellular mycobacterial growth by both inducible nitric oxide synthase-dependent and inducible nitric oxide synthase-independent pathways. *J Immunol* **166**:6728--6734.
6. **Emile, J. F., N. Patey, F. Altare, S. Lamhamedi, E. Jouanguy, F. Boman, J. Quillard, M. Lecomte-Houcke, O. Verola, J. F. Mousnier, F. Dijoud, S. Blanche, A. Fischer, N. Brousse, and J. L. Casanova.** 1997. Correlation of granuloma structure with clinical outcome defines two types of idiopathic disseminated BCG infection. *Journal of Pathology* **181**:25-30.
7. **Emile, J. F., N. Patey, F. Altare, S. Lamhamedi, E. Jouanguy, F. Boman, J. Quillard, M. Lecomte-Houcke, O. Verola, J. F. Mousnier, F. Dijoud, S. Blanche, A. Fischer, N. Brousse, and J. L. Casanova.** 1997. Correlation of granuloma structure with clinical outcome defines two types of idiopathic disseminated BCG infection. *Journal of Pathology* **181**: 25-30.
8. **Flesch, I., and S. Kaufmann.** 1987. Mycobacterial growth inhibition by interferon-gamma-activated bone marrow macrophages and differential susceptibility among strains of *Mycobacterium tuberculosis*. *J Immunol* **138**:4408-4413.
9. **Flesch, I. E., and S. H. Kaufmann.** 1990. Activation of tuberculostatic macrophage functions by gamma interferon, interleukin-4, and tumor necrosis factor. *Infect Immun* **58**:2675-2677.

10. **Flynn, J. L., and J. Chan.** 2001. Immunology of tuberculosis. *Annu Rev Immunol* **19**:93--129.
11. **Flynn, J. L., M. M. Goldstein, J. Chan, K. J. Triebold, K. Pfeffer, C. J. Lowenstein, R. Schreiber, T. W. Mak, and B. R. Bloom.** 1995. Tumor necrosis factor-alpha is required in the protective immune response against *Mycobacterium tuberculosis* in mice. *Immunity* **2**:561-572.
12. **Fratazzi, C., R. D. Arbeit, C. Carini, M. K. Balcewicz-Sablinska, J. Keane, H. Kornfeld, and H. G. Remold.** 1999. Macrophage apoptosis in mycobacterial infections. *J Leukoc Biol* **66**:763-764.
13. **Grode, L., P. Seiler, S. Baumann, J. Hess, V. Brinkmann, A. Nasser Eddine, P. Mann, C. Goosmann, S. Bander mann, D. Smith, G. J. Bancroft, J. M. Reyrat, D. van Soolingen, B. Raupach, and S. H. Kaufmann.** 2005. Increased vaccine efficacy against tuberculosis of recombinant *Mycobacterium bovis* bacille Calmette-Guerin mutants that secrete listeriolysin. *J Clin Invest* **115**:2472-2479.
14. **Guyot-Revol, V., J. A. Innes, S. Hackforth, T. Hinks, and A. Lalvani.** 2006. Regulatory T cells are expanded in blood and disease sites in patients with tuberculosis. *Am J Respir Crit Care Med* **173**:803-810.
15. **Hinchey, J., S. Lee, B. Y. Jeon, R. J. Basaraba, M. M. Venkataswamy, B. Chen, J. Chan, M. Braunstein, I. M. Orme, S. C. Derrick, S. L. Morris, W. R. Jacobs, and S. A. Porcelli.** 2007. Enhanced priming of adaptive immunity by a proapoptotic mutant of *Mycobacterium tuberculosis*. *J Clin Invest* **117**:2279-2288.
16. **Huse, M., B. F. Lillemeier, M. S. Kuhns, D. S. Chen, and M. M. Davis.** 2006. T cells use two directionally distinct pathways for cytokine secretion. *Nature Immunology* **7**:247-255.
17. **Ishii, N., K. Nakahigashi, T. Baba, M. Robert, T. Soga, A. Kanai, T. Hirasawa, M. Naba, K. Hirai, A. Hoque, P. Ho, Y. Kakazu, K. Sugawara, S. Igarashi, S. Harada, T. Masuda, N. Sugiyama, T. Togashi, M. Hasegawa, Y. Takai, K. Yugi, K. Arakawa, N. Iwata, Y. Toya, Y. Nakayama, T. Nishioka, K. Shimizu, H. Mori, and M. Tomita.** 2007. Multiple High-Throughput Analyses Monitor the Response of *E. coli* to Perturbations. *Science* **316**:593-597.
18. **Keane, J., M. K. Balcewicz-Sablinska, H. G. Remold, G. L. Chupp, B. B. Meek, M. J. Fenton, and H. Kornfeld.** 1997. Infection by *Mycobacterium tuberculosis* promotes human alveolar macrophage apoptosis. *Infect Immun* **65**:298-304.
19. **Keane, J., S. Gershon, R. P. Wise, E. Mirabile-Levens, J. Kasznica, W. D. Schwieterman, J. N. Siegel, and M. M. Braun.** 2001. Tuberculosis associated

- with infliximab, a tumor necrosis factor alpha-neutralizing agent. *N Engl J Med* **345**:1098-1104.
20. **Keane, J., H. G. Remold, and H. Kornfeld.** 2000. Virulent *Mycobacterium tuberculosis* strains evade apoptosis of infected alveolar macrophages. *J Immunol* **164**:2016-2020.
 21. **Kramnik, I., W. F. Dietrich, P. Demant, and B. R. Bloom.** 2000. Genetic control of resistance to experimental infection with virulent *Mycobacterium tuberculosis*. *Proc Natl Acad Sci U S A* **97**:8560-8565.
 22. **Kristensen, N. N., M. Gad, A. R. Thomsen, B. Lu, C. Gerard, and M. H. Claesson.** 2006. CXC chemokine receptor 3 expression increases the disease-inducing potential of CD4⁺ CD25⁻ T cells in adoptive transfer colitis. *Inflamm Bowel Dis* **12**:374-381.
 23. **Krombach, F., S. Münzing, A. M. Allmeling, J. T. Gerlach, J. Behr, and M. Dörger.** 1997. Cell size of alveolar macrophages: an interspecies comparison. *Environ Health Perspect* **105 Suppl 5**:1261-1263.
 24. **Laster, S. M., J. G. Wood, and L. R. Gooding.** 1988. Tumor necrosis factor can induce both apoptic and necrotic forms of cell lysis. *J Immunol* **141**:2629-2634.
 25. **Lin, P. L., S. Pawar, A. Myers, A. Pegu, C. Fuhrman, T. A. Reinhart, S. V. Capuano, E. Klein, and J. L. Flynn.** 2006. Early events in *Mycobacterium tuberculosis* infection in cynomolgus macaques. *Infect Immun* **74**:3790-3803.
 26. **Marino, S., I. Hogue, C. Ray, and D. Kirschner.** 2008. A methodology for performing global uncertainty and sensitivity analysis in systems biology. *J Theor Biol* (in press).
 27. **Marino, S., D. Sud, H. Plessner, P. L. Lin, J. Chan, J. L. Flynn, and D. E. Kirschner.** 2007. Differences in reactivation of tuberculosis induced from anti-TNF treatments are based on bioavailability in granulomatous tissue. *PLoS Comput Biol* **3**:1909-1924.
 28. **Mason, C. M., E. Porretta, P. Zhang, and S. Nelson.** 2007. CD4⁺CD25⁺transforming growth factor--producing T cells are present in the lung in murine tuberculosis and may regulate the host inflammatory response. *Clinical & Experimental Immunology* **148**:537-545.
 29. **Mohan, K., Z. Ding, J. Hanly, and T. B. Issekutz.** 2002. IFN-gamma-inducible T cell alpha chemoattractant is a potent stimulator of normal human blood T lymphocyte transendothelial migration: differential regulation by IFN-gamma and TNF-alpha. *J Immunol* **168**:6420-6428.

30. **Mohan, V. P., C. A. Scanga, K. Yu, H. M. Scott, K. E. Tanaka, E. Tsang, M. M. Tsai, J. L. Flynn, and J. Chan.** 2001. Effects of tumor necrosis factor alpha on host immune response in chronic persistent tuberculosis: possible role for limiting pathology. *Infect Immun* **69**:1847-1855.
31. **Ordway, D., M. Henao-Tamayo, M. Harton, G. Palanisamy, J. Troudt, C. Shanley, R. Basaraba, and I. Orme.** 2007. The Hypervirulent Mycobacterium tuberculosis Strain HN878 Induces a Potent TH1 Response followed by Rapid Down-Regulation. *J Immunol* **179**:522-531.
32. **Pan, H., B.-S. Yan, M. Rojas, Y. Shebzukhov, H. Zhou, L. Kobzik, D. Higgins, M. Daly, B. Bloom, and I. Kramnik.** 2005. Ipr1 gene mediates innate immunity to tuberculosis. *Nature* **434**:767-772.
33. **Paul, S., P. Laochumroonvorapong, and G. Kaplan.** 1996. Comparable growth of virulent and avirulent Mycobacterium tuberculosis in human macrophages in vitro. *J Infect Dis* **174**:105-112.
34. **Peters, W., J. G. Cyster, M. Mack, D. Schlöndorff, A. J. Wolf, J. D. Ernst, and I. F. Charo.** 2004. CCR2-dependent trafficking of F4/80dim macrophages and CD11cdim/intermediate dendritic cells is crucial for T cell recruitment to lungs infected with Mycobacterium tuberculosis. *J Immunol* **172**:7647-7653.
35. **Ridley, M., C. Heather, I. Brown, and D. Willoughby.** 1983. Experimental epithelioid cell granulomas tubercle formation and immunological competence: An ultrastructural analysis. *The Journal of Pathology* **141**:97-112.
36. **Riggs, T., A. Walts, N. Perry, L. Bickle, J. N. Lynch, A. Myers, J. Flynn, J. J. Linderman, M. J. Miller, and D. E. Kirschner.** 2008. A comparison of random vs. chemotaxis-driven contacts of T cells with dendritic cells during repertoire scanning. *J Theor Biol* **250**:732-751.
37. **Roach, D., A. Bean, C. Demangel, M. France, H. Briscoe, and W. Britton.** 2002. TNF Regulates Chemokine Induction Essential for Cell Recruitment, Granuloma Formation, and Clearance of Mycobacterial Infection. *J Immunol* **168**:4620-4627.
38. **Roberts, T., N. Beyers, A. Aguirre, and G. Walzl.** 2007. Immunosuppression during active tuberculosis is characterized by decreased interferon- gamma production and CD25 expression with elevated forkhead box P3, transforming growth factor- beta , and interleukin-4 mRNA levels. *J Infect Dis* **195**:870-878.
39. **Rook, G. A., J. Steele, M. Ainsworth, and B. R. Champion.** 1986. Activation of macrophages to inhibit proliferation of Mycobacterium tuberculosis: comparison of the effects of recombinant gamma-interferon on human monocytes and murine peritoneal macrophages. *Immunology* **59**:333-338.

40. **Sakaguchi, S., N. Sakaguchi, M. Asano, M. Itoh, and M. Toda.** 1995. Immunologic self-tolerance maintained by activated T cells expressing IL-2 receptor alpha-chains (CD25). Breakdown of a single mechanism of self-tolerance causes various autoimmune diseases. *J Immunol* **155**:1151-1164.
41. **Segovia-Juarez, J. L., S. Ganguli, and D. Kirschner.** 2004. Identifying control mechanisms of granuloma formation during *M. tuberculosis* infection using an agent-based model. *J Theor Biol* **231**:357-376.
42. **Stein, J., and C. Nombela-Arrieta.** 2005. Chemokine control of lymphocyte trafficking: a general overview. *Immunology* **116**:1-12.
43. **Styblo, K.** 1980. Recent advances in epidemiological research in tuberculosis. . *Adv Tuberc Res* **20**:1-63.
44. **Theus, S., K. Eisenach, N. Fomukong, R. F. Silver, and M. D. Cave.** 2007. Beijing family *Mycobacterium tuberculosis* strains differ in their intracellular growth in THP-1 macrophages. *Int J Tuberc Lung Dis* **11**:1087-1093.
45. **Thornton, A. M., and E. M. Shevach.** 1998. CD4+CD25+ immunoregulatory T cells suppress polyclonal T cell activation in vitro by inhibiting interleukin 2 production. *J Exp Med* **188**:287-296.
46. **Valente, A. J., D. T. Graves, C. E. Vialle-Valentin, R. Delgado, and C. J. Schwartz.** 1988. Purification of a monocyte chemotactic factor secreted by nonhuman primate vascular cells in culture. *Biochemistry* **27**:4162-4168.
47. **van Buul, J., and P. Hordijk.** 2004. Signaling in Leukocyte Transendothelial Migration. *Arterioscler Thromb Vasc Biol* **24**:824-833.
48. **Velmurugan, K., B. Chen, J. L. Miller, S. Azogue, S. Gurses, T. Hsu, M. Glickman, W. R. Jacobs, S. A. Porcelli, and V. Briken.** 2007. *Mycobacterium tuberculosis* nuoG Is a Virulence Gene That Inhibits Apoptosis of Infected Host Cells. *PLoS Pathog* **3**.
49. **Warrender, C., S. Forrest, and F. Koster.** 2006. Modeling intercellular interactions in early *Mycobacterium* infection. *Bull Math Biol* **68**:2233-2261.
50. **Winthrop, K. L.** 2006. Risk and prevention of tuberculosis and other serious opportunistic infections associated with the inhibition of tumor necrosis factor. *Nat Clin Pract Rheumatol* **2**:602-610.
51. **Yan, B. S., A. V. Pichugin, O. Jobe, L. Helming, E. B. Eruslanov, J. A. Gutierrez-Pabello, M. Rojas, Y. V. Shebzukhov, L. Kobzik, and I. Kramnik.** 2007. Progression of pulmonary tuberculosis and efficiency of bacillus Calmette-

Guerin vaccination are genetically controlled via a common *sst1*-mediated mechanism of innate immunity. *J Immunol* **179**:6919-6932.

52. **Yurchenko, E., M. Tritt, V. Hay, E. Shevach, Y. Belkaid, and C. Piccirillo.** 2006. CCR5-dependent homing of naturally occurring CD4⁺ regulatory T cells to sites of *Leishmania major* infection favors pathogen persistence. *J. Exp. Med.* **203**:2451-2460.
53. **Zhang, M., J. Gong, Y. Lin, and P. Barnes.** 1998. Growth of Virulent and Avirulent *Mycobacterium tuberculosis* Strains in Human Macrophages. *Infect Immun* **66**:794-799.
54. **Zhou, Z., M. C. Connell, and D. J. Macewan.** 2007. TNFR1-induced NF- κ B, but not ERK, p38MAPK or JNK activation, mediates TNF-induced ICAM-1 and VCAM-1 expression on endothelial cells. *Cell Signal* **19**:1238-1248.

Chapter 5

Conclusions and Future Directions

5.1 Summary of Results

The work presented here uses a series of mathematical and computational models to analyze the roles of signaling in macrophage activation and infection with *Mycobacterium tuberculosis*. We explore two major levels of signaling: intracellular signaling pathways and spatial intercellular communication.

5.1.1 Activation of Killing Effectors in Macrophages

The network of components involved in upregulating nitric oxide production in mouse macrophage models appears to have three distinct functional modules, with several components feeding into NO production that results in feedback by NO. To understand the function of this system, we used a mathematical model to predict characteristics of macrophage responses for different possible designs selected for by evolution. This elucidated design principles that explain how macrophages are capable of balancing a usual quiescent state with the need for production of high levels of NO required to kill some pathogens, including *M. tuberculosis*. The results predict that feedback regulation of NF- κ B and Stat1 pathways has an important role for NO activity in the system. This network design allows macrophages to reach very high levels of NO production due to synergistic activation of iNOS transcription, but is antagonistic to NO

production if only one of the complementary pathways (NF- κ B or Stat1) is activated. Therefore, this design represents a type of logical AND gate with a continuous component that allows intermediate states.

5.1.2 Kinetics of Activation and Macrophage-*M. tuberculosis* Interactions

We next examined implications of macrophage functional design in *M. tuberculosis* infection. The model, analogous to a cell culture experiment, predicts that negative feedback by NO reduces the efficacy of killing intracellular bacteria by macrophages compared to a positive feedback design. However, the model also predicts that negative feedback speeds NO induction, which may be advantageous in some activation scenarios. Simulations of several scenarios for possible timing of TNF- and IFN- γ -induced activation indicate a kinetic advantage for systems with negative feedback if the activation signals are received at the time of *M. tuberculosis* infection, and not before. Negative feedback may also induce an overshoot of NO production beyond the activated steady state that contributes to the kinetic advantage of initial macrophage activation occurring only after infection.

5.1.3 Roles of Intercellular Signaling in Granuloma Formation

An agent-based model of granuloma formation allowed us to determine the role of signaling networks in immune responses to *M. tuberculosis* that extend beyond the intracellular level to the cellular level. Sensitivity analysis of model parameters indicates a changing role over time for TNF- and T cell-related parameters in the first 50 days post-infection. With parameters varied in uncertainty analysis, the model predicts that changes

in the timing of T cell recruitment alter the kinetics of bacterial elimination: a first wave of elimination occurs with innate immunity, and a second follows soon after initial T cell arrival. This suggests that if T cells were properly primed by a vaccine, the infection may be more quickly and effectively cleared.

TNF-focused sensitivity analysis combined with perturbation of individual TNF activities or combinations of them gave predictions for the effects of the four primary TNF roles in granuloma dynamics (Figure 4.1). The results suggest that pleiotropy is an essential feature of TNF function: loss of single TNF activities did not result in predicted granuloma structures comparable to TNF deletions or depletions. Granuloma structures and cell kinetics in simulations with deleted TNF-mediated apoptosis activity predict a hyper-inflammatory state caused by an effective positive feedback loop, suggesting an important role for anti-inflammatory cytokines in ensuring robustness of the system.

5.2 Future Directions: Macrophage Activation Models

The analyses in this work were performed using two types of computational models operating at different space and time scales. The difference between these approaches allowed the study of complementary types of signaling roles in macrophage activation and *M. tuberculosis* infection. We now present a plan for integrating the two approaches for a detailed model of macrophage activation that will permit directly addressing questions that each of the approaches can not answer independently-i.e. building a detailed multi-scale model of the role of macrophages in granuloma formation (Figure 5.1). This type of model would capture cellular-scale interactions and

intercellular signals, with a detailed representation of their effects on intracellular signaling.

5.2.1 Integrating a biochemical network into individual macrophage agents

The ordinary differential equation model used in Chapters 2 and 3 allowed an accurate representation of biochemical events averaged over a population of macrophages, much like a cell culture experiment. In this type of model, activating cytokines and bacterial products directly turn on the production of anti-microbial effectors as a deterministic function of the amount of cytokine or bacterial products.

However, this type of model may not be accurate for representing this mechanism in individual agents of an ABM: gene regulation in individual eukaryotic cells, including macrophages, is not deterministic (10). Recent work suggests a “transcriptional burst” model, where transcription randomly transitions between “on” and “off” states (9). Transcriptional stochasticity has distinct implications in the role of intracellular feedback mechanisms (reviewed in 3). For instance, redundancy in signaling pathways may reduce variability in single cells (6). Addressing the role of intracellular macrophage signaling implemented in an agent-based model approach calls for an appropriate single-cell representation intracellular events. This approach would allow more accurate prediction of the interactions between individual macrophages and intracellular mycobacteria.

To do this, we first need to represent levels of individual molecular components in a single macrophage, and distinguish between deterministic and random variables as appropriate. Second messengers NF- κ B and Stat1 and levels of nitric oxide may be represented deterministically with differential equations linked to each activated

macrophage. Levels of regulated mRNAs of interest, including those for the iNOS and TNF genes, are best represented with the transcriptional burst model. The appropriate method to solve this component of macrophage activation is the Gillespie algorithm, which simulates kinetics of random chemical processes using a Monte Carlo approach (1).

5.2.2 Locations of macrophage recruitment and bacterial killing

With a more accurate model of macrophage activation kinetics, we can directly predict the effects of different levels of activation attained on the spectrum of *M. tuberculosis* loads in single cells.

This immediately suggests an approach to more directly examine a model for macrophage recruitment strategies proposed in Chapter 3. Based on the timing of activation signals, we hypothesized that recruitment of macrophages directly to the site of a mycobacterial granuloma would give a kinetic advantage over recruitment more distally, with subsequent migration across the lung parenchyma that may expose migrating cells to activating stimuli before they become infected.

If we added this mechanistic model of single-cell macrophage activation to the ABM here, this hypothesis could be directly tested. Simulations allow tracking and sorting of macrophage agents according to their location of entry into the modeled lung space. This location can be converted into a distance from the site of infection by a number of different methods, such as averaging the coordinate locations of extracellular bacteria or infected macrophages. The computed distance can be plotted versus NO levels, intracellular bacterial numbers, number of bacteria killed by a macrophage, or any

other relevant measured output. A result consistent with the activation timing hypothesis in Chapter 3 would be a positive correlation between the number of intracellular bacteria in each macrophage and recruitment distance of each macrophage. Repeated analysis for different times would reveal if there is a changing role for this effect between establishment phase of infection (with initial T cell infiltration) and later points after infection.

A possible consequence of recruitment strategies affecting macrophage activation levels in *M. tuberculosis* infection is a potential role for bacterial mechanisms that affect host cell recruitment mechanisms to improve intracellular survival. While macrophages are the preferred environment for bacterial growth in *M. tuberculosis* infections, sufficiently activated macrophages are capable of attaining bactericidal levels of activation. This suggests a selective advantage for Mtb infections promoting mechanisms of recruitment that minimize activation levels at the time of infection. One mechanism we propose testing for this effect is the level of chemokines induced by bacteria.

5.2.3 Feedforward and redundancy of feedback in macrophage activation

The biochemical model of macrophage activation presented in previous chapters is a simplification that subsumed levels of feedforward and feedback into a simple activation/response/feedback model. However, the JAK/STAT signaling pathway has several other characteristics that raise interest for their possible role in individual macrophages. Two genes induced by the activated Stat1- α homodimer with probable functional consequences for iNOS induction are interferon regulatory factor (IRF)-1 and suppressor of cytokine signaling 1 (SOCS1).

IRF-1 positively regulates iNOS transcription in mouse macrophage models (5), making it reminiscent of a coherent feed-forward loop with Stat1 (11; Figure 5.2). That is, Stat1 induces both iNOS and IRF-1 while IRF-1 in turn contributes to iNOS induction. This type of regulatory motif has been shown to cause a sign-sensitive delay in production of the co-regulated gene (4) (here, iNOS), such that increases in the rate of transcription are delayed but decreases are not.

On the other hand, SOCS1 is an anti-inflammatory feedback regulator that negatively regulates Stat1 (12) and NF- κ B (2, 7). Combined with the apparent NO-induced negative feedback of these regulators, these macrophage activation pathways appear to have redundant mechanisms for negative feedback regulation (Figure 5.2).

By including these mechanisms in a biochemical model that is integrated into the agent-based model, we could test hypotheses about design principles that have evolved to respond to, or minimize, uncertainty involved with gene regulation. The role of these mechanisms in the level, stability or predictability of macrophage responses may also have implications in the host-pathogen interaction with *M. tuberculosis*.

One hypothesis for the role of multiplicity and redundancy in activation signaling pathways is that co-regulation of IRF-1, SOCS1 and iNOS by Stat1 reduces variability in gene expression levels, making activation in a single macrophage more predictable or switch-like.

Chromosomal linkage between multiple genes also affects co-regulation in the transcriptional burst model of gene regulation: genes at the same locus have periods of activity at identical times while those at separate loci undergo uncorrelated bursts (9). This adds another dimension to how these mechanisms may function. In humans, IRF-1,

SOCS1 and iNOS are located on chromosomes 5, 16 and 17, respectively (8). This suggests that the three genes undergo uncorrelated transcriptional activity periods.

We propose simulations comparing scenarios where one or more of the regulated genes undergo coupled or uncoupled transcriptional bursts. This approach may then be carried out with each feedback interaction altered or removed from the system.

5.2.4 Shortcomings and alternative approaches

The proposed model integrates detailed biochemical kinetics using the Gillespie algorithm with intercellular interactions in cells representing an entire mycobacterial granuloma. While this approach is flexible and potentially useful, it has the possible shortcoming of high computational cost arising from the need to compute intracellular states of macrophage cells in a near-continuous manner.

One possible alternative approach to prevent this shortcoming is to lose some of the proposed mechanistic detail. For example, nitric oxide kinetics could be prescribed with rules that reflect different hypotheses without directly computing the kinetics of each individual macrophage cell. This approach would represent an intermediate step between the simple rule-based model used in Chapter 4 and the Gillespie algorithm approach proposed above, trading off some flexibility for computational tractability.

5.2.5 Effects of biochemical network design on mycobacterial granuloma formation

Spatio-temporal aspects of signaling captured by the granuloma model allow predictions for how variability in cytokine signals (extrinsic uncertainty) interacts with randomness in gene regulation (intrinsic uncertainty) to give variable levels of nitric

oxide expression. One interesting aspect of the regulatory pathways co-induced by JAK/STAT signaling is that their role appears to be primarily to gain control over pro-inflammatory signaling. That is, their relevant effects here may be primarily to modulate iNOS. (We note that other genes induced by the Stat1 pathway, such as CIITA, may have pro-inflammatory effects; the hypothesis presented here primarily concerns co-regulated genes feeding into iNOS expression.) An overarching theme of these regulatory pathways is a trade off between high levels of activation and the ability of macrophages to effectively kill *M. tuberculosis*.

We therefore propose studies to determine how changes in these regulatory pathways affect mycobacterial granuloma structure and bacterial levels. We can define performance criteria based on bacterial killing and levels of cytokine produced to determine how the trade-off between activation and modulation of activation affects bacterial survival. This would link the effects of intracellular signaling to granuloma structure, providing an integrated, multi-scale model of intracellular signaling in *M. tuberculosis* infection.

Figures

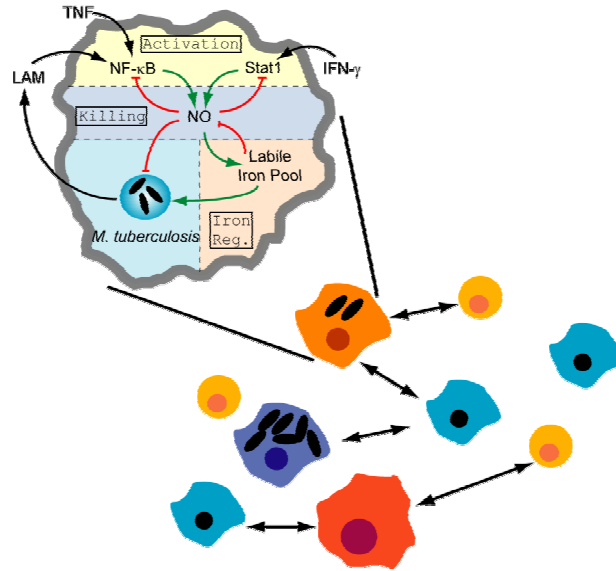


Figure 5.1. Conceptualization of a multi-scale model of intra- and inter-cellular signaling in *M. tuberculosis* infection.

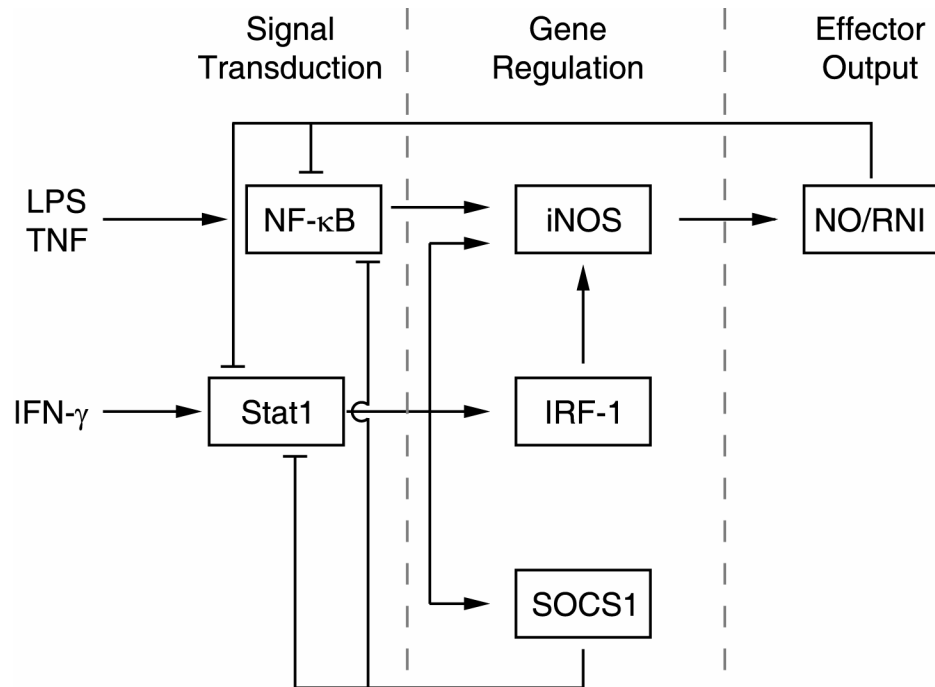


Figure 5.2. Macrophage activation pathways involved with iNOS induction have layers of regulation from other genes regulated by Stat1. IRF-1 forms a coherent feed-forward loop regulating iNOS induction. SOCS1 provides negative feedback to Stat1 and NF- κ B.

5.3 References

1. **Gillespie, D.** 1976. A general method for numerically simulating the stochastic time evolution of coupled chemical reactions. *Journal of Computational Physics* **22**:403-434.
2. **Kinjyo, I., T. Hanada, K. Inagaki-Ohara, H. Mori, D. Aki, M. Ohishi, H. Yoshida, M. Kubo, and A. Yoshimura.** 2002. SOCS1/JAB is a negative regulator of LPS-induced macrophage activation. *Immunity* **17**:583-591.
3. **Maheshri, N., and E. K. O'Shea.** 2007. Living with noisy genes: how cells function reliably with inherent variability in gene expression. *Annu Rev Biophys Biomol Struct* **36**:413-434.
4. **Mangan, S., and U. Alon.** 2003. Structure and function of the feed-forward loop network motif. *Proc Natl Acad Sci U S A* **100**:11980-11985.
5. **Martin, E., C. Nathan, and Q. W. Xie.** 1994. Role of interferon regulatory factor 1 in induction of nitric oxide synthase. *J Exp Med* **180**:977--984.
6. **McAdams, H., and A. Arkin.** 1999. It's a noisy business! Genetic regulation at the nanomolar scale. *Trends in Genetics* **15**:65-69.
7. **Nakagawa, R., T. Naka, H. Tsutsui, M. Fujimoto, A. Kimura, T. Abe, E. Seki, S. Sato, O. Takeuchi, K. Takeda, S. Akira, K. Yamanishi, I. Kawase, K. Nakanishi, and T. Kishimoto.** 2002. SOCS-1 participates in negative regulation of LPS responses. *Immunity* **17**:677-687.
8. **Pruitt, K. D., T. Tatusova, and D. R. Maglott.** 2007. NCBI reference sequences (RefSeq): a curated non-redundant sequence database of genomes, transcripts and proteins. *Nucleic Acids Res* **35**.
9. **Raj, A., C. Peskin, D. Tranchina, D. Vargas, and S. Tyagi.** 2006. Stochastic mRNA Synthesis in Mammalian Cells. *PLoS Biology* **4**:e309.
10. **Ross, I. L., C. M. Browne, and D. A. Hume.** 1994. Transcription of individual genes in eukaryotic cells occurs randomly and infrequently. *Immunol Cell Biol* **72**:177-185.
11. **Shen-Orr, S., R. Milo, S. Mangan, and U. Alon.** 2002. Network motifs in the transcriptional regulation network of *Escherichia coli*. *Nat Genet* **31**:64-68.
12. **Yoshimura, A., T. Naka, and M. Kubo.** 2007. SOCS proteins, cytokine signalling and immune regulation. *Nature Reviews Immunology* **7**:454-465.